DYNAMIC ANALYSIS OF COUPLED ARTICULATED TOWER AND FLOATING PRODUCTION SYSTEMS

Ismail Hakkı Helvacıoglu, B Sc, M Sc

Thesis submitted for the Degree of Doctor of Philosophy

Department of Naval Architecture and Ocean Engineering
University of Glasgow

November 1990

ProQuest LLC.
789 East Eisenhower Parkway
P.O. Box 1346
Ann Arbor, MI 48106 – 1346

CONTENTS

LIST OF FIGURES

CHAPTER 3

CHAPTER 4

CHAPTER 5

CHAPTER 6

CHAPTER 7

APPENDICES

LIST OF TABLES

ACKNOWLEDGEMENTS

The author is grateful for the advice and help of all members of the staff of the Department of Naval Architecture and Ocean Engineering at the University of Glasgow during the research study reported in the thesis.

The author is particularly indebted to

Professor D. Faulkner, Head of Department, for making this research possible, and for his continuous encouragement,

Dr. A. Incecik, Superintendent of the Hydrodynamics Laboratory, for supervising this research and for his tireless assistance, encouragement and support,

Dr. M. Söylemez for his stimulating discussions and valuable assistance in completing the thesis,

Mr. D. Percival for his advice and assistance during the development of the computer programs,

Mr. O. Yılmaz for allowing his data to be used in the comparison studies and for his contribution towards the completion of the thesis,

Mr. R. B. Christison and the staff at the Hydrodynamics Laboratory for their assistance during the experimental work, and

his parents for their support and encouragement throughout this work.

Finally, the financial support from the Turkish Ministry of Education and the Science and Engineering Research Council, U.K. is gratefully acknowledged.

DEDICATED TO MY PARENTS

DECLARATION

Except where reference is made to the work of others,
this thesis is believed to be original.

SUMMARY

In this thesis, motion and structural response characteristics of coupled articulated tower and ship systems under various types of environmental loading are investigated.

In Chapter 1, the main objectives of the study are explained. A discussion of the previous investigations carried out on the subject is presented briefly. The main characteristics of the existing and proposed structures, the accepted criteria for the environment in which these structures are working or are proposed to work and the assumptions underlying the theoretical analysis are summarized. The detailed literature review is left to each individual chapter. The outline of the thesis is also explained in this chapter in order to guide the reader.

Chapter 2 deals with the modelling of environmental loading on coupled articulated tower and ship systems. Wave, wind and current are chosen as prime loading effects on these systems. The flow regimes of vertical surface piercing cylinders are shown. The application of Morison's equation is discussed. The Froude-Krylov forces are derived for the wave induced force calculations on the box-shaped barges which represent the storage tanker. The second order wave forces present in regular and irregular waves on the box-shaped barges are also discussed. Various formulations in defining the short crested seas, steady current as well as static and dynamic wind are given.

Chapter 3 is concerned with the prediction of the motion and structural response of single articulated tower and ship systems under first and second-order wave, current, and steady and dynamic wind excitation. Although these environmental forces may occur at the same time to yield a combined effect on the structure, the emphasis here is placed upon the effect of each excitation force individually. The dynamic motion equations which are based on simple (1-DOF) and detailed (4-DOF) mathematical models are derived and solved in the frequency domain by utilizing some linearization procedures. The analytical predictions are compared with experimental measurements reported in the literature. Some parametric studies are presented including the effect of yoke length

variation and the effect of different hydrodynamic coefficients on the surge response of the system and on the yoke forces. In the last section of this chapter, the effect of directional spreading of waves on the motion and structural response of the coupled system are investigated through the different energy spreading assumptions.

Chapter 4 aims to obtain the motion equations for a double articulated tower by using the Lagrange method. A double articulated tower configuration which consists of five cylindrical elements is considered. The same configuration is also used during the model tests described in Chapter 7. First order wave forces are considered as excitation forces. The shear forces and bending moments as well as the axial tension and wave induced force distribution along the tower are presented for a number of wave frequencies. The parametric studies include the sensitivity of the natural frequency of the system to the geometric changes, the effect of increasing water depth and deck weight on motion response, a comparison of the angular motion and the joint force values of the double articulated tower with the values of a geometrically similar single articulated tower.

In Chapter 5 a motion response analysis of a double articulated tower and ship system in regular waves is presented. 2-DOF and 5-DOF mathematical models are considered. The results of the two mathematical models are compared with each other as well as with the experimental measurements carried out at the Hydrodynamics Laboratory. The shear force and bending moment distributions along the double articulated tower with the barge connected to it are shown. The motion and structural response values of the coupled double articulated tower and ship system are compared with the values of a geometrically similar single articulated tower and ship system. This chapter ends with some parametric studies which examine the effect of various geometrical changes on the system responses as well as on the yoke forces including the yoke length and the yoke orientation.

In chapter 6 the time domain simulation procedure is applied to the motion equations to obtain motion response characteristics of three different configurations. These are a single articulated tower, a coupled articulated tower and ship system and a rigid yoke moored ship. In the first and second cases, the motion equations of the system are solved

by employing the time domain simulation procedure and comparing these with the frequency domain solutions. In the third case, the yawing oscillations of a yoke-moored barge about a fixed point are examined. The external forces acting on the ship consist of the steady wind and current forces, the steady component of the second order wave forces and incident wave forces. This analysis shows the dominant environmental effect on a particular ship configuration.

In Chapter 7, a description of model tests carried out in regular waves is presented. These tests are:

- motion response measurements with a double articulated tower over a range of wave frequencies and wave heights,
- motion response and the yoke force measurements with a coupled double articulated tower and a rectangular box-shaped barge
- motion response measurements for a barge model moored by means of linear springs located on the fore and aft ends of the model.

In addition to the measurements listed above, the added mass, drift force coefficients and still water and wave damping coefficients of the barge model were measured. The numerical filtering procedure developed to analyse the data obtained from the free oscillation tests in waves is described in Appendix C.

In the final Chapter 8, the main emphasis is placed on drawing overall conclusions and on making some recommendations for future studies on this subject.

CHAPTER 1

INTRODUCTION

1.1 ARTICULATED TOWERS AS COMPLIANT STRUCTURES

The advantages of compliance on strength has been known for many years, even by poets. In one of his fables, La Fontaine (1621-1695) compares a reed and an oak as follows:

...the Reed says to the Oak:'Springs from a kindly heart; but do not fret;
you and not I, should pay the winds respect
I bow, but never crack!'
{The Oak and the Reed}

Compliant systems are designed to withstand environmental loads by their ability to deflect from an equilibrium position when they are subjected to environmental loading. Their ability to move allows them to effectively reduce the imposed loads. Difficulties in design arise when the compliant systems are located in ever increasing depths and subjected to extremely hostile environmental conditions.

An articulated tower is a surface piercing circular cylinder which is connected to the sea bed by means of a universal joint. Since it has freedom to oscillate around the universal joint the articulated tower can be classified as a compliant structure.

In order to show the effect of becoming compliant on the structural loading, a simple cylindrical tower is considered. Firstly, the tower is connected to the sea bed by means of a universal joint. Secondly, the universal joint is removed and the tower is fixed at the sea bottom. The shear force and bending moment distributions along the tower are calculated under sinusoidal wave excitation (the wave height is 2 m and the wave frequency is 0.6 rad/s). Two tower configurations and the shear force and bending moment distributions along these towers are shown in Fig.1.1. This figure shows clearly that the freedom of oscillation under the external forces reduces extensively the loads on the articulated tower structure.

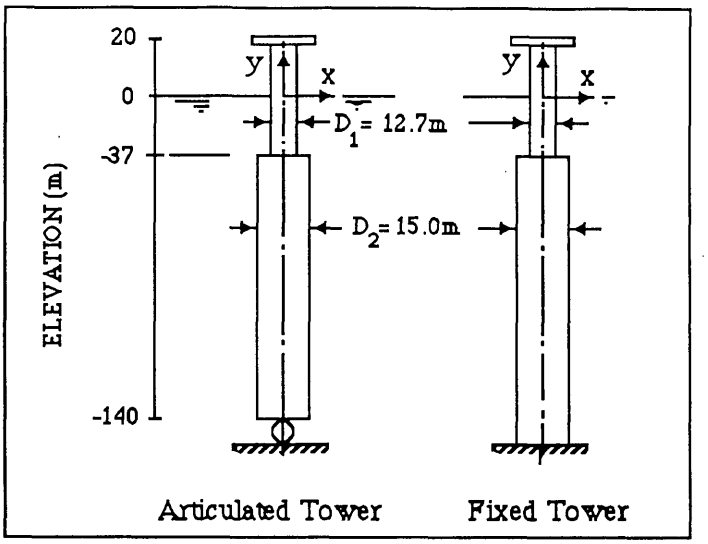

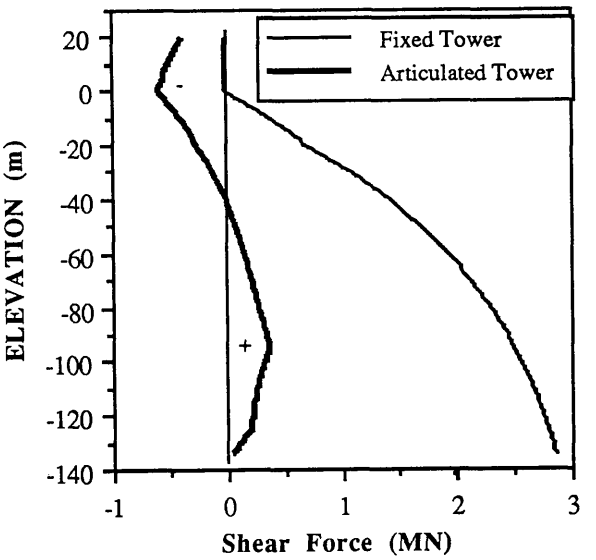

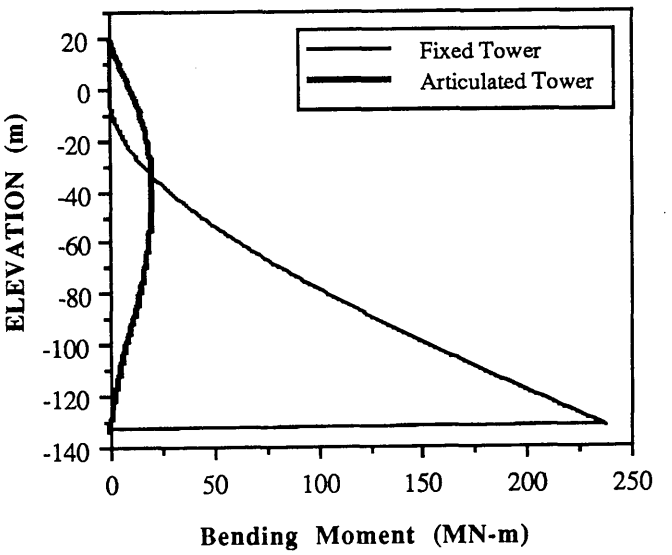

Fig.1.1 Comparison of articulated tower and fixed tower

Articulated towers have been used in rough seas as mooring devices for shuttle tankers, as flare platforms, as support for production facilities and as permanent mooring for production and storage tankers. In the latter case, the function of the articulated tower is to provide a mooring point for a production and storage vessel and allow for the exportation of oil.

The main characteristics of the existing and proposed articulated towers and articulated tower based floating production systems are presented in Table 1.1. The accepted criteria for the environment in which these structures are working, or are proposed to work, and the assumptions for the theoretical analysis are also given in this table. Chronological order is followed. Papers referring to the same prototypes are placed in the same column.

The usage of the articulated tower in deeper waters requires a strong and massive construction. Detailed analysis of large diameter articulated towers has been subject to investigation for some time (see Drake (1984) and Wu (1987)). A large diameter configuration causes large added mass and wave action forces and consequently very large bending moments. In order to avoid the large bending moments at the middle of the tower, a second articulation is introduced. This type of articulated tower is called a double articulated tower (see Table 1.1, Jain and Kirk (1977) and Millar et al (1979)). A dynamic analysis of the double articulated tower concept in regular waves is part of the study considered in this thesis.

1.2 ARTICULATED TOWER BASED FLOATING PRODUCTION SYSTEMS

Ship based systems have attracted operators who purchase them at relatively low cost and convert them into a combination of production and storage units (see Smulders and Remery(1979)). Also the large ship deck areas allow for the necessary space and payload requirements of larger fields.

The ship can be moored to an articulated tower by means of a bow hawser or a rigid yoke mechanism. In the former case, the system has a large degree-of-freedom in the horizontal plane. Therefore, the behaviour of the moored ship may be rather unstable. On the other hand, the rigid yoke connection eliminates the instability problem in the horizontal plane by coupling the surge and sway oscillations of the ship by angular response of the tower in pitch and roll. The rigid connection mechanism also protects the tower from overriding the ship.

It has been reported (Drawe et al 1986) that without rigid yoke assembly, ships can not stay moored to the single point mooring terminals in waves above 4.5 m and can not berth in waves above 2.4 m. Therefore, the articulated tower and yoke mechanism must be designed to hold the ship in the most severe weather conditions. The permanent rigid yoke moored storage vessel overcomes the downtime associated with the connect /disconnect of the shuttle tanker.

The large number of papers published on the analysis of coupled systems over the last few years clearly reflects an increasing interest in this field (see Romeling et al (1984), Snowden et al (1985) and Chadhuri(1986)).

1.3 SCOPE OF STUDY

In designing the coupled articulated tower and ship systems, it is necessary to consider vessel structural and seakeeping characteristics, including joint probability of the environmental effects and structural survivability during storm conditions.

The overall aim of this research is to establish a closer understanding of the relationship between the environmental loading and the dynamic behaviour of these compliant structures. The solution of the dynamic and structural problems will allow safer designs of these systems.

The research conducted during this study resulted in the development of design and analysis tools for predicting the motion and structural response of coupled articulated

tower and ship systems under first- and second-order wave, current as well as static and dynamic wind induced loading. The developed tools are very suitable for parametric design studies in which the effect of changes in various geometrical and environmental parameters on the performance of the articulated tower based systems could be determined. The computer programs written during the study can be run on personal computers which are commonly available in today's design offices.

The results of predictions obtained from the mathematical models developed in this study are verified with the results of experiments carried out by other researchers and published in the open literature. In addition to that a limited amount of experimental investigation is carried out during this study in order to verify the mathematical models.

1.4 STRUCTURE OF THESIS

This thesis is organized as follows:

In Chapter 2, the modelling of the environmental loading on the coupled articulated tower and ship systems is explained. Chapter 3 is devoted to the single articulated tower and ship system. The environmental loading calculation procedure described in Chapter 2 is applied to motion equations reported in Chapter 3. In Chapter 4, motion equations for a double articulated tower are derived and solved in the frequency domain. The shear force and bending moment distributions along the tower are calculated. Some parametric studies regarding the effect of variations of the tower configuration on the dynamic behaviour of the tower are presented. In Chapter 5, the double articulated tower motion equations are coupled with the motion equations of the ship. The effect of the second articulation is examined in terms of motion and structural response values. Time domain analysis is applied to the motion equations in Chapter 6. In carrying out the time domain analysis of coupled floating systems the emphasis is placed upon the non-linearities due to the existence of the articulated tower. The mathematical models developed in Chapters 4 and 5 are compared in Chapter 7 with experimental model tests. Chapter 8 is devoted to overall conclusions and recommendations for the future work.

TABLE II

1. Concept Name and Source of Reference	AMMPR Caldwell & Gammage (1977)	Tower-Tanker System Chakrabarti & Cotter (1978)	SALM System Millar et al (1979), Jain & Kirk (1977)
2. Technical Description	Articulated Multiline Marine Production Riser System	A loading tanker (54 000 dwt) is moored to a single tower by a mooring arm or a nylon hawser.	Single anchor leg mooring system, an export terminal for tankers up to 120 000 dwt.
3. Field data	Gulf of Mexico, d=457m	Garoupa field, Brazil,d=122m	North Sea, Thistle field, d=160m
4. Environmental Loading (static and dynamic)	Current =1.1m/s; max. wave crest heigth=7.6~9.1m, max.wave trough= 6.1~7.6m, dominant wave period =9s~12s	Current=1.54m/s; wind=22m/s; irregular waves:Hs=10.7m, Tp=10s(1 year storm)	Wind=26m/s; Hw=7m, T=5~20s.
5. Dynamic solution type	A finite element procedure that is employed to calculate the motion responses	Linearized frequency domain analysis	The eom are derived from Lagrange's equation and are solved in the time domain by a step-by step solution technique.
6. Method of structural analysis	n/a	n/a	The finite element approach is adopted to calculate the SF&BM distributions along the structure (McNamara & Lane,1984)
7. Used commercial computer programs (if any)	n/a	n/a	n/a
8. Model test data	Scale=1:3.5, a prototype structure in 52m of water.	CBI Labs., Ill.; Scale=1:48; Hw=2.4 ~9.6m; Freq.=0.25~0.91rad/s; (irregular waves consist of 8 components)	n/a
9. Typical motion and force values	Max. hor. displacement of the buoy top is 26m; max. load at the mooring device is 66.7kN; max. middle unv. joint angle is 72deg.	Max. values (per unit wave amp.): tilt angle=0.3deg; mooring arm load=437kN horizontal pin load=269kN	Max. values in survival cond. (Hw=30m, T=16s); top displ.=19m; SF=0.45MN; BM=6 MNm. Natural freq.=0.23rad/s and 0.7rad/s.
10. Comments	The prototype tests has larger dynamic horizontal buoy motion because no ship is attached to the buoy to restrain it.	Secondary peak at 0.31rad/s is observed. More reseach on drift forces on the system is needed.	n/a

N.B. i) All values refer to the full scale dimensions, including model test results;

ii) Following abreviations are adopted: d=water depth, Hs=significant wave height, Hw=wave height, T=wave period, Tz= zero crossing period, Tp= peak period, SF=shear force, BM=bending moment, nat. freq.=natural frequency, hor.=horizontal, ver.=vertical, f.=force, n/a=not avaliable

1	Articulated Single Point System Olsen et al. (1978), Korbijn(1979) Sorheim(1980)	Test-CONAT Kokkinowrachos & Mitzlaff(1981), Butt et al. (1980)	Articulated Loading Platform and Tanker Naess (1980)	SALM- VLCC Mack et al (1981)
2	Computation of the motions and loads of an articulated SPM system for a large tanker (130 000 dwt)	Concrete Articulated Tower	Model tests of a loading tanker(150 000 dwt) moored to a single tower by means of a hawser	A tanker(210 000 dwt) is connected to a single anchor leg mooring by a rigid yoke.
3	North Sea, d=145m	North Sea, d=30m	North Sea, d=147.5m	North Sea, d=82m
4	Several enviromental conditions are considered: No.11 is Current=1.3m/s; Wind=50m/s; Hw=30m.	Current=1m/s, wind=35m/s, Hw=12m, T=9s	Current=0.5m/s, wind=24m/s, Hs=5.5m (operational); current=1.2m/s, wind=46.5m/s , Hs=16.5m (survival); P-M spectrum.	100 year survival storm: current= 1.3m/s; wind=43.9m/s, Hs=14.4m, Tz=16.4s; (JONSWAP spectrum)
5	The nonlinear emotion equations are solved in the time domain using numerical integration techniques.	The eom are derived from Lagrange's equation and are solved in the time domain by a step-by step solution technique.	n/a	n/a
6	Structural analysis program (NV 337) calculates SF&BM distribution along the tower.	n/a	n/a	The fatigue analysis for the rigid arm was based on AWS-X modified fatigue curves.
7	A computer program (NV 429) is used to predict the hydrodynamic motions and loads on the articulated towers including the single point moored tanker.	n/a	n/a	ANSYS finite element computer program is used to calculate stresses and displacements for the universal joint components.
8	NSMB; Scale 1:70, Model tests are performed in irregular seas only.	Full scale measurement carried out at 30m water depth, damping ratio is measured as 0.017.	NHL Ship and Ocean Lab.; Scale=1:70; P-M spectrum is created.	n/a
9	Max. values (current=0.77m/s, wind= 20.6m/s,Hw=5.5m,T=10s, thrust astern= 147.1KN) : surge=30m; sway=35m; bow hawser tension=2.9MN	Max. inclination angle is 40 deg.	Natural freq.=0.11rad/s, logarithmic damping decrement=0.46; max. values: tilt angle= 9.3deg.; shear force=4.26MN; hawser tension=2.89MN	Design vertical reaction=29.4MN.
10	The tanker may affect the wave field around the tower by 0~10% as far as water particle velocity and accelerations are concerned.	Hydrodynamic analysis on the basis of potential theory is necessary in the estimation of the Cm and Cds.	In the presence of current, directional instability of the tanker causes large transverse excursions.	Design load cases were developed at each location by considering phasing relationships obtained from model tests

1	ALP Kim & Luh (1982)	Articulated Platforms Kirk & Bose (1982)	SALS System Langley & Kirk (1982)	SALM Wagenaar & Davison (1983); Haverty, McNamara & Moran (1982)
2	Articulated Loading Tower	Random motion analysis of 3 deep water articulated tower configurations (Elf tower and ARCOLPROD towers)	A tanker (240 000 dwt) is moored to riser which is placed under tension by a submerged buoyancy chamber (single cylinder buoy or U-shape chamber)	A tanker (200 000 dwt) is moored to a riser by means of a rigid yoke.
3	North Sea, d=147.5m	Deep waters, d = 300m, 250m, 210m	North Sea, d=160m.	Tazerka Field, Tunisia, d=140m
4	Regular waves only	Current=1.5 m/s; JONSWAP and P-M spectra; 100 year storm Hs=15m, Tp=17.2s; average winter storm, Hs=7.5m, Tp=12.1s.	JONSWAP and P-M spectra; Hs=15m, Tav=14s.	Current=1.05 m/s; wind=17m/s; Operational conditions: Hs=8.5m, T=14s.
5	Linearised freq. domain analysis	Spectral methods with the nonlinear drag force being linearized by the method of Tung &Wu(1975)	Linearised spectral analysis	n/a
6	n/a	n/a	n/a	n/a
7	n/a	n/a	n/a	n/a
8	see Naess (1982)	see Olsen et al (1978)	NSMB; Current=1.23m/s; wind=33m/s; ISSC spectrum, Hs=10.4m, Tav=12.4s.	n/a
9	Maximum values: pitch resp.=3 deg/m; Nat. fre.=0.12rad/s; total wave excitation f.=125t/m; SF at joint=150t/m; axial f.at j.=33t/m	Max. BM at 50m below the tower deck is 715MNm; max. SF at the joint is 16.5MN; max. deck acceleration is 0.23g, (Hs=15m)	R.m.s. values(Hs=4m) : riser angle=4 deg., yoke f.(ver.)=0.8MN, yoke f.(hor.)=1.3MN, riser tension=2.8MN; nat. freq.=0.027rad/s; max. static offset due to drift forces=14m.	Max. values in operational cond.: surge=6m; heave=5m; Static offset of tanker=47m;
10	More model tests in regular waves is recommended.	Elastic mode bending is important for d>350m. Inclusion of current decrease the max. BM by 3% and increase the SF at j. by 7%.	The presence of current increase r.m.s. joint forces by 4%, decrease r.m.s. surge responses.	n/a

1	A Tanker and SALM System Olson et al. (1983)	Multi Articulated Tower and a Floating Vessel Dumazy & Leturcq (1983)	Articulated Tower Andersson & Matsson(1983)
2	A tanker (50 000 dwt) is connected to a Single Anchor Leg Mooring by means of rigid yoke (hinged at the stern)	A double articulated tower is moored to a tanker (230 000 dwt) by a mooring hawser or a yoke (stern connection)	Application of a Finite Element Program to the Articticulated Tower Motion Analysis
3	Hondo Field, California, d=149m	North Sea, d=300m	d=135m
4	Current=1m/s; Wind=40m/s; Hw=12.3m	Current=1.5m/s; wind=41m/s; Hs=17m, Tz=6s (survival); wind=26m/s,Hs=8m, Tz=9s (operational); JONSWAP and P-M spectra.	Regular waves; Hw=30m, T=17s.
5	n/a	3-D program was used to calculate hydrodynamic properties. Slow drift motion and forces are calculated in time domain	Finite Elemet Program which takes into account the displaced position when calculating the wave induced forces are introduced.
6	n/a	n/a	n/a
7	n/a	ELFSIM (time domain simulation program)	ADINA (Automatic Dynamic Incremental Nonlinear Analysis)
8	n/a	The model tests were carried out by DSRL in Copenhagen. Irregular uni-directional waves are considered.	n/a
9	The period of response to wave drift forces is 314s. The second mode of vibration (oscillation of the intermediate unv. joint) is 28s.	Survival condition: max. lower column response= 21.5deg.; max. upper column response=34.6deg.; max. yoke force=13.9 MN	Max. Inclination = 7.59 degrees Natural freq.=0.12 rad/s.
10	n/a	The DAT is designed to have low natural frequency (0.05and 0.19 rad/s),The tower-tanker system nat. freq. is 0.017rad/s. Damping ratio in waves is 0.12	For non-slender structures NMIWAVE can be used as a pre-program for ADINA.

1	Single Anchor Leg Mooring Rigid Arm (SALMRA) Houlie, M. et al (1983)	Articulated Production Tower Butt et al. (1984)	Bi-Articulated Column and Tanker Römeling, Marol & Sand (1984)
2	Double articulated tower is moored to a tanker by means of a rigid yoke	Production towers in water depths of more than 300m.	Model test of a double articulated tower and tanker (250 000 dwt) system in directional waves
3	Northern North Sea, d=375m	North Sea, d > 300m	North Sea, d=160m
4	wind=47m/s; P-M spectrum; Hs=5.4~17m, Tz=7.6~12.5s.	Regular waves only	Wind=15m/s; JONSWAP spectrum; Hs=8.8m,Tp=12.7s, headings between 0~30degrees.
5	n/a	Linearized frequency domain analysis	Dynamic analysis with nonlinear F.E. program in random sea
6	n/a	Bending moment distribution is given.	n/a
7	n/a	n/a	TRITON (diffraction program) DYN (F.E. program) TENSION (frequency domain analysis program)
8	Norwegian Maritime Labs., Scale=1:55, Tests were carried out in uni- and multi-directional seas ('cos square' spreading function is considered)	n/a	DHI Offshore Test Basin; scale 1:100; 2-D and 3-D wave fields are created.
9	Yoke Force=29.4kN in uni-dir. seas (Hs=12.2m), yoke Force= 98.1 kN in multi-dir. seas (Hs=11.8m), 4 times higher sig. sway motion in multi-dir. seas, 8 times higher sig. roll motion in multi-dir. seas.	Max. values when d=300m and Hw=2m; tilt angle= 0.1deg.; joint force=3.4MN; bending moment= 360MNm.	Normalized surge response (Tower with tanker): Uni-Dir. waves : 9.4m(high freq.), 34.1m (low freq.) 34.1m(low freq.), Multi-Dir. waves : 9.3m(high freq.) , 32.1m(low freq.)
10	All motions are increased in multi-dir. seas except the surge motion and the longitudinal yoke load.	In order to reduce the loads acting on the joint,the use of light weight concrete and the aerodynamic design of the deck structure will be investigated.	The tanker motions in sway, roll, pitch and yaw are larger in multi-dir. waves than in uni-dir. waves; larger transverse forces are noted in multi-dir case.

1	HDW, Articulated Loading Tower Schellin & Koch(1985), Ostergaard & Schellin(1987)	Articulated Column-Based Floating Production System Snowden et al (1985)	SALM-Tanker Chaudhuri (1986)
2	Loading platform for LNG transfer	A tanker (195 000 dwt) is permanently moored to an articulated column by means of a rigid yoke.	A tanker(250 000 dwt) is connected to a Single Anchor Leg Mooring by means of a mooring arm.
3	North Sea, d=180m	North Sea, d=169m	Northern North Sea, d>300m
4	Regular and irregular waves	JONSWAP and P-M spectra; Hs=14.5m, Tz=13.5; Davenport wind spectrum.	100 year storm condition: current=1.5m/s, wind= 31m/s, Hs=15.8m,Tp=18.8s; JONSWAP spectrum.
5	Time domain simulation; 3 sets of computations: 1. Cm=2 and Cd=1 2. Selected coefficients based on Sarpkaya's experiments 3. Coefficients calculated using potential theory	Linearized freq. domain, time domain and spectral analysis.	Non-linear finite element analysis of the SALM -Tanker system for extreme and operational environment.
6	n/a	SF & BM along the tower (with or without a tanker connected to it) are calculated.	n/a
7	GLTOWER,(time domain simulation program)	n/a	n/a
8	Hamburg S.M.B.; Scale=1:32.75; regular waves: Hw=1.9~5.6m and T=6~15s; irregular waves (No.111): Hs=9.1m, Tp=10.7s.	TEL labs.; scale=1:169; max. Hw=16.9m, Hs=15.2m.	n/a
9	Measured max. values for Hw=2m: top motion=1.3m; joint force(hor.)=490kN; joint force(ver.)=210kN; Calculated max. values in irregular seas(No.111): top motion=6.76m; joint force(hor.)=3016kN .	Max. values(for Hw=2m): surge=1m; heave=1m; pitch=0.6 deg.; yoke force= 3MN; column bending moment=100 MNm; horizontal joint force=1.9MN.	Max. surge r.a.o.=0.4, max. heave r.a.o.=2.25; mean drift offset=65m, slow drift motion amp. and period=45m and 450s, resp.; base joint hor. f.=8.6MN; intermediate joint hor. f.=8.4MN.
10	Morison's equation can be used adequately; the influence of Cd on the tower response and forces at joint is small. Set 3 gives the best correlation with experiments.	The effect of the nonlinearities due to wave and current interaction and non-colinear forces on the system should be investigated.	The effect of the steady drift force on the motion of the system is difficult to calculate due to the large variability of damping in vessel motions.

CHAPTER 2

ENVIRONMENTAL LOADING ON COMPLIANT STRUCTURES

2.1 GENERAL DESCRIPTION

In determining the external forces acting on compliant structures accurate definition of the environmental is essential. The magnitude of these forces as well as their frequency range must be known in order to accurately predict the behaviour of a compliant structure.

A coupled articulated tower and ship system comprises two hydrodynamically different structures (see Fig.2.1): An articulated tower which is a vertical surface piercing cylinder, free to oscillate about an articulating joint, and a ship which is a bluff body floating in waves.

This chapter deals with the modelling of the environmental forces acting on coupled articulated tower and ship systems. The wave, wind and current forces are prime loading effects on these systems. The different flow regimes around vertical surface piercing cylinders are shown. The application of Morison's equation is discussed. The Froude-Krylov forces are derived for the wave induced force calculations on a box-shaped barge which represents a storage tanker. The second order wave forces present in regular and irregular waves on a box-shaped barge are also discussed. Various formulations in defining the short-crested seas, steady current as well as static and dynamic wind are given.

2.2 FIRST ORDER WAVE FORCES

2.2.1 INTRODUCTION

The flow regimes which affect a coupled tower-ship system are defined before a formulation of wave forces acting on these systems is given.

The wave forces acting on offshore structures were classified by Hogben(1976) under three headings, inertia+drag, inertia and diffraction. Fig.2.2 shows the different flow regimes as a function of wave height, member diameter and length values. In deep

water applications, Fig.2.2 can be used to identify the appropriate method of wave force calculation for a structural member in a particular flow field:

$H/D > 1$	Morison's equation (inertia+drag)
$D/\lambda < 0.2$ and $H/D < 1$	either Morison's equation or diffraction method
$D/\lambda > 0.2$	wave diffraction method.

Existing articulated towers have a diameter range of 6m to 15m at the S.W.L. If we consider a sea state having a wave height range of 2m to 15m and a wave length range of 1540m to 43m (which corresponds to ω=0.2~1.2 rad/s), the variables in Fig.2.2 are calculated as follows:

Diameter: 6m

$$H/D = 0.33\ (H = 2m) \Rightarrow 4.0\times10^{-3} \le D/\lambda \le 0.14$$
$$H/D = 2.5\ (H = 15m) \Rightarrow 4.0\times10^{-3} \le D/\lambda \le 0.05$$

Diameter: 15m

$$H/D = 0.13\ (H = 2m) \Rightarrow 9.0\times10^{-3} \le D/\lambda \le 0.35$$
$$H/D = 1.0\ (H = 15m) \Rightarrow 9.0\times10^{-3} \le D/\lambda \le 0.14$$

Fig.2.2 shows that the articulated towers generally work in the inertia regime. The application of Morison's equation is therefore considered adequate. For large diameter articulated towers (e.g. D=25m) diffraction force calculations have been carried out by Drake, Eatock-Taylor and Matsui (1984). They found that when Morison's approach is applied to large diameter towers, it over-predicts the wave loads in the range of higher frequencies. However, the advantage of the easy applicability of Morison's equation to the relatively small diameter towers (e.g. off-loading or mooring towers) has been recognized by many researchers (see Kirk and Jain (1977), Chakrabarti and Cotter (1979), Schellin and Koch (1985)).

The characteristic dimensions of a production/storage vessels range between 40 and 55 m. Hence, for the ship-shaped structures the diffraction regime is dominant. In formulating the wave forces acting on the production/storage ship, the ship is represented in this study by a rectangular box-shaped barge.

In the following sections, the wave force calculation on vertical surface piercing cylinders and on rectangular box-shaped type bluff bodies will be discussed.

2.2.2 FIRST ORDER WAVE FORCES ON VERTICAL SURFACE PIERCING CYLINDERS

In calculating the wave loads on the cylinders, the assumption of incompressible, unbounded fluid of uniform depth is made. For a stationary cylinder in a plane flow field, the total time-varying loading per unit length is given by Morison and others (1950) as follows

$$f = C_M \rho \pi \frac{D^2}{4} \dot{U} + C_D \rho \frac{D}{2} U|U| \tag{2.1}$$

where D is the diameter of the cylinder; ρ, water density and U and U are the water particle velocity and acceleration, respectively (these terms can be derived from the flow velocity potential as presented in Table 2.1). C_M and C_D which are inertia and drag coefficients for the circular cylinder, are based on experimental data (see Sarpkaya and Isaacson (1981). They are functions of several parameters, i.e.

$$C_M = C_M(R_e, \text{KC, cylinder roughness, etc.})$$
$$C_D = C_D(R_e, \text{KC, cylinder roughness, etc.})$$

in which R_e and KC are the Reynolds number and the Keulegan-Carpenter number, respectively.

If the structure, in our case a surface piercing cylinder, is oscillating in the flow, Morison's equation can be modified to obtain the effective loading per unit length as

$$f = C_M \rho \pi \frac{D^2}{4} \dot{U} + C_D \rho \frac{D}{2} (U - \dot{x}) |U - \dot{x}| \qquad (2.2)$$

where $\dot{x}$ is the rigid-body velocity of the section.

The C_M and C_D coefficients obtained from oscillating vertical cylinders are different than those obtained from fixed cylinders in oscillatory flow.

Chakrabarti and Cotter(1984) conducted experiments to investigate the interaction of waves with an oscillating tower. The tower was tested at 3 inclination angles and in 3 different excitation modes. These three different modes were i) tower fixed in regular waves, ii) tower forced to oscillate in still water, iii) tower allowed to oscillate freely in one plane in regular waves. It was found that in the case of the free tower, the flow field in the vicinity of the tower was affected by both the oncoming waves and the tower oscillations, but because of the presence of the waves, the flow field tended to be similar to that around the fixed tower in waves. They concluded that the coefficients obtained from the forced oscillating tower in still water and from the fixed cylinder in waves are generally applicable to a free tower in waves(see Fig.2.3). On the other hand, they proposed further investigation into the use of C_D as a relative velocity drag term when the KC number is low.

Kokkinowrachos et al (1985) carried out full scale pendulum tests by pulling a large scale(1:25) articulated tower model with a tug to an angle of roughly 18 deg in relatively calm seas. The tower was then released from the slip hook. They measured the oscillations of the tower. They also simulated the free oscillation tests using a time domain, nonlinear analysis technique. In the numerical simulation, the drag coefficient was chosen as C_D=0.7 and 1.6. For C_D=1.6 a good agreement between the measured and calculated time histories was achieved.

In conclusion, the hydrodynamic coefficients for surface piercing circular cylinders can be chosen from the results of model tests although further investigation into the oscillating cylinders at low KC numbers is necessary. In this study, C_M=2.0 and C_D=1.0 were used as the inertia and drag coefficients, respectively, unless otherwise indicated.

The total force on the cylinder can be found by integrating the force per unit length along the cylinder:

$$F = \int_{-d}^{0} f(y,t)dy \tag{2.3}$$

The moment of these wave forces around the seabed can be given as follows

$$M = \int_{-d}^{0} (y+d)f(y,t)dy \tag{2.4}$$

The first assumption of this method is that the flow around each section is not influenced by the flow around adjacent sections. This assumption becomes questionable when a cross flow is present. The second assumption is that the effect of the free surface is negligible. One should therefore use Morison's equation with a correction factor for the free surface effects (see Chakrabarti (1970)).

2.2.3 FIRST ORDER WAVE FORCES ON RECTANGULAR BOX-SHAPED BARGES

In this section, the effect of first order forces on the ship will be discussed. In a regular wave train, the ship is subject to incident waves. There are two distinct effects of these waves as they meet the ship. As they strike the ship they get reflected or diffracted from the hull and scattered in all directions. At the same time, since the ship is free to move in surge, the waves will set the ship in motion. The motion of the ship will generate waves and these waves will radiate out in all directions. In the case of first order

calculation these two problems may be treated separately and can be added together linearly. The incident and diffracted waves on the ship produce external forces and are computed on the wetted hull surface when ship is at rest, assuming small amplitude motions. The radiated waves produce forces on the ship which are proportional to the amplitude of motion of the ship. The component inphase with the ship rigid-body acceleration is the added mass component and the component inphase with the ship rigid-body velocity is the damping force component.

An investigation is carried out to find simple but accurate methods of calculating the wave forces on the ship. The ship is modelled as a rectangular box-shaped barge having the same displacement as the ship. The wave excitation forces on the barge are calculated by using the Froude-Krylov approximation. The effect of diffracted wave is taken into account by an approximate method.

Surge Force

The horizontal pressure forces on the rectangular box-shaped barge(see Fig.2.4) can be written by integrating the dynamic wave pressure component in x direction as follows

$$F_{Px} = -\int_{V}(\frac{\partial p}{\partial x})dv \tag{2.5}$$

where p is given in Table 2.1 and dv=B(x)dxdy. Since the breadth of the barge is constant along the barge length, the volume integral is reduced to the following form:

$$F_{Px} = \int_{-L_S/2}^{L_S/2}\int_{-T_S}^{0}\rho g\zeta_a k e^{ky}\sin(kx-\omega t)B_S dydx \tag{2.6}$$

where ρ is density of water; g, gravitational acceleration; ζ_a, wave amplitude; k, wave number; ω, angular frequency; L_S,B_S,T_S are barge length, breadth and draught,

respectively.

The integral given in Eq.(2.6) becomes

$$F_{Px} = -2\rho g\zeta_a \frac{B_S}{k}(1 - e^{-kT_S})\sin(k\frac{L_S}{2})\sin(\omega t) \tag{2.7}$$

On the other hand, the wave particle acceleration induced forces on the barge (the effect of diffracted waves) in x direction can be approximated by

$$F_{Ax} = m_{AD,x}B_S[\dot{U}_x\Big|_{\substack{x=-L_S/2 \\ y=-T_S/2}} + \dot{U}_x\Big|_{\substack{x=L_S/2 \\ y=T_S/2}}]$$

or

$$F_{Ax} = -2m_{AD,x}B_S\zeta_a\omega^2 e^{-T_S/2}\cos(k\frac{L_S}{2})\sin(\omega t) \tag{2.8}$$

where $m_{AD,X}$ is the added mass of a rectangular plate with a unit width oscillating in x direction:

$$m_{AD,x} = \rho\frac{\pi}{4}T_S^2$$

The added-mass values of rectangular geometries with various aspect ratios are given in Sarpkaya and Isaacson(1981).

The total wave force in x direction is given by the following equation

$$F_{Tx} = F_{Px} + F_{Ax}$$
$$= -2\zeta_a B_S[\rho g\frac{1}{k}(1 - e^{-kT_S})\sin(k\frac{L_S}{2}) + m_{AD,x}\omega^2 e^{-T_S/2}\cos(k\frac{L_S}{2})]\sin(\omega t) \tag{2.9}$$

Heave Force

The vertical pressure forces on the barge can be calculated by integrating the dynamic pressure at the bottom of the barge along the hull length as follows:

$$F_{Py} = \int_{-L_S/2}^{L_S/2} B_S \rho g \zeta_a e^{-kT_S} \cos(kx - \omega t) dx \tag{2.10}$$

On the other hand, vertical inertia forces in the heave mode of motion due to the wave particle acceleration can be written as follows

$$F_{Ay} = \int_{-L_S/2}^{L_S/2} m_{AD,y} \dot{U}_y \Big|_{y=-T_S/2} dx \tag{2.11}$$

where $m_{AD,y}$ is added mass per unit length of a rectangular section in dimensions $B_S \times T_S$ in heave, or $m_{AD,y} = \rho \frac{\pi}{2} C_{VH} (B_S/2)^2$ where C_{VH}=1.5; U_y is the vertical component of water particle acceleration.

Thus, performing the above integrations, total heave forces on the barge can be given in the following simplified form:

$$\begin{aligned} F_{Ty} &= F_{Py} + F_{Ay} \\ &= 2\zeta_a \frac{e^{-kT_S}}{k} (\rho g B_S - m_{AD,y}\omega^2) \sin(k\frac{L_S}{2}) \cos(\omega t) \end{aligned} \tag{2.12}$$

Pitch Moment

Considering an element of hull dx and including the moment arm x in Eqs.(2.10) and (2.11), the pitch moment about the gravity centre of the barge is written as follows

$$M_{T\psi} = \int_{-L_S/2}^{L_S/2} x dF_{Py} + \int_{-L_S/2}^{L_S/2} x dF_{Ay} \tag{2.13}$$

After the integration of Eq.(2.13), the pitch moment can be written as follows

$$M_{T\psi} = \zeta_a \frac{e^{-kT_S}}{k} (\rho g B_S - m_{AD,y}\omega^2) [\frac{2}{k} \sin(k\frac{L_S}{2}) - L_S \cos(k\frac{L_S}{2})] \sin(\omega t) \tag{2.14}$$

When the waves approach the barge with a heading angle, the wave exciting forces can be calculated by using the velocity potential which takes into account the arbitrary wave heading angle. The derivation of surge and sway forces for an arbitrary wave approaching angle are presented in Appendix B.

2.2.4 COMPARISON OF FROUDE-KRYLOV APPROXIMATION WITH DIFFRACTION THEORY AND WITH MEASUREMENTS

In this section, the Froude-Krylov approximation is compared with the experimental results reported by van Oortmerssen(1976). In his thesis, van Oortmerssen, applied the three dimensional source distribution technique (3D) to calculate wave forces on a Very Large Crude Carrier (200 000 dwt) and compared the numerical predictions with extensive model test results. Since these experiments were carried out in shallow water the formulae given in Eqs.(2.6)-(2.14) were modified to include the shallow water effects. Then the Froude-Krylov forces on the barge which has the same displacement as the tanker were calculated. The results are plotted in Figs.2.5-2.10. Both the 3D theory and Froude-Krylov approximation correlate well with the experimental measurements. Figs.2.6 and 2.7 show surge and sway forces calculated in 45 degrees heading angle. The advantage of the Froude-Krylov approximation is that the computing time spent on force calculation is very small. This is even more important in time domain calculations for the simulation of non-linear behaviour of the tanker in waves. On the other hand,

Froude-Krylov approximation over estimates the wave forces at higher frequencies.

Constant added mass and damping values at infinite frequency are employed in this thesis on the assumption that the added mass and damping do not vary much over the range of frequencies considered in this study.

The effect of different bow and stern shapes of the rectangular barge on the Froude-Krylov forces is examined by considering three configurations (see Fig.2.11). Fig.2.12 shows that the surge exciting forces do not change when the bow and stern shapes differ.

There are some other analytical methods available for calculating the wave forces on large tankers. One such method is the elliptical cylinder approximation (see Muga and Fong (1976)). Yılmaz (1990) adopted this method to calculate the wave forces on the tanker geometry given by van Oortmerssen (1976). The results presented in Figs.2.13-2.16 show that the elliptical cylinder approximation is also an alternative method in calculating the wave forces on tankers.

2.3 SECOND-ORDER WAVE FORCES

2.3.1 INTRODUCTION

In this section, the effects of second-order wave forces on the coupled systems are discussed. In particular, attention is paid to the prediction of forces acting on a surface piercing vertical circular cylinder and on a rectangular box shaped barge.

If we assume that the water is homogeneous, inviscid, incompressible and irrotational, the wave forces acting on a floating structure can be deduced from the following equation:

$$\vec{F} = -\int_{S_B} p\vec{n}ds \tag{2.15}$$

where S_B is the wetted surface; $\vec{n}$ is the normal vector; p is the dynamic pressure at a point on the structure's surface. The pressure p can be obtained using the Bernoulli equation as follows

$$p = -\rho\left(\frac{\partial\phi}{\partial t} + \frac{1}{2}\left|\nabla\phi\right|^2 + gy\right) \tag{2.16}$$

The pressure itself is nonlinear and it is usual to expand the wave forces in a form of perturbation series

$$\vec{F} = \vec{F}^{(0)} + \varepsilon\vec{F}^{(1)} + \varepsilon^2\vec{F}^{(2)} + \ldots \tag{2.17}$$

where $\vec{F}^{(0)}$ is the zeroth order (buoyancy) forces; $\vec{F}^{(1)}$ the first order (linear) forces; $\vec{F}^{(2)}$ the second order forces, etc.

This expansion indicates that the zeroth order forces are much larger than the first order forces, and the latter are much larger than the second order forces, and so on. As an example, for a tanker with a displacement of 200000 dwt the surge force is typically 1900 tons and the second order force is 25 tons(or less).

The first order forces are important because they are oscillatory so they give rise to oscillatory motions(see Section 2.2) whereas the buoyancy forces are constant. The steady part of the second order forces is much smaller than the hydrostatic forces and their oscillatory part much smaller than the first order forces. However, three modes of motions, namely surge, sway and yaw induce no buoyancy forces at all. Since there are no other steady forces associated with these motions, the steady part of the second order wave forces becomes important. In addition, the frequency range of the first order forces is restricted between 0.2 and 2.0 rad/s. This is not the case for the second order forces which have a nonlinear character so they are contained in every frequency well above or below the range of the linear forces. The high frequency ship longitudinal vibration modes may be excited by the high frequency components of those second order forces.

This phenomenon is important from the point of view of structural design. On the other hand the second order forces are very important since they may induce slowly varying surge, sway and yaw motion oscillations for low frequencies, typically below 0.2 rad/s.

The evaluation of the second order forces on the floating structures follows two approaches, namely the "far field" approach and the "near field" approach. In the far field approach, the hydrodynamic properties of the body are evaluated on a control surface far away from the body (see Maruo(1960) and Newman(1967)). In the near field approach, introduced by Pinkster(1979), the hydrodynamic properties are evaluated on the surface of the body. The advantage of the latter approach is that the components of the second order forces can be examined separately.

The second order force components arising from potential flow considerations on a floating object can be summarized as follows (see Pinkster, 1979) :

I.Drift force due to the relative wave elevation.

$$-\tfrac{1}{2}\rho g \int_{WL} \zeta_r^2 \vec{n}_L dl$$

II.Pressure drop due to velocity squared term in Bernoulli's equation.

$$\iint_{S_O} -\tfrac{1}{2}\rho \left|\nabla\phi^{(1)}\right|^2 \vec{n}_S dS$$

II.Pressure due to product of gradient of first order pressure and first order motion.

$$-\int_{S_O} -\rho\left(\vec{X}^{(1)} \frac{\partial\left(\nabla\phi^{(1)}\right)}{\partial t}\right) dS$$

IV.Drift force due to products of first order angular motions and inertia forces.

$$\alpha^{(1)} M \frac{\partial^2 \vec{X}^{(1)}}{\partial t^2}$$

V. Drift force due to second-order potentials ,

$$\int_{S_O} \rho \frac{\partial \phi^{(2)}}{\partial t} \vec{n}_S dS$$

In the above expressions, ρ is the water density; g, the gravitational acceleration; WL, the mean water line; ζ_r, the relative wave elevation; n_L, unit normal vector to WL; S_O the mean underwater surface of the structure; $\phi^{(1)}$ first order velocity potential; n_S unit normal vector to S_O; $X^{(1)}$ first order translational motion; $\vec{\alpha}^{(1)}$ first-order angular motion; M the mass of the structure and $\phi^{(2)}$ second-order velocity potential.

Derivations of these drift force components are given in detail in Pinkster(1979). Fig.(2.17) taken from the same reference shows a comparison between the magnitudes of the drift force components for a rectangular barge.

In the following section, the second order steady forces on vertical cylinders are considered. The second order forces acting on fixed and oscillatory vertical cylinders are compared with each other. Some approximate formulations for calculating the steady drift forces are also presented. In the Section 2.3.3, second order steady forces on box-shaped rectangular barges floating in regular waves are examined. Various approximate formulae which calculate the steady forces in regular seas are presented. These formulae were derived to predict the added resistance of ships in waves and reported in several publications. In the Section 2.3.4, the second order wave forces in irregular waves are introduced. The approximate formulae given by Pinkster and Bowers are discussed in the same section. Some parametric studies are performed to show the effect of sea spectrum parameters as well as the structure dependent coefficients. The results of these parametric

studies are also presented.

2.3.2 SECOND ORDER WAVE FORCES ON VERTICAL SURFACE PIERCING CYLINDERS

The second order wave forces on articulated columns in regular waves cause a steady pitch due to a mean drift force. This mean force can be derived analytically for fixed or oscillating vertical cylinders. Drake et al (1984) examined the effect of placing progressively more slender articulated columns in deeper waters. That study showed that drift forces increase as the depth of water increases. Drake et al also concluded that in deep waters the steady drift forces on an articulated column tend to be equal to the drift force on a fixed cylinder (see, Fig.2.18). Therefore, in predicting the second-order wave forces, the articulated tower can be modelled as a fixed vertical cylinder for deep water applications. There are a number of studies dealing with the calculation of the second order forces on fixed vertical cylinders:

Havelock (1940) derived a closed form of expression for the steady second order force on a large vertical cylinder in deep waters. His theory was later extended by MacCamy and Fuchs (1954) for finite water depths. Chakrabarti (1984a) obtained a complete expression for the second order steady force on a fixed vertical cylinder by making use of MacCamy and Fuchs' theory. This is given in the following:

The potential drift force has two components-the wave elevator term and the velocity head term. The total of these two components can be written as follows

$$\bar{F}_{C,1} + \bar{F}_{C,2} = 2\rho g \zeta_a^2 D \frac{1}{\pi^2 (ka)^3} \sum_{n=0}^{\infty} \left[1 - \frac{n(n+1)}{(ka)^2} \right]^2 \frac{1}{A_n A_{n+1}} \qquad (2.18)$$

where D is the diameter of the circular cylinder (a=D/2); $A_n(ka) = J'^2_n(ka) + Y'^2_n(ka)$ and J'_n, Y'_n are the derivation of Bessel functions of the first and second kind, respectively.

This force can be normalized with respect to $\frac{1}{2}\rho g\zeta_a^2 D$. This nondimensional steady drift force approaches a constant value of 0.666 in deep water for high values of ka. The potential component of the drift forces on the vertical cylinder is shown in Fig.2.19.

This formulation makes use of the second order diffraction-radiation theory. However, the drift forces due to the viscous drag, the second component of the Morison equation, may also be important, especially for more slender bodies. The regions of importance of the viscous and potential drift forces were discussed by Standing et al (1981). They showed that the drag and diffraction regions for a fixed vertical column can be separated using the following equation

$$\frac{H}{D} = 60\left(\frac{D}{\lambda}\right)^2 \tag{2.19}$$

The curve obtained using Eq.(2.19) is plotted in Fig.2.20 and separates the drag and diffraction regions.

In order to calculate the viscous drift forces acting on the vertical cylinder use of the Morison equation is made. In the absence of current, the drag forces on the fixed column have a steady component. In deep waters, this component is given by

$$\bar{F}_D = \frac{4\pi}{3} C_D \rho g \zeta_a^3 (ka) \tag{2.20}$$

where C_D is the drag coefficient; D, the diameter of the cylinder; a, the radius of the cylinder; ζ_a, the wave amplitude, and k is the wave number. The above expression is derived by Standing et al (1981) and Chakrabarti (1984a).

The viscous components of the drift forces are compared with the potential drift forces in Fig.2.19. The wave height over diameter ratio, H/D is taken as 0.125. The C_D

coefficient is considered to be equal to 1. As can be seen in Fig.2.19, the magnitude due to the viscous forces is quite small compared to the potential force. The viscous forces show a linearly increasing trend for the ka values considered in the study. Fig.2.21 shows the variation of drift forces for different H/D ratios. In calculating the results presented in Fig.2.21, H and D values were selected as follows

1. D=6m, H=2m,
2. D=6m, H=8m,
3. D=12.7m, H=2m,
4. D=12.7m, H=8m.

As Fig.2.21 indicates, the second order forces are drag dominated up to 0.85 rad/s while for higher frequency values the potential drift force dominates. The viscous effect becomes more predominant for large wave heights (H=8m) since the viscous drift forces increase with the cube of the wave amplitude. Increasing the column diameter gives larger potential drift forces. For H=8m the viscous drift forces are 9% of the potential drift forces at 1 rad/s wave frequency.

2.3.3 SECOND ORDER WAVE FORCES ON RECTANGULAR BOX-SHAPED BARGES

There are several analytical and experimental investigations reported in the literature regarding the calculation of drift forces on floating structures. Chakrabarti (1980) reviews the various analytical and experimental studies carried out on the drift forces acting on ship-shaped structures. He showed that the drift force coefficients are quite sensitive to the shape of the structures as well as the techniques and assumptions used in the calculation procedures.

Remery and Hermans (1971) tested a rectangular barge moored in a head sea with linear springs. The mean drift forces were measured and the drift force coefficient, $R(\omega)$, was calculated. A similar type of experiment is carried out in this study and presented in Chapter 7.

The estimation of the second order forces due to the wave potential can be performed by applying numerical hydrodynamic techniques. These techniques were presented by Pinkster and van Oortmerssen(1977), Molin(1979), Clauss et al (1980) and Standing et al (1981). For bluff bodies such as tankers and barges, the contribution due to relative wave height provides the major component as shown in Fig.2.17.

The steady drift forces on the ship can be calculated by referring to the formulae published in the literature for predicting added resistance in waves. These formulae are applied on the assumption that the advance speed on the body is zero. In the following, some formulae to calculate the steady drift forces on ships are given. These formulations are then modified to calculate the drift forces on a rectangular box shaped barge which has the same displacement as the ship.

Fujii and Takahashi(1975)'s formula, which was derived from Havelock(1940)'s calculation method of the drifting force on a fixed obstacle, is given in the following form

$$\bar{F}_B = \alpha_1(1+\alpha_2)\frac{1}{2}\rho g\zeta_a^2 B_S \overline{\sin^2\beta} \tag{2.21}$$

where $\alpha_1 = \pi^2 I_1^2 / \left(\pi^2 I_1^2 + K_1^2\right)$ is the correction factor for finite draft; α_2, the correction factor for advance speed (α_2 = 0 for barge); $I_1 = I_1(kT_S)$, $K_1 = K_1(kT_S)$, modified Bessel functions of the first and second kind, respectively; T_S, ship draught; β, slope of the tangent of the water plane curve with respect to the longitudinal centerline of the ship and β=90° for rectangular box shaped barge.

Kwon (1982) proposed a new formula for the increase in resistance in waves as follows

$$\bar{F}_B = C_V C_S C_T \frac{1}{2}\rho g\zeta_a^2 \int_{S_R} \left(\frac{dy}{ds}\right)^3 ds \tag{2.22}$$

where C_V is the correction factor for advance speed (Cv = 1 for barge); C_S, the scattering

coefficient (C_S = 1 for rectangular barge); C_T =1-exp(-2kT_S), the correction factor for finite draft, and S_R, the reflection region of the body surface.

The integration term in the above equation can be reduced to the following form

$$\int_{-B_S/2}^{B_S/2} \sin^2 \beta dy \tag{2.23}$$

This integration gives the value of B_S in the case of a rectangular barge. Kwon's formula gives good approximation to the drift forces on bluff bodies in the shorter wave length range, $\lambda/L_S < 1$.

The drifting coefficients for a rectangular box shaped barge can be calculated analytically by dividing these forces by $\frac{1}{2}\rho g \zeta_a^2 B_S$. These coefficients as obtained from different approaches are compared with each other in Fig.2.22.

2.3.4 STEADY AND LOW FREQUENCY SECOND ORDER WAVE FORCES IN IRREGULAR WAVES

As was discussed in Section 2.3.1, the drift forces acting on a floating structure in regular waves are proportional to the square of the wave amplitude. In the presence of irregular waves, the wave elevation at a point can be considered as the sum of a large number of regular waves:

$$\zeta(t) = \sum_{i=1}^{N} \zeta_i \cos(\omega_i t + \varepsilon_i) \tag{2.24}$$

The square of the wave elevation is given by

$$\zeta^2(t) = \sum_{i=1}^{N} \sum_{j=1}^{N} \zeta_i \zeta_j \cos(\omega_i t + \varepsilon_i) \cos(\omega_j t + \varepsilon_j) \tag{2.25}$$

The low frequency second order wave forces can be obtained by introducing the low frequency part of the wave elevation square,

$$\zeta^2(t) = \sum_{i=1}^{N} \sum_{j=1}^{N} \frac{1}{2}\zeta_i \zeta_j \cos\{(\omega_i - \omega_j)t + (\varepsilon_i - \varepsilon_j)\} \tag{2.26}$$

into the steady force equation, $F^{(2)}(t) = \frac{1}{2}\rho g B_S \zeta_a^2 R^2(\omega)$, as follows

$$F^{(2)}(t) = \sum_{i=1}^{N} \sum_{j=1}^{N} \zeta_i \zeta_j P_{ij} \cos\{(\omega_i - \omega_j)t + (\varepsilon_i - \varepsilon_j)\}$$
$$+ \sum_{i=1}^{N} \sum_{j=1}^{N} \zeta_i \zeta_j Q_{ij} \sin\{(\omega_i - \omega_j)t + (\varepsilon_i - \varepsilon_j)\} \tag{2.27}$$

where P_{ij} and Q_{ij} are the in-phase and out-phase parts of the second order transfer function, respectively.

The expressions given above were derived by Pinster (1979). $F^{(2)}(t)$ is a second order force which varies slowly with a frequency which is composed of a difference of the frequencies present in an irregular wave train. This force will cause large oscillation when it applies to a linearly moored system. The reason for this is that the frequency difference $(\omega_i - \omega_j)$ in irregular waves is likely to coincide with the natural frequency of the compliant system which has low damping characteristics in the surge, sway and yaw motions.

Making use of the sea spectrum $S_\zeta(\omega)$ the steady drift force in irregular seas can be written as follows

$$F^{(2)}_{STEADY} = 2\int_0^\infty S_\zeta(\omega)\left[\frac{F^{(2)}}{\zeta_a^2}\right]d\omega \tag{2.28}$$

The spectrum of the low frequency forces can be determined by

$$S_F(\mu) = 8 \int_0^\infty S_\zeta(\omega)\, S_\zeta(\omega + \mu) \left[\frac{F^{(2)}}{\zeta_a^2}(\omega, \omega + \mu) \right]^2 d\omega \tag{2.29}$$

Pinkster proposed an approximate method in his earlier paper (see Pinkster(1974)) to calculate the mean and slowly varying second order forces in irregular waves by using the coefficients obtained from mean drift forces in regular waves. This method is commonly adopted for practical purposes (see, Arai et al (1977), Langley and Kirk(1980)) since it is easy to compute or measure the steady drift forces in regular waves.

In the case of bluff bodies such as tankers and barges the steady drift forces in irregular seas can be calculated as follows

$$F^{(2)}_{STEADY} = \rho g B_S \int_0^\infty S_\zeta(\omega) R^2(\omega) d\omega \tag{2.30}$$

where $S_\zeta(\omega)$ is the wave amplitude spectrum; $R(\omega)$, drift force coefficient (see Fig.2.22).

The spectrum of slowly varying wave drifting force can be given in the following form (see, Pinkster(1974))

$$S_F(\mu) = 2(\rho g B_S)^2 \int_0^\infty S_\zeta(\omega) S_\zeta(\omega + \mu) R^4(\omega + \mu/2) d\omega \tag{2.31}$$

Pinkster's method does not take into account the second order horizontal pressure gradient. As was discussed by Standing et al (1981) Pinkster's method is valid when wave diffraction effects are dominant and gradient effects are small.

The other approximate method emerges from the theoretical work of Bowers (1976) and is given by

$$S_{SF}(\mu) = 2(\rho g B_S)^2 (1 - T_S / d)^2 \int_0^\infty S_\zeta(\omega) S_\zeta(\omega + \mu) \sin^2 \alpha d\omega \qquad (2.32)$$

with $\alpha = L_S / 2g[(\omega + \mu)^2 - \omega^2]$ for deep water applications.

It should be noted that the latter method is developed for ship shaped structures. The second order force spectra calculated by the two methods are shown in Fig.2.23. As can be seen from these figures, there is a large discrepancy between the methods for a high sea state, corresponding to a wind velocity of 26 m/s (H_S=14.4m), whereas in a lower sea state when wind velocity is 18 m/s (H_S=6.9m) the two methods yield closer predictions to the second order force spectra. The difference may be attributed to the term which takes into account the water depth in the expression given by Bowers.

In order to explore the effects of several parameters on the second order force spectra the following studies are performed: Firstly two parameters JONSWAP wave spectrum are considered (see Chakrabarti(1984b)). The gamma factor of the spectrum is altered from 1.0 to 7.0. In addition, five zero crossing periods are taken into account. Secondly, different drift force coefficients for a rectangular box shaped barge (see, Fig.2.22) are considered.

The wave amplitude spectrum of sea waves is shown in Figs.2.24 and 2.25 while the second order wave spectra are shown in Figs.2.26 and 2.27. The effect of the increasing gamma factor (i.e. increasing peakness of the spectrum) on the second order wave spectrum is quite significant in the low frequency range ($\omega < 0.15$ rad/s). On the other hand the trend of the spectra does not differ much throughout the.remaining frequency range (see, Fig.2.26). As can be seen from Fig.2.25, increasing zero the crossing period creates narrow band spectra with sharp peaks. Fig.2.27 shows that the higher zero crossing periods yield smaller area under the second-order wave spectra. The shape of the spectrum with Tz=11.5 s becomes very similar to the white noise spectrum. The second order wave force spectra (SOWFS) for the barge which has 47m beam and 14m draught are given for three sea states in Figs.2.28, 2.29 and 2.30. Employment of

the different drift coefficients in force calculations causes dramatic changes in force spectra as shown in Fig.2.28. This trend is the same for the other sea states. The gamma factor of 3.3 and the zero crossing period of 11.5s give the lowest magnitudes among the sea states considered here. As the gamma factor decreases to a magnitude of 1.0, the SOWF spectrum values are almost doubled. The largest SOWFS in magnitude is observed for a less severe sea state of Tz=9.5s and γ=3.3.

Making use of the drift coefficients obtained for regular seas (see, Fig.2.19), the spectrum of low frequency order forces on vertical cylinders can be calculated as follows

$$S_{FC}(\mu) = 2(\rho g D)^2 \int_0^\infty S_\zeta(\omega) S_\zeta(\omega+\mu) R_C^4(\omega+\mu/2)\, d\omega \qquad (2.33)$$

in which R_C denotes the drift coefficient for surface piercing cylinders and D is the diameter of the column. The diameter of the 12.7m and the representative wave height of 8.5m is used in Fig.2.31 to give an example of the SOWF spectrum calculation for vertical cylinders. Although the viscous drift force coefficient is small in magnitude, it causes a larger and broader force spectrum than the potential force coefficient (see Fig.2.32).

2.4 SHORT-CRESTED WAVES

The distribution of wave energy is not only in the frequency domain but also in the directions of wave propagation. The concept of the directional spectrum therefore arose to provide a means of describing short-crested waves. In this section various formulations for defining short-crested waves are given.

The directional wave spectrum is generally represented by the following equation

$$S(\omega, \alpha) = S(\omega) G(\omega; \alpha) \qquad (2.34)$$

where $S(\omega)$ is the wave amplitude spectrum; α , the angle of the wave propagation; ω wave frequency; $G(\omega; \alpha)$, the directional spreading function which represents the directional distribution of the total sea energy.

Our knowledge of the directional distribution of sea energy is very limited due to the lack of field measurements. However, there are a number of proposed equations which can be utilized to model short-crested waves (see Goda, 1985):

The first proposed form of directional spreading function is a cosine-squared distribution in the range of $\pm \pi / 2$ (Arthur, 1949)

$$G(\alpha) = \begin{cases} \frac{2}{\pi} \cos^2 \alpha & |\alpha| \le \frac{\pi}{2} \\ 0 & |\alpha| > \frac{\pi}{2} \end{cases} \tag{2.35}$$

Kingsman(1965) gave another formula based on data obtained from a series of streophotographs as follows

$$G(\omega, \alpha) = \frac{1}{\pi}\{1 + (0.50 + 0.82 \exp[-\frac{1}{2}(\frac{\omega}{\omega_o})^4])\cos 2\alpha$$

$$+ 0.32 \exp[-\frac{1}{2}(\frac{\omega}{\omega_o})^4]\cos 4\alpha\} \quad |\alpha| \le \frac{\pi}{2} \tag{2.36}$$

where $\omega_o = g / V_5$, and V_5 is the wind sped at 5m above the sea surface.

On the other hand, Mitsuyasu et al. (1975) proposed a formula based on field measurements with clover leaf-type instrument buoys located at two Japanese sites:

$$G(\omega, \alpha) = G_o \cos^{2s}(\frac{\alpha}{2}) \tag{2.37}$$

where G_o is the coefficient of the directional distribution so that Eq.(2.37) must satisfy the following relation

$$\int_{-\pi}^{\pi} G(\omega, \alpha)d\alpha = 1$$

The following expression is given for G_o:

$$G_o = [\int_{-\pi}^{\pi} \cos^{2s}(\frac{\alpha}{2})d\alpha]^{-1} \quad \text{or} \quad G_o = \frac{1}{\pi}2^{2s-1}\frac{\Gamma^2(s+1)}{\Gamma(2s+1)} \tag{2.38}$$

The parameter s represents the degree of directional spreading. The estimation of the value of this parameter requires careful study into the nature of waves at the design site. Mitsuyasu et al (1975) show that s takes a maximum value around the frequency of the spectral peak and that the value of s decreases as the wave frequencies become smaller or greater than the frequency of the spectral peak. They also show that the larger the value of s, the sharper is the distribution function and the more concentrated is the directional energy distribution. When s approaches infinity the waves become uni-directional. Mitsuyasu et al (1975) propose the following form for calculating values of s:

$$s = \begin{cases} s_{max}(\frac{\omega}{\omega_p})^5 & \text{when} \quad \omega \le \omega_p \\ s_{max}(\frac{\omega}{\omega_p})^{-2.5} & \text{when} \quad \omega > \omega_p \end{cases} \tag{2.39}$$

where ω_p is peak frequency. The recommendations based on the measured data in the field give the following values for the s_{max} for engineering applications (Goda,1984)

-wind waves, $s_{max} = 10$
-swell with short decay distance, $s_{max} = 25$
-swell with long decay distance, $s_{max} = 75$

In Fig.2.33 , the aforementioned three directional spreading functions are shown. The same sea condition is applied to each case, namely the significant wave height, H_S=16.5m and the peak period, Tp=20.3s. Mitsuyasu type spreading function has a parameter s_{max}=10.

Fig.2.33 only compares the spreading function diagrammatically. The effect of spreading function on the motion and structural response is also dependent upon the appropriate R.A.O. function (i.e. the sensitivity of the structure motion to the directional waves) which will be shown in Chapter 3.

2.5 WIND FORCES

The coupled articulated tower and ship compliant systems are more susceptible to the dynamic effects of wind than the conventional fixed-bottom platforms. This is especially true in the low frequency range of wind spectra to which this type of system is exposed.

Considering the overall behaviour of the structures subject to wind loading we need the following information regarding

- the wind environment,
- the relation between that environment and the forces it induces on the structure, and
- the behaviour of the structure under the action of these forces.

The mean velocity field of the wind is of the boundary-layer type where the fluid motion is that of a turbulent flow. This type of flow can be characterized by a power-law expression(see Davenport, 1967):

$$\bar{V} = \bar{V}_{10}\left(\frac{y}{10}\right)^{0.16} \tag{2.40}$$

The flow past the structure can be regarded as quasi-steady and therefore, fundamental equations of aerodynamics can be used to formulate the relationship between the incident velocity fluctuations and the wind force fluctuations on the structure:

$$F_W(t) = \frac{1}{2}\rho_a C_D A_p V^2(t) \tag{2.41}$$

where ρ_a is air density (=0.0012 t/m^3); C_D, drag coefficient; A_P, projection area (m^2); V(t), wind velocity (m/s) and t indicates the time dependency of the variable.

Substituting $V(t)= \bar{V} + v(t)$, where $\bar{V}$ is the steady component of the wind velocity and v(t) is the fluctuating wind velocity, one can write the following equation:

$$F_W(t) = 0.5\, \rho_a\, C_D\, A_P [\, \bar{V}^2 + 2\, \bar{V}\, v(t) + v^2(t)] \tag{2.42}$$

By ignoring the higher order terms, the mean wind force is given by

$$F_W^M = \frac{1}{2}\rho_a C_D A_P \bar{V}^2 \tag{2.43}$$

and the dynamic wind force is given by

$$F_W^D(t) = \rho_a C_D A_P \bar{V}\, v(t). \tag{2.44}$$

The gustiness of the wind field is expressed as a fluctuation about the mean wind field at a given elevation. The fluctuations present in the wind generate an oscillation about the system's static displacement. In order to model the gustiness of the wind field, the power spectral density of the wind must be specified. The wind spectrum is necessary to represent the frequency content of the velocity fluctuations. There are several descriptions of the wind spectra. Three of the more common spectra are shown in Fig.2.34.

Harris(1970) has described the wind spectrum by

$$S_w(f) = \frac{4\kappa \tilde{f} \bar{V}_{10}^2}{f(2+\tilde{f}^2)^{5/6}} \tag{2.45}$$

where $\tilde{f} = \frac{Lf}{\bar{V}_{10}}$; f is frequency (Hz); L, length scale(= 1200m); $\bar{V}_{10}$, wind speed at a height of 10m and κ, drag coefficient (=0.005, in open country).

The Davenport spectrum is given by

$$S_w(f) = \frac{4\kappa \tilde{f}^2 \bar{V}_{10}^2}{f(1+\tilde{f}^2)^{4/3}} \tag{2.46}$$

with same meaning of the descriptive terms (see Davenport(1967)).

Kaimal has proposed a slightly different form for the spectral density. Kaimal's version represents the nondimensional frequency $\tilde{f}$ as follows

$$\tilde{f} = \frac{fy}{\bar{V}(y)}$$

and the spectral function is given by

$$S_w(f) = \frac{200\,\kappa \tilde{f}\, \bar{V}_{10}^2}{f(1+50\tilde{f})^{5/3}} \tag{2.47}$$

The power spectrum of wind forces is related to the spectrum of wind gustiness by

$$S_{WF}(f) = S_W(f)\ TF^2 \tag{2.48}$$

where wind force transfer function TF is given as follows

$$TF = \frac{F_W^D}{v(t)} \tag{2.49}$$

In addition to that expression, an aerodynamic admittance function is introduced to take into account the turbulence around the structure as follows(see, Kareem and Dalton (1982))

$$|\aleph(f)|^2 = \frac{1}{1+\left(\frac{2f\sqrt{A_p}}{3\bar{V}_{10}}\right)} \tag{2.50}$$

Due to its viscous origin, the estimation of wind loads depends on drag and lift coefficients determined as a result of model tests. Some data is available for well-known geometric shapes(see Fig.2.35, Horner(1965)). In the case of a large ship subject to winds approaching from various directions, scale model tests may be considered the only way of calculating wind forces. OCIMF (1977) undertook an investigation into the computation of wind and current loads on VLCCs (Very Large Crude Carriers) in the 150000 to 250000 dwt class. The data obtained in the form of nondimensional coefficients are used by several investigators (see, Ractliffe&Clarke(1980) and Nienhuis(1986)).

The horizontal and lateral wind drag coefficients for a loaded tanker are reproduced in Figs. 2.36 and 2.37. For values larger than 180 deg. the negative value of the force coefficient can be used.

2.6 CURRENT FORCES

The effect of current on hydrodynamic loading of offshore structures may be treated either as a complex phenomenon where the interaction of waves and currents is taken into consideration or as a relatively simple phenomenon where the interaction is neglected and the current effect is simply superimposed on the wave effects.

In this thesis the second approach is followed. In addition to that the current flow is considered as a quasi-steady flow which consists of several horizontal layers parallel to

each other. The distribution of the current profile is suggested by DnV(1974) in the following form:

$$V_C(y) = V_T(1 + \frac{y}{d})^{1/7} + V_W(1 + \frac{y}{d}) \tag{2.51}$$

where y is the vertical distance(m); d, depth of water (m); V_T, the speed due to tidal and circulation current at the free surface(=0.75 m/s); V_W, the speed due to the wind at the free surface(=0.8 m/s).

A typical current profile of 100 m water depth was shown in Fig.2.38. The variation in velocity and direction of the current is very low. Therefore, the current may be considered as a steady phenomenon.

If one knows the current velocity profile for a particular place one can calculate the current induced forces by using appropriate drag coefficients. The current load per unit length on the vertical cylinder can be written as follows:

$$dF_C^T = \frac{1}{2}\rho C_D D V_C^2 dy \tag{2.52}$$

where D is the diameter; ρ, water density(t/m^3); C_D, drag coefficient due to steady flow measurement(=1.0 for circular cylinders); V_C, current velocity(m/s^2). The integration of this force from the sea bed to the water surface is required.

In order to calculate the longitudinal current forces acting on the ship, the slender body approximation is made. This approximation assumes that the longitudinal current forces are due mainly to frictional resistance.

The following expression is used by Remery and van Oortmerssen (1973) for the determination of the longitudinal current forces for tanker shaped bodies.:

$$F_{CX}^S = C_C \frac{1}{2}\rho S V_C^2 \tag{2.53}$$

where C_C is the friction coefficient(=0.075 (log R_e - 2)$^{-2}$); S, wetted surface(m^2); R_e, Reynolds number(=V_C / υL_S) and υ, kinematic viscosity of water(m^2/s).

The lateral current forces on the ship can be calculated either by employing the cross flow principle given by Faltinsen et al (1979) or by using the experimental data obtained for ships(see, OCIMF(1977)). The former method uses the drag coefficient for cross-flow past an infinitely long cylinder with a cross-sectional area equal to the ship cross-section and its image above the free surface. The formulation is given as follows

$$F_{CY}^{S} = \frac{1}{2}\rho \int_{L_S} C_{DY}(x) T_S(x) V_C |V_C| dx \tag{2.54}$$

In the later method, the formulation given by OCIMF(1977) makes use of the drag coefficients obtained experimentally for different current heading angles. The current force calculation is made by taking into account the appropriate drag coefficient (see Fig.2.39) for a particular current heading angle as follows

$$F_{CY}^{S} = \frac{1}{2}\rho C_{DY}(\alpha) L_S T_S V_C^2 \tag{2.55}$$

where α is the current approaching angle.

In addition to the direct effect of the current as an excitation force, the presence of current modifies the wave length. The new wave length was given by Brebbia and Walker(1979) for deep waters as follows

$$\lambda' = 2\pi g \frac{1}{\left[\omega - \frac{2\pi V_C}{\lambda}\right]^2} \tag{2.56}$$

2.7 CONCLUSIONS

In Chapter 2, the modelling of the environmental loading on the coupled articulated tower and ship system were discussed. Some findings of the limited investigation on the environmental force calculation are given as follows:

Characteristic dimensions of the coupled articulated tower and ship systems were examined in order to find an appropriate method of wave force calculation. It was found that the articulated towers work in the inertia regime whereas ship shape structures work in the diffraction regime.

The application of Morison's equation to the force calculation procedure is considered adequate for articulated towers. The wave excitation forces on the ship were calculated by summing the Froude-Krylov components of the wave forces with the approximated diffraction forces.

In predicting the second-order wave forces the articulated tower can be modelled as a fixed vertical cylinder for deep water applications. The potential and viscous components of the wave drift forces for a vertical surface piercing cylinder were compared. It was shown that for higher frequency values the potential drift force dominates. The viscous effect becomes more predominant for large wave heights.

The steady drift forces on the ship can be calculated by referring to the formulae given by Kwon and Fujii&Takahashi for predicting the added resistance of ship-shaped structures in waves. Making use of this formulae, the drift coefficients for a structure can be calculated. Nondimensional drift coefficients which are obtained for regular seas can be quite useful in calculating the steady or slowly varying second order wave forces on ships.

Pinkster's formulae to calculate the second order forces in irregular waves was compared with Bowers'. The discrepancy between these methods was found to be large for high sea states.

Several parametric studies on the second order force spectra reveal that the various gamma factors in the JONSWAP spectrum and the various drift coefficients cause considerable changes in force spectra.

In addition to the different wind spectra formulations, the different spreading functions are given in this chapter. The drag coefficients for VLCCs in air and in water are adopted from the current literature and presented in this chapter.

TABLE 2.1

Deep water approximation to linear wave theory (Sarpkaya and Isaacson (1982))

Range of validity	$kd > \pi$ or $\frac{d}{\lambda} > \frac{1}{2}$
Velocity potential	$\phi = \frac{g}{\omega}\zeta_a e^{ky} \sin(kx - \omega t)$
Dispersion relation	$c^2 = \frac{\omega^2}{k^2} = \frac{g}{k}$
Wave length	$\lambda = \frac{gT^2}{2\pi}$
Surface elevation	$\zeta = \zeta_a \cos(kx - \omega t)$
Pressure	$p = \rho g \zeta_a e^{ky} \cos(kx - \omega t)$
Horizontal particle displacement	$\xi = -\zeta_a e^{ky} \sin(kx - \omega t)$
Vertical particle displacement	$\eta = \zeta_a e^{ky} \cos(kx - \omega t)$
Horizontal particle velocity	$U_x = \zeta_a \omega e^{ky} \cos(kx - \omega t)$
Vertical particle velocity	$U_y = \zeta_a \omega e^{ky} \sin(kx - \omega t)$
Horizontal particle acceleration	$\dot{U}_x = \zeta_a \omega^2 e^{ky} \sin(kx - \omega t)$
Vertical particle acceleration	$\dot{U}_y = -\zeta_a \omega^2 e^{ky} \cos(kx - \omega t)$

(The coordinate system is shown in Fig.2.4)

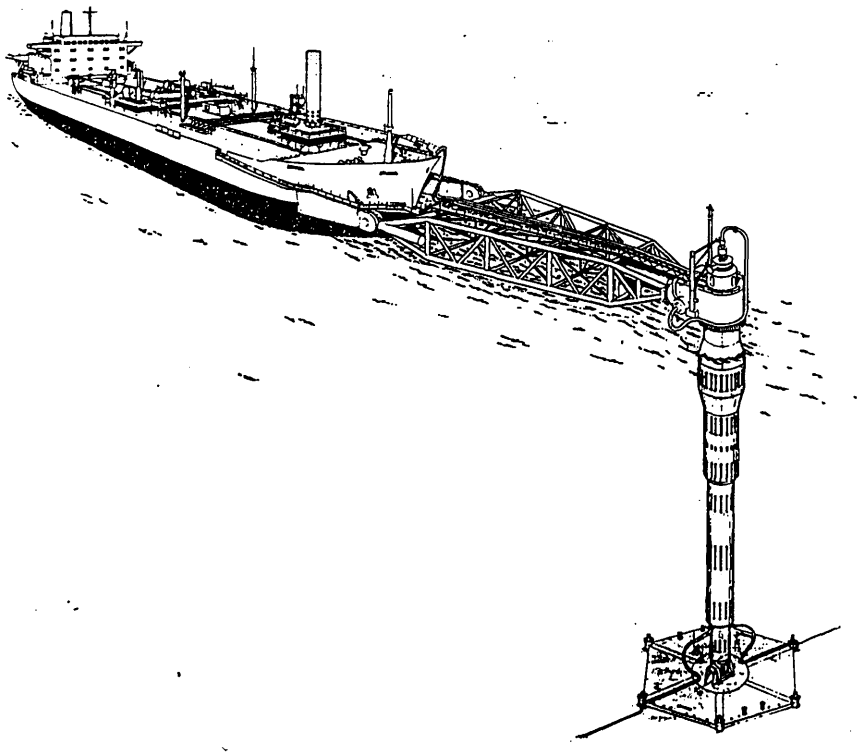

Fig.2.1 Coupled articulated tower and ship configuration

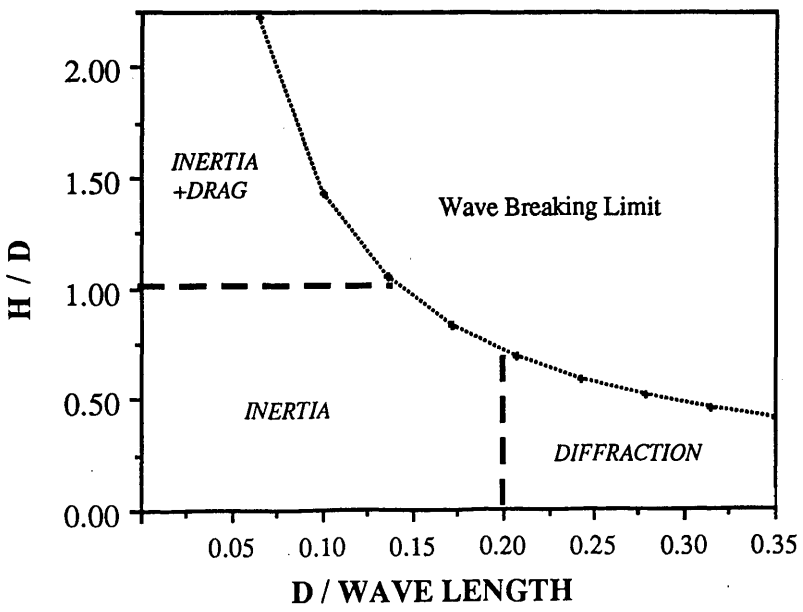

Fig.2.2 First order wave force regime for vertical cylinders

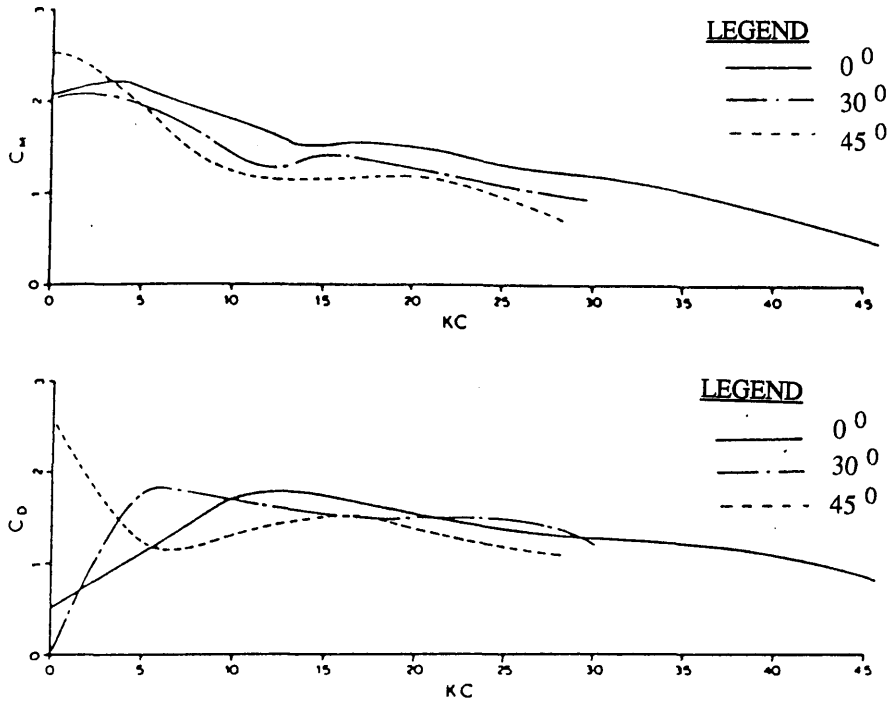

Fig.2.3 C_M and C_D values for fixed tower at 0, 30, 45 deg in waves when ($0<Re<10^5$)

(Chakrabarti and Cotter (1984))

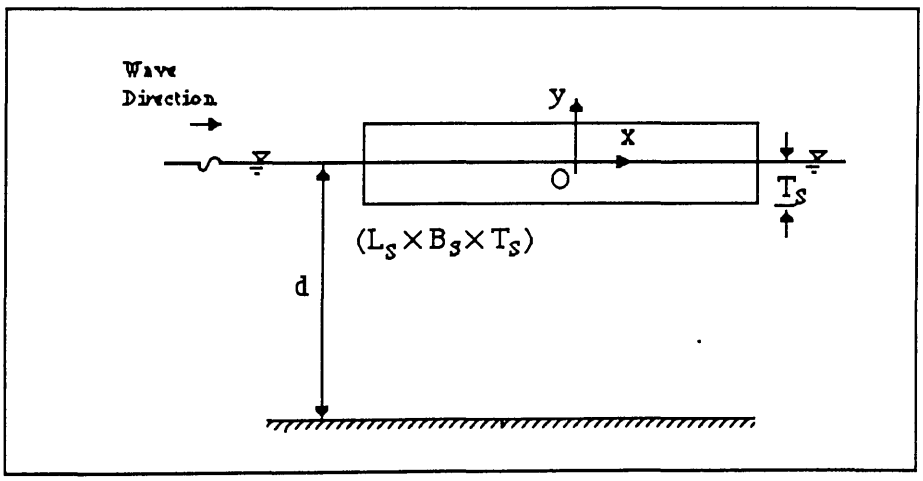

Fig.2.4 Coordinates for rectangular box-shaped barge

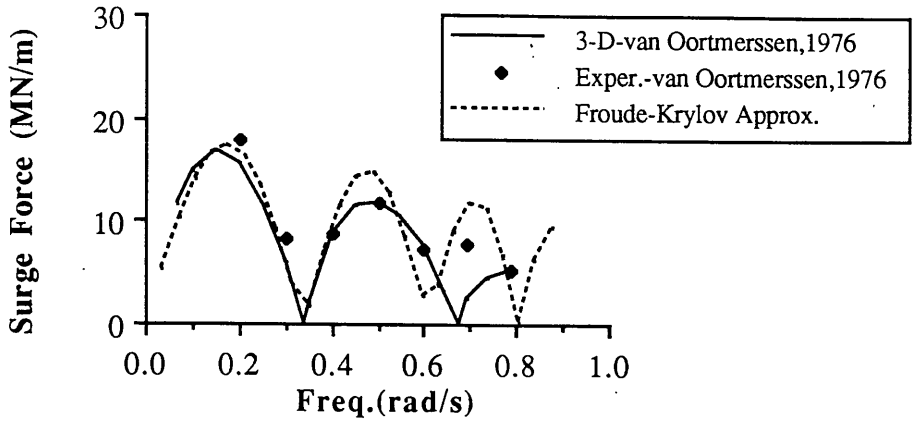

Fig.2.5 Comparison of surge exciting forces in regular waves; heading angle is 180 deg.

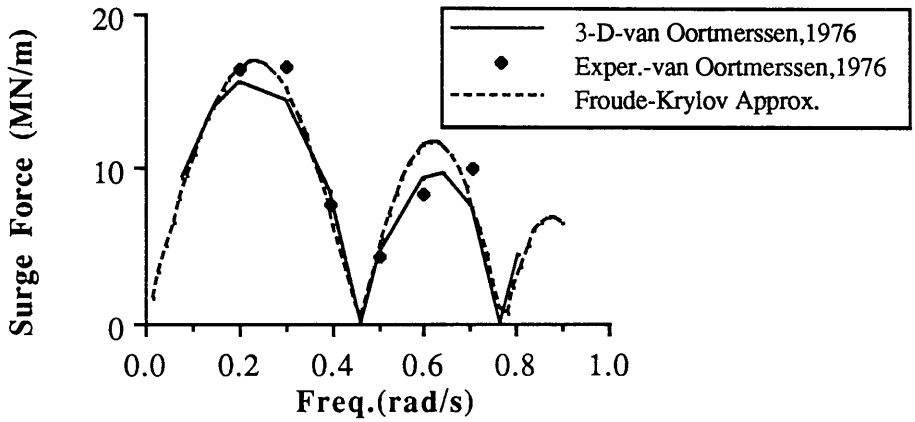

Fig.2.6 Comparison of surge exciting forces in regular waves; heading angle is 225 deg.

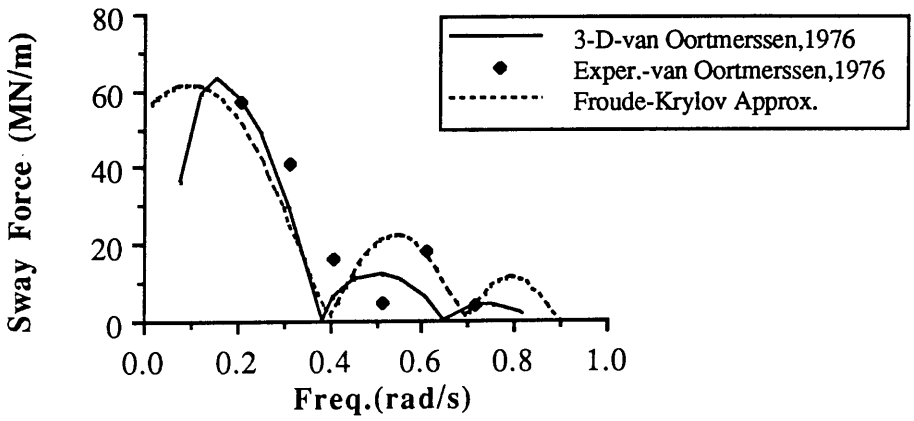

Fig.2.7 Comparison of sway exciting forces in regular waves; heading angle is 225 deg.

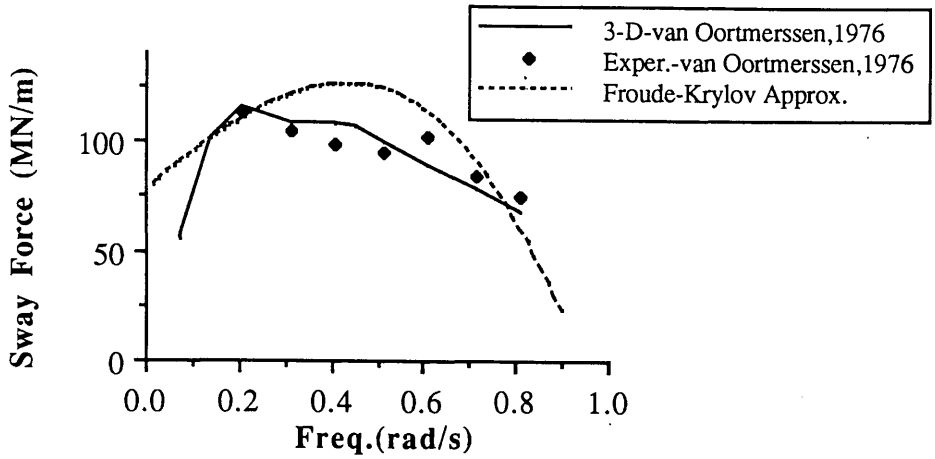

Fig.2.8 Comparison of sway exciting forces in regular waves; heading angle is 270 deg.

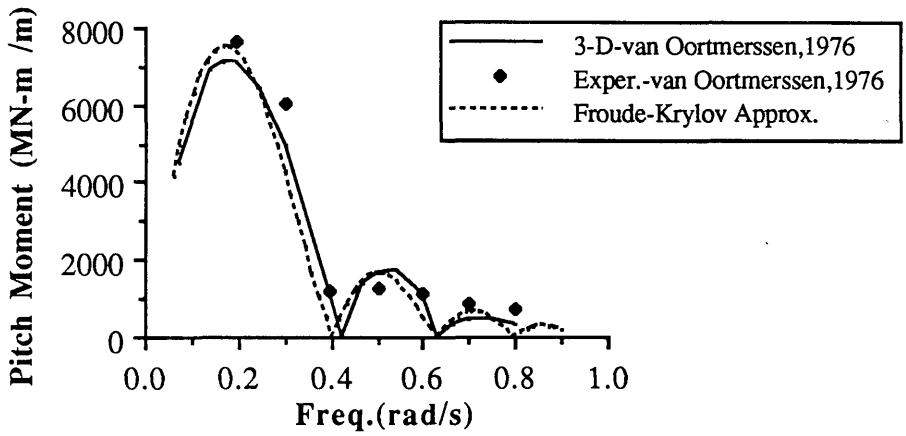

Fig.2.9 Comparison of pitch moments in regular waves; heading angle is 180 deg.

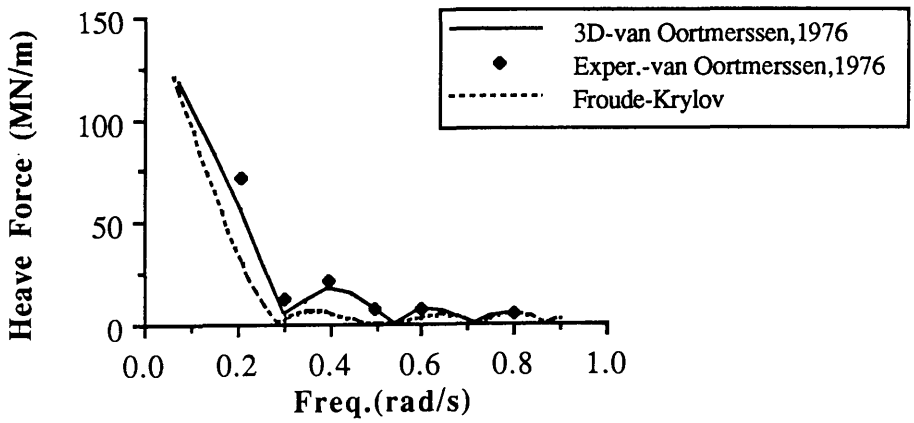

Fig.2.10 Comparison of heave exciting forces in regular waves; heading angle is 180 deg.

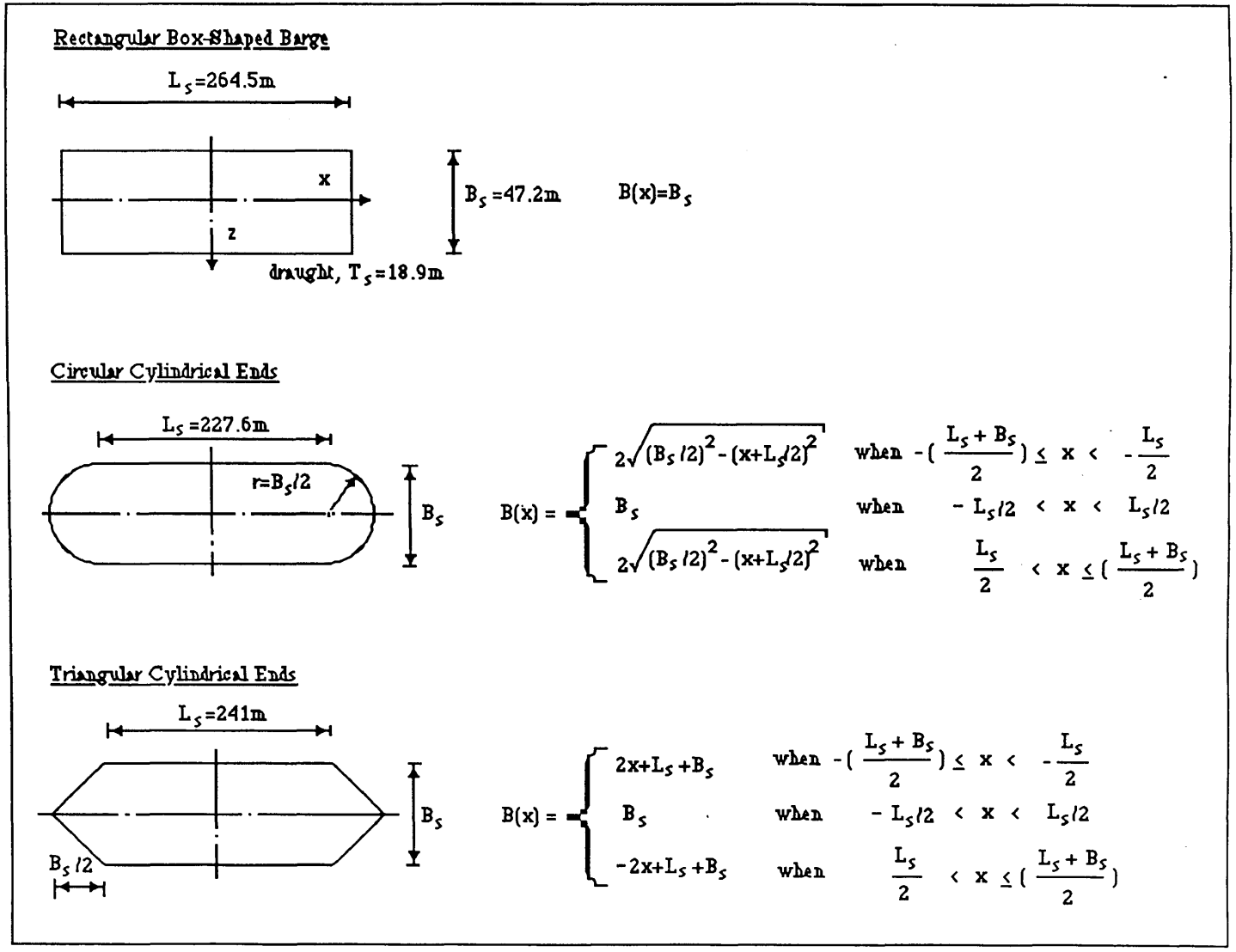

Fig.2.11 Different bow and stern shapes for rectangular barges

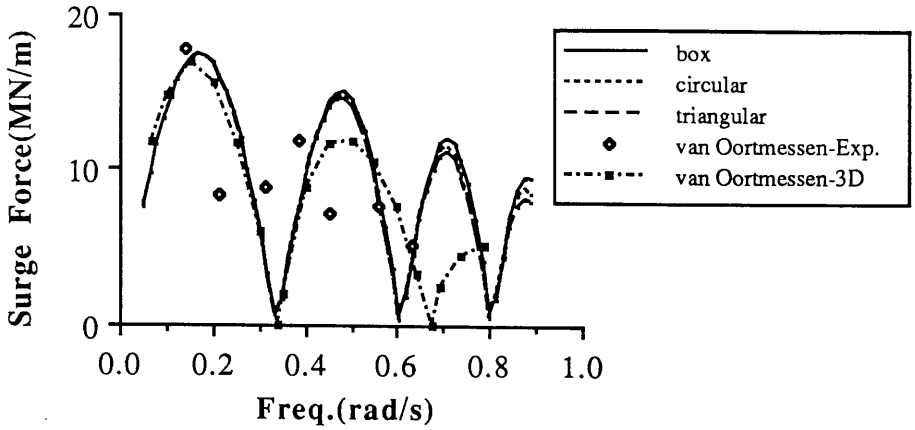

Fig.2.12 Effect of different bow and stern shapes on Froude-Krylov forces

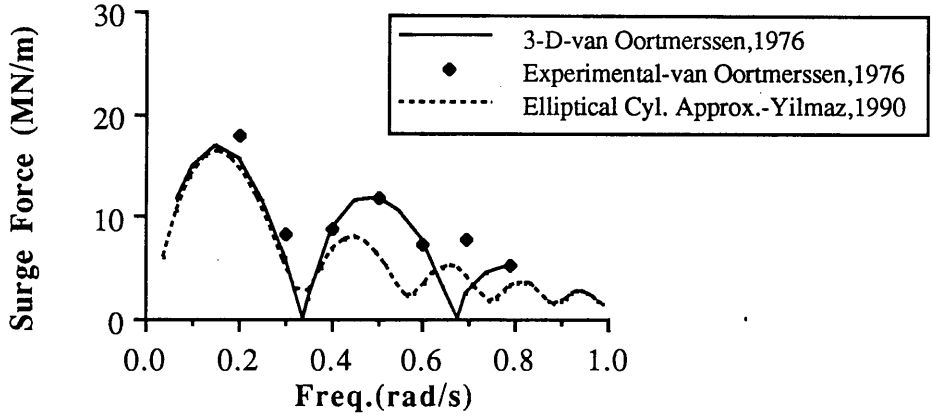

Fig.2.13 Comparison of surge exciting forces in regular waves; heading angle is 180 deg.

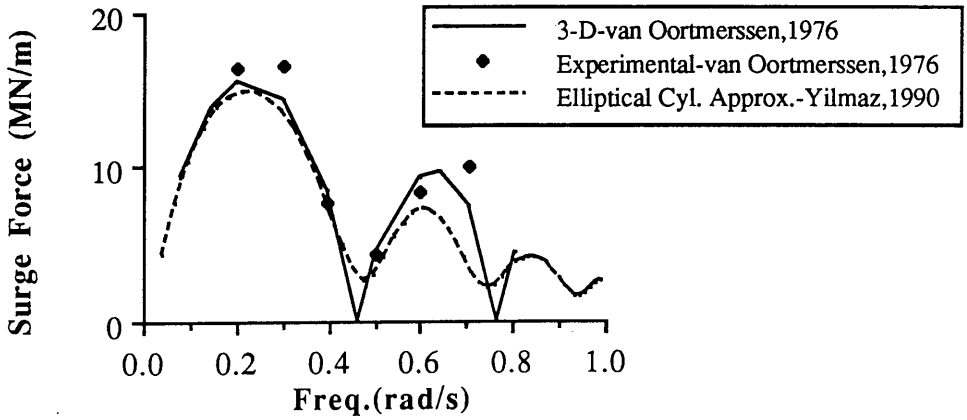

Fig.2.14 Comparison of surge exciting forces in regular waves; heading angle is 225 deg.

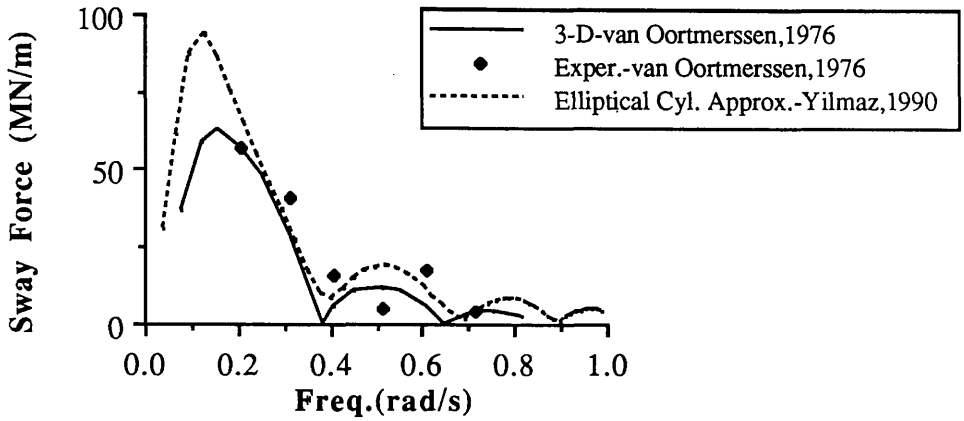

Fig.2.15 Comparison of sway exciting forces in regular waves; heading angle is 225 deg.

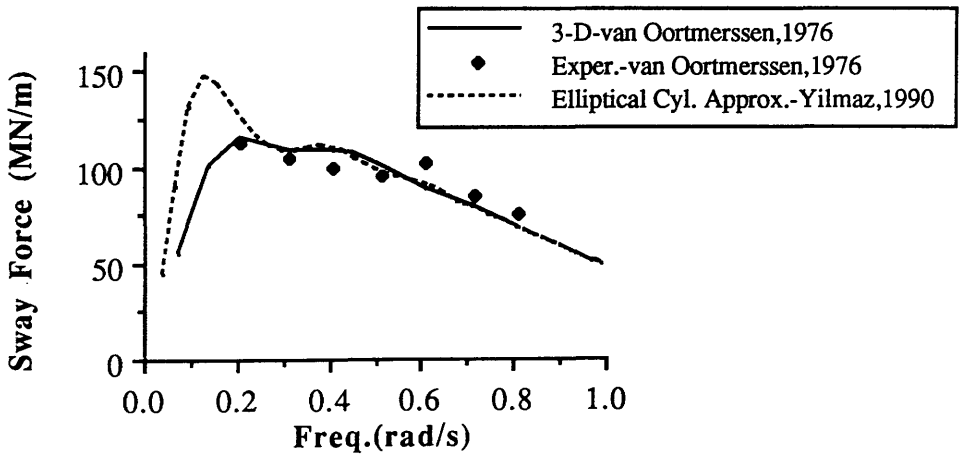

Fig.2.16 Comparison of sway exciting forces in regular waves; heading angle is 270 deg.

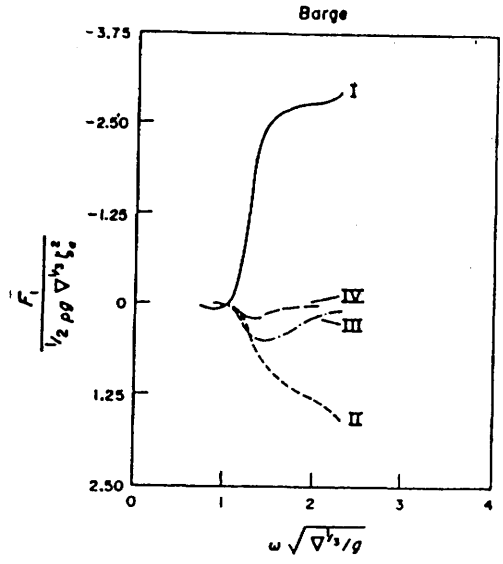

Fig.2.17 Components of computed steady drift force in surge (Pinkster(1979))

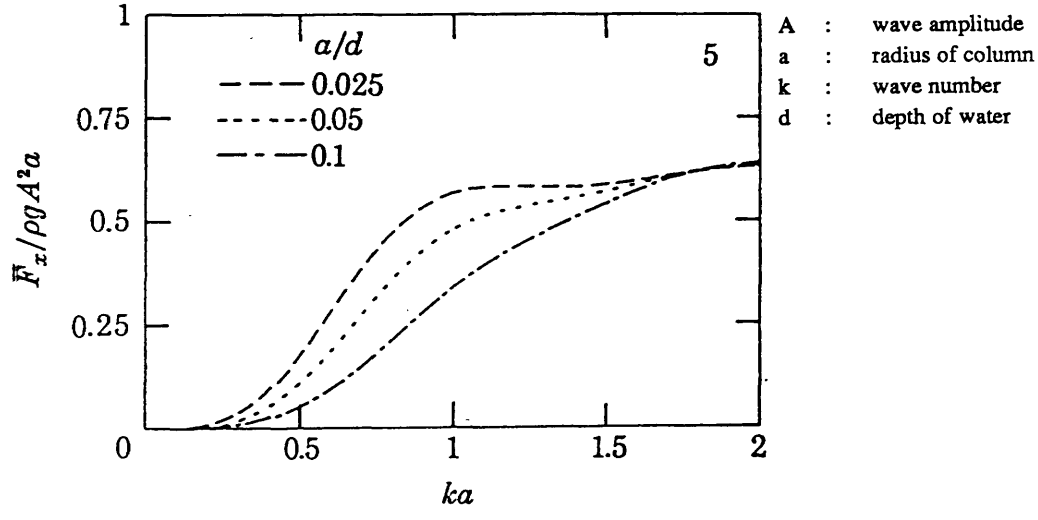

Fig.2.18 Normalized steady drift forces on an articulated column

(Drake et al (1984))

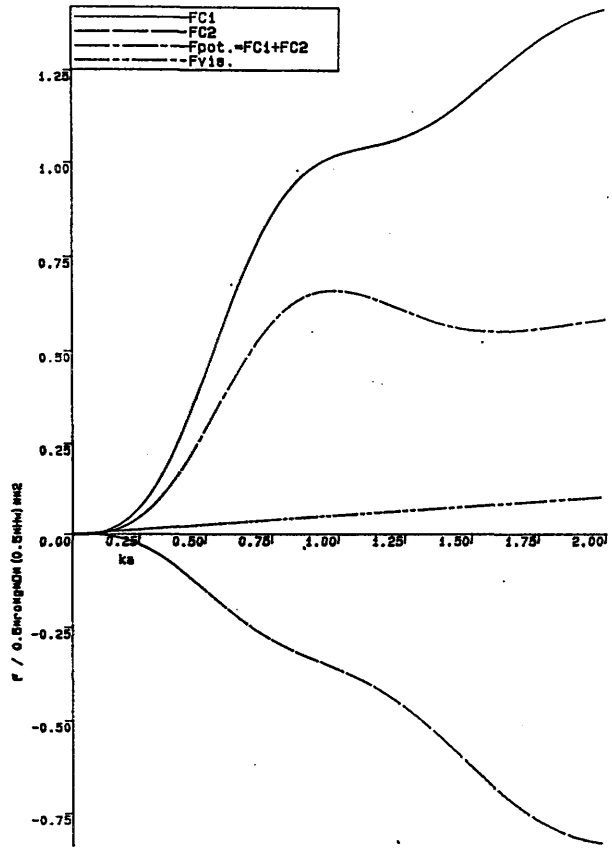

Fig.2.19 Normalized steady drift forces on vertical cylinder

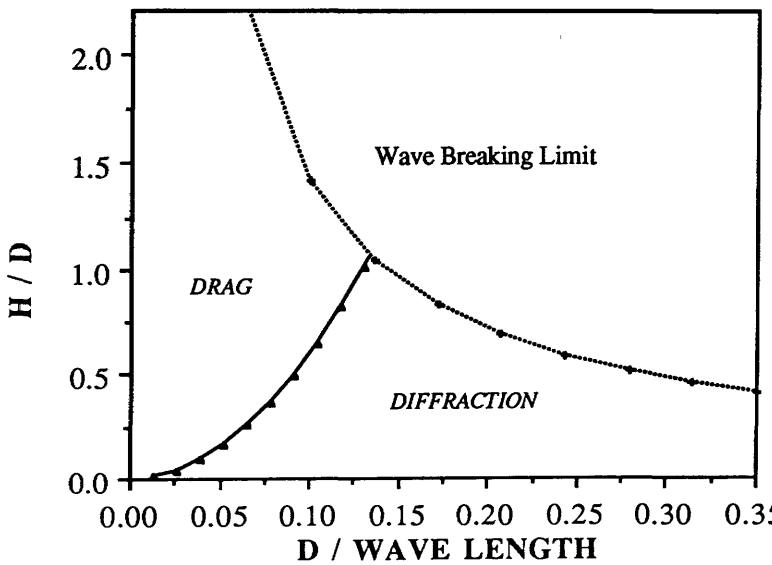

Fig.2.20 Second order force regime for vertical cylinder

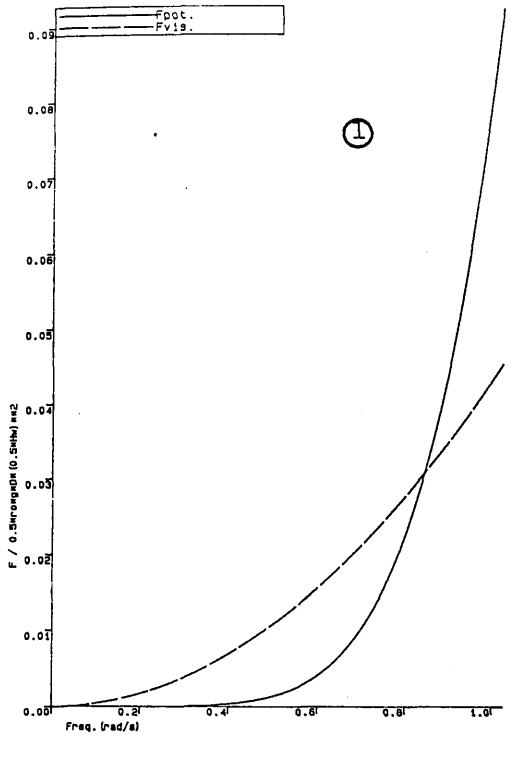

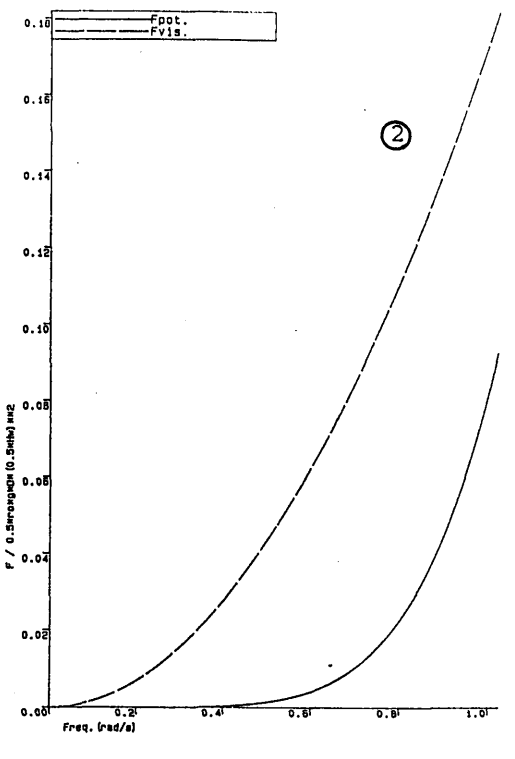

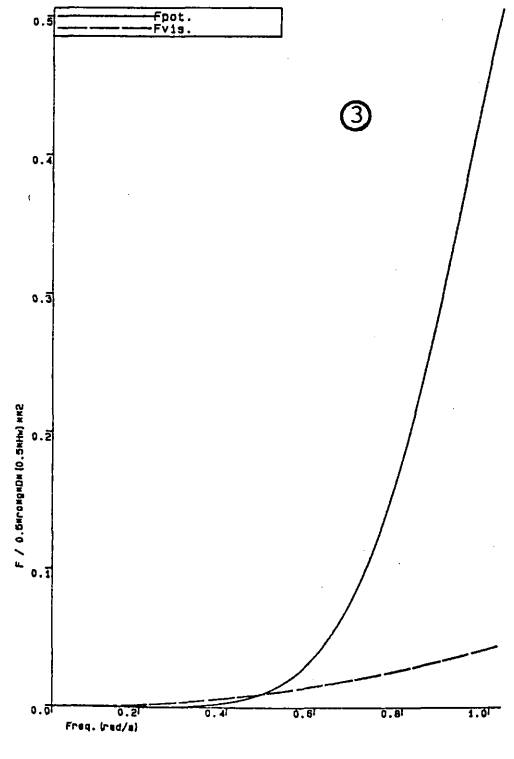

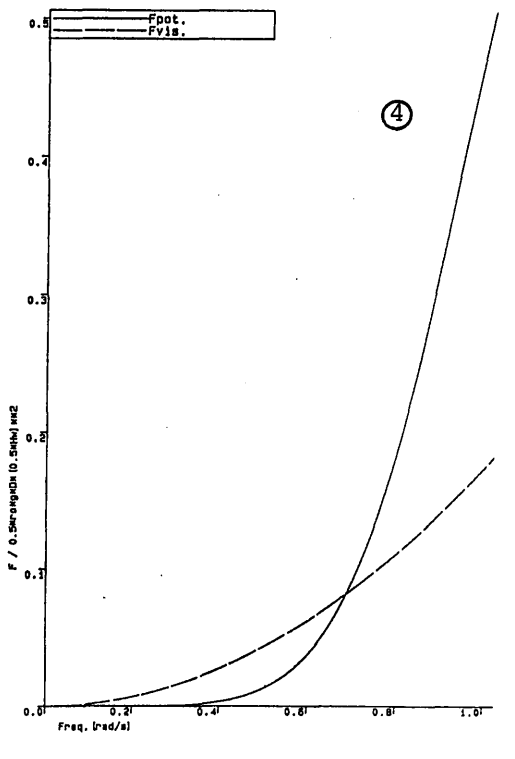

Fig.2.21 Variation of drift force coefficient on vertical cylinder for different H/D ratios

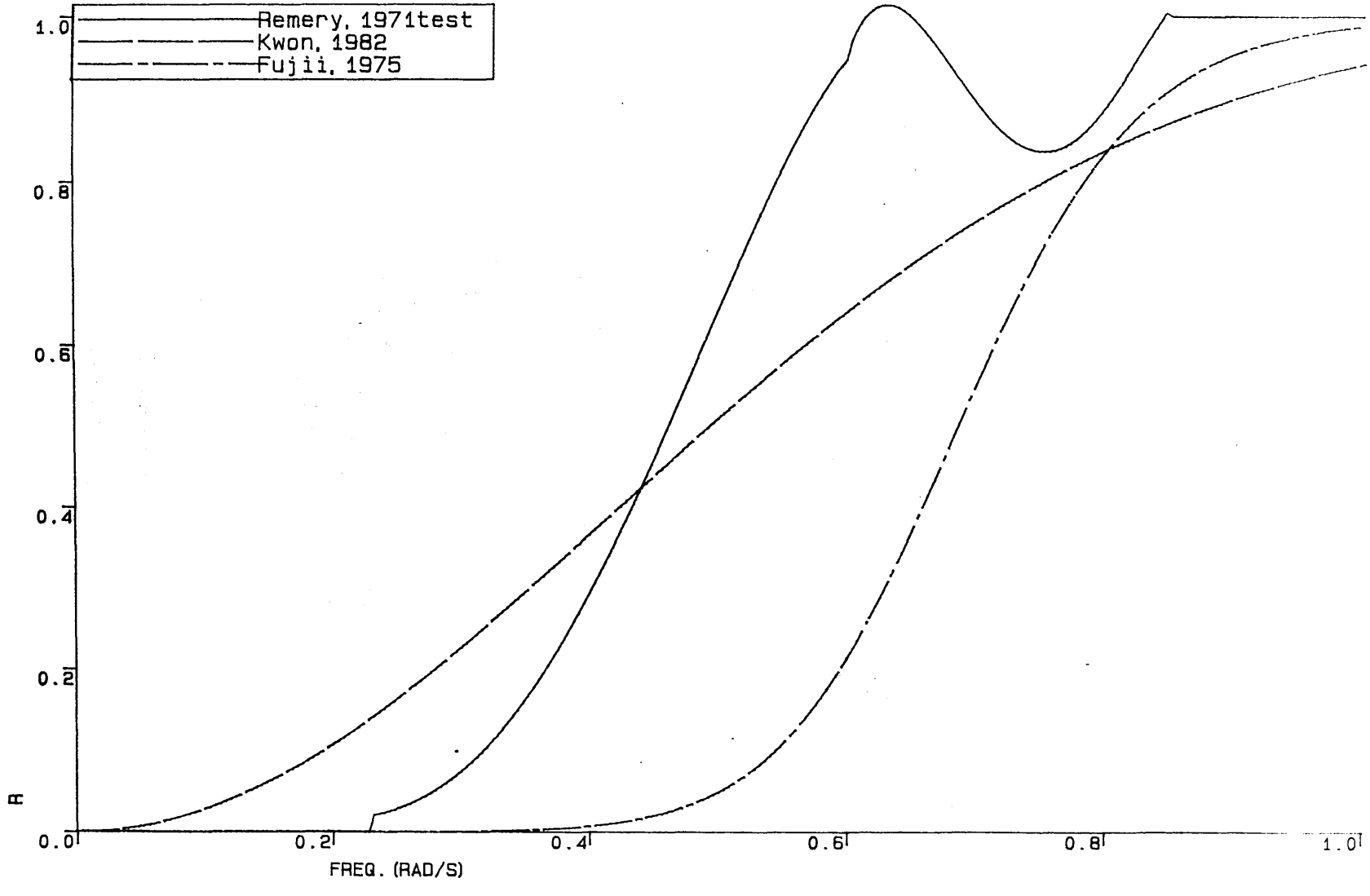

Fig.2.22 Comparison of drift force coefficient on rectangular box-shaped barge

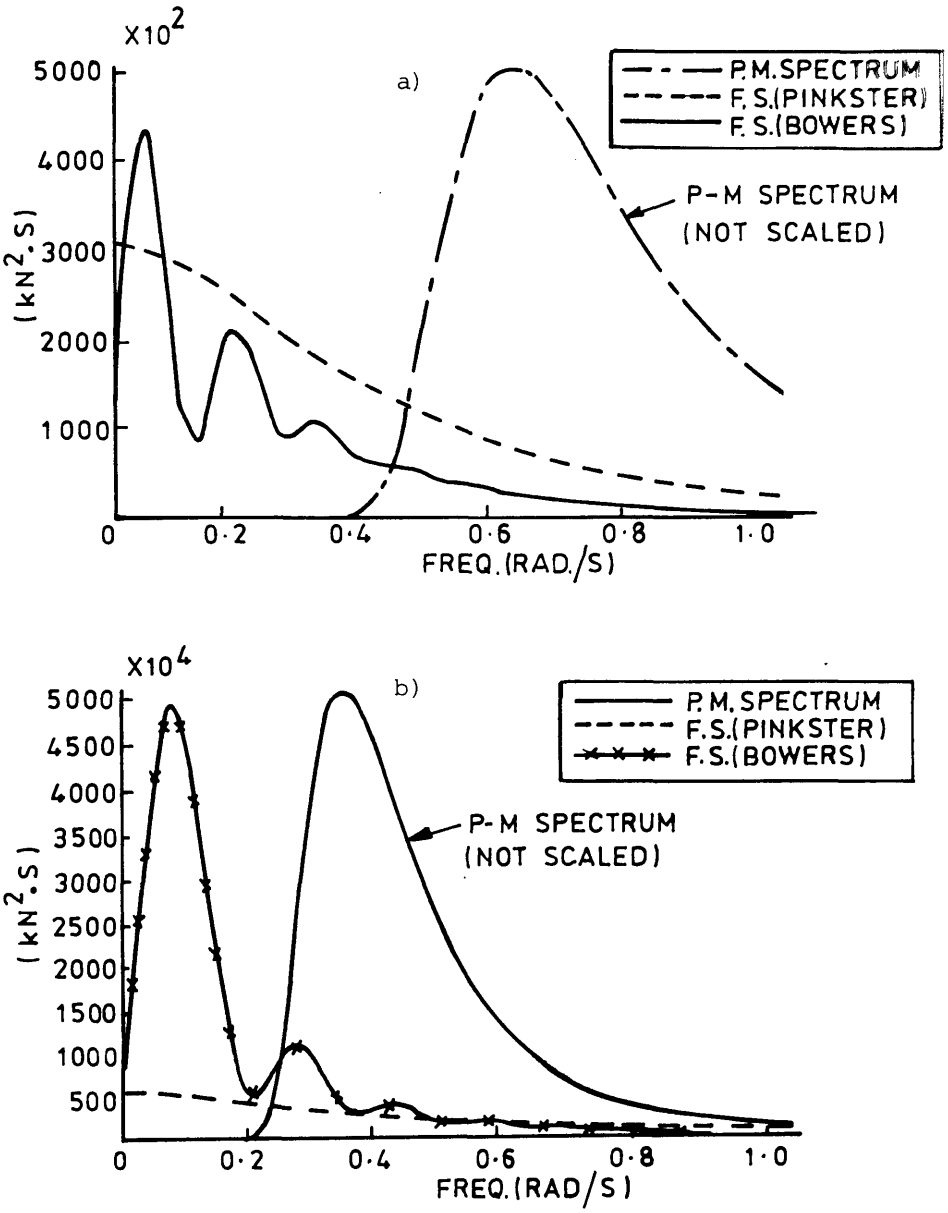

Fig.2.23 Comparison of second order force spectra for different sea states

a) V_W=18m/s (H_S=6.9m) b) V_W=26m/s (H_S=14.4m)

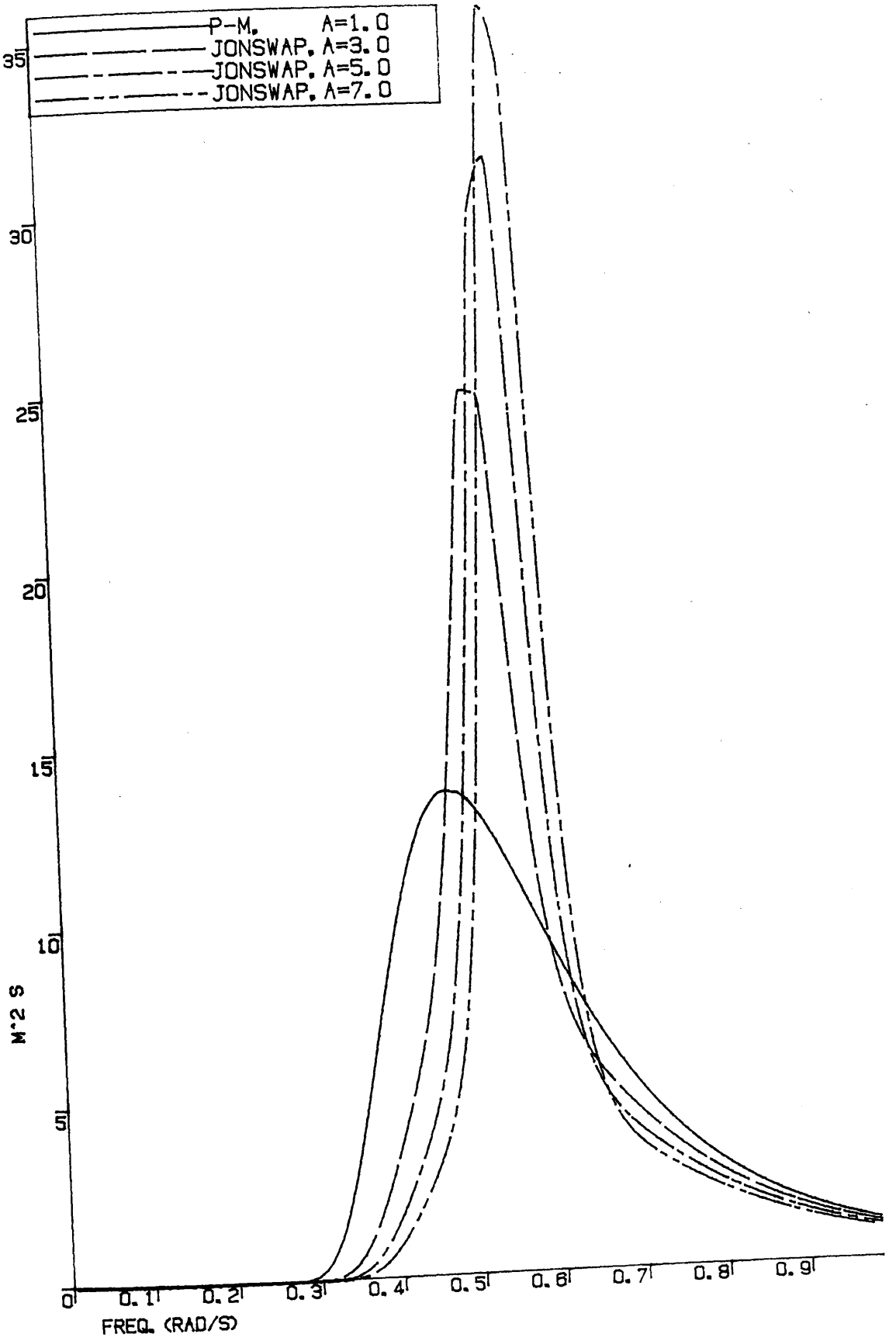

Fig.2.24 Effect of gamma factor variation on first order wave spectrum

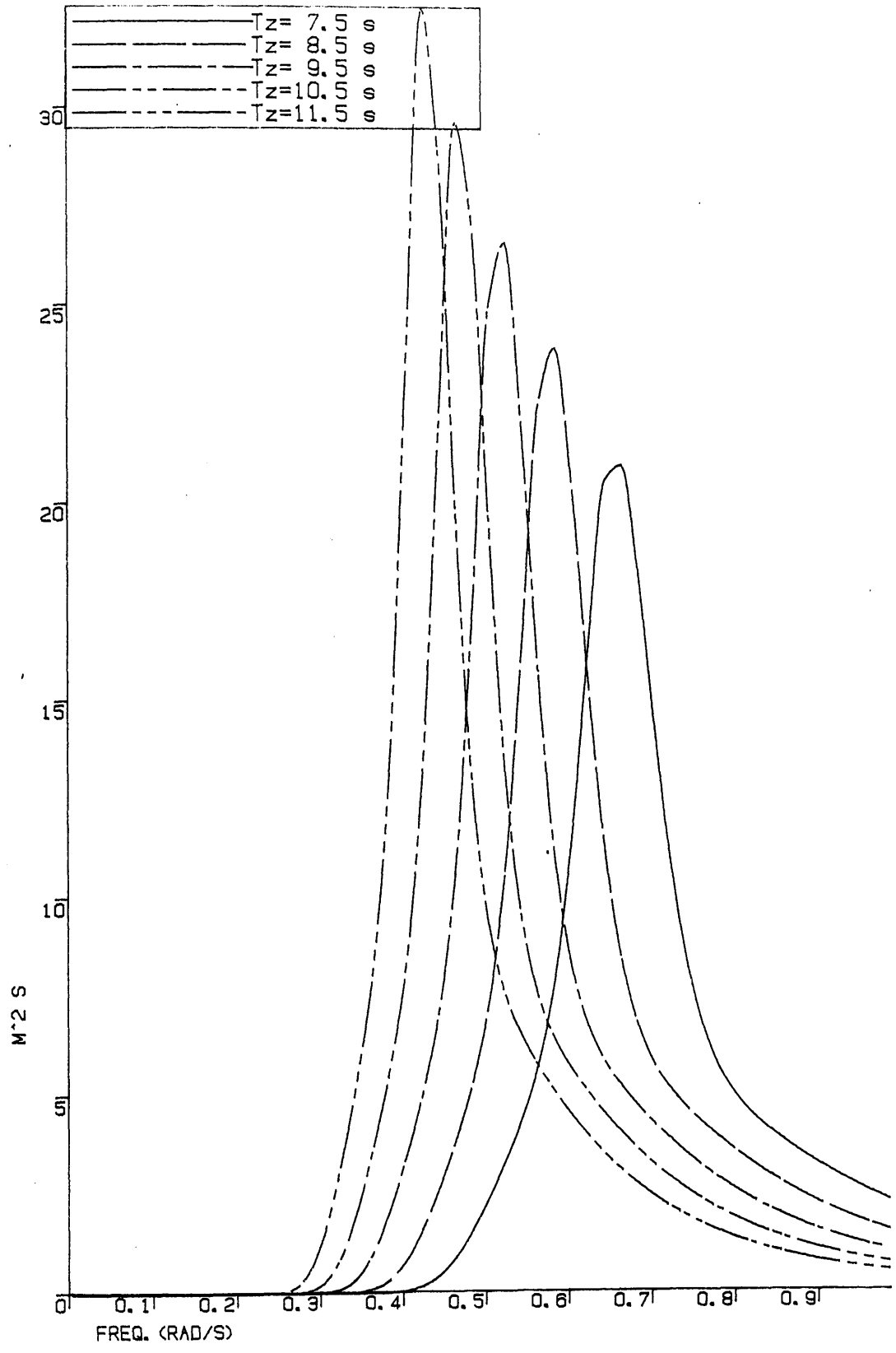

Fig.2.25 Effect of zero crossing period variation on first order wave spectrum

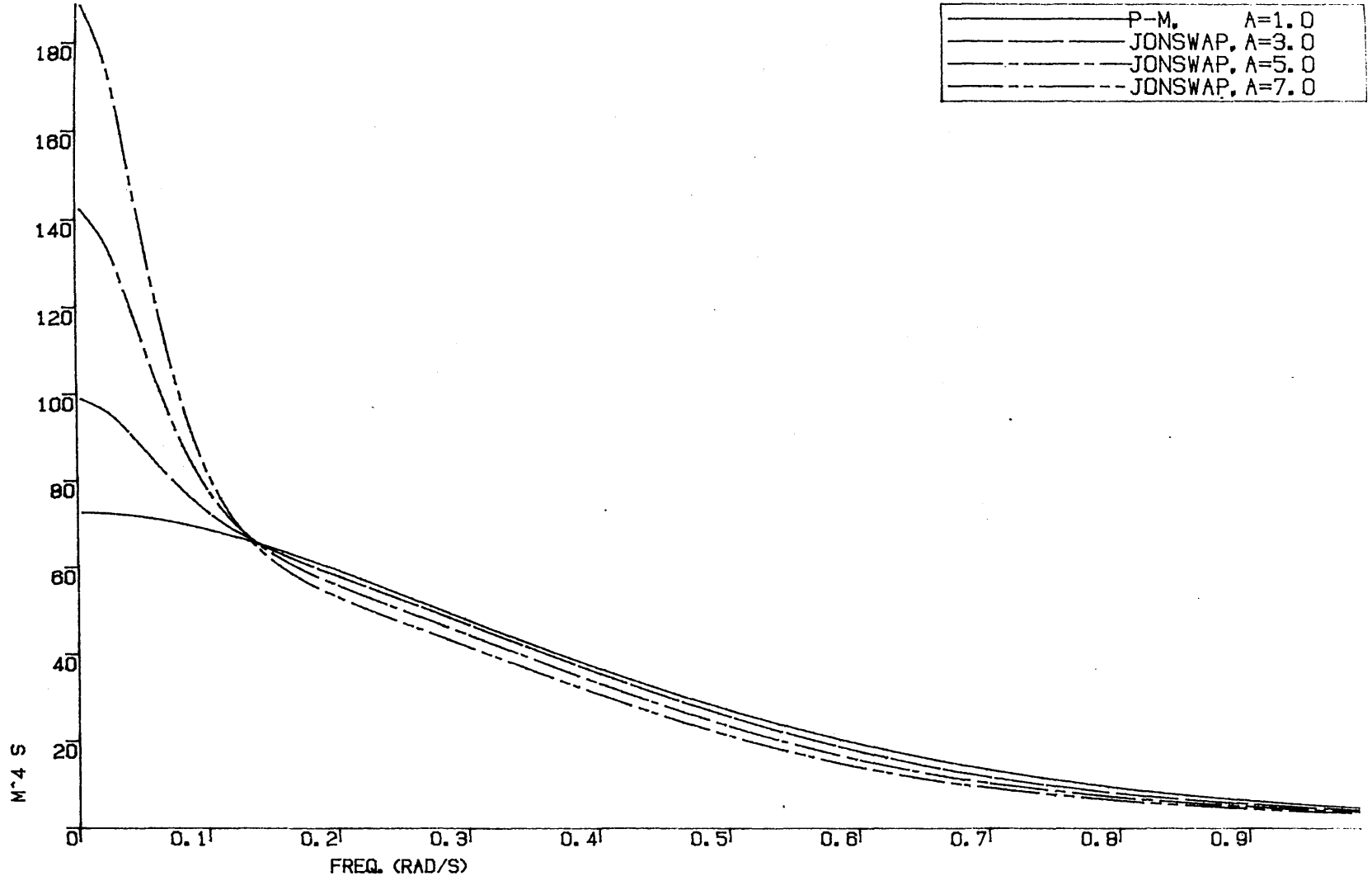

Fig.2.26 Effect of gamma factor variation on second order wave spectrum

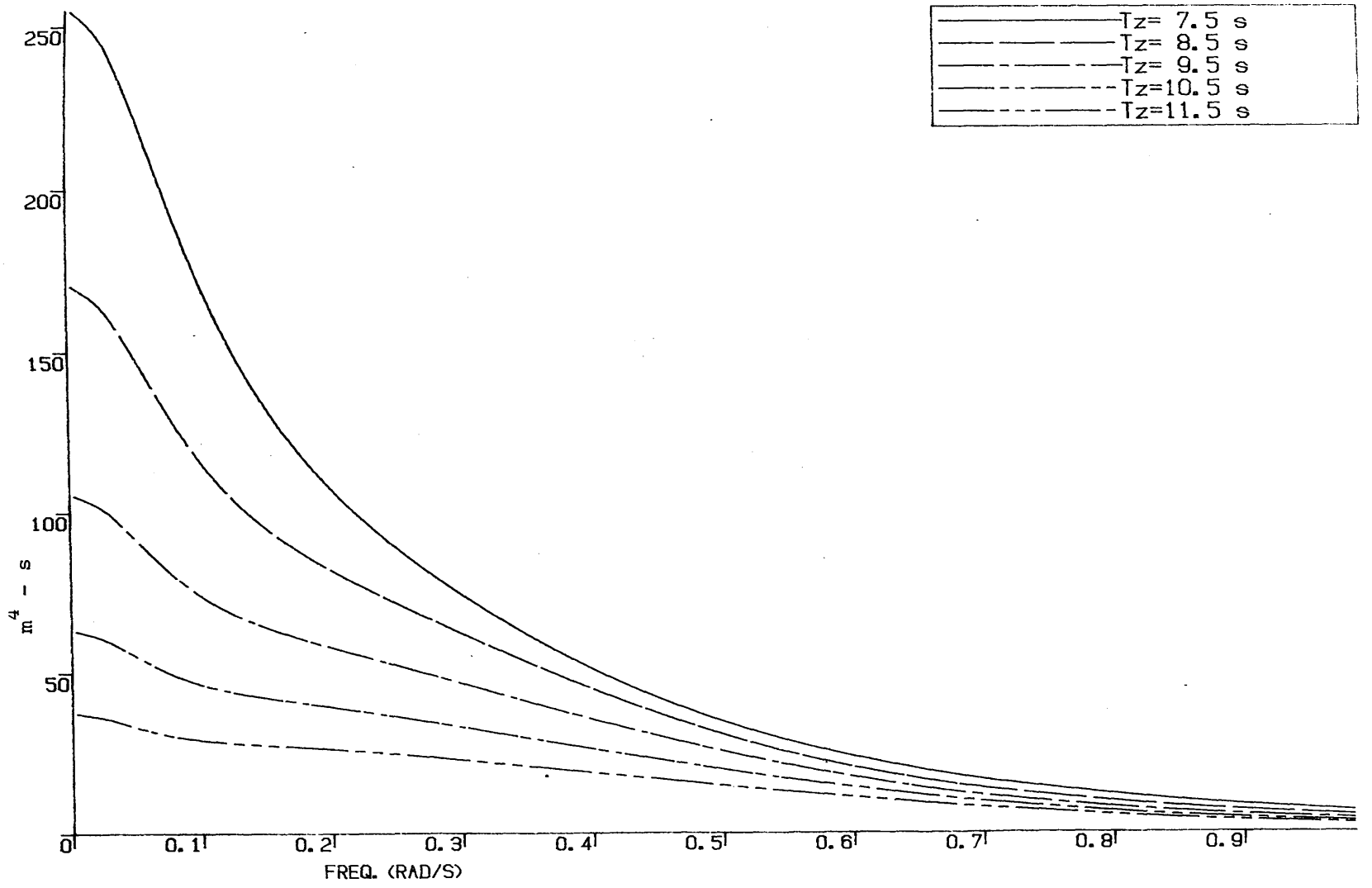

Fig.2.27 Effect of zero crossing period variation on second order wave spectrum

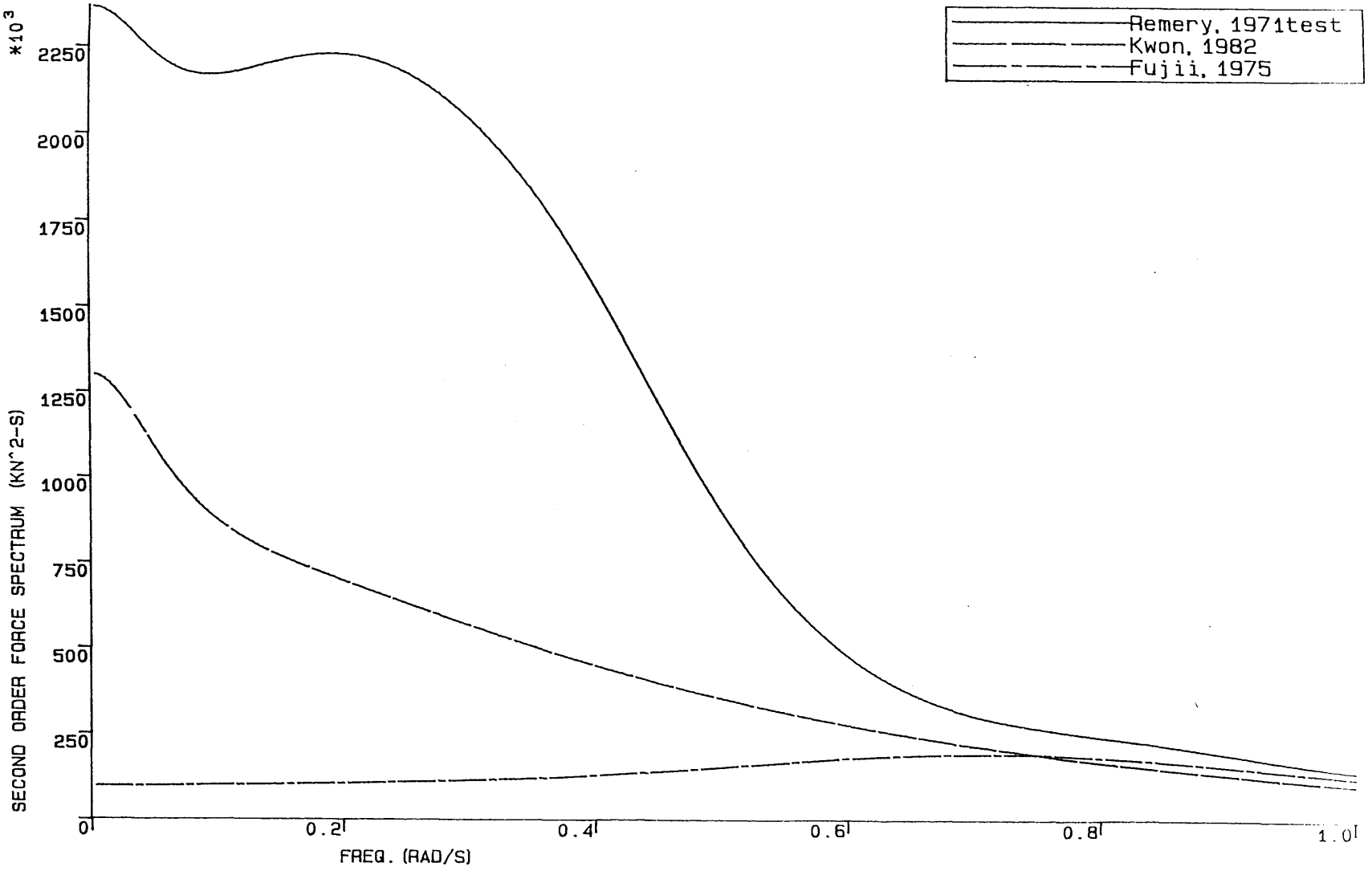

Fig.2.28 Effect of different drift force coefficients on second order force spectrum

H_S=8.5m T_Z=11.5s Gamma Factor=3.3.

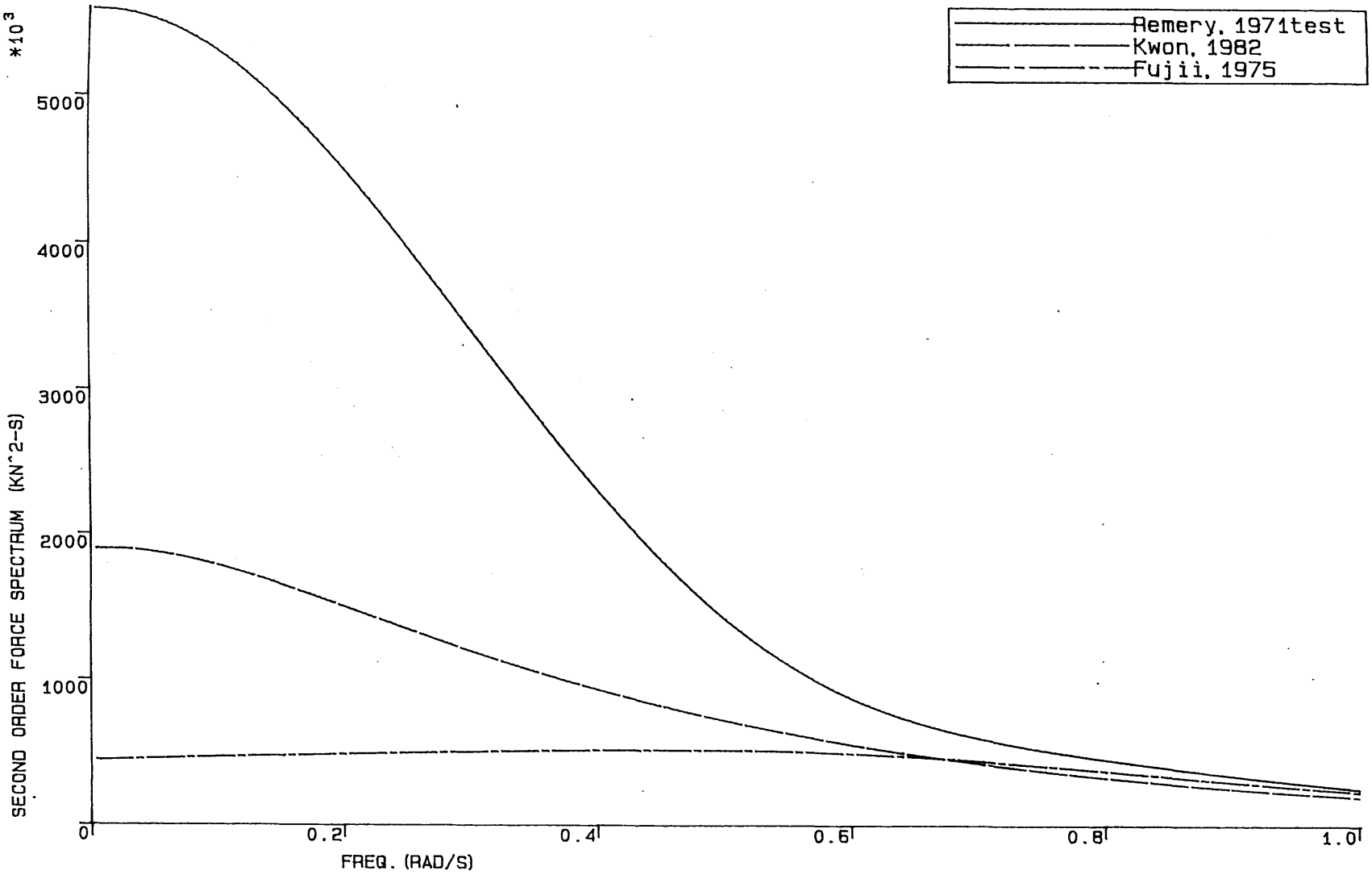

Fig.2.29 Effect of different drift force coefficients on second order force spectrum

H_S=8.5m T_Z=9.5s Gamma Factor=1.0.

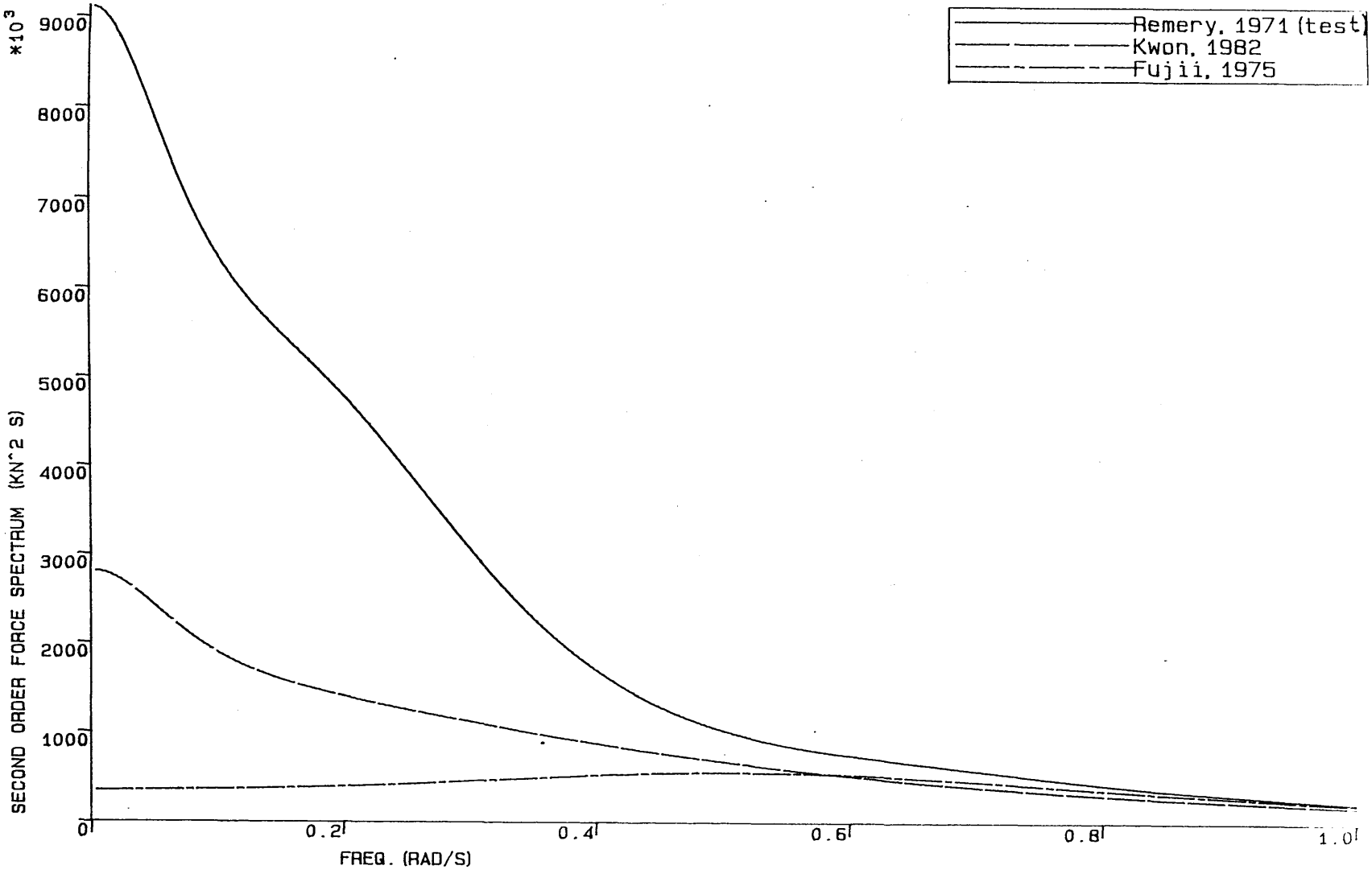

Fig.2.30 Effect of different drift force coefficients on second order force spectrum

H_S=8.5m T_Z=9.5s Gamma Factor=3.3.

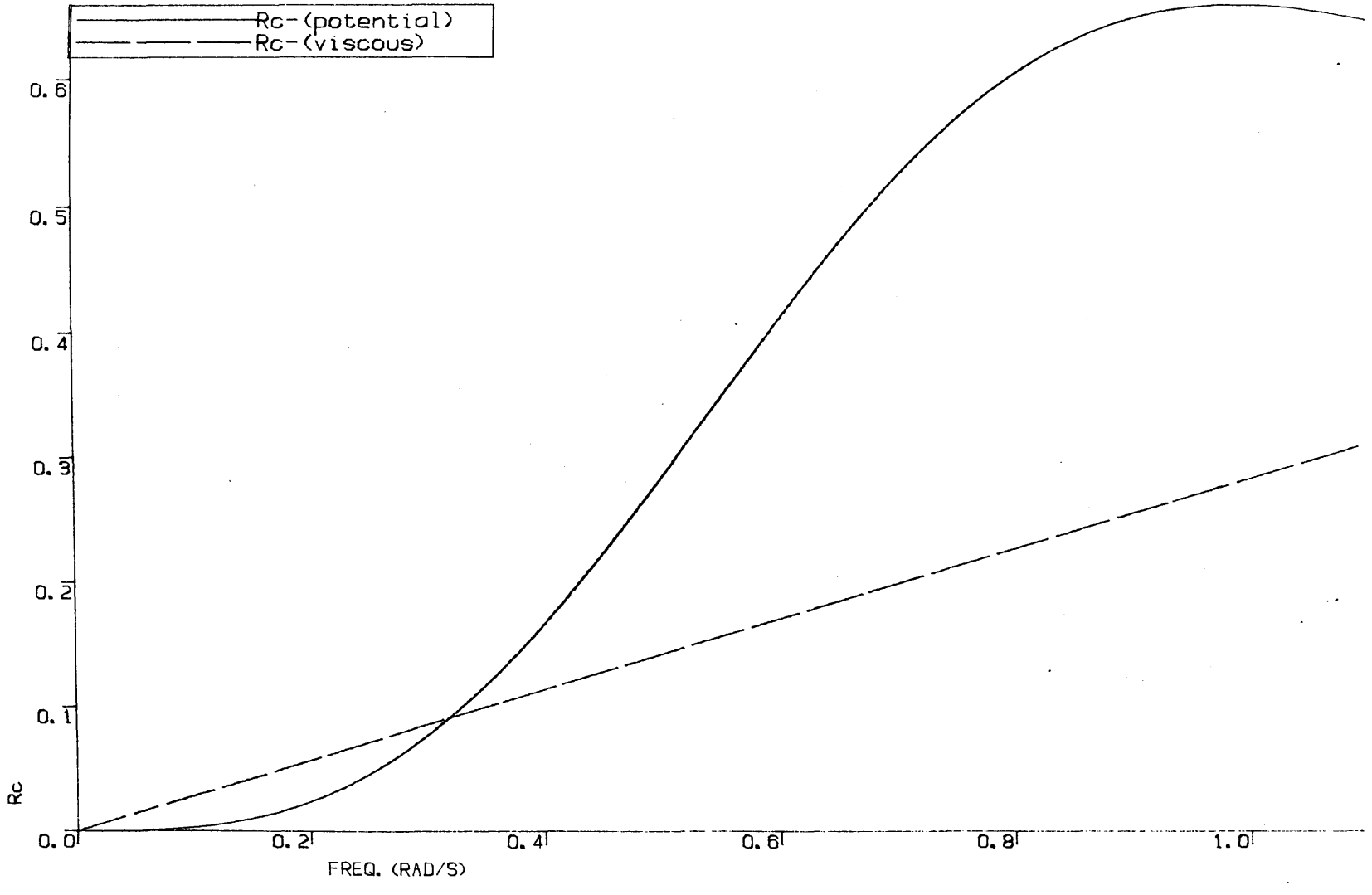

Fig.2.31 Comparison of drift force coefficient for vertical column:
viscous vs potential D=12.7m H_W=8.5m.

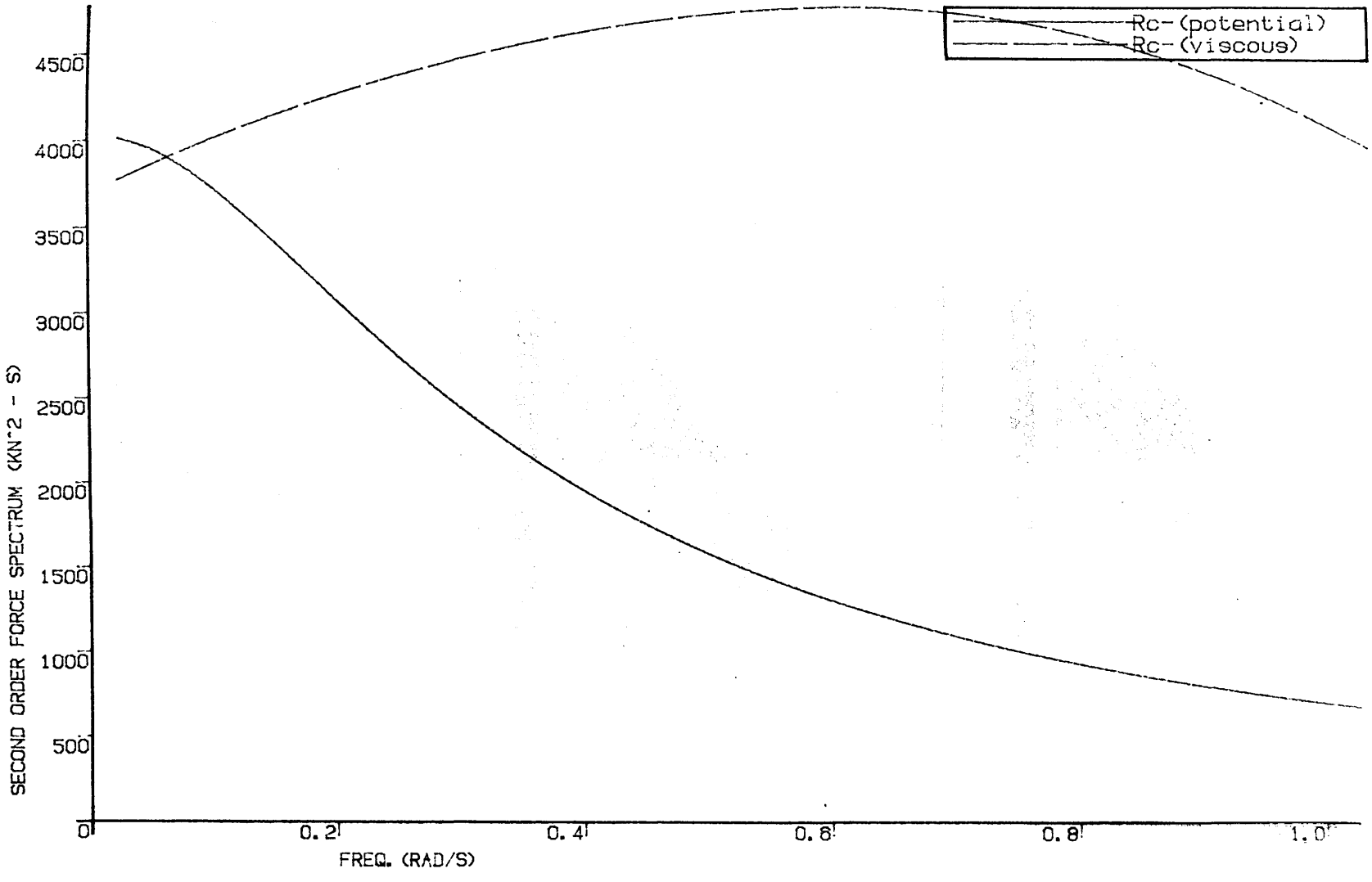

Fig.2.32 Comparison of second order force spectrum for a vertical cylinder: viscous vs potential

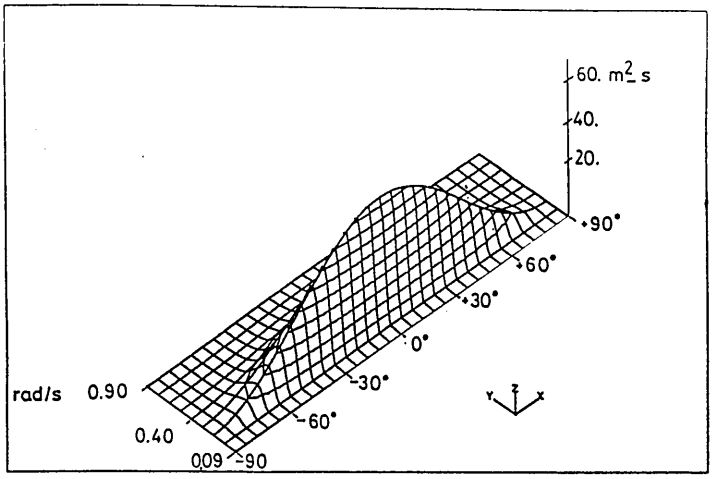

SPREADING FUNCTION NO.1 (ARTHUR . 1949)
JONSWAP SPECTRUM, Hws=16.5m, Tp=20.3s

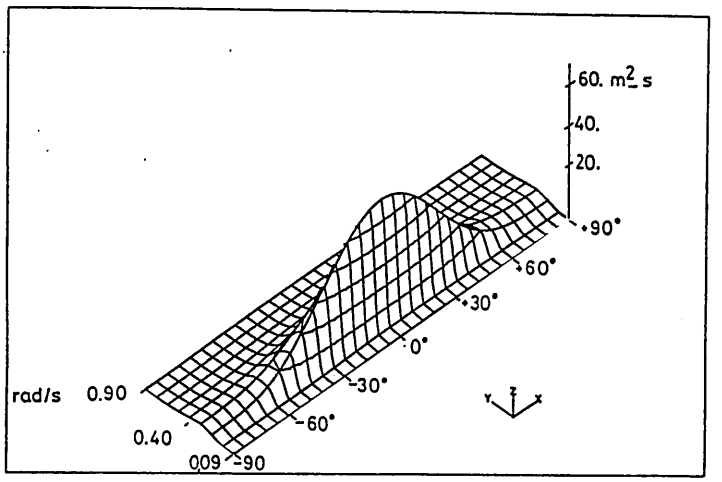

SPREADING FUNCTION NO.2 (KINSMAN . 1965)
JONSWAP SPECTRUM, Hws=16.5m, Tp=20.3s

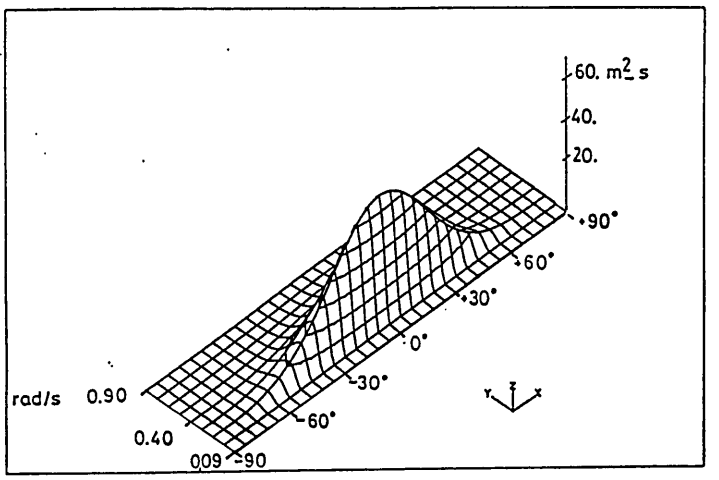

SPREADING FUNCTION NO.3 (MITSUYASU, 1975)
JONSWAP SPECTRUM, Hws=16.5m, Tp=20.3s.

Fig. 2.33 Schematic comparison of three directional spreading functions

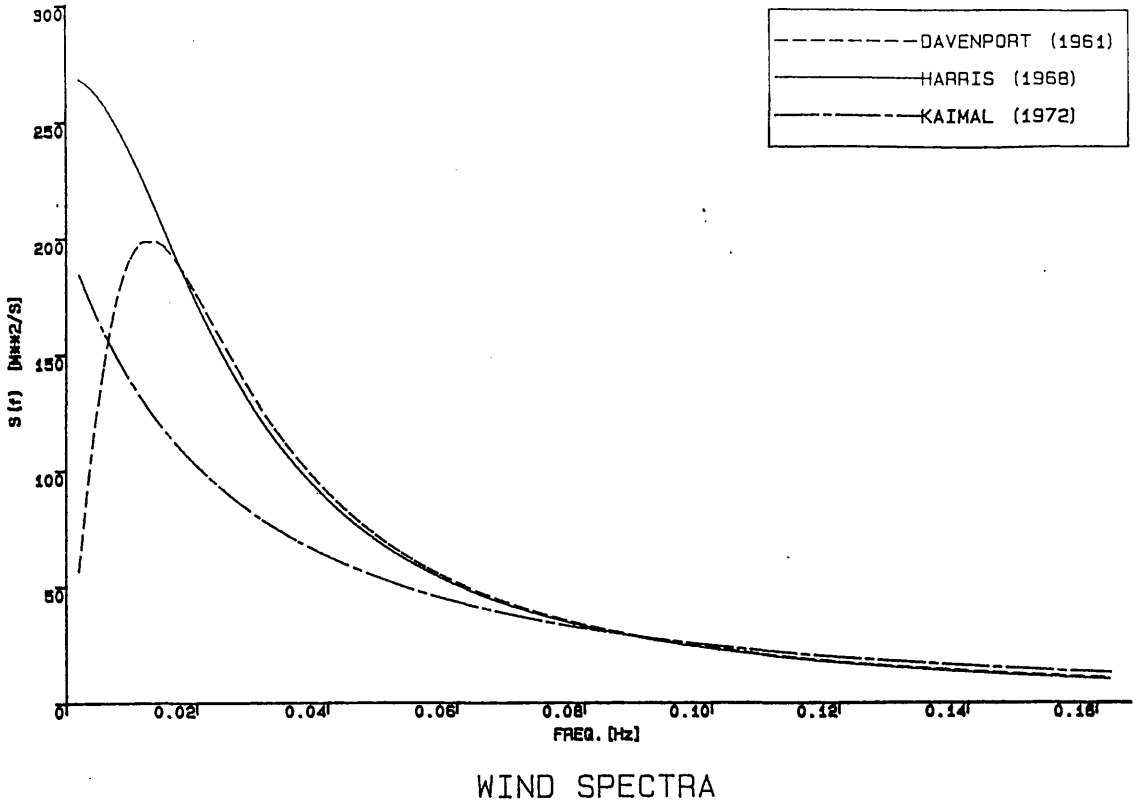

Fig.2.34 Comparison of three wind spectra when $\bar{V}_{10}$=30m/s

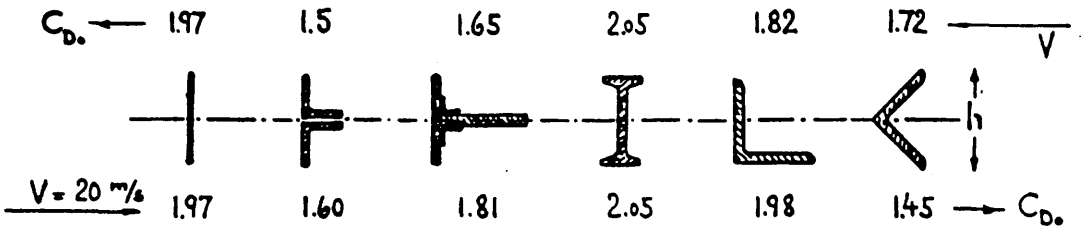

Fig.2.35 Drag coefficients in air for different geometrical shapes (Horner(1965))

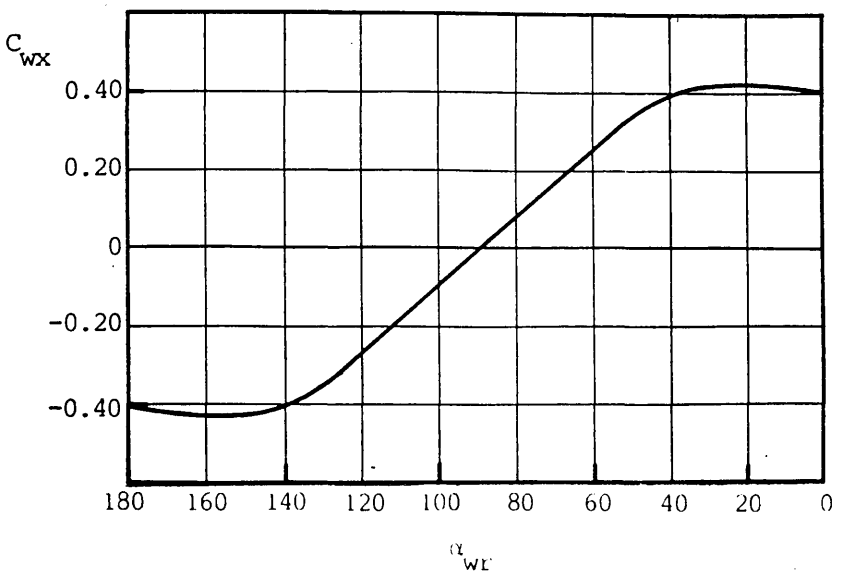

Fig.2.36 Horizontal wind force coefficient for loaded tanker (OCIMF(1977))

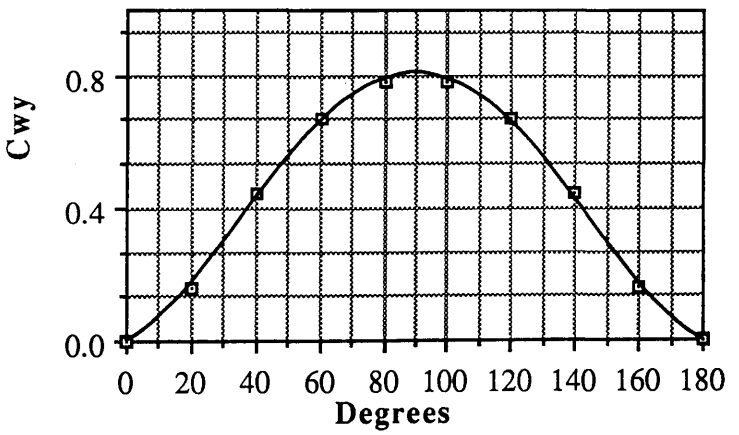

Fig.2.37 Lateral wind force coefficient for loaded tanker (OCIMF (1977))

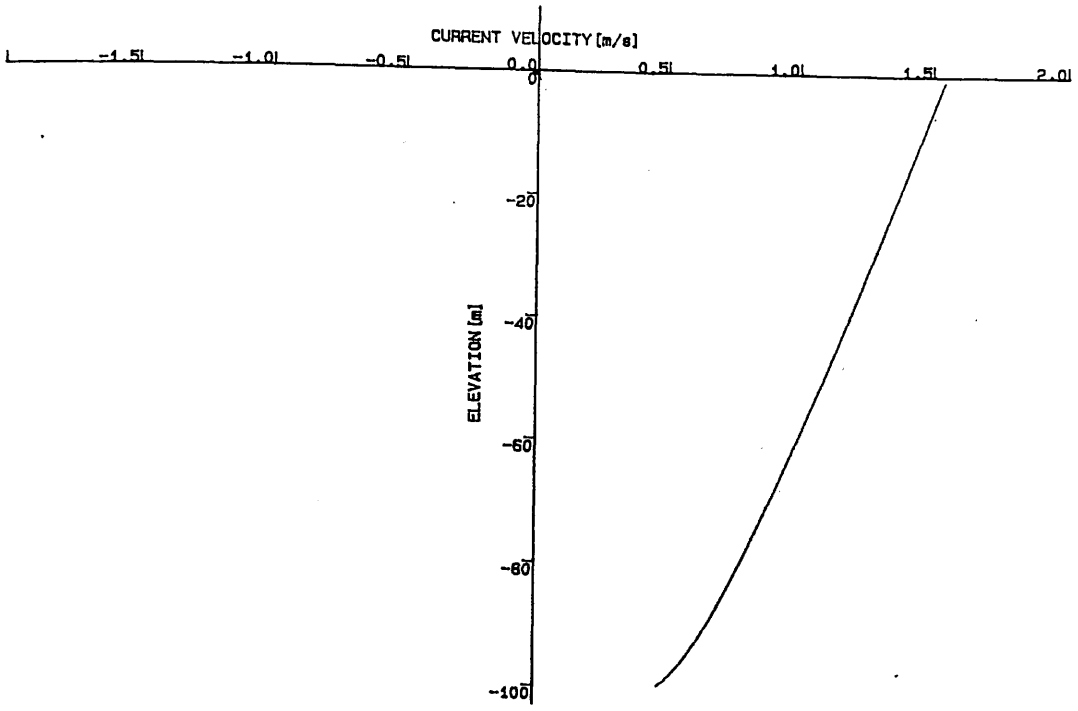

Fig.2.38 Current profile recommended by DnV (1974)

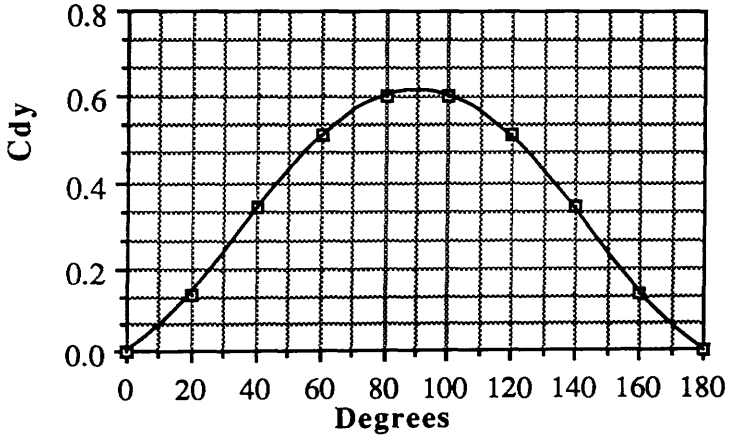

Fig.2.39 Lateral current force coefficient for loaded tanker (OCIMF, 1977)

CHAPTER 3

COUPLED SINGLE ARTICULATED TOWER AND SHIP SYSTEM

3.1 GENERAL DESCRIPTION

Coupled articulated tower and ship systems are used as storage and offloading systems in marginal fields(see Mack et al (1981)). A typical structure is shown in Fig.3.1.

The ship is connected to the articulated tower by means of a rigid yoke mechanism which allows the ship to weatherwane around the tower. The tower buoyancy provides the necessary restoring force to moor the tanker and carries the weight of the loading pipes as well as the yoke mechanism. The yoke connection is a universal one at the tower end. At the tanker end, the yoke is connected to the ship by means of two articulations at the port and starboard sides of the tanker. This connection allows relative heave and pitch motions of the ship. Only the lateral and transverse loads are transferred from the articulated tower to the storage ship through the yoke mechanism. The produced oil can be stored on tanker until it is off-loaded to a shuttle tanker moored in tandem astern.

A review of the theoretical and experimental studies of coupled articulated tower-ship systems published in the literature is given in the following.

Smulders and Remery (1979) described the various types of yoke-single buoy mooring systems either installed or under fabrication. The advantages of permanent moored systems over soft moored systems were discussed. Operational properties and fields of application of yoke moored tankers were reviewed.

Chakrabarti and Cotter (1978) gave an analysis technique and model test results of an articulated tower and a tanker system in head seas. The wave forces were assumed to be colinear with wind and current forces. They assumed that the dynamic oscillations took place about a static off-set resulting from the steady forces. The problem was considered as a 3-DOF(degrees of freedom) system. The oscillation of the tower in the plane of wave motion and the surge and pitch motions of the ship were taken into account in the analysis. The added mass and damping coefficients of the tower and the tanker were obtained from their free damped oscillations. The nonlinear drag term was

linearised.

Naess (1980) reported the tank test measurements of motions and loads on an articulated tower with and without a tanker moored to it, in non-colinear wind, current and random sea environment. The tension in the mooring line as well as the joint forces were presented for various sea conditions.

A more extensive analysis of a Single Anchor Leg Storage (SALS) system was given by Langley and Kirk (1982). In this analysis, a SALS system which consists of a mooring chain placed under high tension by a submerged buoyancy chamber and a welded steel tubular yoke structure attached to the vessel by pivots was employed. A linearised spectral analysis technique to predict random rigid-body motions and pivot forces due to first and second order wave forces was presented.

Snowden et al (1985) described the development of floating production systems. The figures presented in this paper include the motion and structural response of a coupled single articulated tower and tanker system. The response values were obtained from the solutions of 4-DOF modelling of the coupled tower and ship system which takes into account pitch of the tower, surge, heave and pitch of the ship. The experimental results reported by Snowden et al (1985) will be used in this chapter to validate the mathematical modelling for a single articulated tower-ship system. This model and a comparison between the test results and the analytical predictions will be discussed in Section 3.2.4.

Gernon and Lou (1987) modelled the Articulated Loading Platform(ALP) and tanker system analytically as a 2-DOF system: the pitch motion of the tower and the surge motion of the tanker. The hawser connecting the tanker to the ALP was modelled as a nonlinear spring. Morison's equation was used to evaluate the wave force on the ALP. The incident and diffracted wave potentials as well as the forced motion potential were expressed in terms of Mathieu functions. These potentials were used to calculate the wave forces on the tanker as well as the hydrodynamic coefficients for a defined frequency. With the full expression of the first-order potential, the second order forces

were evaluated according to the "near field" approach of Pinkster (1979). The Wilson-θ step-by-step integration technique was used in order to predict the motion behaviour of the ALP and the tanker with respect to a fixed coordinate system for each time step.

This chapter is concerned with the prediction of the motion and structural response of single articulated tower and ship systems under the first and second-order wave, current, and steady and dynamic wind excitation. Although these environmental forces may occur at the same time to yield a combined effect on the structure, the emphasis here is placed upon the effect of each excitation force individually. The dynamic motion equations which are based on simple (1-DOF) and detailed (4-DOF) mathematical models are derived and solved in the frequency domain by utilizing some linearization procedures. Motion equations could also be solved in the time domain including the nonlinear effects. This procedure is left to Chapter 6. Developed mathematical models are applied to a coupled articulated tower and ship configuration given by Snowden et al (1985). The analytical predictions are compared with experimental measurements reported in the same reference in order to validate the analytical models and the assumptions regarding the force calculations. Some parametric studies are presented including the effect of yoke length variation and the effect of different hydrodynamic coefficients on the surge response of the system, on the yoke forces and on the shear forces at the base joint. The effects of static and dynamic forces acting on the coupled system are compared. In the last section of the Chapter 3, the effects of directional spreading of waves on the motion and structural response of the coupled system are also investigated through various energy spreading assumptions.

3.2 MOTION EQUATION FOR COUPLED SINGLE ARTICULATED TOWER AND SHIP SYSTEM

3.2.1 SIMPLE MODEL FOR COUPLED SAT-SHIP SYSTEM, 1-DOF

In this section, a simple mathematical model for a coupled single articulated tower and ship system is developed to predict motion responses and yoke forces under uni-

directional wave excitation. In this mathematical modelling, the ship is assumed to be a rigid extension of the tower and to have only surge oscillations about the articulating joint of the tower. The yoke is assumed to have infinite stiffness and to remain parallel to the water surface.

Throughout the development of the mathematical model the following assumptions are made:

- Wave and motion amplitudes are small.

- The tower can be divided into several elements and the sectional dimensions of these elements are small compared to the wave length. The Morison approach is applied to determine the wave loading on the articulated tower.

- The interference between the tower elements as well as between the tower elements and ship is negligible.

- Hydrodynamic forces due to rigid-body velocity can be linearised and the wave forces due to wave particle velocities can be neglected.

- The tower and ship oscillate as a rigid body.

- The friction on the joint between the tower and the foundation and on joints of the yoke mechanism is neglected.

Considering the coupled system as a single degree of freedom system by taking into account only the pitch angles of the tower and the surge motions of the ship the equation of motion can be written as follows (see, Fig.3.1)

$$I_\theta \ddot{\theta} + B_\theta \dot{\theta} + K_\theta \theta = M_\theta \tag{3.1}$$

where $I_\theta = I_{\theta\theta} + I_{AD,\theta} + I_{M,S} + I_{AD,S}$

$B_\theta = B_{\theta\theta} + B_{xx}$

$K_\theta = g (\rho \nabla_T \overline{KB} - W_T \overline{KG})$

$M_\theta = M_{T\theta} + M_{XS,I} + M_{XS,D}$

and, I_θ is the total mass moment of inertia of the coupled system which is calculated about the articulated joint; $I_{\theta\theta}$ is the mass moment of inertia of the tower; $I_{AD,\theta}$, the added-mass moment of inertia of the tower; $I_{M,S}$, the mass moment of inertia of the ship; $I_{AD,S}$, the added-mass moment of inertia of the ship; B_θ, the damping coefficient of the coupled system; $B_{\theta\theta}$, the damping coefficient of the tower in pitch oscillation and B_{xx}, the damping coefficient of the ship in surge oscillations. The calculation of damping coefficients will be explained further in Section 3.2.3.

The stiffness coefficient K_θ arises from the difference between the buoyancy and the gravity forces when the articulated tower is displaced from its equilibrium position. $\overline{KB}$ and $\overline{KG}$ are the centre of buoyancy and gravity of tower measured from the articulated joint, respectively; ∇_T, displacement of tower; W_T, mass of tower; g, gravitational acceleration and ρ, water density.

In the right hand side of the equation: $M_{T\theta}$, moment of the wave inertia forces on the tower; $M_{XS,I}$, the moment of incident wave pressures on the ship and $M_{XS,D}$, the moment of diffracted wave pressures on the ship. Wave forces acting on the single articulated tower and ship system were explained in detail in Chapter 2, Section 2.2. The excitation moments due to the waves can be calculated by using the moment arm, d_{yoke} from the sea bed to the force acting point (see Fig.3.2).

Total wave exciting moment on the coupled system can also be expressed in terms of in-phase and out-phase components as

$$M_\theta = a \sin \omega t + b \cos \omega t. \qquad (3.2)$$

Eq.(3.1) can be expressed in the following form after dividing both sides of the equation by I_θ

$$\ddot{\theta} + 2\zeta\omega_n \dot{\theta} + \omega_n^2 \theta = \underline{A} \sin\omega t + \underline{B} \cos\omega t \tag{3.3}$$

where $2\zeta\omega_n = B_\theta / I_\theta$, $\omega_n^2 = K_\theta / I_\theta$, $\underline{A} = a / I_\theta$, $\underline{B} = b / I_\theta$; ω_n, is the natural frequency of the system and ζ is the damping ratio of the system.

The solution of the differential equation, Eq.(3.3) is given as,

$$\theta = X_1 \sin \omega t + X_2 \cos \omega t. \tag{3.4}$$

If Eq.(3.4) is derived with respect to time and substituted into Eq.(3.3), the unknown coefficients of the solution can be obtained as:

$$X_1 = \frac{\underline{A}(\omega_n^2 - \omega^2) + 2\zeta\omega_n\omega\underline{B}}{(\omega_n^2 - \omega^2)^2 + (2\zeta\omega_n\omega)^2} \quad \text{and} \quad X_2 = \frac{\underline{B}(\omega_n^2 - \omega^2) + 2\zeta\omega_n\omega\underline{A}}{(\omega_n^2 - \omega^2)^2 + (2\zeta\omega_n\omega)^2} \tag{3.5}$$

Maximum pitch response of the tower becomes,

$$\theta_{max} = \sqrt{(X_1^2 + X_2^2)}. \tag{3.6}$$

In order to obtain the horizontal yoke forces, the moments of the yoke forces about the joint are incorporated into the motion equation of the single articulated tower as follows:

$$F_R(t)\, d_{yoke} = [I_{\theta\theta} + I_{AD,\theta}]\, \ddot{\theta} + B_{\theta\theta}\, \dot{\theta} + K_\theta\, \theta - M_{T\theta} \tag{3.7}$$

where d_{yoke} is the distance between the yoke attachment point of the column and the joint.

F_R can be determined in terms of the tower's geometrical particulars and the motion response of the system by substituting Eq.(3.4) into Eq.(3.7). Thus,

$$F_R(t) = \frac{1}{d_{yoke}} \{ -\omega^2 [I_{\theta\theta} + I_{AD,\theta}] (X_1 \sin\omega t + X_2 \cos\omega t)$$

$$+ \omega B_{\theta\theta} (X_1 \cos\omega t - X_2 \sin\omega t) + K_\theta (X_1 \sin\omega t + X_2 \cos\omega t) - \bar{M}_{T\theta} \sin\omega t \}. \qquad (3.8)$$

For two different time steps with a 90 degrees phase lag between them, one can write two yoke force values as

$$F_{R,1} = \frac{1}{d_{yoke}} (-\omega^2 [I_{\theta\theta} + I_{AD,\theta}] X_2 + \omega B_{\theta\theta} X_1 + K_\theta X_2) \qquad \text{when} \quad t = 0$$

and

$$F_{R,2} = \frac{1}{d_{yoke}} (-\omega^2 [I_{\theta\theta} + I_{AD,\theta}] X_1 - \omega B_{\theta\theta} X_2 + K_\theta X_1 - \bar{M}_{T\theta}) \text{ when } t = T_o / 4 \qquad (3.9)$$

in which T_o is one period.

The maximum yoke force can then be obtained from the following equation

$$(F_R)_{max.} = \sqrt{(F_{R,1}^2 + F_{R,2}^2)} \qquad (3.10)$$

The application of this 1-DOF mathematical model on the coupled tower-ship system will be discussed in Section 3.2.4.

3.2.2 DETAILED MODEL FOR COUPLED SAT-SHIP SYSTEM, 4-DOF

In this Section, a detailed mathematical model to predict the dynamic response of the coupled system by taking into account heave and pitch motions of the ship, pitch motions

of the tower as well as finite stiffness and arbitrary angle for the yoke is presented.

In the 4-DOF mathematical model, the dynamic response of the system and the governing equations can be given as follows (see Fig.3.3):

Heave motion of the ship

$$(M + M_{AD,y})\ddot{y} + B_{yy}\dot{y} + K_{yy}y = F_{Ty} - F_R \sin \alpha \tag{3.11}$$

where M is the mass of the ship; $M_{AD,y}$ the added mass of the ship in heave; B_{yy} , the damping coefficient in heave; K_{yy}, the stiffness coefficient of the ship in heave; F_{Ty}, the heave forces on the ship due to regular waves (see Eq.(2.12)); α, the yoke inclination angle and F_R, the axial yoke force.

Surge motion of the ship

$$(M + M_{AD,x})\ddot{x} + B_{xx}\dot{x} = F_{Tx} + F_R \cos \alpha \tag{3.12}$$

where $M_{AD,x}$ is the added mass of the ship in surge; B_{xx}, the damping coefficient in surge and F_{Tx}, the surge forces on the ship due to regular waves (see Eq.(2.9)).

Pitch motion of the ship

$$(I_{\psi\psi} + I_{AD,\psi})\ddot{\psi} + B_{\psi\psi}\dot{\psi} + K_{\psi\psi}\psi = M_{T\psi} - F_R[H \cos \alpha + (L_S / 2)\sin \alpha] \tag{3.13}$$

where $I_{\psi\psi}$ is the mass moment of inertia of the ship in pitch; $I_{AD,\psi}$, added mass moment of inertia of the ship in pitch; $B_{\psi\psi}$, damping coefficient in pitch; $K_{\psi\psi}$, stiffness coefficient of the ship in pitch and $M_{T\psi}$, wave induced moments on the ship in pitch (see Eq.(2.14))

Angular motion of the tower

$$(I_{\theta\theta} + I_{AD,\theta})\ddot{\theta} + B_{\theta\theta}\dot{\theta} + K_{\theta\theta}\theta = M_{T\theta} + F_R L_1 \cos\alpha \tag{3.14}$$

where $I_{\theta\theta}$ is the mass moment of inertia of the tower ; $I_{AD,\theta}$, added mass moment of inertia of the tower; $B_{\theta\theta}$, damping coefficient of the tower; $K_{\theta\theta}$, stiffness coefficient; $M_{T\theta}$, wave induced moments on the tower and L_1, the moment arm between the joint and the yoke.

These equations are coupled by writing the kinematic compatibility equation which can be expressed in terms of motion amplitudes of the ship and the tower, geometrical characteristics of the ship and tower and stiffness of the yoke as follows

$$F_R = c\{y\sin\alpha - x\cos\alpha + \psi[H\cos\alpha + (L_S/2)\sin\alpha] - \theta L_1\cos\alpha\} \tag{3.15}$$

where c is stiffness coefficient for the yoke or $c = AE/L_y$; A, cross sectional area of the yoke; E, modulus of elasticity and other terms are defined in Fig.3.3.

The resulting equation is given in matrix form as follows

$$[M]\{\ddot{X}\} + [B]\{\dot{X}\} + [K]\{X\} = \{F\} \tag{3.16}$$

where

$$[M] = \begin{bmatrix} M + M_{AD,y} & 0 & 0 & 0 \\ 0 & M + M_{AD,x} & 0 & 0 \\ 0 & 0 & I_{\psi\psi} + I_{AD,\psi} & 0 \\ 0 & 0 & 0 & I_{\theta\theta} + I_{AD,\theta} \end{bmatrix}$$

$$[B] = \begin{bmatrix} B_{yy} & 0 & 0 & 0 \\ 0 & B_{xx} & 0 & 0 \\ 0 & 0 & B_{\psi\psi} & 0 \\ 0 & 0 & 0 & B_{\theta\theta} \end{bmatrix}$$

$$\{F\} = \begin{Bmatrix} F_{Ty} \\ F_{Tx} \\ M_{T\psi} \\ M_{T\theta} \end{Bmatrix}$$

in which

$M = \rho L_S B_S T_S$,

$M_{AD,y} = \rho (\pi/2)(B_S/2)^2 C_{VH} L_S$,

$B_{yy} = 2\zeta[(M+M_{AD,y})K_{yy}]^{0.5}$,

$K_{yy} = \rho g L_S B_S$,

$M_{AD,x} = \rho (\pi/4) B_S^2 C_{VS} T_S$

$B_{xx} = (1/2)\, \rho\, C_{DS}\, B_S T_S$

$I_{\psi\psi} = (M/12)(D_B^2+L_S^2)$

$I_{AD,\psi} = \rho (\pi/2) (L_S/2)^4 C_{VP} B_S$

$B_{\psi\psi} = 2\, \zeta\, [(\, I_{\psi\psi}+I_{AD,\psi})\, K_{\psi\psi}]^{0.5}$

$K_{\psi\psi} = \rho\, g\, \overline{GM}_L\, L_S\, B_S\, T_S$

$B_{\theta\theta} == \; 2\, \zeta\, [(\, I_{\theta\theta}+I_{AD,\theta})\, K_{\theta\theta}]^{0.5}$

$K_{\theta\theta} = g\, (\, \rho\, \nabla_T\, \overline{KB} - W_T\, \overline{KG}\,)$

ζ = damping ratio

$\overline{GM}_L$ = longitudinal metacentric height of ship

The coefficients of the stiffness matrix can be expressed in terms of the geometrical characteristics of the ship, the tower and the yoke mechanism as follows

$[K] = k_{ij}$ or,

$k_{11} = K_{yy} + c \sin^2\alpha$,

$k_{12} = -c \cos\alpha \sin\alpha$,

$k_{13} = c\, [H \cos\alpha + (L_S / 2) \sin\alpha] \sin\alpha$,

$k_{14} = -c\, L_1 \cos\alpha \sin\alpha$,

$k_{21} = -c \cos\alpha \sin\alpha$,

$k_{22} = c \cos^2\alpha$,

$k_{23} = c\,[\,H\cos\alpha + (L_S/2)\sin\alpha]\cos\alpha,$

$k_{24} = c\,L_1\cos^2\alpha,$

$k_{31} = c\sin\alpha\,[\,H\cos\alpha + (L_S/2)\sin\alpha],$

$k_{32} = -\,c\cos\alpha\,[\,H\cos\alpha + (L_S/2)\sin\alpha],$

$k_{33} = K_{\psi\psi} + c\,[\,H\cos\alpha + (L_S/2)\sin\alpha]^2$

$k_{34} = -c\,L_1\cos\alpha\,[\,H\cos\alpha + (L_S/2)\sin\alpha],$

$k_{41} = -c\,L_1\sin\alpha\cos\alpha\,,$

$k_{42} = c\,L_1\cos^2\alpha,$

$k_{43} = -c\,[\,H\cos\alpha + (L_S/2)\sin\alpha]\,L_1\cos\alpha,$

$k_{44} = K_{\theta\theta} + c\,L^2{}_1\cos^2\alpha$

Eq.(3.16) is a homogeneous second-order linear differential equation and the solution of the equation can be assumed to take the following form :

$$\{X\} = \begin{Bmatrix} y_1 \sin\,\omega t + y_2 \cos\,\omega t \\ x_1 \sin\,\omega t + x_2 \cos\,\omega t \\ \psi_1 \sin\,\omega t + \psi_2 \cos\,\omega t \\ \theta_1 \sin\,\omega t + \theta_2 \cos\,\omega t \end{Bmatrix} \tag{3.17}$$

The solution of Eq.(3.15) can be obtained by substituting Eq.(3.17) into Eq.(3.16) and solving 8 simultaneous linear equations with 8 unknowns comprising the in-phase and out-phase components of the displacement vector. The NAg subroutine, F04AEF, is considered suitable to solve the matrix equation. The axial yoke force can be predicted using the kinematic compatibility equation, Eq.(3.15). The maximum yoke force in the frequency domain may be obtained following the procedure given in deriving Eq.(3.10).

3.2.3 DISCUSSION ON DAMPING COEFFICIENT CALCULATION

When the coupled tower-ship system oscillates in still water the damping forces occur in order to slow down the system motion. Since the restoring stiffness for articulated towers will be mainly linear, it can be expected that the damping, whether it be linear or nonlinear, will be the dominant mechanism for limiting the resonant response.

Damping forces are assumed to be proportional to the square of the relative water particle velocity. There are two ways to calculate the viscous damping forces on the system : The first one is to measure the forces by using a geometrically similar prototype oscillating in still water; the second is to calculate the forces by utilizing the appropriate damping coefficients for each part of the system. In the case of a single degree-of-freedom mathematical model the moments of the viscous damping forces with respect to the articulated joint at the sea bed can be written as follows:

Viscous damping moment on the articulated tower

$$M_D^T = \int_{-d}^{0} \frac{1}{2}\rho C_D D[\dot{\theta}(y+d)]\left|\dot{\theta}(y+d)\right|(y+d)dy \tag{3.18}$$

Viscous damping moment on the ship in surge direction

$$M_D^S = \frac{1}{2}\rho C_{DS} B_S T_S \dot{x}|\dot{x}|d_{yoke} \tag{3.19}$$

where C_D and C_{DS} are the drag coefficients for the tower and the ship in surge direction, respectively and $\dot{x}$ is the velocity of ship in surge direction ($=\dot{\theta}d_{yoke}$). Other terms are defined in Fig.3.2. The nonlinear term, $\dot{\theta}|\dot{\theta}|$ in Eqs.(3.18) and (3.19) should be linearized in order to solve the equation of motion, Eq.(3.1) in frequency domain. Defining the angular velocity terms as Fourier series and ignoring the higher order terms gives the following result

$$\dot{\theta}|\dot{\theta}| = \frac{8}{3\pi}\omega\theta_{max}\dot{\theta}$$

where θ_{max} is given by Eq.(3.6). After the linearization of Eqs.(3.18) and (3.19), the damping coefficients can be written as follows

$$B_{\theta\theta} = \frac{4}{3\pi}\rho C_D \omega\theta_{max}\int_{-d}^{0} D(y+d)^3\,dy \tag{3.20}$$

$$B_{xx} = \frac{4}{3\pi}\rho C_{DS}\, B_S\, T_S\, d_{yoke}^3\, \omega\theta_{max} \qquad (3.21)$$

where d is the depth of water. The iteration procedure is employed to find the motion dependent damping.

In calculating the damping coefficients using 4-DOF mathematical model, each degree of freedom is treated individually. The viscous damping forces due to the ship are calculated by assuming that the ship is represented by an oscillating plate which has a cross sectional area of $T_S \times B_S$. It is also assumed that the damping in heave and pitch motions of the ship is less than critical damping and can be calculated by choosing a damping ratio, ζ, less than the unity.

3.2.4 COMPARISON OF TWO MODELS: 1-DOF VS 4-DOF

In this section, the motion and structural response values obtained from 1-DOF and 4-DOF mathematical models are compared with each other and with the experimental measurements reported by Snowden et al (1985). The configuration of SAT-Ship system given in Fig.3.1 is used. The response values are non-dimentionalised with respect to wave amplitude.

The motion equations given in Eqs.(3.1) and (3.16) are applied to the coupled tower-ship configuration shown in Fig.3.1. The surge response and the yoke forces obtained from 1-DOF and 4-DOF mathematical models are compared with the experimental measurements reported by Snowden et al (1985). Figs.3.4 and 3.5 show the surge response of the system and the axial yoke force, respectively. The heave and pitch responses of the ship are presented in Figs.3.6 and 3.7. Comparisons between the predictions and the measurements show a reasonable agreement.

It can be noted that the harmonic wave forces acting on the coupled system are calculated in two different ways for 1-DOF and 4-DOF systems. In the latter, the origin of the system is at the centre of the ship, therefore the force calculation procedure

explained in Chapter 2 Section 2.2.3 could be used. On the other hand, wave forces on the tower could be calculated by taking into account the distance between the centre of the tower and the origin. In the case of the 1-DOF system, the origin is placed at the centre of the tower. Therefore, the force calculation on the ship is performed by integrating the pressure and acceleration forces from the bow to the stern of the ship (see Fig.3.2).

Since the two mathematical models yield reasonably close results, the 1-DOF model may be found more suitable for further studies which will be dealt with in the following sections.

3.3 CALCULATION OF SHEAR FORCE AND BENDING MOMENT DISTRIBUTION ALONG THE SINGLE ARTICULATED TOWER WHEN IT IS COUPLED WITH A SHIP

The articulated tower is subjected to external forces due to waves and due to its motion. The in-phase and out-phase components of the mooring forces also act at the top of the tower. In designing such structures, the shear force and bending moment distribution along the column should be predicted. The large bending moments which are likely to occur at the middle of the tower should be calculated.

In Appendix A, the load, shear force and bending moment calculation procedure for the single articulated tower is described. The tower is divided into a number of differential elements. Wave and motion induced forces are calculated on each element. The shear forces are obtained by numerically integrating the structural load distributions. The bending moments are obtained by numerically integrating the shear force distributions. The shear force and bending moment distributions for a unit wave amplitude at wave frequencies of 0.4 rad/s and 1.0 rad/s are given in Figs.3.8 and 3.9, respectively.

The horizontal shear forces at the base joint are compared with the experimental values published by Snowden et al (1985) in Fig.3.10. Fig.3.11 shows a comparison

between the theoretical and experimental bending moment values at 49m. In general, the agreement between the theory and the experiment is satisfactory.

3.4 PARAMETRIC STUDIES

The parametric studies are performed by using the simplified 1-DOF motion equation for the coupled system.

Firstly, the effect of yoke length variation on the motion and structural responses of the system are examined (see Figs.3.12-3.14). The total wave exciting force acting on the coupled system is dependent of the distance between the ship and the tower. The changes in yoke length alter the total force acting on the system and in turn affect joint forces and the motion responses. The yoke length is varied between 37 and 57 metres. The change of yoke length shows no significant difference in surge response predictions as illustrated in Fig.3.12. It can be seen from Fig.3.13 that there is no significant change in the yoke force in the frequency range between 0.0 and 0.6 rad/s. Although larger variations are predicted when wave frequency becomes larger than 0.6 rad/s this region would have low wave energy and therefore would not have significant importance from the point of view of maximum design stress. However, large variations on yoke force occurring in the range between 0.6 to 1.0 rad/s should be considered for fatigue life. The shear force variation at the base joint shows the same trend as the axial yoke forces (see Fig.3.14). The smaller the yoke length larger the shear forces become at the joint.

Secondly, the effect of added mass variation on the motion and structural response values are examined. Since the acceleration force component of the surge force on the ship was calculated using an approximate method (see Chapter 2, Section 2.2.3) the sensitivity of yoke forces and surge responses of the coupled system to the acceleration forces is studied by altering the added mass of the ship. It is assumed that the ship added mass is 5, 10 and 15% of the ship's displacement. Fig.3.15 shows that the effect of added mass variation on surge response is not significant. It is predicted that the three-fold increase in the added mass reveals a 30% increase in yoke forces and in shear forces at the higher frequency range as shown in Figs.3.16 and Fig.3.17.

As was discussed in Section 3.2.3, the viscous damping on the articulated tower is calculated using the drag coefficient experimentally measured for the circular cylinders. In order to examine the effect of different drag coefficients on the motion and structural response of the coupled system, three different C_D coefficients are considered. Figs.3.18-3.20 show that the motion and structural response values do not vary significantly.

Finally, the effect of water depth on the motion and structural response of the system is investigated. Figs.3.21 and 3.22 shows that an increase in water depth from 138m to 178m (about 28% increase) reveals very little increase in surge motion response values. The yoke forces increase by 2% as the water depth increases. On the other hand, the shear forces at the base joint decrease slightly as the water depth increases (see Fig.3.23). It can be seen from Fig.3.24 that the natural frequency of the system is not sensitive to changes of water depth.

3.5 EFFECTS OF STEADY FORCES ON COUPLED SYSTEM

In this section, the steady surge response of the coupled system due to steady wind and current forces as well as second-order wave effects are considered. The steady axial yoke forces due to various environmental effects are compared.

The steady angular response due to static loading can be obtained by the following expression

$$\theta_{MEAN} = \frac{M_{MEAN}}{K_\theta} \tag{3.22}$$

where M_{MEAN} is the moment of the steady forces w.r.t. the articulation point and K_θ is the restoring coefficient due to the tower buoyancy.

The steady forces on the system due to current are calculated by employing the current profile given in Eq.(2.51). Eqs.(2.52) and (2.53) are used to determine the

current forces on the tower and on the ship, respectively. The C_D value for the vertical cylinder is chosen as 1.0 for steady flow.

The steady forces on the system due to the wind are calculated by considering a wind profile given in Eq.(2.40). The mean wind force is then determined from Eq.(2.43). The drag coefficients for the ship are obtained by making use of OCIMF(1977)'s data for tankers.

In addition to the steady wind and current forces on the system the steady component of second-order forces occurs in irregular seas. This force is proportional to the wave amplitude square. The steady drift force on the circular cylinder in irregular seas was given by Pinkster(1974) as follows (see also Eq.(2.28))

$$\tilde{F}_d = \rho g D \int_0^\infty S_\zeta(\omega) R^2(\omega) d\omega \tag{3.23}$$

where $S_\zeta(\omega)$ is the wave amplitude spectrum and $R(\omega)$ is the drift force coefficient.

The steady drift force on the ship can be calculated by replacing the value D with B (breadth of ship) and using the appropriate drift force coefficients. For the application presented in this section, a normalized form of Eq.(2.18) is used to calculate the drift force coefficient of the vertical cylinder. Kwon's formula(see Eq.(2.22)) is employed to calculate the drift force coefficient for the ship.

The steady surge response of the coupled system due to steady wind and current forces as well as second-order wave effects are shown in Fig.3.25. It is assumed that the wind does not effect the current speed. Therefore, the surge response values due to current are the same along the wind velocity range considered here. Fig.3.25 also shows that the static surge due to second order forces has the largest value. On the other hand, the static off-set due to current forces is comparatively high. Fig.3.26 shows the steady yoke forces for different wind velocities. It can be noted that the steady yoke forces due

to current are as large as the yoke forces due to oscillatory first-order wave forces.

3.6 EFFECTS OF DYNAMIC FORCES ON COUPLED SYSTEM

In this section, dynamic effects due to waves and wind on the coupled system surge response are considered.

The dynamic loads on the system consist of the three following components:

- loads due to irregular seas (first order waves),
- loads due to the gustiness of the wind field and
- loads due to second order wave forces.

The r.m.s. surge of the ship is calculated for the above dynamic loads. The configuration given in Fig.3.1 is considered. The dynamic response in irregular seas is determined by the Pierson-Moskowitz wave amplitude spectrum. The minimum range of the spectrum is 0.2 rad/s. Since the natural frequency of the 1-DOF system is 0.024 rad/s in surge mode of motion, the peak values of the surge transfer function are out of dominant wave energy range. This is not the case for the spectrum of the second order wave forces (see Fig.3.27). The peak of the surge transfer function is in the higher range of the second-order wave force spectrum. The second-order force spectrum of the coupled system is determined by simply adding the force spectrum of the ship to the force spectrum of the articulated tower. The latter force spectrum is very small in comparison with the former one as shown in Fig.3.27.

The spectrum of the motion response can be written as follows

$$S_M(\omega) = (1 / K_\theta)\, S_F(\omega)\, Q \tag{3.24}$$

where $S_F(\omega)$ is the second-order force spectrum which is given in Eq.(2.31); K_θ, the stiffness coefficient and Q, the magnification factor which is given by,

$$Q = \frac{1}{\sqrt{((1-r^2)^2 + (2\zeta r)^2)}} \quad \text{and } r=\omega/\omega_n.$$

where ζ is the damping ratio and ω_n is the natural frequency of the system.

The integration of the response spectrum reveals the r.m.s. surge response. In order to compare the second-order force spectrum calculation methods, the r.m.s. surge response values were calculated using Pinkster's an Bowers' methods(see, Eqs.(2.31) and (2.32)). Fig.3.28 shows that the two methods yield similar surge response values up to a significant wave height of 9m. As the significant wave height increases Bowers' method gives larger values than Pinkster's. The prediction of the surge response due to second-order wave forces is compared with experimental measurements in Table 3.1. Comparisons between the predictions and the model tests show that both Pinkster's and Bowers' methods agree reasonably well with the experimental measurements in low sea states. As the significant wave height increases Pinkster's methods correlate better with the measurements (see Table 3.1).

The calculation procedure for the response spectra due to wind can be written as follows

$$R_S(f) = S_W(f)\left[\left(TF^2_{SHIP}\,\aleph^2_{SHIP}\right) + \left(TF^2_{TOWER}\,\aleph^2_{TOWER}\right)\right] \tag{3.25}$$

where

$$TF_{SHIP} = \rho_a C_{D,\,SHIP}\, A_{P,\,SHIP}\, \bar{V}\, d_{yoke} \frac{Q}{K_\theta}$$

$$TF_{TOWER} = \rho_a C_{D,\,TOWER}\, A_{P,\,TOWER}\, \bar{V}\, d_{yoke} \frac{Q}{K_\theta}$$

in which, d_{yoke} is the moment arm for the wind force; $A_{P,\,TOWER}$, air projection area

for the part of the tower above S.W.L.; $A_{P,SHIP}$ air projection area for the ship $C_{D,TOWER}$ and $C_{D,SHIP}$ are the drag coefficients in air for the tower and the ship, respectively. Other terms are defined in Section 2.5.

R.m.s. angular response could then be found by using the following expression:

$$\theta_{rms} = [\int_0^\infty R_S(f)df]^{0.5} \tag{3.26}$$

The r.m.s. surge response due to dynamic wind is calculated using three wind spectra given in Eqs.(2.45)-(2.47). The frequencies of the wind spectra range from very low values and continue with a broad band character. The three wind spectra reveal different r.m.s. surge values due to the difference in their shape (see Table 3.2).

The r.m.s. surge responses of the coupled system due to first order wave spectrum as well as second-order forces and dynamic wind spectra are compared in Table 3.2. As can be seen from Table 3.2 the surge motions of the coupled system due to dynamic wind forces are as significant as the surge motion due to first order wave forces. Table 3.2 also shows that the damping factor is quite an important factor in determining the motion responses.

3.7 EFFECT OF SHORT-CRESTED WAVES ON COUPLED SYSTEM

Utilizing the uni-directional waves in designing compliant structures is a conservative approach (see Tiegen(1983) and Standing et al (1986)). This will result in predicting of larger motions and forces than using a more realistic short-crested sea. In this section, an attempt is made first to investigate the directional sensitivity of the surge and sway motions as well as the yoke forces of the coupled system, and secondly to apply different energy spreading functions to predict responses in short-crested waves.

The 1-DOF motion equation for the coupled single articulated tower and ship system is used in the motion analysis in short-crested waves. Analogous to Eq.(3.1) the following equations can be written for the angular motion of the coupled system in surge and sway direction as follows

$$I_\theta \ddot{\theta} + B_\theta \dot{\theta} + K_\theta \theta = M_{T\theta} \tag{3.27}$$

$$I_\eta \ddot{\eta} + B_\eta \dot{\eta} + K_\eta \eta = M_{T\eta} \tag{3.28}$$

where I_θ is the total mass moment of inertia of the coupled system in surge direction; B_θ, the damping coefficient of the coupled system in surge direction; K_θ, the stiffness coefficient; $M_{T\theta}$, the moment of the external forces in surge direction; I_η, the total mass moment of inertia of the coupled system in sway direction; B_η, the damping coefficient of the coupled system in sway direction; K_η, the stiffness coefficient and $M_{T\eta}$, the moment of the external forces in sway direction.

It is assumed that the wave height and motion responses are small so that the equations describing motions of fluid and the structure can be linearized. The forces and responses are assumed to be linearly proportional to wave height. The moments due to wave forces, $M_{T\theta}$ and $M_{T\eta}$, are calculated at one direction. The transfer functions are calculated at 15 degree intervals for the constant powers. The integrals are approximated by summation. The calculation procedure of the wave forces acting on a rectangular barge while taking into account arbitrary wave propagation angle are summarized in Appendix B. Wave induced forces on the articulated tower are calculated from Morison's formula under the assumption that the water particle kinematic remains unaffected by the presence of the ship. The added mass and damping coefficients for both structures are taken as constant values (e.i. independent of the wave frequency). This simplification procedure on the wave forces and on the hydrodynamic coefficients results in a considerable amount of time saving during the numerical calculations.

Figs.3.29 and 3.30 compare the excitation forces acting on the articulated tower-ship system. Different wave headings are used namely, 0, 30, and 60 degrees for the surging forces; 30, 60 and 90 degrees for the swaying forces. As is seen from Figs.3.29 and 3.30, the wave forces on the articulated column are rather low compared with the forces on the barge; but their magnitude is not insignificant.

In order to predict the response values in short-crested waves the response transfer functions in different propagation angles should be known.

Eqs.(3.27) and (3.28) are solved independently to calculate the surge and sway transfer functions for different wave propagation angles. Similarly, axial and shear forces on the yoke for different wave directions are calculated as described in Section 3.2.1, Eq.(3.7). Two dimensional and three dimensional representations of the motion and structural response values are shown in Figs.3.31-3.38. As was shown in Figs.3.31-3.38, the motion and structural response behaviour of the coupled system is directionally sensitive. After obtaining the transfer functions in different propagation angles, the directional response spectrum is then determined with the following equation

$$S_{DR}(\omega, \bar{\alpha}) = S(\omega) \int_{\alpha_{min}}^{\alpha_{max}} G_O \cos^{2s}\left(\frac{\alpha - \bar{\alpha}}{2}\right) [RAO\ (\omega, \alpha)]^2 d\alpha \qquad (3.29)$$

where S_{DR} is the directional response spectrum; α, the angle of the wave propagation; $\bar{\alpha}$, the principal angle of the wave propagation; and G_O, directional spreading function as described in Chapter 2, Eq.(2.38).

Eq.(3.29) is applied to the transfer function curves given in Figs.3.35-3.38 to predict significant surge and sway motions as well as axial and shear forces on the yoke. In these predictions the JONSWAP spectrum is adopted and directional spreading parameter, s is varied according to Eq.(2.39) and arbitrarily, independent of the wave frequency.

The results of these predictions are shown in Figs.3.39-3.42. These figures reveal that the motion and structural response calculations carried out in multi-directional waves gave significantly different values than those obtained in uni-directional waves. Maximum response values obtained in multi-directional seas are lower than the maximum values obtained in uni-directional seas. On the other hand, minimum response values obtained in short-crested waves are higher than the minimum response values obtained in uni-directional waves. It should also be noted that as the values of the directional spreading parameter increase, the response values approach those obtained using uni-directional waves.

3.8 CONCLUSIONS

The simple (1-DOF) and detailed (4-DOF) mathematical models developed to predict the motion response of the coupled articulated tower and ship system and the yoke forces under first-order wave excitation show a reasonably good correlation with each other and with the experimental measurements. Since the two mathematical models yield reasonably close results, the simple model may be found more suitable for preliminary design studies.

Parametric studies have shown that variations of yoke length have no significant effect on yoke forces and motion responses of the coupled articulated tower-ship system. The effect of various added mass values on the motion and structural response values were investigated. It has been found that added mass variation has an important impact on the response values at the higher frequency range. On the other hand, different drag coefficients have almost no effect on the response values. The motion and structural response values were found to be insensitive to water depth variations when the water depth increased from 138m to 178m.

It was found that the current force has the dominant effect on steady surge response of the system although the steady second-order forces may result in larger surge off-set where the wind velocity is greater than 18m/s.

The dynamic forces become important if the peak value of the spectrum is closer to the natural frequency of the system. The coupled articulated tower and ship system has the natural frequency of the order of 0.024 rad/s. Therefore, the effect of wind and second-order force spectrum can be considered very important for this type of compliant structure. R.m.s. surge responses of the system due to three wind spectra were calculated and presented in Table 3.2. It was found that the Davenport wind spectrum gives lower surge response values than the other two wind spectra. The magnitudes were very sensitive to the damping ratio.

Two methods were considered to calculate the second order force spectra; Pinkster's method and Bowers' method. Both methods gave the same r.m.s. surge values up to a significant wave height of 9m. Beyond that point, Bowers' method predicted larger values than Pinkster's.

The effect of directional spreading of waves on the motion and structural response of the coupled single articulated tower and ship system were investigated through different energy spreading assumptions. The motion and structural response predictions in multi-directional waves gave significantly different results from those obtained in uni-directional waves. Since maximum structural response values were about 20% ~ 25% lower than those predicted from uni-directional wave analysis it is believed that some savings in terms of structural weight may be achieved by introducing multi-directional wave analysis into design procedures. It can also be seen that multi-directional wave analysis gives more realistic results for fatigue calculations.

Table 3.1

Low Frequency Surge Response of Coupled System at Fig.(3.1) (r.m.s. values in metres)		
P-M Spectrum	Hs=10.0m Tz=12.0s	Hs=14.5m Tz=13.5s
Model Test (Snowden et al. 1985)	6.58	7.91
Prediction (Pinkster's Method)	5.58	9.17
Prediction (Bowers' Method)	6.29	12.51

Table 3.2

Surge Response of Coupled System at Fig.(3.1) (r.m.s. values in metres)				
Environmental Effects	Wind Velocity (m/s)†	ζ : damping factor 0.05	0.10	0.15
First Order Wave Effect in Irregular Seas (P-M Spectrum)	20	0.30	0.30	0.30
	30	2.06	2.06	2.06
	40	5.40	5.40	5.40
Second Order Wave Effect in Irregular Seas (P-M Spectrum)	20	6.10	4.45	3.36
	30	13.32	9.72	7.33
	40	18.79	13.71	10.36
Dynamic Wind (Davenport Spectrum)	20	0.39	0.29	0.23
	30	0.61	0.46	0.35
	40	0.82	0.61	0.47
Dynamic Wind (Harris Spectrum)	20	0.63	0.47	0.36
	30	1.16	0.87	0.67
	40	1.78	1.34	1.03
Dynamic Wind (Kaimal Spectrum)	20	0.50	0.38	0.29
	30	0.95	0.71	0.55
	40	1.48	1.11	0.86
† wind velocity at 10m above the water surface				

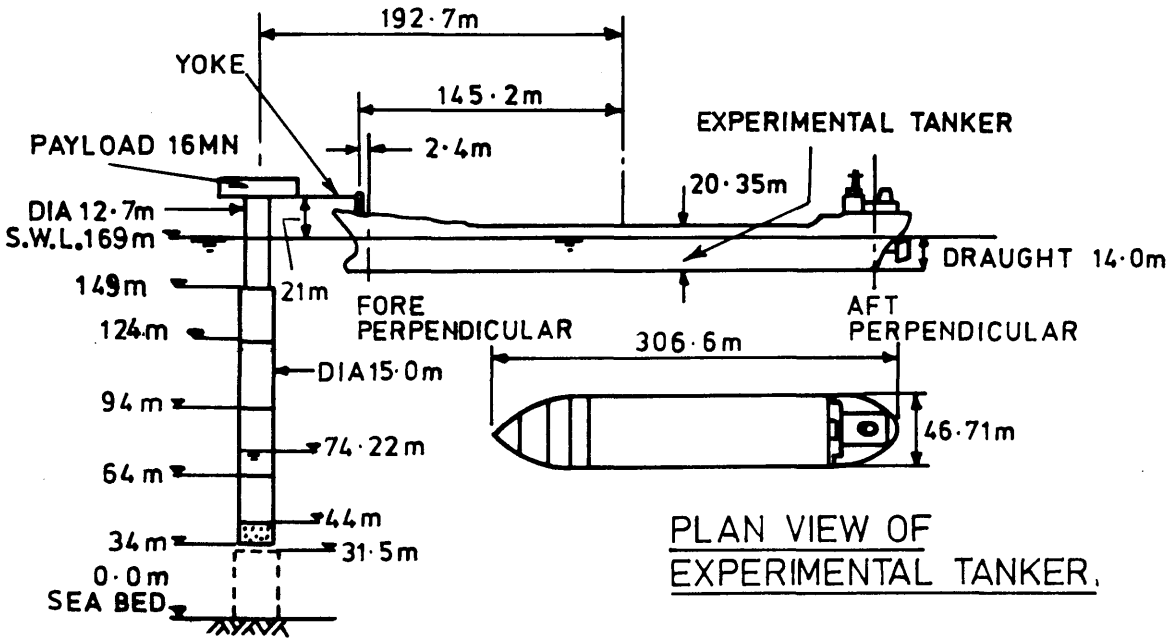

Fig.3.1 Articulated tower and ship configuration (Snowden et al,1985)

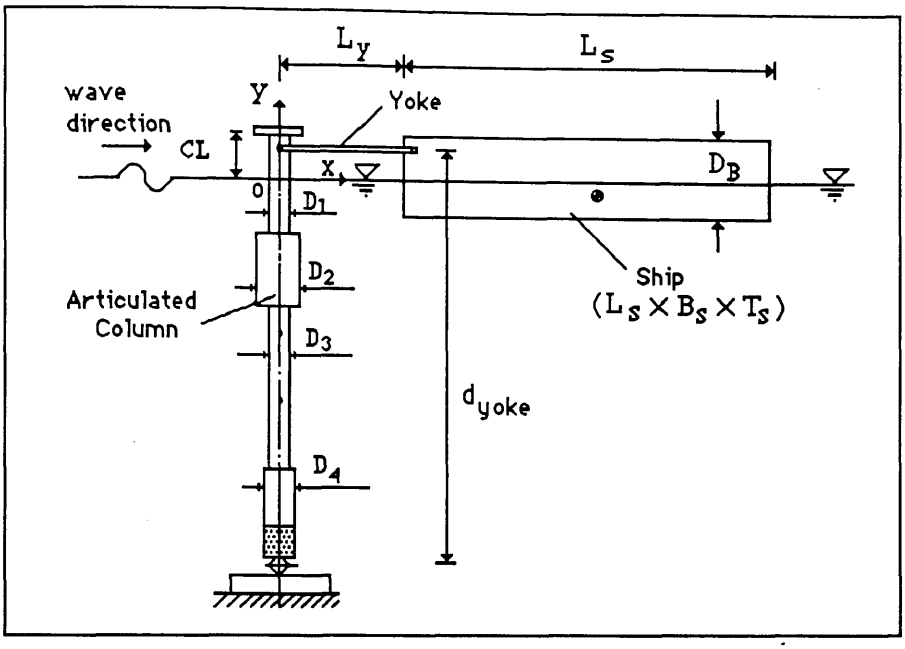

Fig.3.2 Coordinates of 1-DOF system

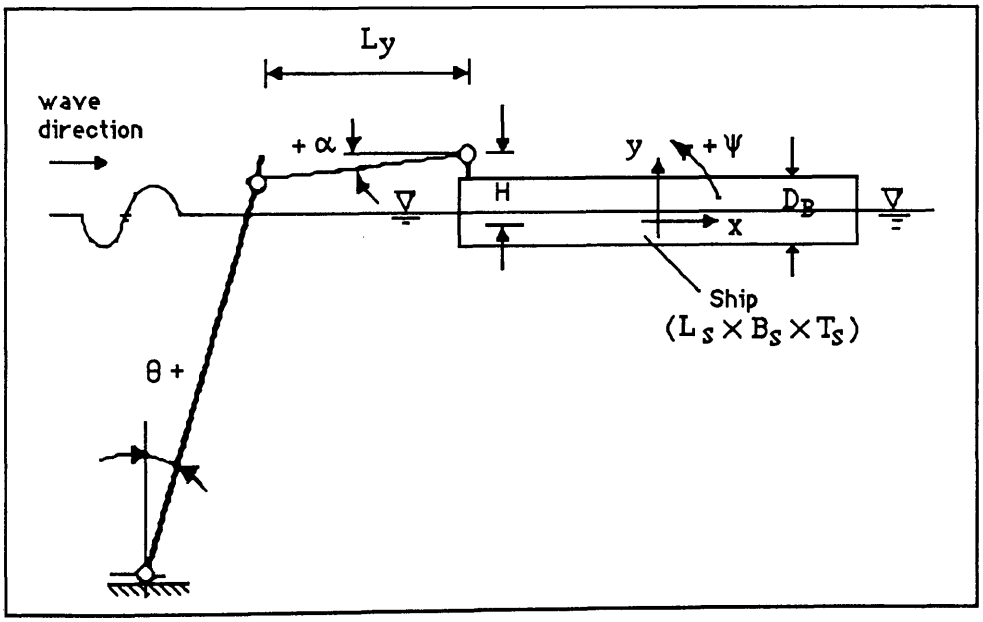

Fig.3.3 Coordinates of 4-DOF system

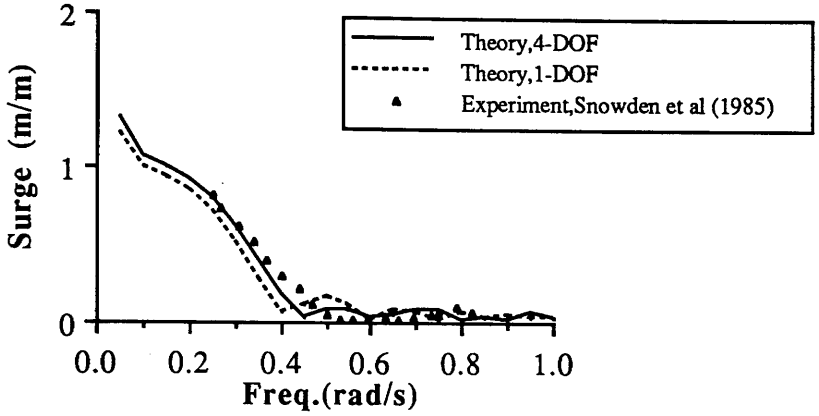

Fig.3.4 Comparison on ship surge

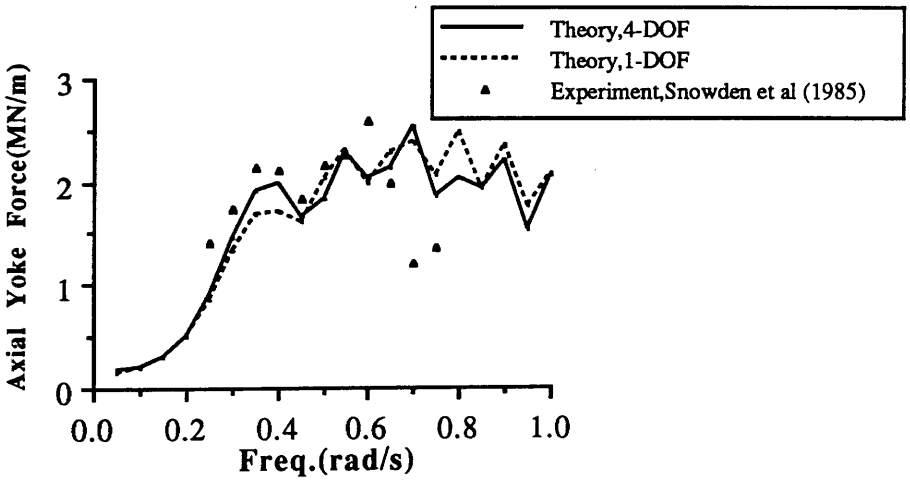

Fig.3.5 Comparison on axial yoke force

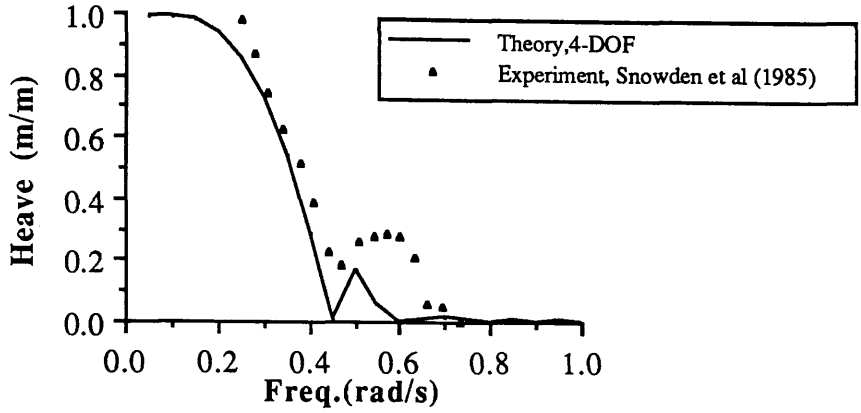

Fig.3.6 Comparison on ship heave

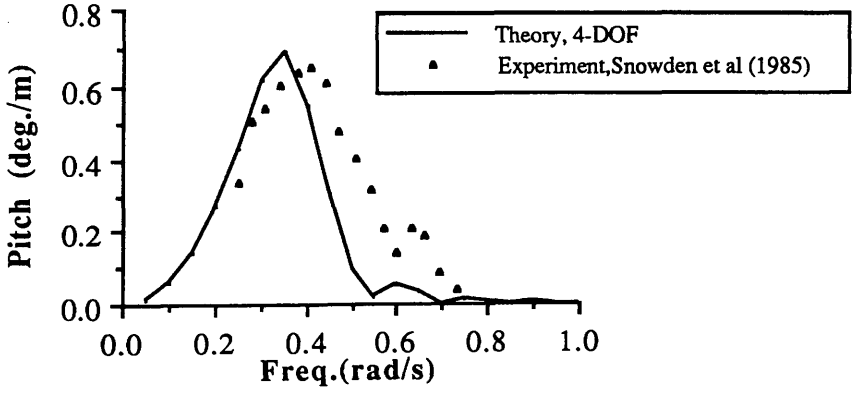

Fig.3.7 Comparison on ship pitch

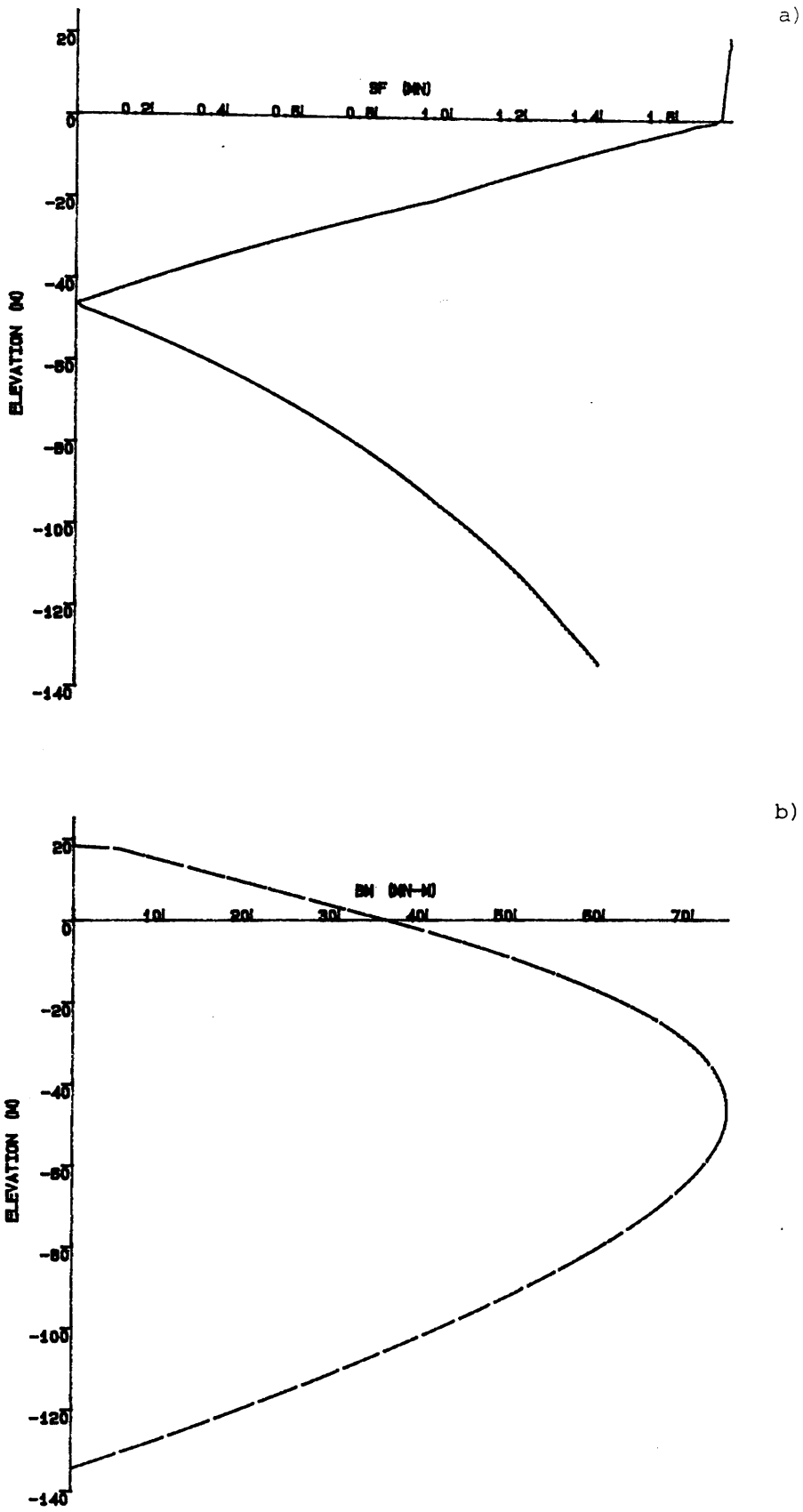

Fig.3.8 Shear force and bending moment distribution along tower in presence of ship.

Freq.= 0.4 rad/s; ζ_a = 1m, a) Shear force b)Bending moment.

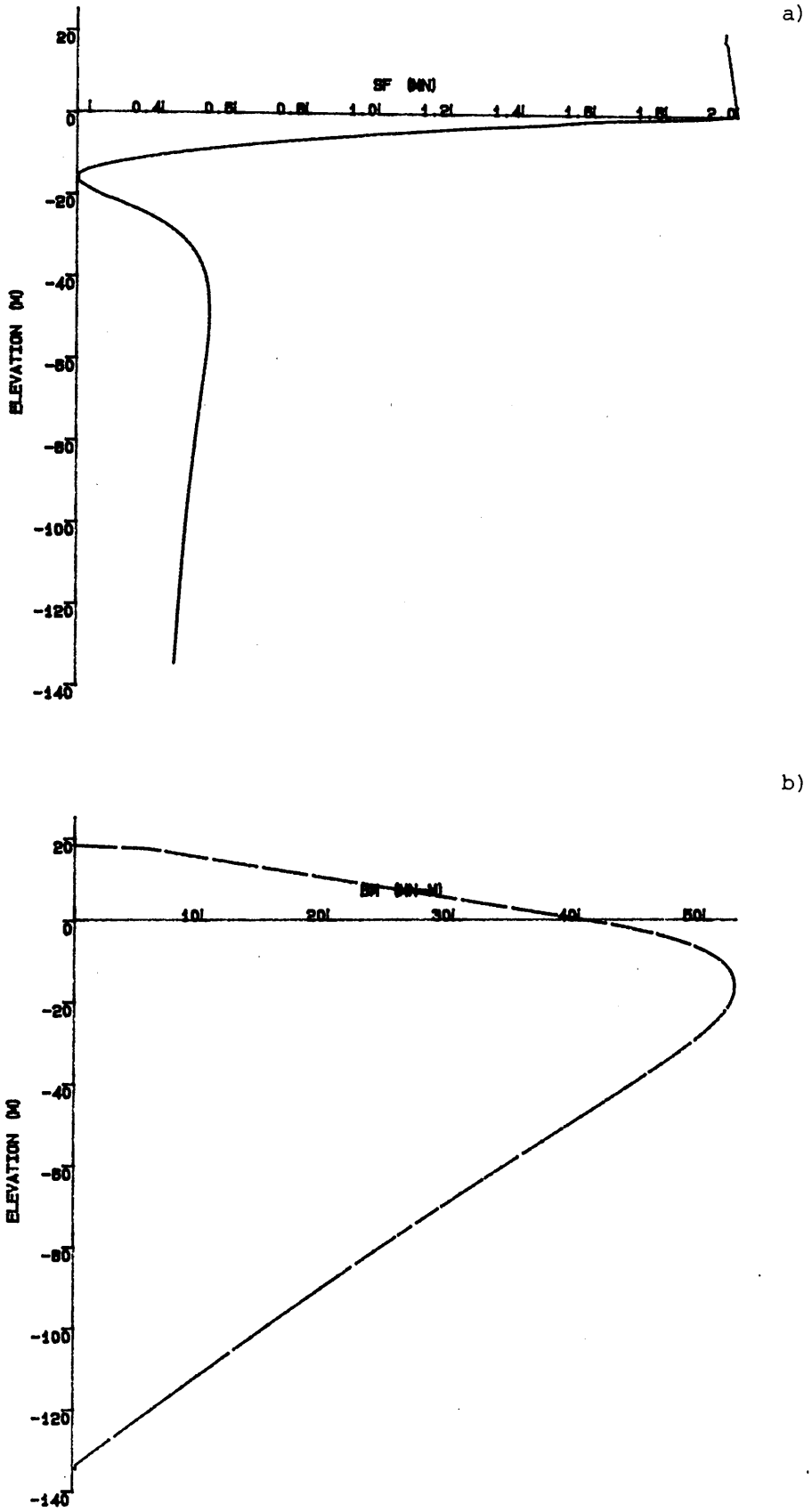

Fig.3.9 Shear force and bending moment distribution along tower in presence of ship.

Freq.= 1.0 rad/s; ζ_a = 1m, a) Shear force b)Bending moment.

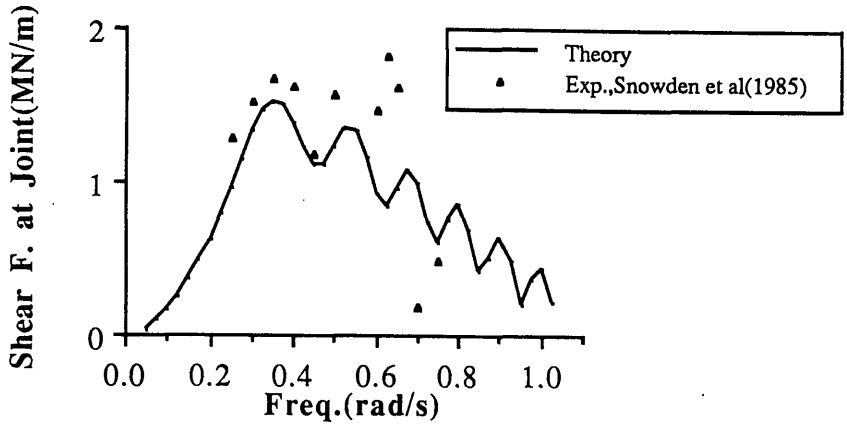

Fig.3.10 Comparison of horizontal shear force at base joint

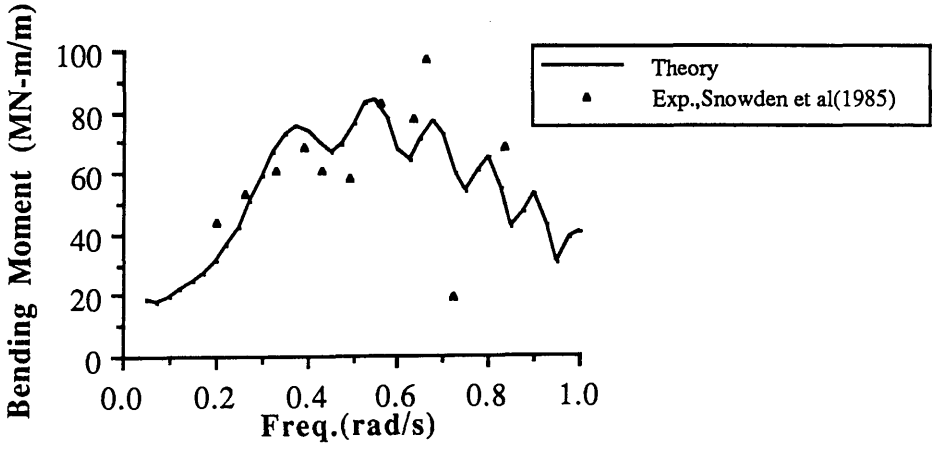

Fig.3.11 Comparison of bending moment at 49m below SWL

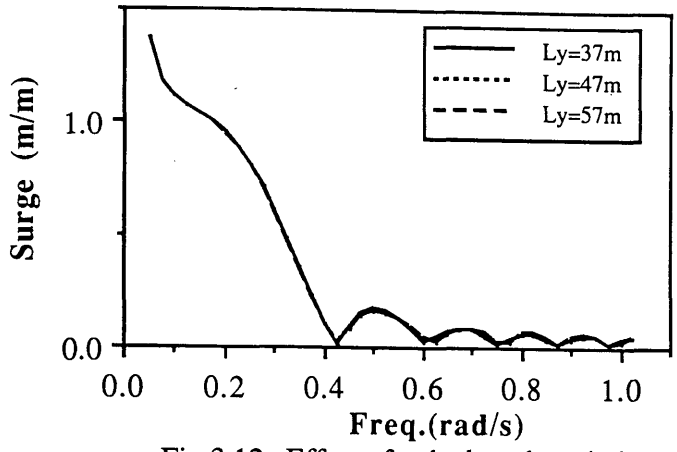

Fig.3.12 Effect of yoke length variation on surge motion response of ship

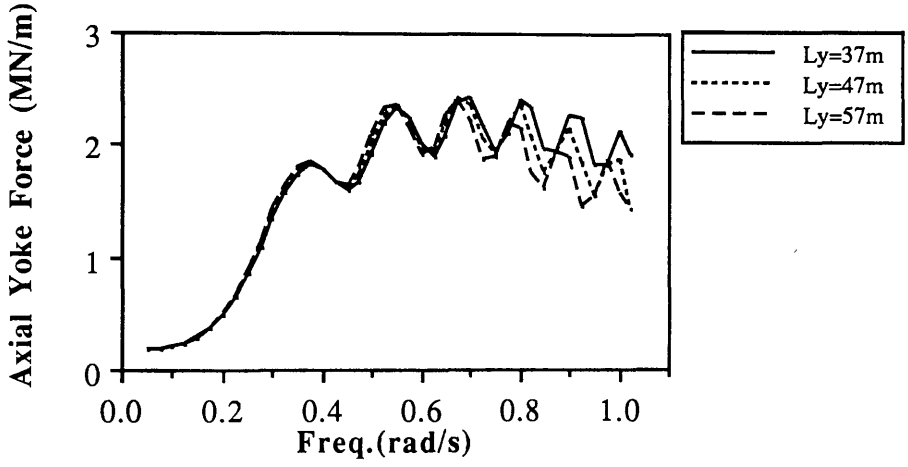

Fig.3.13 Effect of yoke length variation on axial yoke force

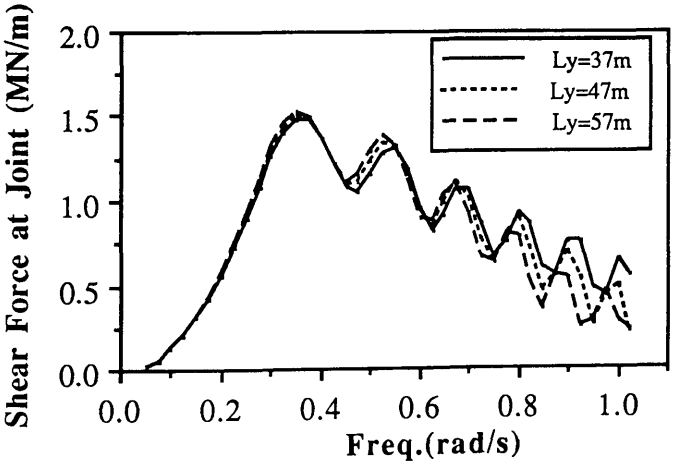

Fig.3.14 Effect of yoke length variation on shear force at base joint

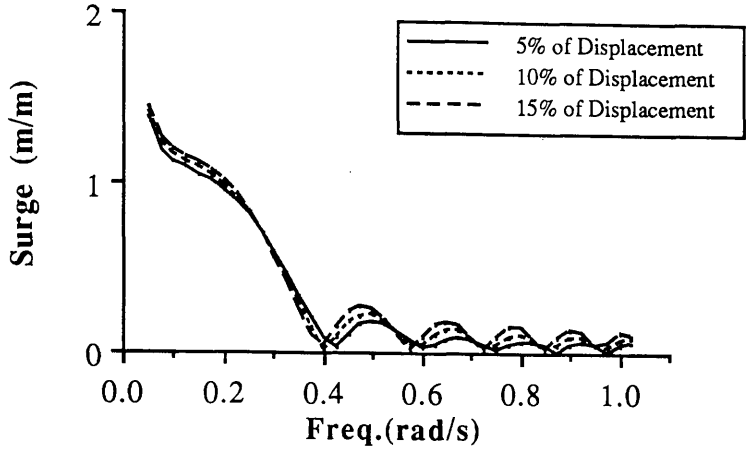

Fig.3.15 Effect of added mass variation on surge motion response of ship

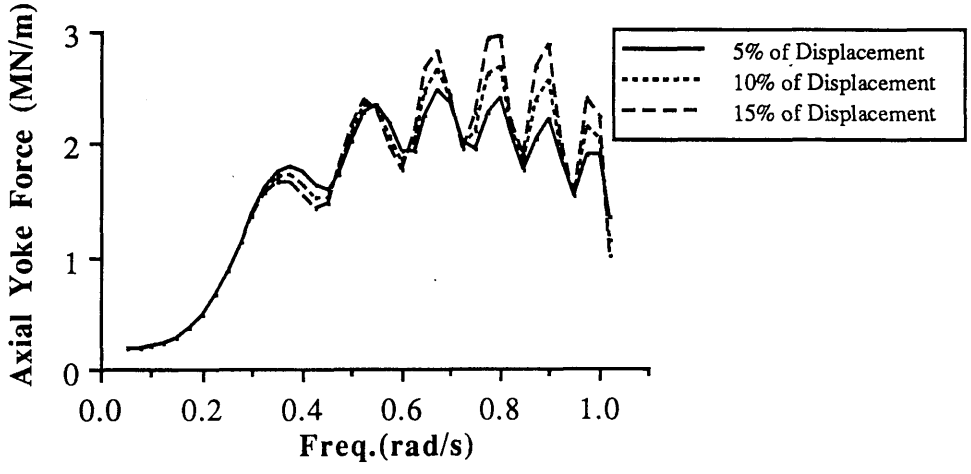

Fig.3.16 Effect of added mass variation on axial yoke force

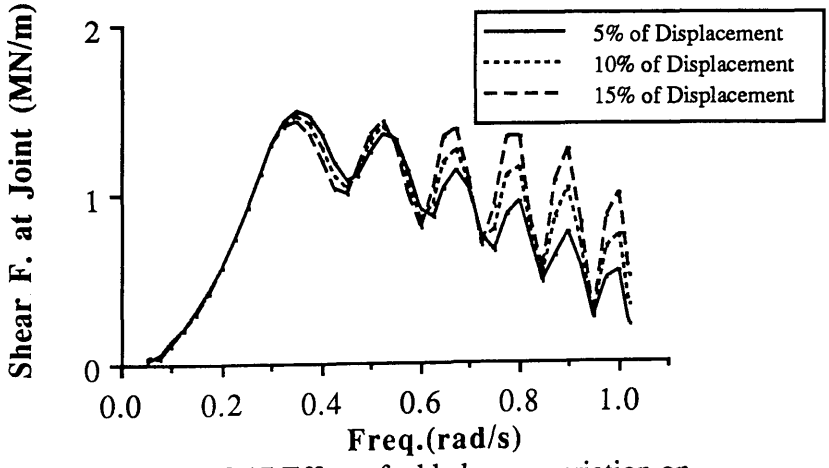

Fig.3.17 Effect of added mass variation on shear force at base joint

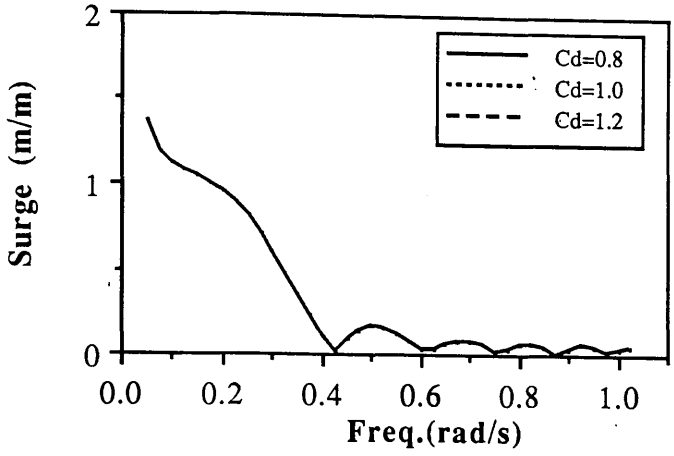

Fig.3.18 Effect of drag coefficient variation on surge motion response of ship

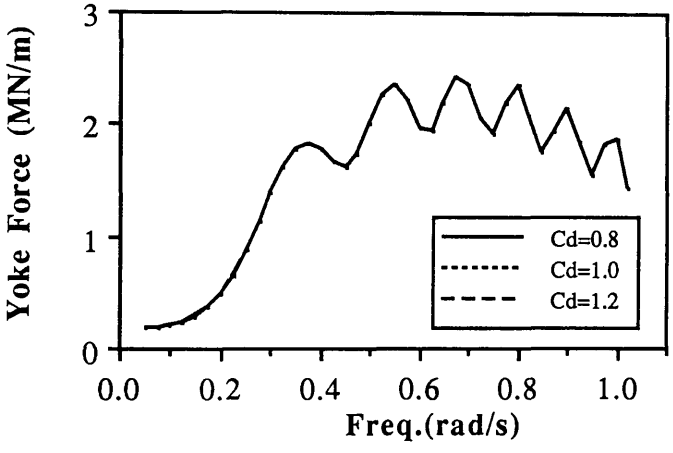

Fig.3.19 Effect of drag coefficient variation on axial yoke force

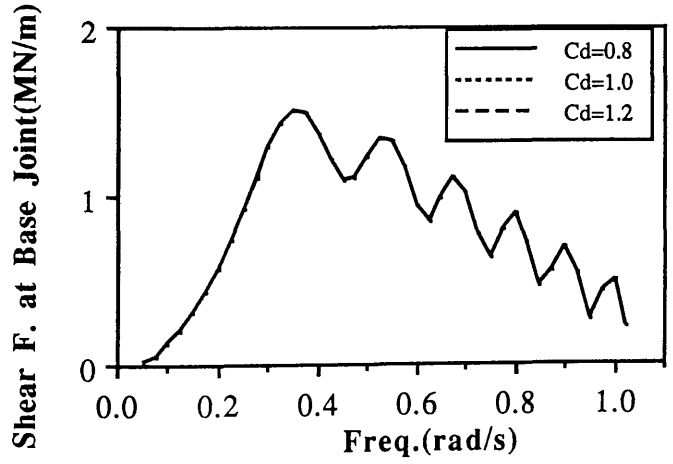

Fig.3.20 Effect of drag coefficient variation on shear force at base joint

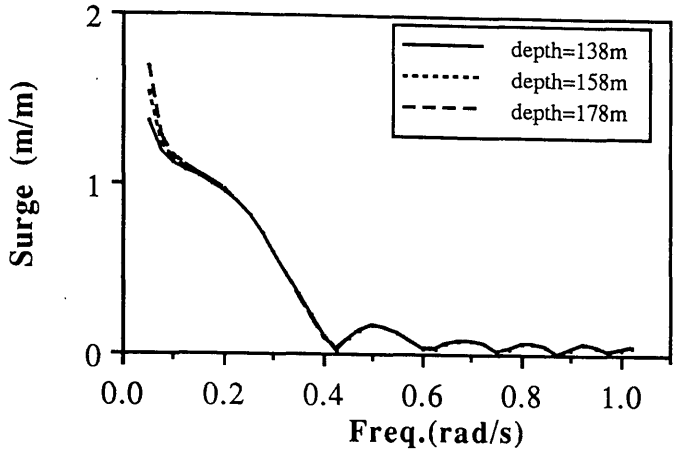

Fig.3.21 Effect of water depth variation on surge motion response of ship

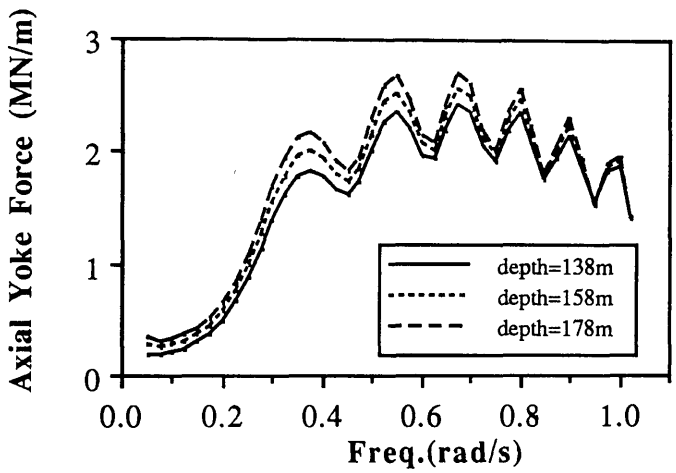

Fig.3.22 Effect of water depth variation on axial yoke force

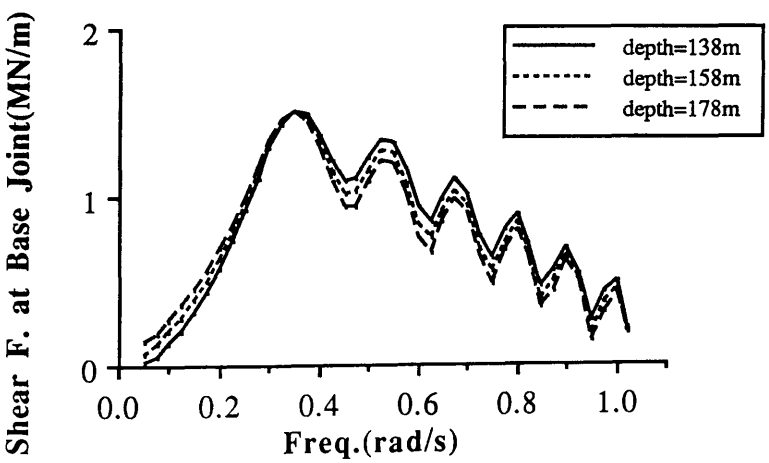

Fig.3.23 Effect of water depth variation on shear force at base joint

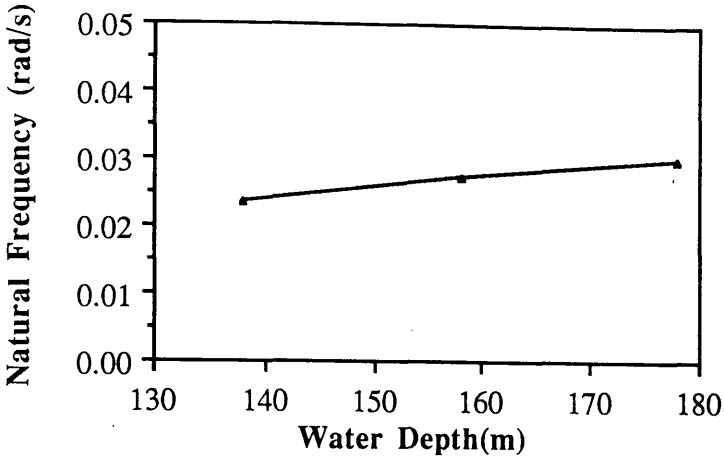

Fig.3.24 Effect of water depth variation on natural frequency of coupled system

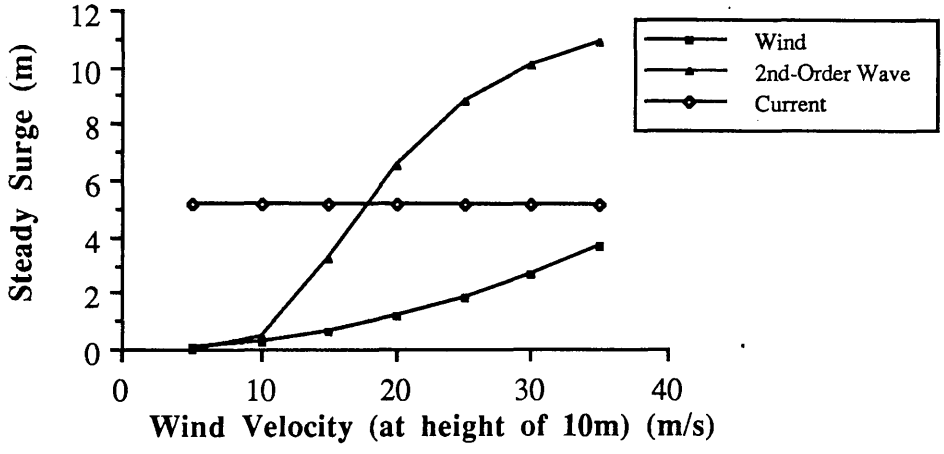

Fig.3.25 Steady surge response due to environmental effects

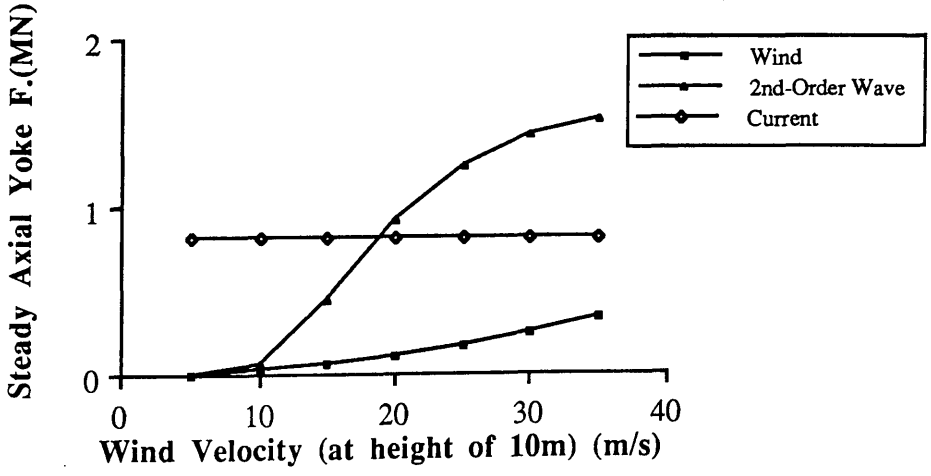

Fig.3.26 Steady yoke force due to environmental effects

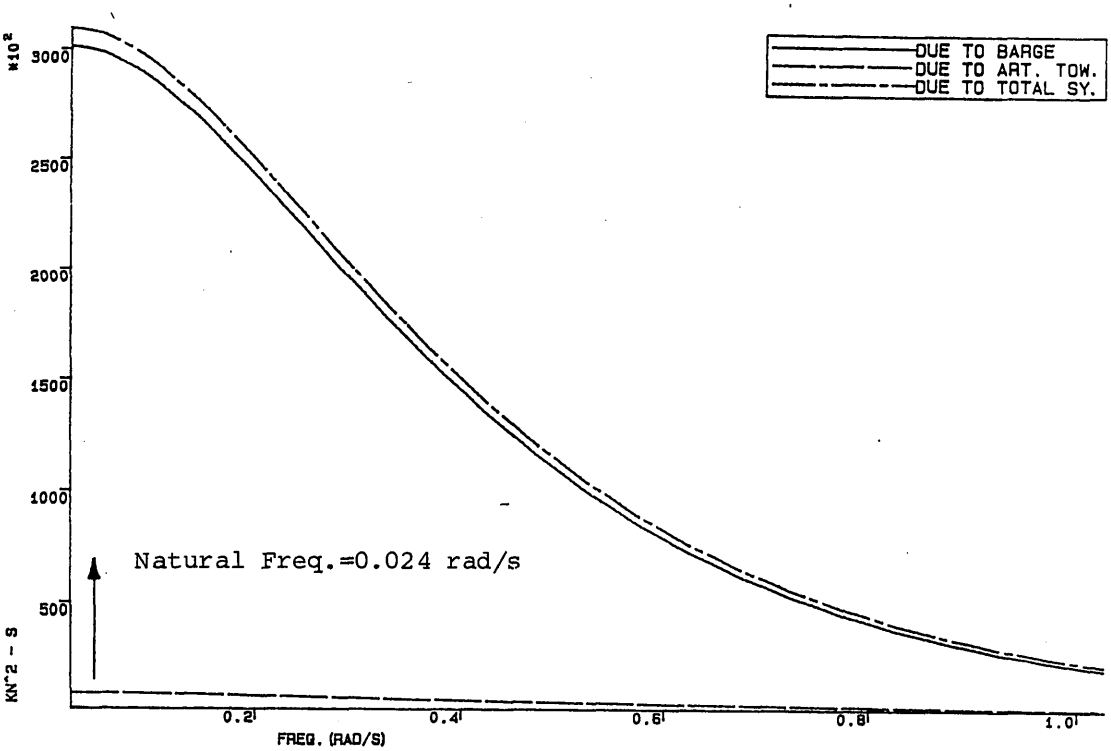

Fig.3.27 Second-order force spectrum for coupled articulated tower-ship system

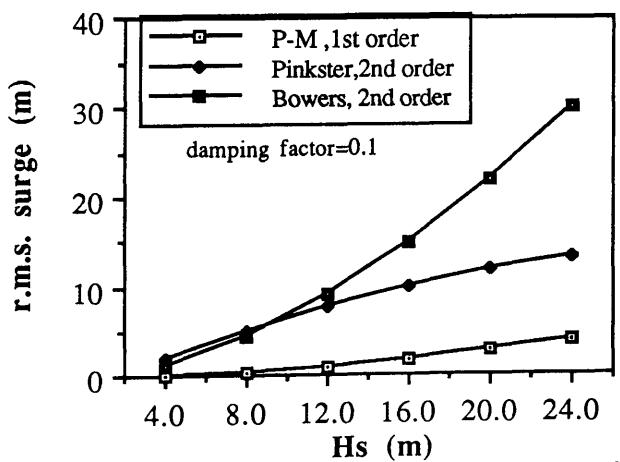

Fig.3.28 Comparison of r.m.s. surge motion response in irregular waves

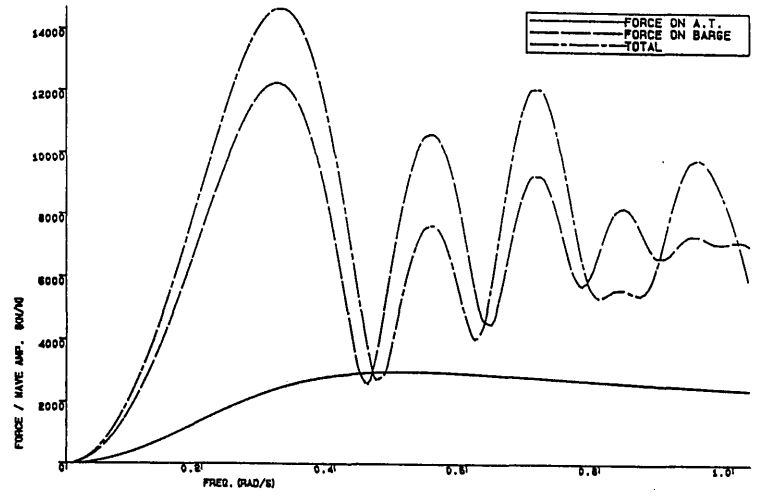

HEADING ANGLE = 0 DEGREES
TEL CONFIGURATION

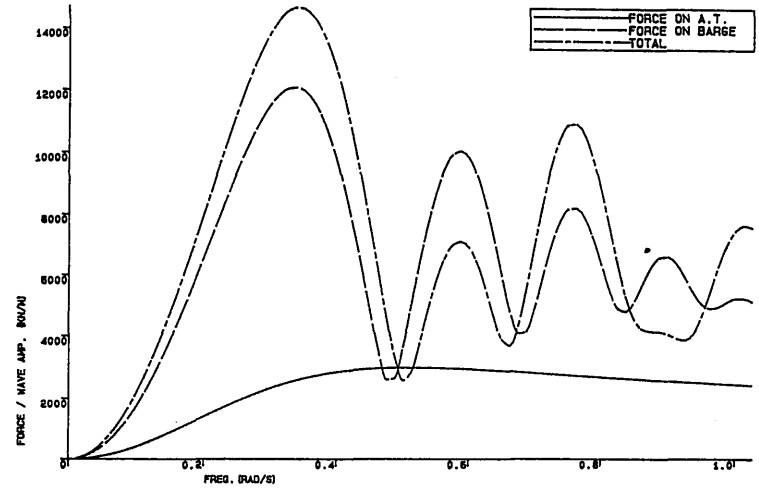

HEADING ANGLE = 30 DEGREES
TEL CONFIGURATION

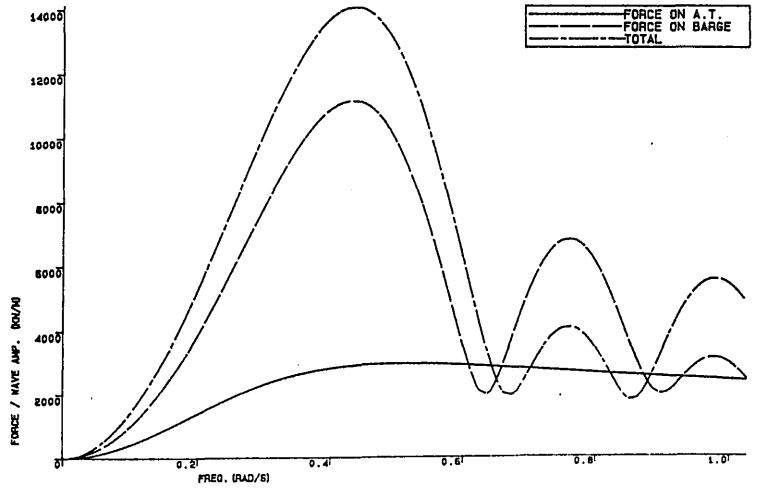

HEADING ANGLE = 60 DEGREES
WAVE INDUCED SURGE FORCES ON THE COUPLED SYSTEM

Fig.3.29 Wave induced surge forces on coupled system

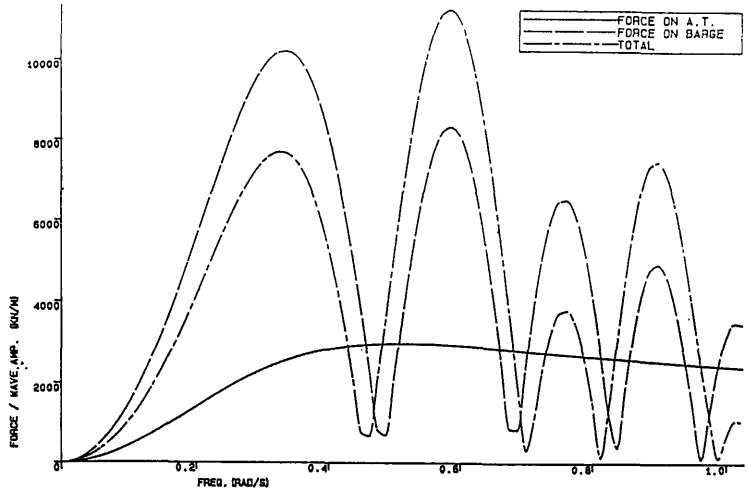

HEADING ANGLE = 30 DEGREES
TEL CONFIGURATION

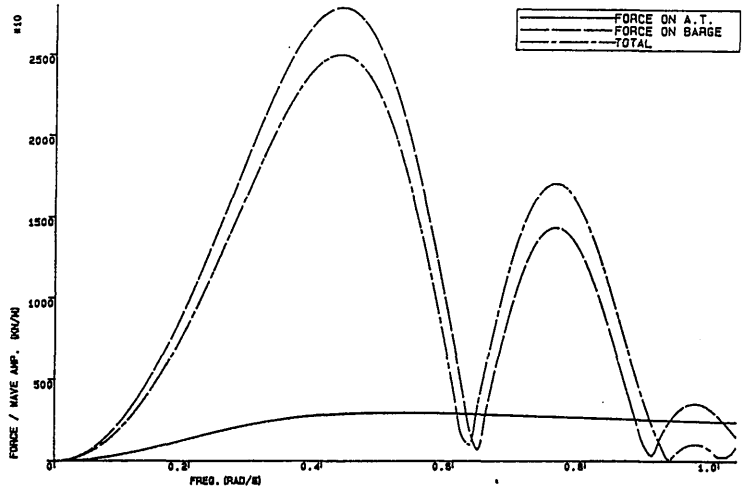

HEADING ANGLE = 60 DEGREES
TEL CONFIGURATION

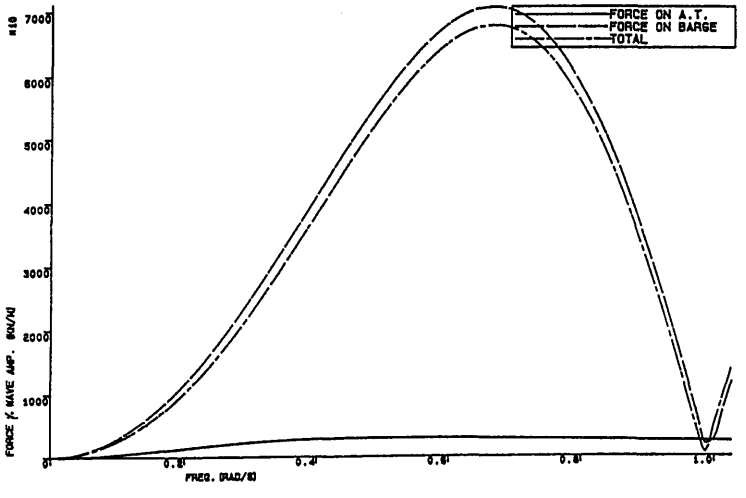

HEADING ANGLE = 90 DEGREES

Fig.3.30 Wave induced sway forces on coupled system

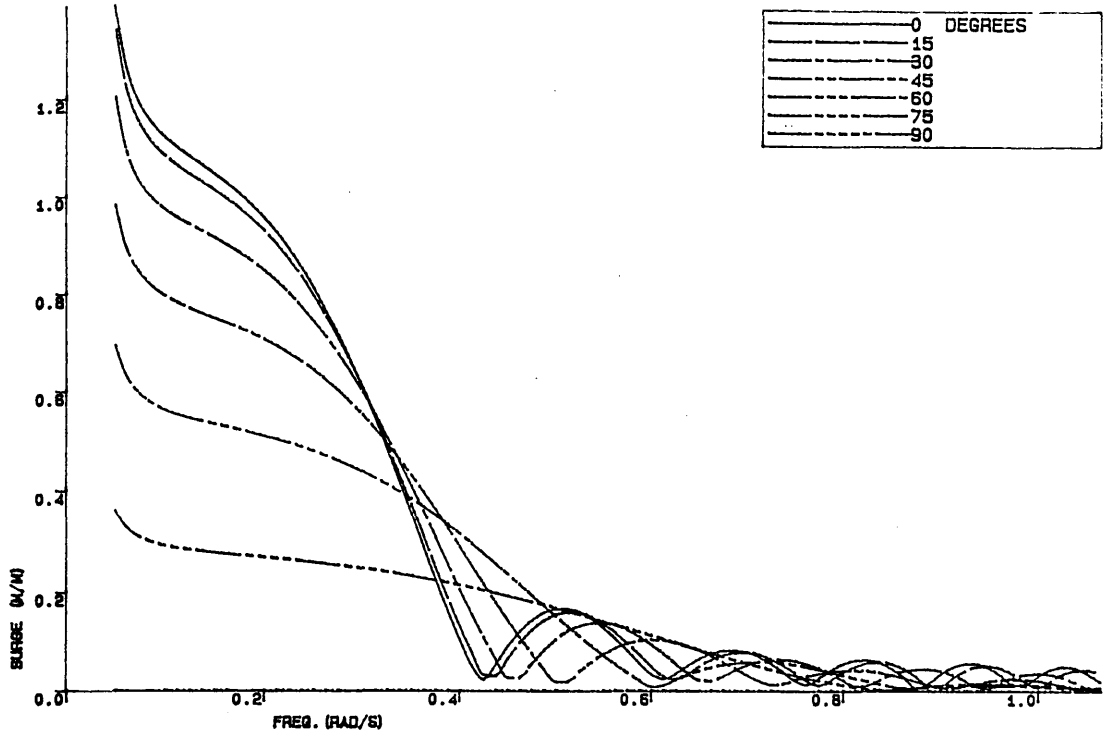

Fig.3.31 Surge transfer function for different wave heading angles

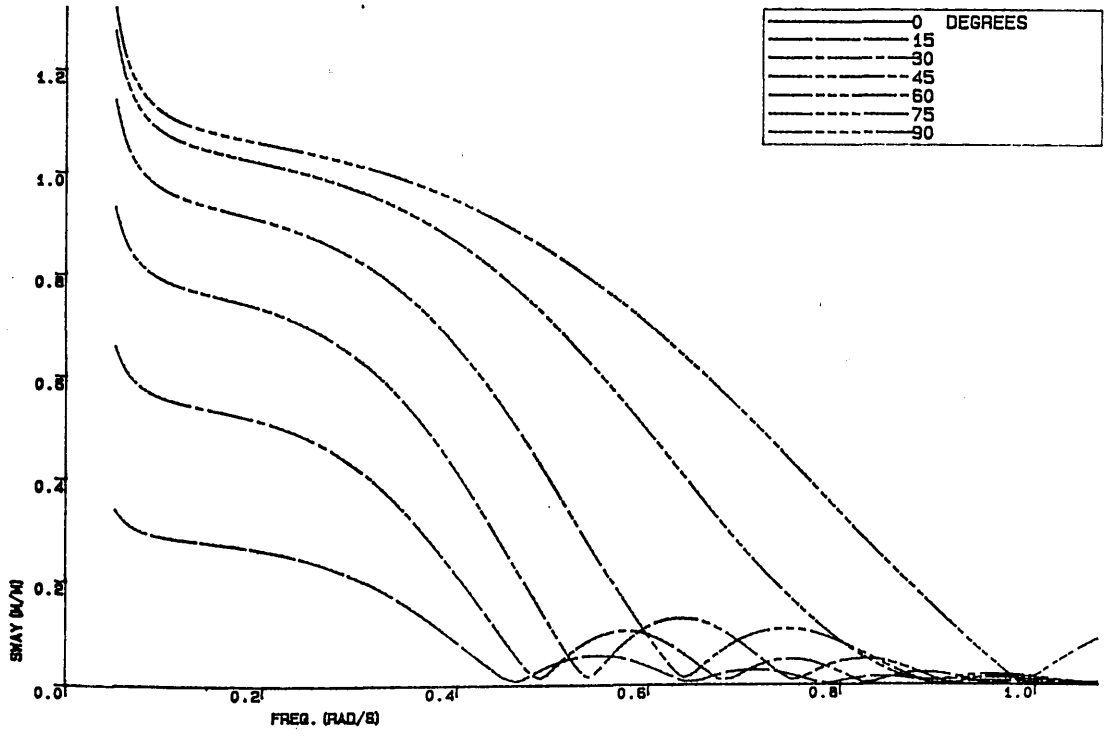

Fig.3.32 Sway transfer function for different wave heading angles

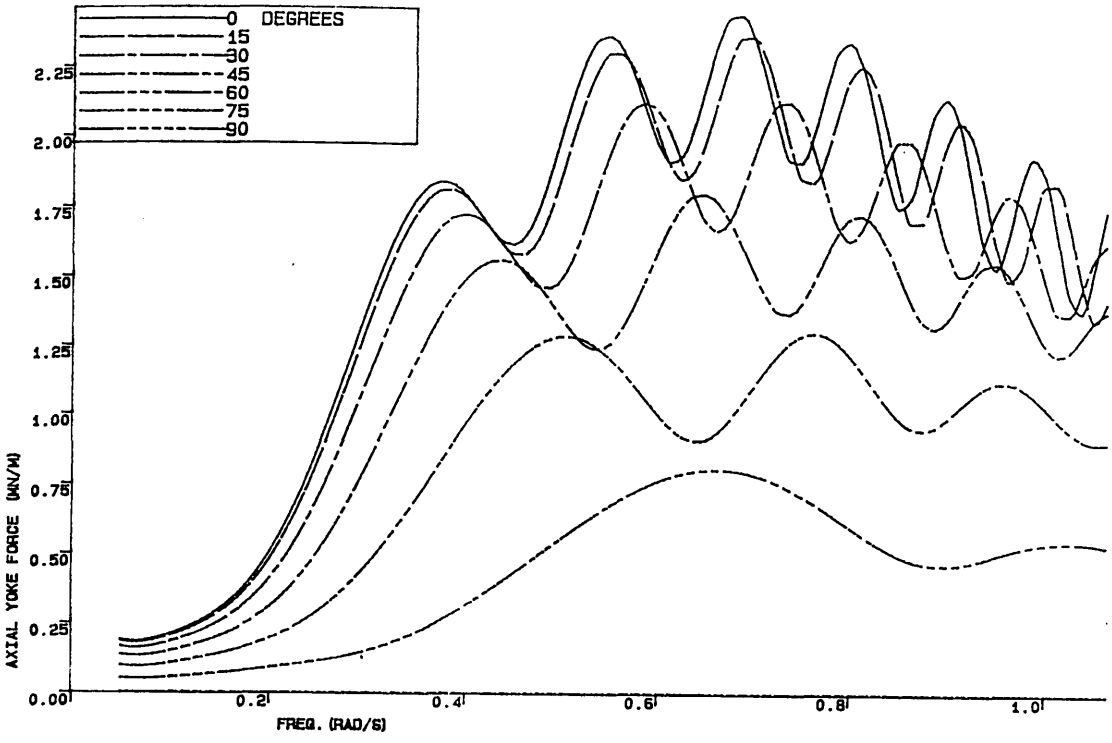

Fig.3.33 Axial yoke force for different wave heading angles

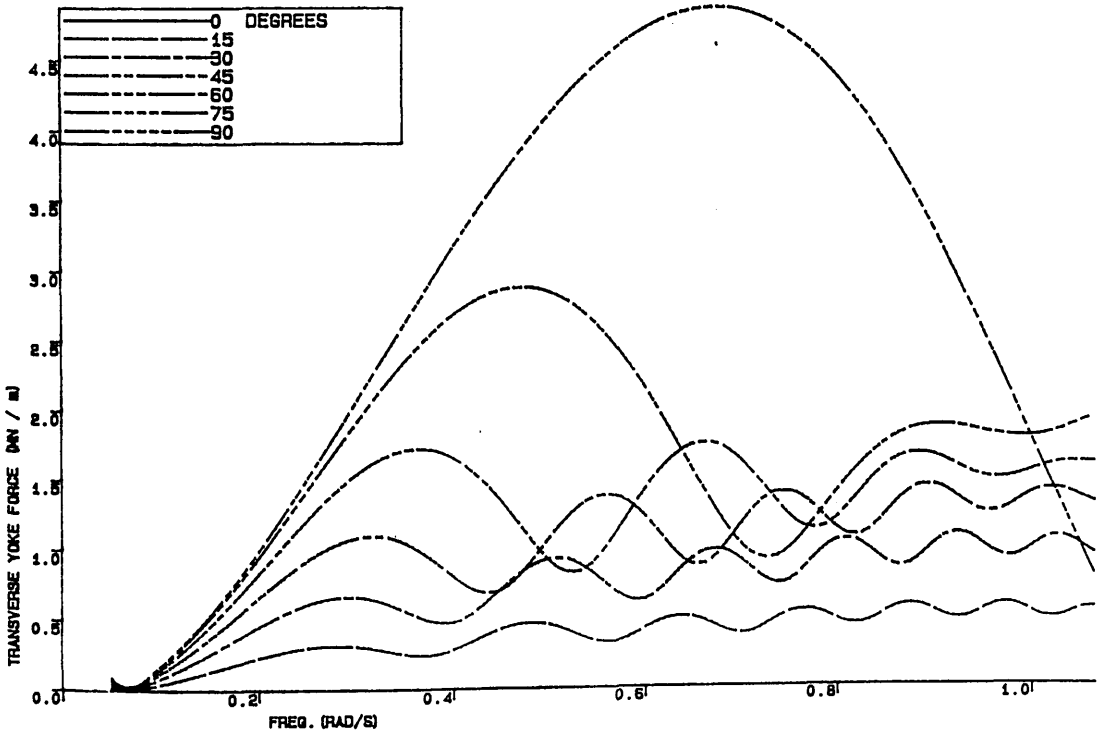

Fig.3.34 Transverse yoke force for different wave heading angles

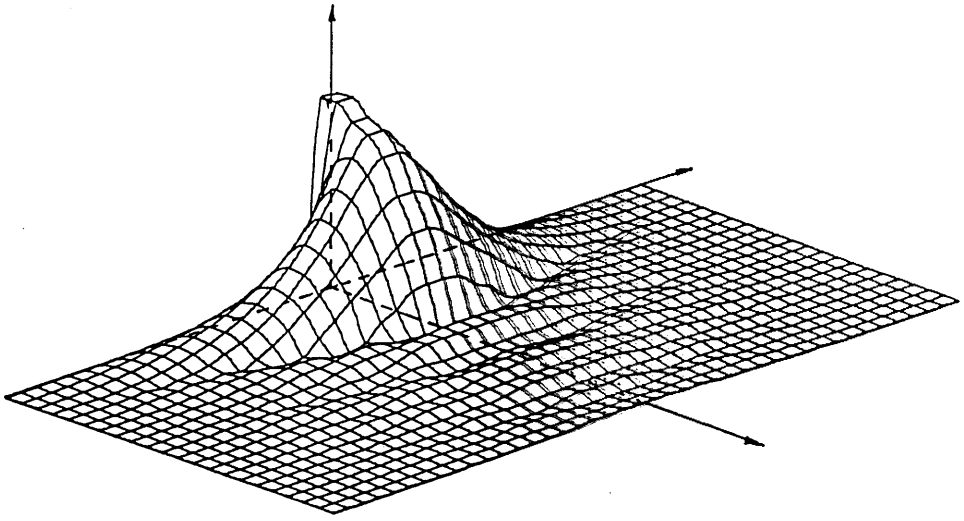

Fig.3.35 Directional surge transfer function

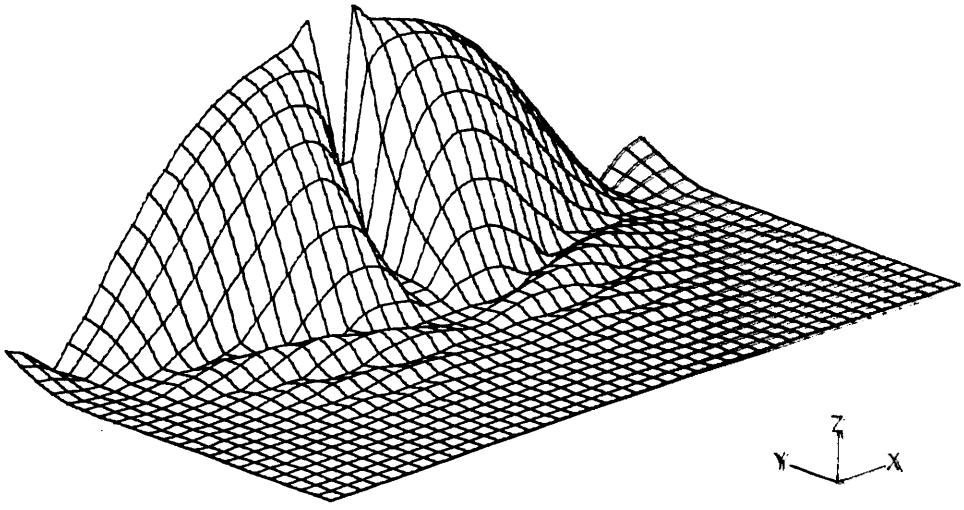

Fig.3.36 Directional sway transfer function

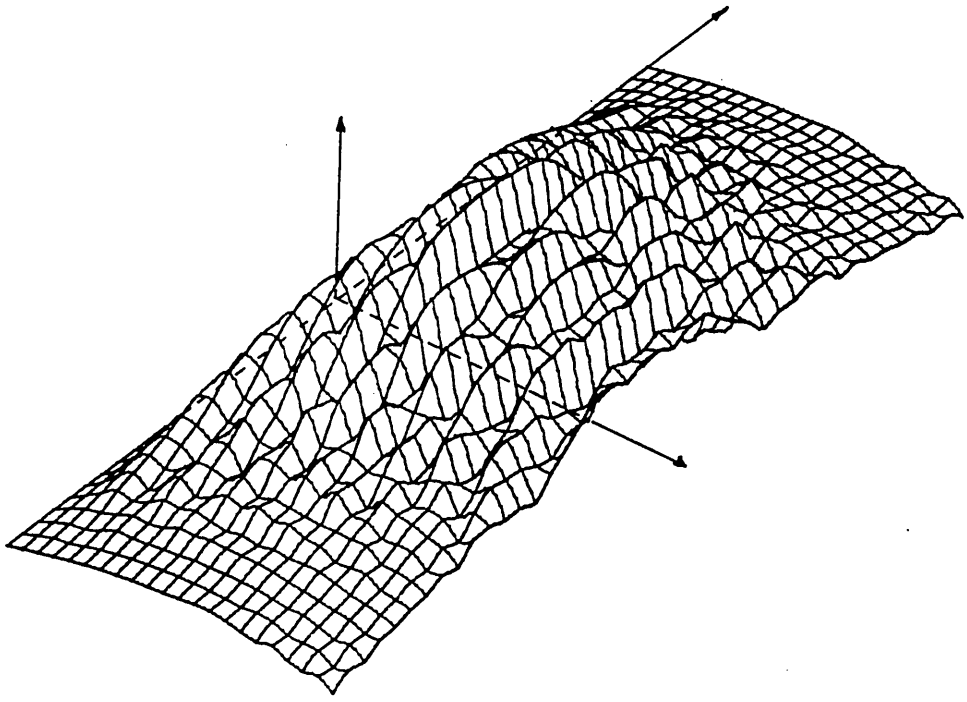

Fig.3.37 Directional axial yoke force transfer function

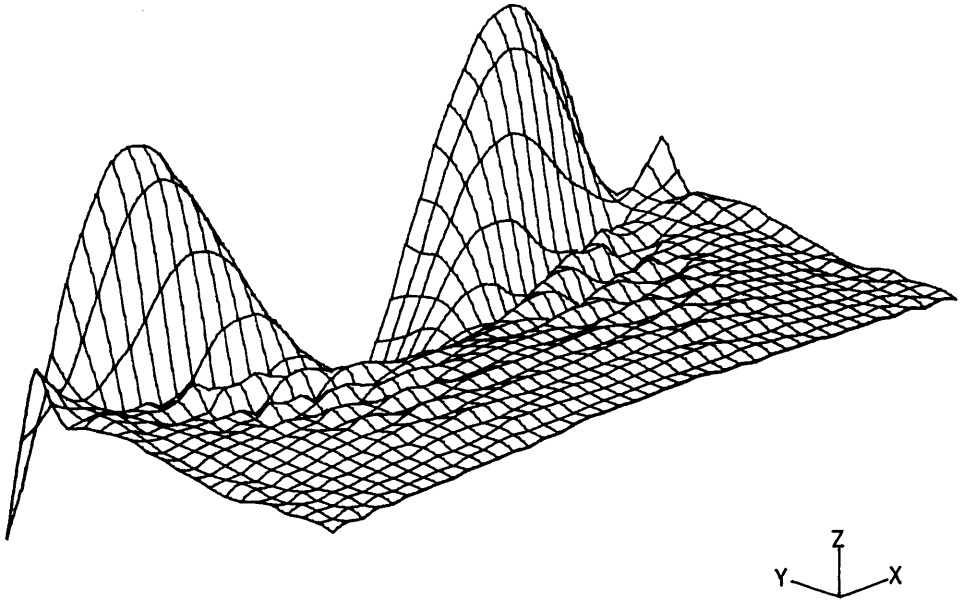

Fig.3.38 Directional transverse yoke force transfer function

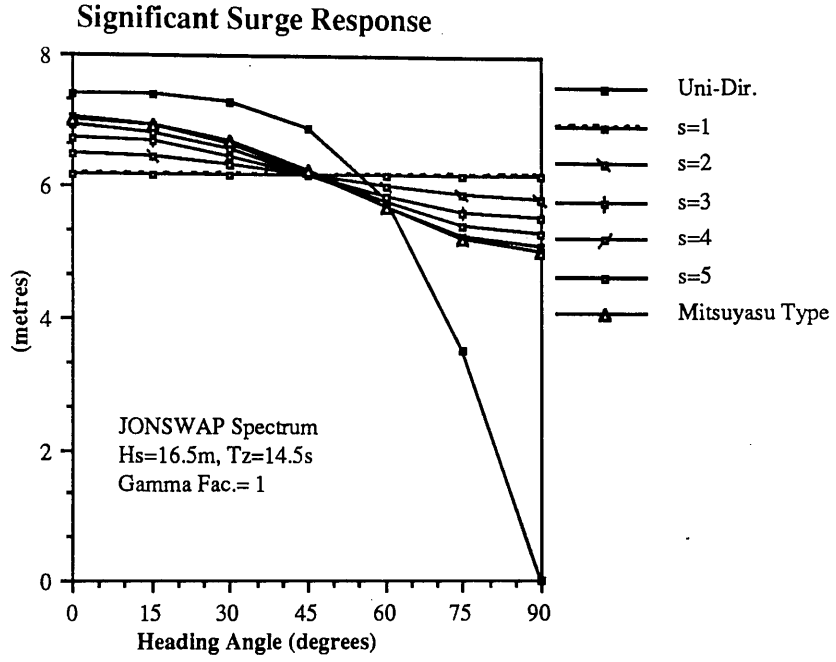

Fig.3.39 Effects of short-crested waves on surge response

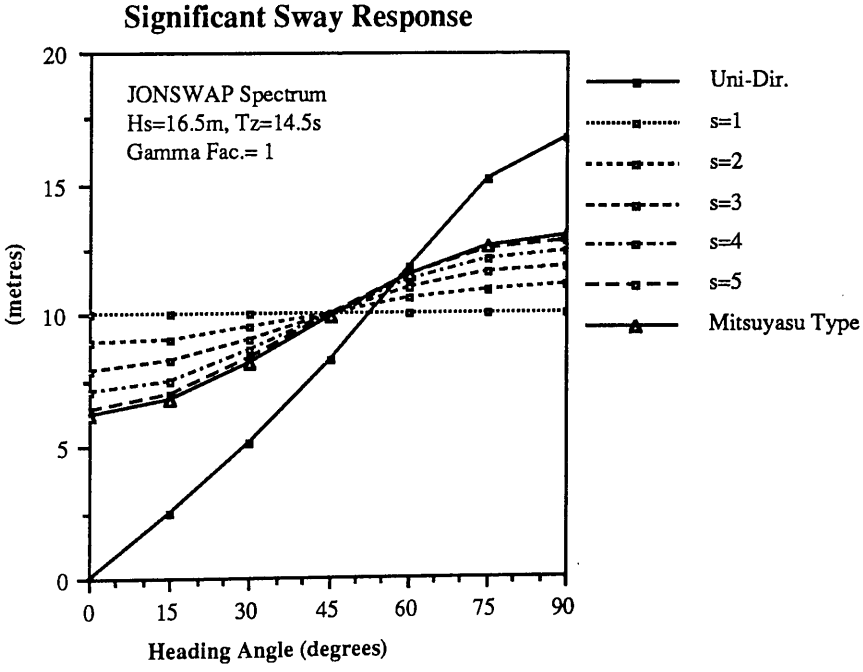

Fig.3.40 Effects of short-crested waves on sway response

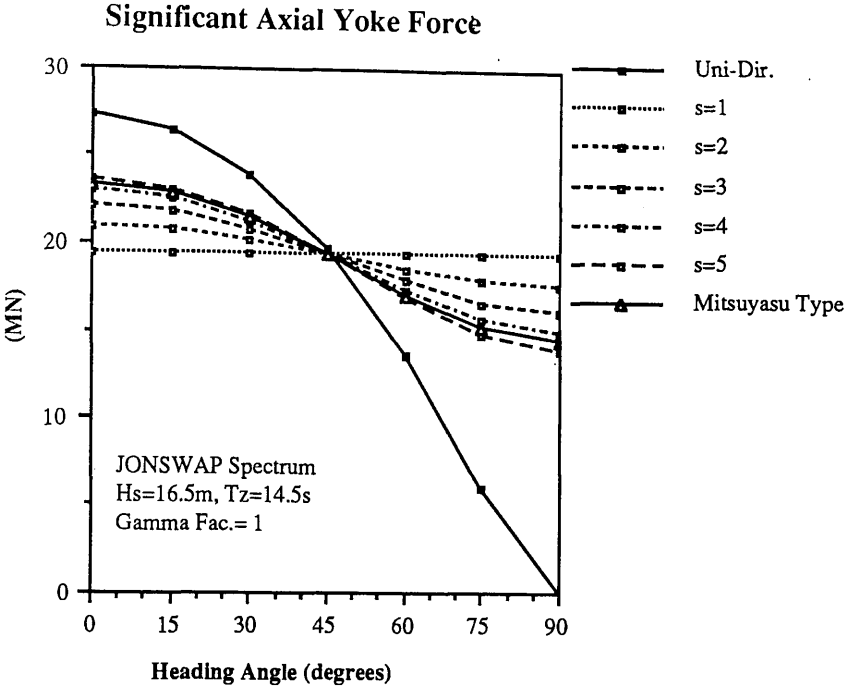

Fig.3.41 Effects of short-crested waves on axial yoke force

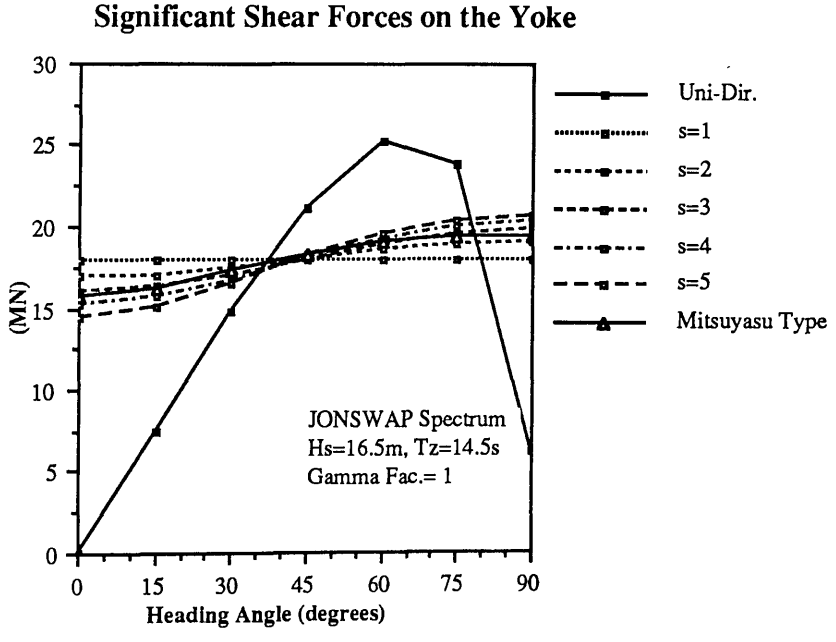

Fig.3.42 Effects of short-crested waves on shear force

CHAPTER 4

DOUBLE ARTICULATED TOWER

4.1 GENERAL DESCRIPTION

The double articulated tower concept was first designed by BNOC(British National Oil Corporation) and installed in 1977 to provide exporting facilities in the Thistle field (see Fig.4.1, duplicated from Goodfellows Ltd.(1986)). The double articulated tower configuration coupled with either a permanently floating structure or with a shuttle transport tanker provides a cost effective alternative to fixed platforms and pipelines in bringing oil to shore via either floating surface or subsea structures. A typical double articulated tower configuration consists of three parts; a deck, an upper column and a lower column. The lower column is connected to the base by means of a universal joint allowing for angular rotations. The bottom part of the column is usually ballasted with water for two reasons. The first one is that the ballast gives extra weight so that it balances the buoyancy of the lower column. The second one is that the ballast prevents the column from buckling under the external pressure. The upper column is connected to the lower one by means of a universal joint. The lower column is also connected to the base with a universal joint. The upper column has a buoyancy chamber which can be designed to provide the required restoring force. This restoring force arises due to an offset position of the upper column which occurs under environmental forces. The size and position of the buoyancy chamber are optimized to limit the maximum inclination angle of the tower and the maximum admissible yoke angle. (The tower may be coupled with a ship via a rigid-yoke). In order to control the axial forces in the intermediate joint, some solid ballast weight may be added in the lower part of the column. This weight may be balanced by increasing the buoyancy chamber diameter.

It is believed that the advantage of the double articulated tower is that the bending moment values along the tower are reduced by including the second joint. Therefore it may prove to be cost effective for deep water applications. The addition of the second articulation is even more important when the tower is connected to a floating vessel. This phenomenon will be considered in Ch.5. On the other hand, towing, installation and maintenance procedures of the double articulated tower may be more difficult and expensive in comparison with the single articulated tower.

In order to design a reliable double articulated tower the following quantities should be known by the designer:

- the angular motions of lower and upper columns,
- the reaction forces at the lower and upper joints, and
- the bending moment and shear force distributions along the tower.

A brief review of the literature on double articulated tower systems is summarized in the following.

Caldwell and Gamage (1977) described a nonlinear computer program that predicts internal reaction forces and motions of a multiline marine production riser exposed to wave and current forces. The method of analysis used in the program involved a finite element procedure that uses a Newton-Raphson iteration technique for large geometric displacement.

Jain and Kirk (1977) analyzed the double articulated tower which was designed for 160m water depth. The equations of motion were derived using Lagrange's equation in spherical coordinates. The tower oscillations were obtained by solving the 4-DOF motion equations in the time domain.

Naftzer and Chakrabarti (1980) analyzed a cylindrical floating storage tank. The storage tank was connected to the sea bed with a single tensioned anchoring leg, so that the tank behaved like an inverted double pendulum. Two degrees of freedom equations were obtained by means of Lagrange's equation and solved in the frequency domain. The added mass and damping for the vessel were obtained from linear radiation theory. The theoretical damping coefficients were found to be small for wave periods above 20s (full scale).

McNamara and Lane (1984) gave a method for the linear and nonlinear motion analysis of offshore systems such as risers and single-leg mooring towers under static and dynamic loading. The technique was based on the finite element approach using

convected coordinates for arbitrary large rotations and includes terms due to buoyancy, gravity, wave and current forces. Sources of numerical stability problems encountered in the mathematical model and the methods adopted to overcome these problems were also discussed.

More recently, Kirk et al. (1985) carried out dynamic response studies of an idealized model of a double articulated spar buoy using two dimensional linear wave theory. Two mathematical models namely the Rigid Body Model and the Finite Element Model were developed. The numerical predictions were compared with the experimental measurements. They concluded that both the Rigid Body Model and FE Model can be used for the motion and structural response analysis of a double articulated spar buoy.

In this Chapter motion equations for a double articulated tower are derived by using the Lagrange method. First, the double articulated tower is modelled as two uniform simple cylinders so that the equations of motion can be tackled easily. Then the resulting expressions are used for the double articulated tower configuration which consists of five cylindrical elements. The latter configuration is also used during the experimental studies which will be described in Chapter 7. First order wave forces are considered as excitation forces. The shear forces and bending moments as well as the axial tension and wave induced force distribution along the tower are presented for a number of wave frequencies. Parametric studies are carried out to investigate the sensitivity of the natural frequency of the system to the geometrical changes and the effect of increasing water depth and deck weight on the motion responses. A comparison of the angular motion and the joint force values of the double articulated tower with the values of a geometrically similar single articulated tower is also given.

4.2 SIMPLE CONFIGURATION: TWO UNIFORM CIRCULAR CYLINDERS

4.2.1 ANALYTICAL MODEL

The equations of motion of the double articulated tower are derived using Lagrange's equation. It is assumed that the structure oscillates as a rigid body and that the angular motions of the upper and lower columns are small (less than 10 degrees). The transverse motions perpendicular to the direction of wave propagation can be neglected.

The oscillation of the system is considered in the plane of two dimensional wave motion. Hence the system is reduced to two degrees of freedom.

In deriving the governing equations, the double articulated tower is assumed to have two circular cylindrical elements connected to each other by an intermediate joint (see Fig.4.2). The lower part of the system is attached to the sea bed. The system motion may be described in terms of the angular motion about the ends of the elements, i.e. θ_1 and θ_2. Both angles are measured from the vertical and are assumed to be small. Referring to Clough and Penzien (1975), the equations of motion are derived from Lagrange's equation, namely,

$$\frac{\partial}{\partial t}\left(\frac{\partial T}{\partial \dot{q}_i}\right) - \frac{\partial T}{\partial q_i} + \frac{\partial V}{\partial q_i} = Q_i \tag{4.1}$$

in which the raised dot denotes differentiation with respect to time; T, total kinetic energy; V, total potential energy; Q_i, generalized forcing functions and q_i, generalized coordinates.

If the generalized coordinates are chosen as θ_1 and θ_2, Lagrange's equation can be expressed in the form

$$\frac{\partial}{\partial t}\left(\frac{\partial T}{\partial \dot{\theta}_i}\right) - \frac{\partial T}{\partial \theta_i} + \frac{\partial V}{\partial \theta_i} = Q_i \quad , \; i = 1, 2 \tag{4.2}$$

where the kinetic energy term is

$$T = \frac{1}{2}I_1\dot{\theta}_1^2 + \frac{1}{2}M_1(\frac{\dot{\theta}_1 L_1}{2})^2 + \frac{1}{2}I_2\dot{\theta}_2^2 + \frac{1}{2}M_2(\dot{\theta}_1 L_1 + \frac{\dot{\theta}_2 L_2}{2})^2, \tag{4.3}$$

the potential energy term is

$$V = \frac{1}{2}(K_{11}\theta_1^2 + K_{22}\theta_2^2) \tag{4.4}$$

with

$$K_{11} = g[(\rho\nabla_1\overline{CB}_1 - W_1\overline{CG}_1) + (\rho\nabla_2 - W_2)L_1]$$

and

$$K_{22} = g[(\rho\nabla_2\overline{CB}_2 - W_2\overline{CG}_2)$$

The forcing functions are

$$Q_1 = -B_{11}\dot{\theta}_1 - B_{12}\dot{\theta}_2 + M_{E1} \tag{4.5}$$

and

$$Q_2 = -B_{21}\dot{\theta}_1 - B_{22}\dot{\theta}_2 + M_{E2} \tag{4.6}$$

where I_i is mass and added mass of inertia about the center of gravity; M_i, mass and added mass; L_i, length; K_{ij} , stiffness coefficient; ∇_i, volumetric displacement; $\overline{CB}_i$, center of buoyancy; $\overline{CG}_i$, center of gravity; W_i, weight; θ_i, angular response from vertical; $\dot{\theta}_i$, angular velocity; ρ, density of water; g, gravitational acceleration; B_{ij} , damping coefficients and M_{Ei}, external moments due to wave excitation and i and j take the values of 1 and 2 indicating the lower and upper cylindrical columns, respectively.

By carrying out the derivations and arranging the terms in Eqs.(4.2)~(4.6), the two degrees of motion equations can be written in matrix form as follows

$$\begin{bmatrix} A_{11} & A_{12} \\ A_{21} & A_{22} \end{bmatrix}\begin{Bmatrix} \ddot{\theta}_1 \\ \ddot{\theta}_2 \end{Bmatrix}+\begin{bmatrix} B_{11} & B_{12} \\ B_{21} & B_{22} \end{bmatrix}\begin{Bmatrix} \dot{\theta}_1 \\ \dot{\theta}_2 \end{Bmatrix}+\begin{bmatrix} K_{11} & 0 \\ 0 & K_{22} \end{bmatrix}\begin{Bmatrix} \theta_1 \\ \theta_2 \end{Bmatrix}=\begin{Bmatrix} M_{E1} \\ M_{E2} \end{Bmatrix} \quad (4.7)$$

where the terms of the first matrix are given as

$$A_{11}=I_1+\frac{M_1L_1^2}{4}+M_2L_1^2$$
$$A_{12}=A_{21}=\tfrac{1}{2}M_2L_2L_1$$
$$A_{22}=I_2+\frac{M_2L_2^2}{4}$$

As a first approach to the solution of the 2 DOF system, the damping and exciting moment terms are set to zero and the following equations are obtained:

$$\begin{aligned} A_{11}\ddot{\theta}_1+A_{12}\ddot{\theta}_2+K_{11}\theta_1=0 \\ A_{21}\ddot{\theta}_1+A_{22}\ddot{\theta}_2+K_{22}\theta_2=0 \end{aligned} \quad (4.8)$$

Since the preceding equations are linear, their steady state solution can be written as:

$$\begin{aligned} \theta_1=\theta_A \sin\ \omega t \\ \theta_2=\theta_B \sin\ \omega t \end{aligned} \quad (4.9)$$

Substituting Eq.(4.9) into Eq.(4.8), the undamped natural periods of the system may be obtained by solving the characteristic equations:

$$\begin{bmatrix} -\omega^2A_{11}+K_{11} & -\omega^2A_{12} \\ -\omega^2A_{21} & -\omega^2A_{22}+K_{22} \end{bmatrix}\begin{Bmatrix} \theta_A \\ \theta_B \end{Bmatrix}=\begin{Bmatrix} 0 \\ 0 \end{Bmatrix} \quad (4.10)$$

which are satisfied for any θ_A and θ_B if the following determinant is zero

$$\begin{vmatrix} -\omega^2 A_{11} + K_{11} & -\omega^2 A_{12} \\ -\omega^2 A_{21} & -\omega^2 A_{22} + K_{22} \end{vmatrix} = 0 \tag{4.11}$$

Letting $\omega^2 = \lambda$, the above determinant leads to the characteristic equation

$$\lambda^2 - \beta_1 \lambda + \beta_2 = 0 \tag{4.12}$$

where

$$\beta_1 = \frac{A_1 K_{11} + A_2 K_{22}}{A_1 A_2 - A_3^2} \quad \text{and} \quad \beta_2 = \frac{K_{11} K_{22}}{A_1 A_2 - A_3^2}$$

The two roots of Eq.(4.12) are

$$\lambda_{1,2} = \frac{\beta_1}{2} \pm \sqrt{\left(\frac{\beta_1}{2}\right)^2 - \beta_2} \tag{4.13}$$

and the natural frequencies of the system are found to be

$$\omega_1 = \sqrt{\lambda_1} \text{ and } \omega_2 = \sqrt{\lambda_2}. \tag{4.14}$$

Having obtained the natural frequencies of the double articulated tower, one can then assess the suitability of the design for a given sea-state. Substitution of these natural frequencies into Eq.(4.10) gives the ratio of the angular responses. For ω_1 and ω_2 , we obtain

$$\left(\frac{\theta_A}{\theta_B}\right)_1 = \frac{\omega_1^2 A_3}{(-\omega_1^2 A_1 + K_{11})} \text{ and } \left(\frac{\theta_A}{\theta_B}\right)_2 = \frac{\omega_2^2 A_3}{(-\omega_2^2 A_1 + K_{11})} \tag{4.15}$$

which are the mode shapes corresponding to the first and second normal modes.

In the second step, the exciting moments which are in phase with the motion are taken into account. The undamped motion equation can be obtained as:

$$\begin{bmatrix} -\omega^2 A_{11} + K_{11} & -\omega^2 A_{12} \\ -\omega^2 A_{21} & -\omega^2 A_{22} + K_{22} \end{bmatrix} \begin{Bmatrix} \theta_A \\ \theta_B \end{Bmatrix} = \begin{Bmatrix} \overline{M}_{E1} \\ \overline{M}_{E2} \end{Bmatrix} \tag{4.16}$$

Solution of this matrix equation gives the angular responses. Calculation of angular responses without damping yields initial response values to be used in solving the damped motion equations since the linearised drag coefficients are a function of the response values.

Second order differential equations, describing the damped oscillations of a double articulated tower were expressed in matrix form in Eq.(4.7). Assuming the solutions of Eq.(4.7) to be

$$\theta_1 = \theta_{11} \sin \omega t + \theta_{12} \cos \omega t$$
and
$$\theta_2 = \theta_{21} \sin \omega t + \theta_{22} \cos \omega t \tag{4.17}$$

the following matrix can be written

$$\begin{bmatrix} -\omega^2 A_{11} + K_{11} & -\omega B_{11} & -\omega^2 A_{12} & -\omega B_{12} \\ \omega B_{11} & -\omega^2 A_{11} + K_{11} & \omega B_{12} & -\omega^2 A_{12} \\ -\omega^2 A_{21} & -\omega B_{21} & -\omega^2 A_{22} + K_{22} & -\omega B_{22} \\ \omega B_{21} & -\omega^2 A_{21} & \omega B_{22} & -\omega^2 A_{22} + K_{22} \end{bmatrix}$$

$$\times \begin{Bmatrix} \theta_{11} \\ \theta_{12} \\ \theta_{21} \\ \theta_{22} \end{Bmatrix} = \begin{Bmatrix} \overline{M}_{E1} \\ 0 \\ \overline{M}_{E2} \\ 0 \end{Bmatrix} \tag{4.18}$$

Solution of matrix Equation (4.18) yields the components of the angular response.

4.2.2 LINEARIZATION OF DAMPING TERMS

The wave damping forces due to the presence of free surface are not considered in this analysis. This assumption may be acceptable since the main volume element of the tower remains well below the free surface. It is also assumed that the damping due to friction in the joints is small and there is no structural damping present in the rigid body motion of either of the columns. Therefore, the only damping effect considered in this analysis is due to the viscosity. In the following, the calculation procedure for the viscous damping forces and their moments on the system is described.

The fluid drag force normal to a small differential element of a vertical cylinder is given by

$$dF_d = \frac{1}{2}\rho C_D D U_S |U_S| dy \tag{4.19}$$

where C_D is the drag coefficient; ρ, the water density ; D, the diameter; U_S, the angular velocity of the element ($U_S = l_i \dot{\theta}$) and l_i, the distance from the appropriate joints.

In order to find the total damping moments on the double articulated tower, Eq.(4.19) should be integrated along the structure. The moment of the damping forces about the base and the intermediate joints can be written, respectively, as follows

Viscous Damping Moment on the Lower Column

$$M_{D1} = \int_{-d}^{-L_2} \frac{1}{2}\rho C_D D_1 [\dot{\theta}_1 (y + d)] \left|\dot{\theta}_1 (y + d)\right| (y + d) dy$$

(damping moment due to the lower column's own motion)

$$+ \int_{-L_2}^{0} \frac{1}{2}\rho C_D D_2 (\dot{\theta}_1 L_1) \left|\dot{\theta}_1 L_1\right| L_1 dy$$

(damping moment which occurs when the lower column sets the upper column into

motion with a velocity of $\dot{\theta}_1 L_1$)

$$+ \int_{-L_2}^{0} \frac{1}{2}\rho C_D D_2[\dot{\theta}_2(y+L_1)]\left|\dot{\theta}_2(y+L_1)\right|L_1 dy \qquad (4.20)$$

(damping moment due to total damping forces acting on the upper column)

Viscous Damping Moment on the Upper Column

$$M_{D2} = \int_{-L_2}^{0} \frac{1}{2}\rho C_D D_2[\dot{\theta}_2(y+L_2)]\left|\dot{\theta}_2(y+L_2)\right|(y+L_2)dy$$

(damping moment due to the lower column's own motion)

$$+ \int_{-L_2}^{0} \frac{1}{2}\rho C_D D_2(\dot{\theta}_1 L_1)\left|\dot{\theta}_1 L_1\right|(y+L_2)dy \qquad (4.21)$$

(damping moment on the upper column due to the motion of the lower column with a velocity of $\dot{\theta}_1 L_1$)

In the above equations, different damping effects are considered separately and are added together linearly. This approximation is made to eliminate the nonlinear terms in the addition of the velocity components. In Eqs.(4.20) and (4.21) $\dot{\theta}_i\left|\dot{\theta}_i\right|$ terms are nonlinear. For a simplified solution of the equations of motion in the frequency domain, Eq.(4.7), these terms should be linearised. The first term of the Fourier series expansion of the angular velocity terms can be written as follows

$$\dot{\theta}_i\left|\dot{\theta}_i\right| \cong \frac{8}{3\pi}\omega(\theta_{i,max})\dot{\theta}_i \qquad (4.22)$$

where

$$\theta_{i,max} = \sqrt{\theta_{i1}^2 + \theta_{i2}^2} \qquad (4.23)$$

Employing this linearization procedure in the damping moment integrations, the damping matrix of the equation of motion may be calculated. The coefficients of the

damping matrix for the case of two uniform circular cylinders are given as follows

$$B_{11} = \frac{1}{3\pi}\rho C_D D_1 \omega\theta_{1,\max} L_1^4 + \frac{4}{3\pi}\rho C_D D_2 \omega\theta_{1,\max} L_1^3 L_2$$

$$B_{12} = \frac{4}{9\pi}\rho C_D D_2 \omega\theta_{2,\max} L_2^3 L_1$$

$$B_{21} = \frac{2}{3\pi}\rho C_D D_2 \omega\theta_{1,\max} L_2^2 L_1^2$$

$$B_{22} = \frac{1}{3\pi}\rho C_D D_2 \omega\theta_{2,\max} L_2^4 \qquad (4.24)$$

In solving the motion equation, the results obtained from undamped motion equations (e.i. Eq.(4.9)) are considered the initial estimate of $\theta_{1,\max}$ and $\theta_{2,\max}$ which are substituted into Eq.(4.7) and a new set of values for $\theta_{1,\max}$ and $\theta_{2,\max}$ are obtained by the new matrix inversion. The process is repeated until a numerical convergence in $\theta_{1,\max}$ and $\theta_{2,\max}$ is reached.

4.2.3 WAVE FORCES AND HYDRODYNAMIC COEFFICIENTS

The wave exciting forces acting on the double articulated tower are considered inertia dominated(see Section 2.2.1). Therefore the drag forces are ignored. Morison's equation is used to calculate the wave excitation forces and their moments about the joint in the vertical position of the structure. The upper and lower columns are divided into segments of unit length. The local wave acceleration is applied to determine the wave force on the segment. These forces are then summed to obtain the total wave induced forces and their moments around the universal joints. The respective description of the wave induced moments on the upper and lower columns are given as follows

$$M_{E1} = A \int_{-d}^{-L_2} D^2(y) e^{ky} (y + d) dy$$

$$M_{E2} = A \int_{-L_2}^{CL} D^2(y) e^{ky} (y + L_2) dy$$

where $A = C_M \rho \frac{\pi}{4} \zeta_a \omega^2 \sin(-\omega t)$.

The inertia coefficient for the force calculation is chosen as C_M=2. A detailed discussion related to the application of Morison equation on the force calculation of articulated tower type of structures is also given in Section 2.2.2.

4.3 ANALYSIS OF GLASGOW UNIVERSITY DOUBLE ARTICULATED TOWER (GUDAT)

4.3.1 SOLUTION OF MOTION EQUATIONS

Motion equations can also be derived for a double articulated tower consisting of more than two cylindrical elements using the Lagrange equation. In order to apply the Lagrange equation, the tower is divided into a number of cylindrical elements. The mass and volume of these elements are represented as m_{1i} and v_{1i}, respectively. The kinetic energy of the system, in this case, is obtained as:

$$T = \frac{1}{2}[A_{11}\dot{\theta}_1^2 + A_{22}\dot{\theta}_2^2 + A_{12}\dot{\theta}_1\dot{\theta}_2 + A_{21}\dot{\theta}_1\dot{\theta}_2] \tag{4.25}$$

in which

$$A_{11} = \sum_{i=1}^{N1} m_{1i} l_{1i}^2 + L_1^2 \sum_{i=1}^{N2} m_{2i} + \rho \sum_{i=1}^{N1} v_{1i} h_{1i}^2 + L_1^2 \rho \sum_{i=1}^{N2} v_{2i}$$

$$A_{22} = \sum_{i=1}^{N2} m_{2i} l_{2i}^2 + \rho \sum_{i=1}^{N2} v_{2i} h_{2i}^2$$

$$A_{21} = A_{12} = L_1 \left(\sum_{i=1}^{N2} m_{2i} l_{2i} + \rho \sum_{i=1}^{N2} v_{2i} h_{2i} \right)$$

where l_{1i} and l_{2i} are the distances of lumped masses from appropriate joints; h_{1i} and h_{2i}, the distances of volume elements from appropriate joints; 1 and 2 represent the lower and

upper columns, respectively.

Here, the expressions given in preceding sections are used for the GUDAT configuration which consists of five cylindrical elements. The tower carries 1218 t deck weight in 297m water depth. The lower column is ballasted by 7810 t weight ($\rho_{BALLAST} = 2.6\ t/m^3$). The physical dimensions as well as the lumped mass distribution along the tower are shown in Fig.4.3. The coefficients of the Eq.(4.7) are given using the geometry of the structure shown in Fig.4.3 as follows

$$A_{11} = m_{11}l^2_{11} + m_{12}l^2_{12} + m_{13}l^2_{13} + m_{14}l^2_{14} + (m_{21}+m_{22}+m_{23}+m_{24}+m_{25})L^2_1 + \rho[V_{11}h^2_{11}+V_{12}h^2_{12}+(V_{21}+V_{22}+V_{23})L^2_1]$$

$$A_{22} = m_{21}l^2_{21} + m_{22}l^2_{22} + m_{23}l^2_{23} + m_{24}l^2_{24} + m_{25}l^2_{25} + \rho(V_{21}h^2_{21}+V_{22}h^2_{22} + V_{23}h^2_{23})$$

$$A_{12} = A_{21} = [m_{21}l_{21} + m_{22}l_{22} + m_{23}l_{23} + m_{24}l_{24} + m_{25}l_{25} + \rho(V_{21}h_{21}+V_{22}h_{22}+V_{23}h_{23})]L_1$$

$$B_{11} = (1/3\pi)\,\rho\, C_D\omega\, \theta_{1,max}\,\{D_5((l_5+\varepsilon_1)^4 - \varepsilon^4_1) + D_4((l_4 + l_5 +\varepsilon_1)^4 - (l_5+\varepsilon_1)^4)\}$$

$$B_{12} = (4/9\pi)\,\rho\, C_D\omega\, \theta_{2,max}\, L_1\{D_3((\varepsilon_2/2 + l_3)^3 - (\varepsilon_2/2)^3) + D_2((\varepsilon_2/2+l_3+l_2)^3 - (\varepsilon_2/2+l_3)^3) + D_1((\varepsilon_2/2+l_3+l_2+l_1)^3 - (\varepsilon_2/2+l_3+l_2)^3)\}$$

$$B_{21} = (2/3\pi)\,\rho\, C_D\omega\, \theta_{1,max}\, L_1^2\,\{D_3((\varepsilon_2/2+l_3)^2 - (\varepsilon_2/2)^2) + D_2((\varepsilon_2/2+l_3+l_2)^2 - (\varepsilon_2/2+l_3)^2) + D_1((\varepsilon_2/2+l_3+l_2+l_1)^2 - (\varepsilon_2/2+l_3+l_2)^2)\}$$

$$B_{22} = (1/3\pi)\,\rho\, C_D\,\omega\, \theta_{2,max}\,\{D_3((\varepsilon_2/2+l_3)^4 - (\varepsilon_2/2)^4) + D_2((\varepsilon_2/2+l_3+l_2)^4 - (\varepsilon_2/2+l_3)^4) + D_1((\varepsilon_2/2+l_3+l_2+l_1)^4 - (\varepsilon_2/2+l_3+l_2)^4)\}$$

$$K_{11} = g[(\rho\nabla_1\overline{CB}_1 - W_1\overline{CG}_1) + (\rho\nabla_2 - W_2)L_1]$$

and

$$K_{22} = g[(\rho\nabla_2\overline{CB}_2 - W_2\overline{CG}_2) \qquad (4.26)$$

Two different C_D coefficients are used in calculating the damping coefficients B_{ij}. These are the values of C_D=1.2 and C_D=4.8. The surge displacements of the lower and upper columns are calculated by solving Eq.(4.7) in an iterative manner. The results are compared with the experimental measurements in Fig.4.4. As can be seen from this figure, the predictions shows good agreement with the measured values when higher C_D coefficients are used. Therefore, the value of C_D=4.8 is employed in the motion analysis of the double articulated tower presented in this chapter. This value should be interpreted as an equivalent coefficient which takes into account the other factors in the motion equation such as water-structure interaction, viscous damping in waves etc.

There are two peaks present in the angular response curves. These are due to the first and second modes of motion as shown in Fig.4.2. It is evident that the lower column response is much smaller than that of the upper column. This is expected since the eigen value analysis gave the ratio of the upper column response to the lower column response as 1.1.

Fig.4.5a shows the phase angle predictions. This figure shows that the upper and lower columns oscillate in phase up to the first natural frequency and they oscillate with a 180 degrees phase difference in the rest of the frequency range. Fig.4.5a also shows the sensitivity of phase angle predictions to increasing wave heights. Similarly, Fig.4.5b shows the sensitivity of upper and lower column surge responses to the increasing wave height. As can be seen from Fig.4.5b, as the wave height increases from 2m to 8m the maximum surge response decrease by a factor of 2 due to the increase in viscous damping in waves.

4.3.2 CALCULATION OF AXIAL FORCE, SHEAR FORCE AND BENDING MOMENT DISTRIBUTION ALONG THE DOUBLE ARTICULATED TOWER

The axial force along the GUDAT configuration (see Fig.4.3) appears as the tension force in the column due to the excess of buoyancy over weight. This force has a static character in the rest position of the tower and is subject to change under the wave loading.

Fig.4.6a shows the axial tension on the double articulated tower in the rest position. The variations of wave induced forces acting horizontally on the column are shown in Fig.4.6b.

The shear forces and bending moments along the columns are obtained by integrating the structural load acting on the differential circular beam elements of the upper and lower columns. The upper and lower columns are divided into a large number of differential elements and the structural load acting on these was calculated as a function of wave and motion induced forces. The components of the horizontal forces acting on the articulated tower are shown in detail in Appendix A. The shear forces are obtained by numerically integrating the structural load distributions. The bending moments are obtained by numerically integrating the shear force distributions. The shear force and bending moment distributions for a unit wave amplitude at wave frequencies of 0.4 rad/s and 1.0 rad/s are given in Figs.4.7 and 4.8, respectively.

When the wave frequency is equal to 0.4 rad/s the maximum bending moments are observed to occur at approximately 57m below the deck on the upper column and at 93m below the middle joint on the lower column. For high frequency motions, e.g. 1.0 rad/s, the distribution of shear forces is different than for low frequency motions. Fig. 4.8 shows that the shear force at the middle joint is smaller than that at the lower joint. The maximum bending moment on the lower column becomes 11.7 MN-m which is approximately 50% less than the maximum bending moment value calculated for 0.4 rad/s.

4.3.3 PARAMETRIC STUDIES

During the parametric studies the wave excitation forces and moments are calculated by taking the wave height as 2m. Therefore, the magnitudes in the figures referred to in this section can be interpreted as the response per unit wave amplitude.

The effect of inertia coefficient variation on the angular responses of the double articulated tower is examined first. Fig.4.9 shows that the angular responses vary linearly with the inertia coefficients. An increase in the inertia coefficient of about 33% yields a 15% increase in the angular response values.

Shear forces at the intermediate and base joints given in Fig.4.10 show the effect of changes in the drag coefficients and hence the viscous damping term of the equations of motion. Fig.4.10 reveals that larger C_D values result in small shear force values. This becomes even more pronounced around the region of the natural frequency.

The maximum bending moment values along the upper and lower columns are shown in Fig.4.11. The effect of damping alters the bending moment values especially around the natural frequency range.

The motion and structural response values of the double articulated tower were compared with those of a geometrically similar single articulated tower. The single articulated tower configuration was modelled by replacing the intermediate joint with a cylindrical element which has the same diameter as the lower column. Fig.4.12 shows the angular response values of both single and double articulated towers. The single articulated tower response curve has a single peak whereas the response curve for the double articulated tower has two peaks. The second peak is at the dominant frequency region for the double articulated tower configuration. In order to improve the motion characteristics of this configuration, the geometric shape of the buoyancy chamber and its place on the upper column may be altered.

The shear forces at the base joint and the maximum bending moments along the tower are compared in Figs. 4.13 and 4.14, respectively. Large response values mean large bending moments and shear forces. Therefore, the shear force and bending moment values of double articulated tower are larger than those for single articulated tower. This leads to the general conclusion that the second articulation present in the double articulated tower concept does not improve the motion and structural response behaviour.

The effect of geometric changes on the natural frequencies of the system is shown in Figs.4.15, 4.16 and 4.17. During this parametric studies, only one parameter and its dependent value are changed. The rest of the dimensions and weight values remain unchanged as shown in Fig.4.3. The overall trend observed from Figs.4.15-4.17 is that the first natural frequency of the system is less sensitive to the geometric changes than is the second natural frequency. Lowering the position of the intermediate articulation downwards increases the second natural frequency (see Fig.4.16a). The effect of water depth variation on the natural frequencies is shown in Fig.4.16b. The increase in water depth was taken into account by changing the length of the lower column while keeping the position of ballast weights unchanged. As is seen from the figures, both natural frequencies are insensitive to increasing water depth.

The natural frequencies are more sensitive to variation in the diameter of the buoyancy chamber than to any other geometrical changes. However, it should be noted that the wave force on the buoyancy chamber also increases in proportion to the diameter square. In order to achieve more stable design configurations, an optimization procedure between the length and diameter of the double articulated tower should be carried out.

The weight distribution along the upper column is quite important. This was shown by changing the deck weight in Fig.4.17b and the ballast weight in Fig.4.18a and b. As is seen from these figures, the second natural frequency is more sensitive to the weight distribution than the first natural frequency.

The effect of variation of the deck weight on the motion response was examined. Fig.4.19a and b shows that the natural frequency reduction is noticeable if the deck weight increases from 200t to 2500t. In addition, the motion response values increase slightly with the exception of the response values at the first natural frequency region in which case the upper column oscillation with 2500t deck weight is higher than the oscillation with 200t.

Fig. 4.20 shows three configurations of double articulated towers designed for different water depths. The angular response curves of two towers shown in Fig.4.20

were presented in Fig.4.21. Although the response values at the first natural frequency are reduced by increasing the depth of water by 50m, the maximum angular response values do not change significantly. This leads to the conclusion that the motion response values are relatively insensitive to water depth variations. The shear forces at the joints decrease with increasing water depth(see Fig.4.22a and b): A 35% increase in water depth causes a 50% decrease in the shear forces at the base joint. Fig.4.23 shows the variations of maximum bending moments on the lower and upper columns for 3 different water depths. The maximum bending moment values decrease slightly with increasing water depth.

4.4 CONCLUSIONS

In this chapter, the motion response characteristics of a double articulated tower concept have been investigated. Comparisons made between theoretical predictions and experimental measurements show that the system is subject to large damping forces due to fluid viscosity. The drag coefficient of 4.8 is used in damping force calculations.

The angular motion and the joint force values of the double articulated tower concept is compared with the values of a geometrically similar single articulated tower. It is shown that the second articulation worsen the motion and structural response behaviour.

Parametric studies carried out for various buoyancy configurations have shown that variations in diameter and in depth of buoyancy tank have a significant effect on the natural frequencies. Similarly, the changes in deck and ballast weight alter the natural frequencies and motion responses occurring at these natural frequencies. However, the magnitude of the angular response does not vary significantly throughout the rest of the wave frequency range.

Although the motion response values increase with increasing deck weight, water depth variation has only a very small effect on the response characteristics.

In order to investigate the effect of local flexural behaviour of the upper and lower columns, the dynamic model developed for a two degrees of freedom system in this chapter can easily be extended to higher degrees of freedom systems. This analysis may prove to be useful for accurate fatigue life calculations.

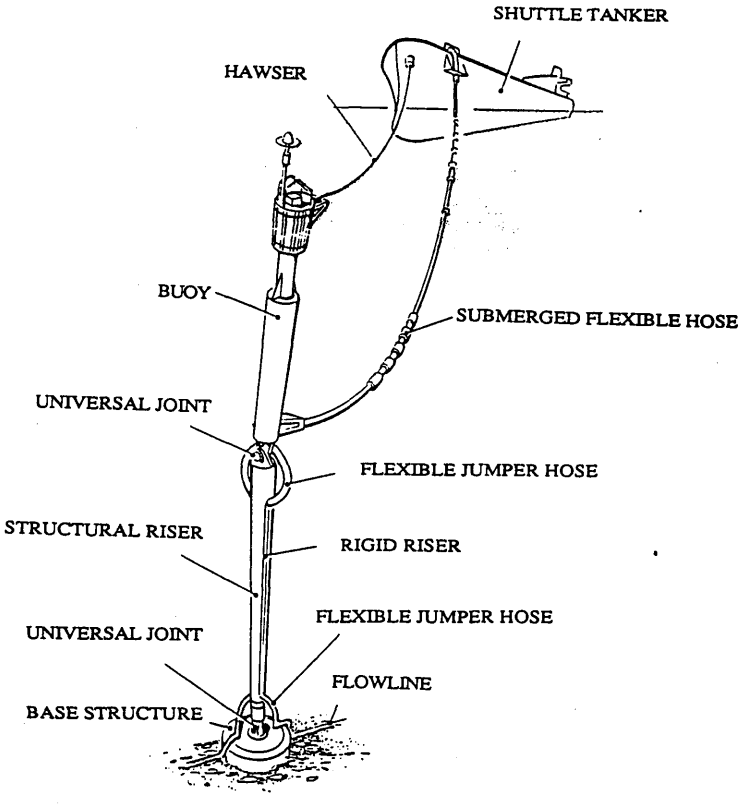

Fig.4.1 THISTLE field SALM system, installed in 1977 (Goodfellows Ltd.,1986)

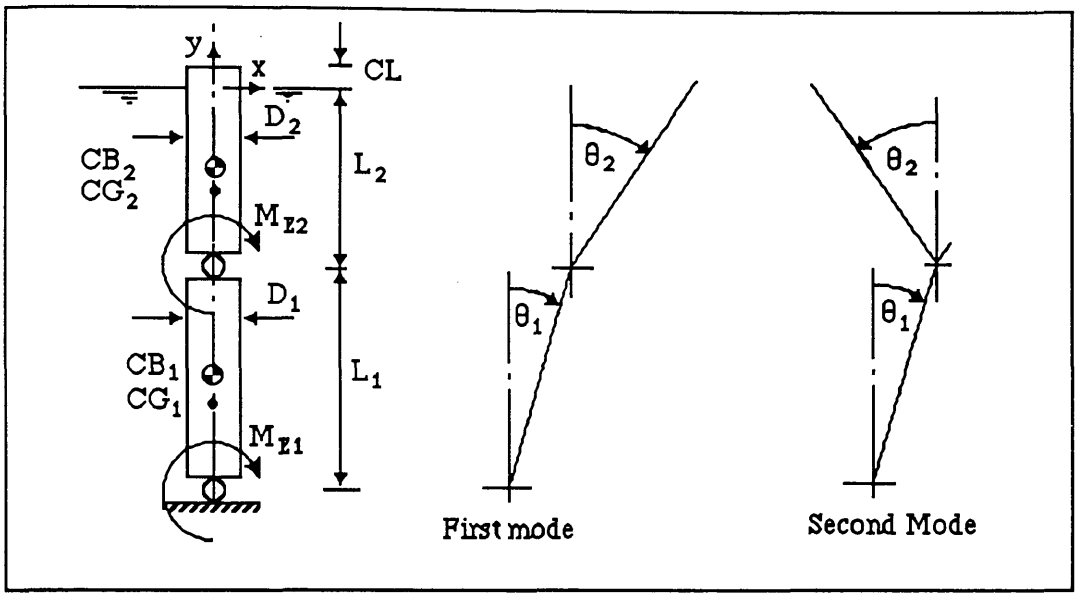

Fig.4.2 Simplified double articulated tower

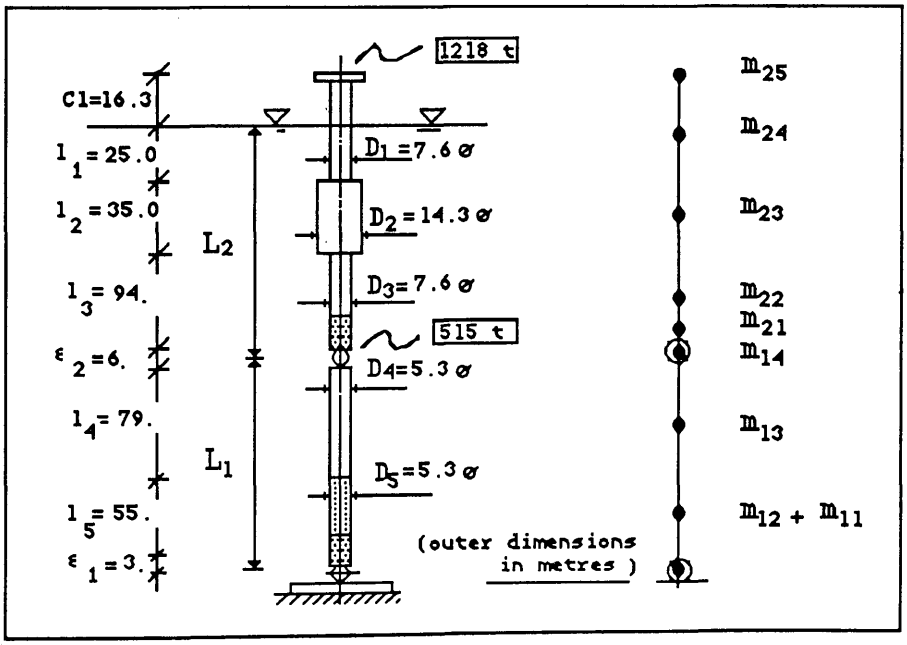

Fig.4.3 Double articulated tower configuration

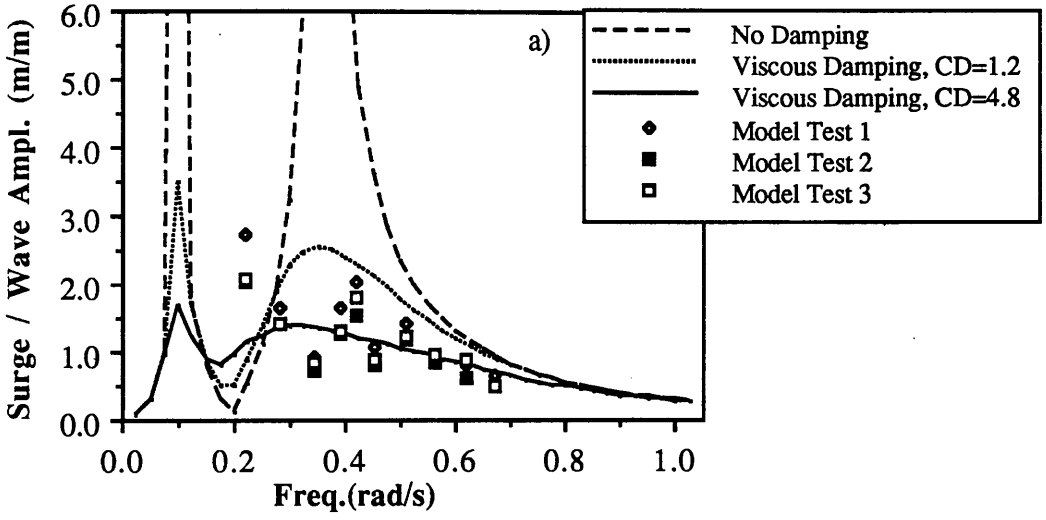

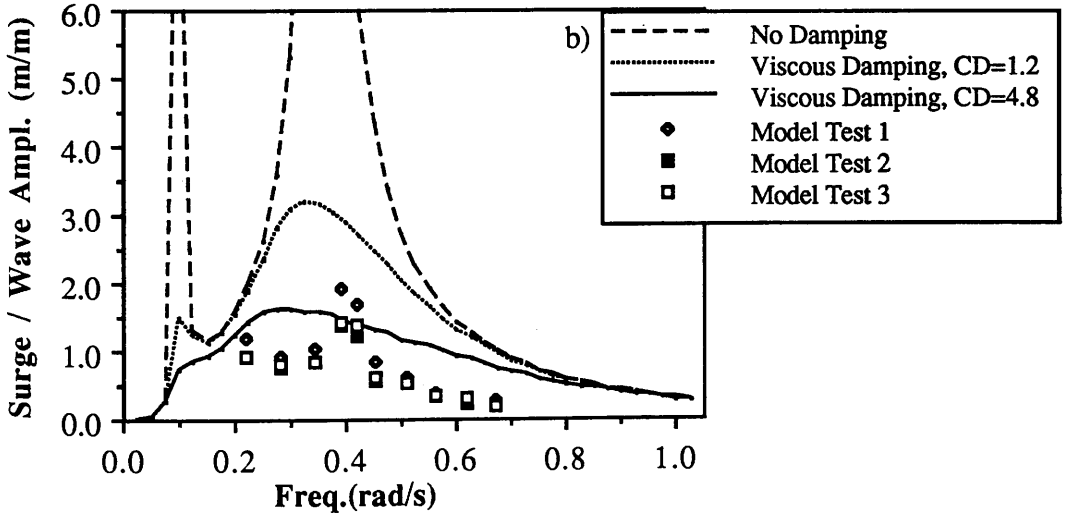

Fig.4.4 Comparison of mathematical model with repeated model test measurements

a) Upper column response b) Lower column response

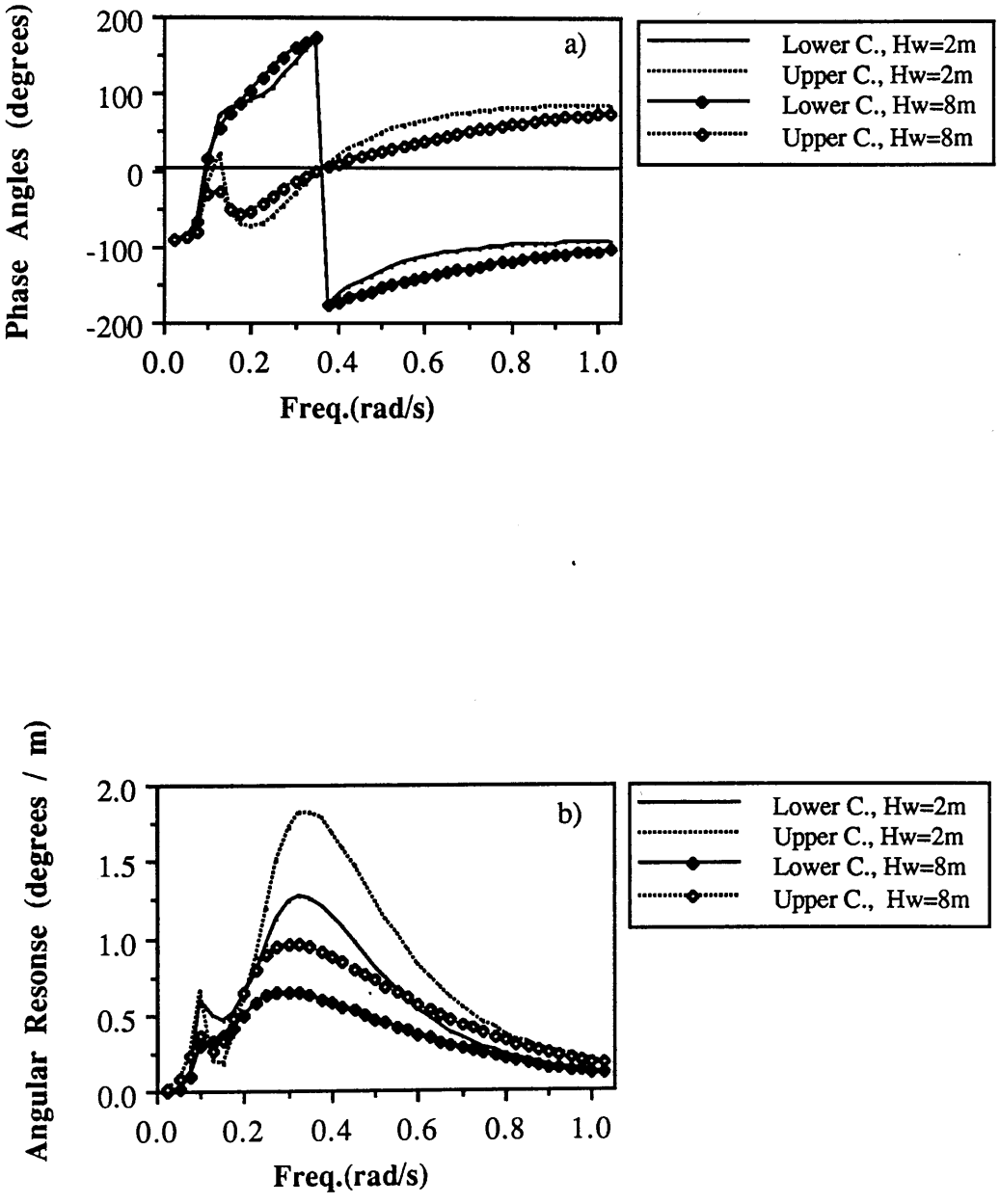

Fig.4.5 Angular response of double articulated tower for different wave heigths

$C_D = 4.8$ a) Phase angles b) Angular response

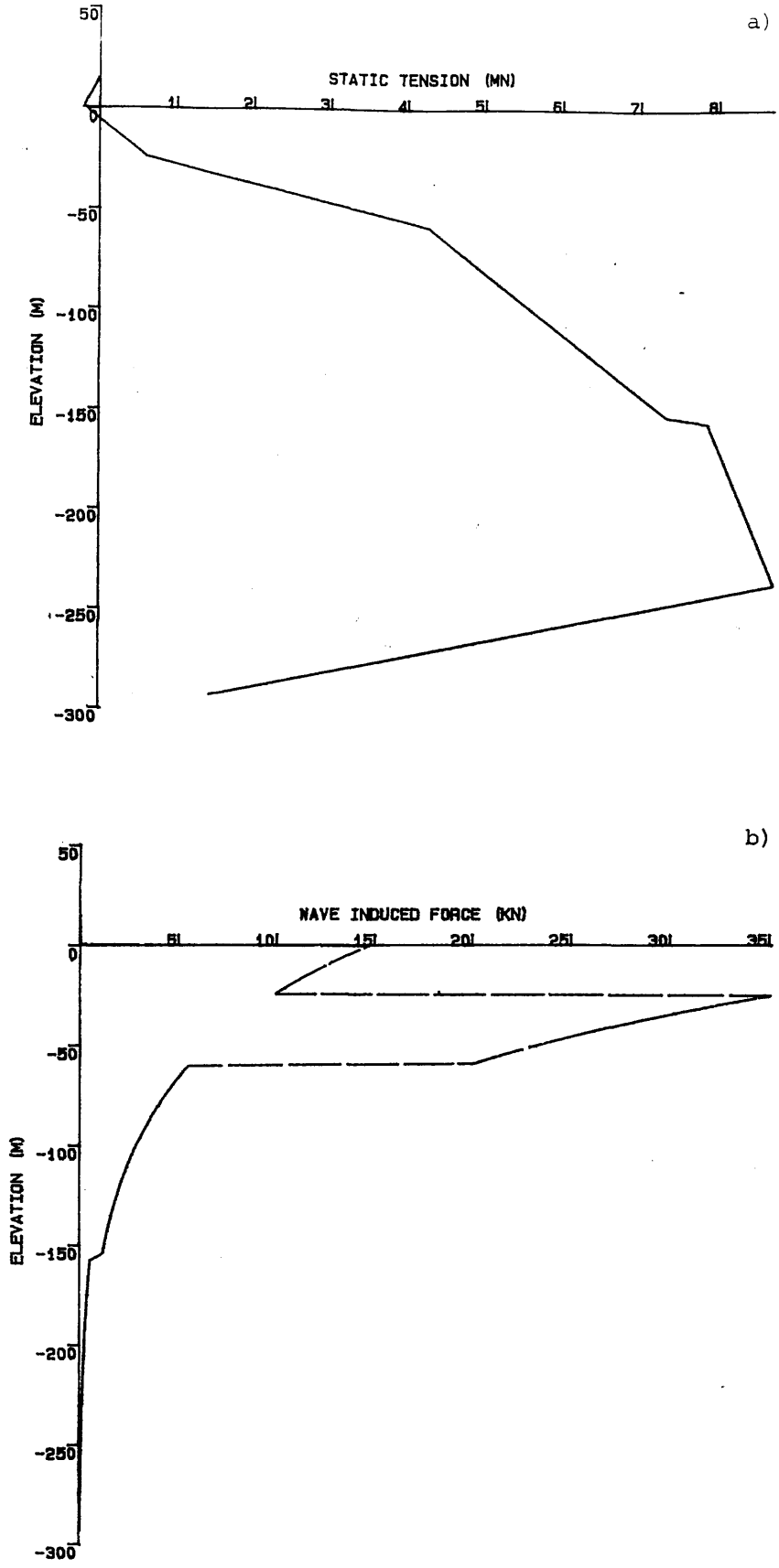

Fig.4.6 Static tension distribution and wave induced forces acting on the double articulated tower, $\omega = 0.4$ rad /s Hw = 2m a) Static tension b) Wave force

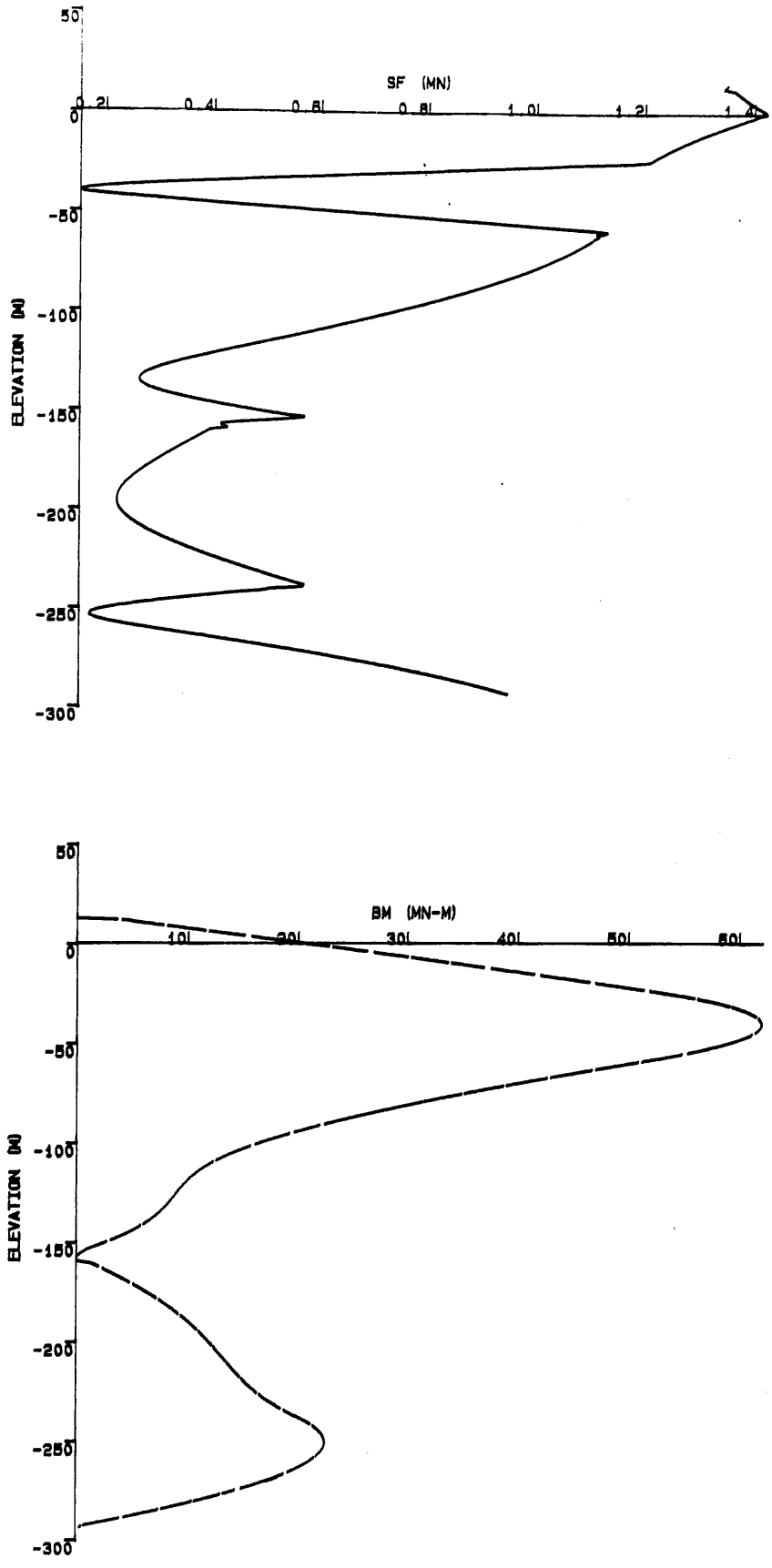

Fig.4.7 Shear force and bending moment distribution along the tower

$\omega = 0.4$ rad /s, Hw = 2m, $C_D = 4.8$ a) Shear force b) Bending moment

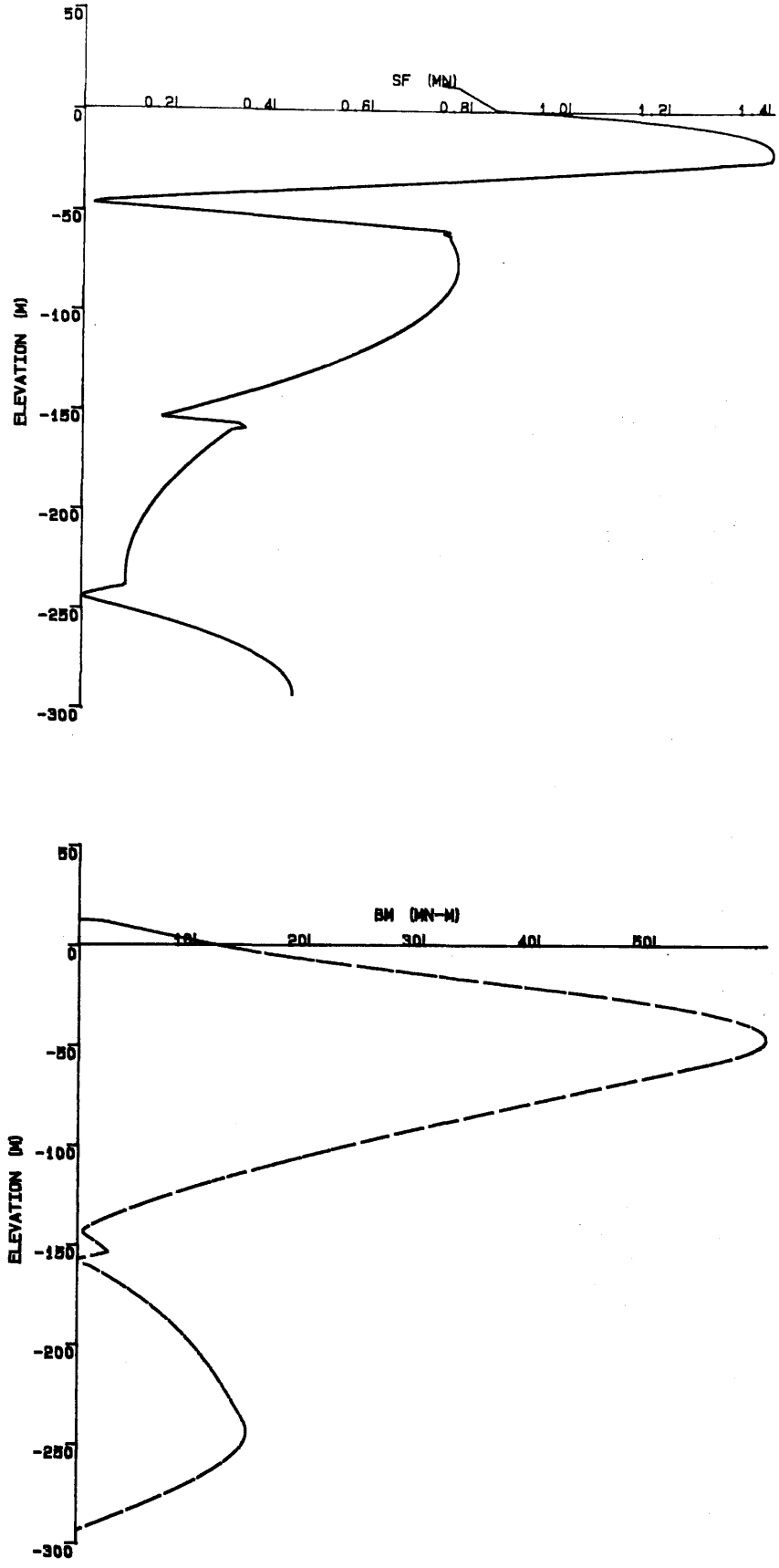

Fig.4.8 Shear force and bending moment distribution along the tower
$\omega = 1.0$ rad /s, Hw = 2m, $C_D = 4.8$ a) Shear force b) Bending moment

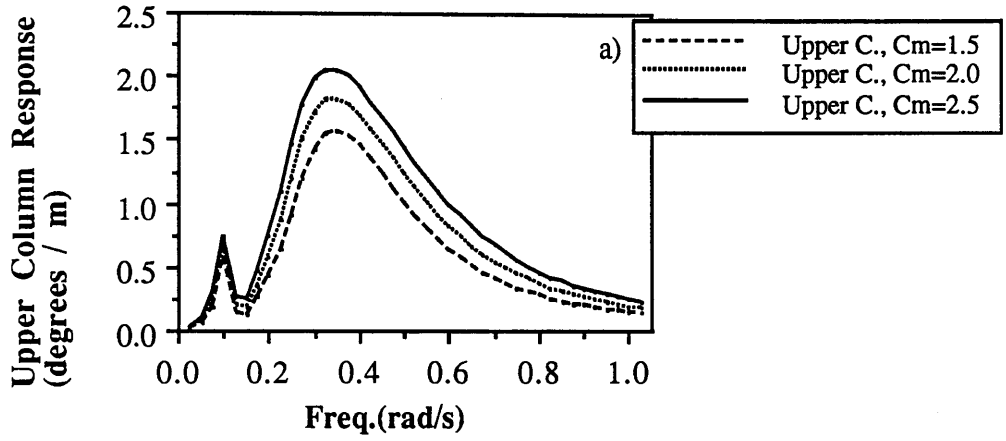

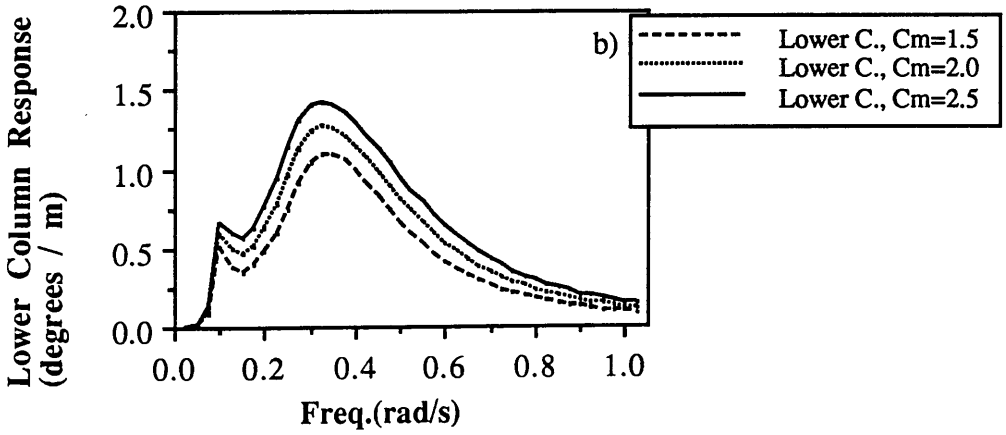

Fig.4.9 Sensitivity of angular response to the C_M coefficient variation

a) Upper column response b) Lower column response

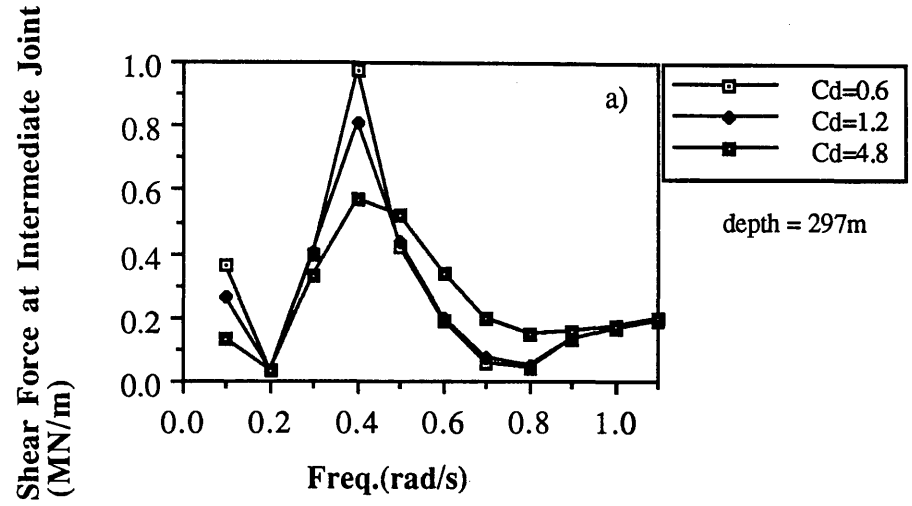

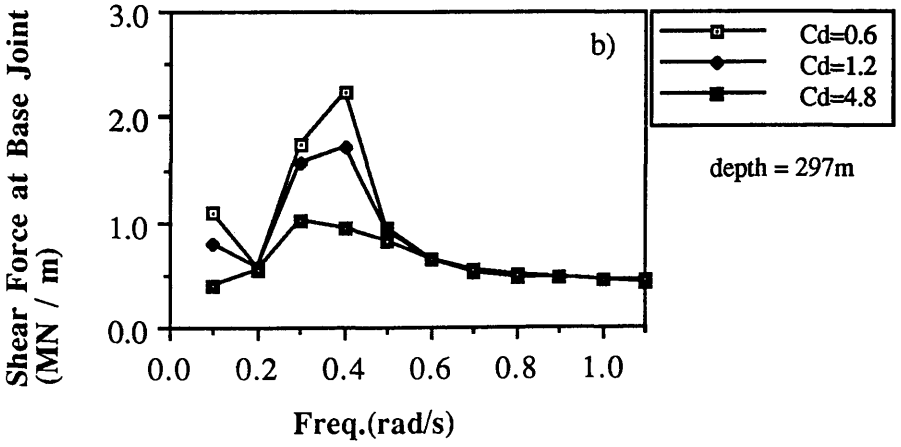

Fig.4.10 The effect of drag coefficient variation on the joint forces

a) Intermediate joint b) Base joint

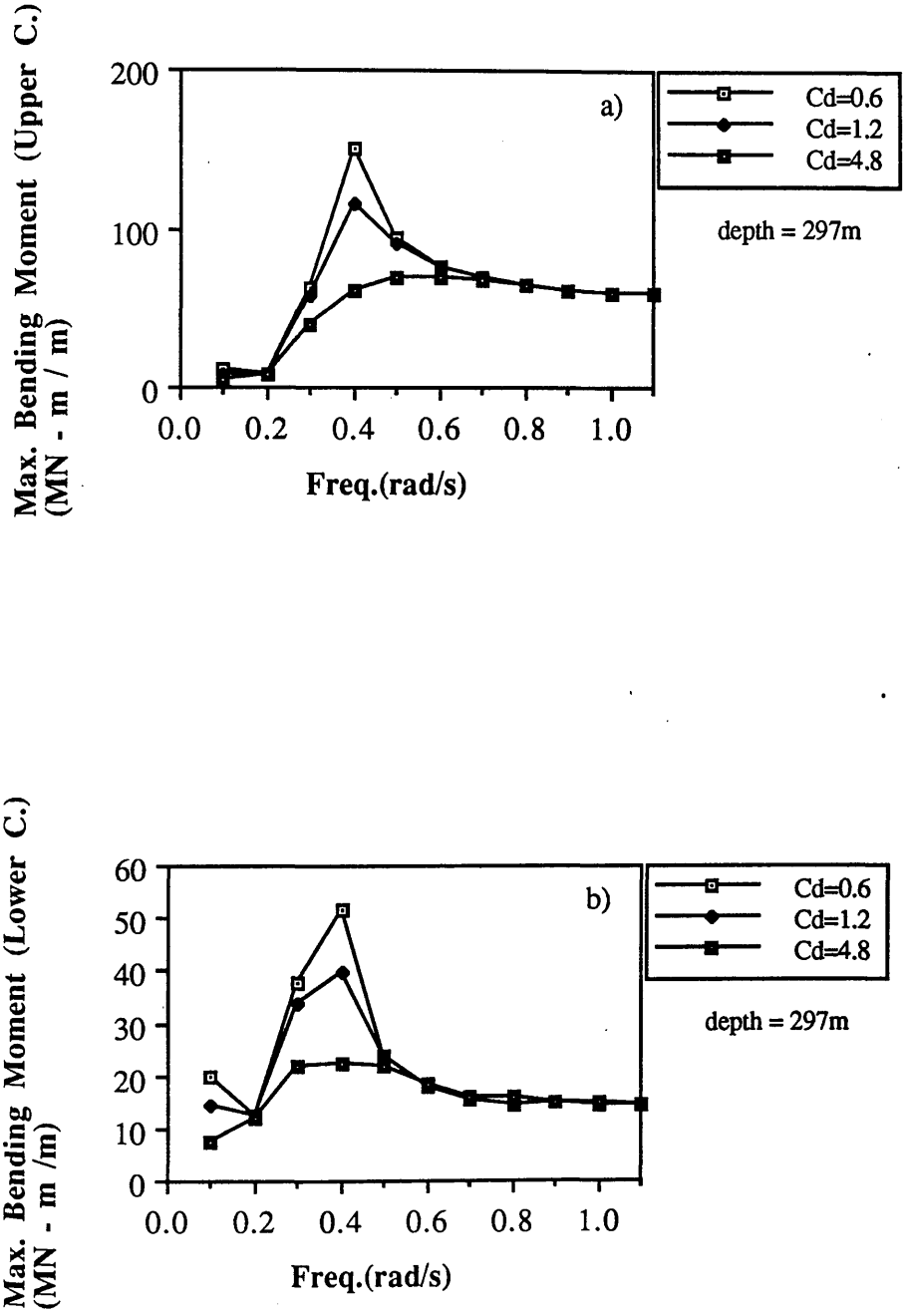

Fig.4.11 The effect of drag coefficient variation on the maximum bending moments

a) Upper column b) Lower column

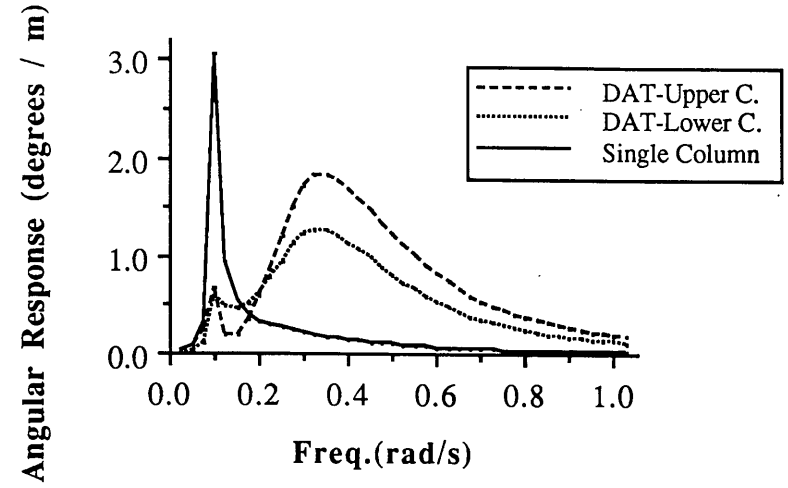

Fig.4.12 Comparison of angular response: DAT vs SAT, Cd=4.8

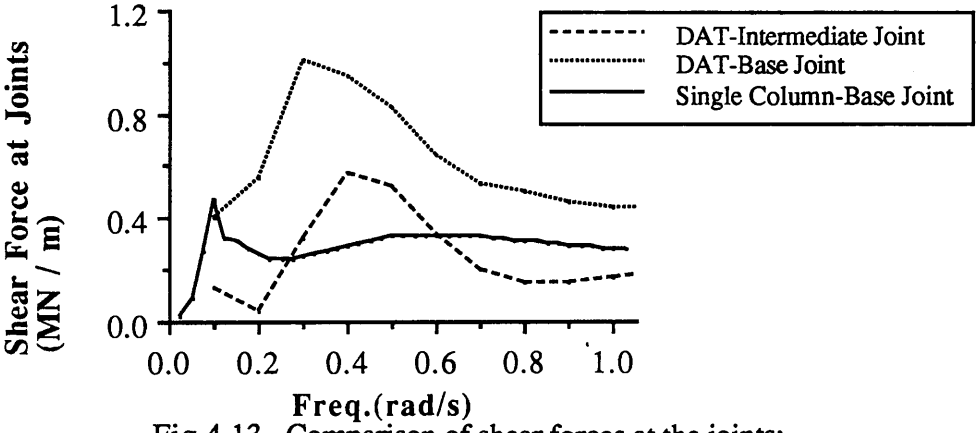

Fig.4.13 Comparison of shear forces at the joints: DAT vs SAT, Cd=4.8

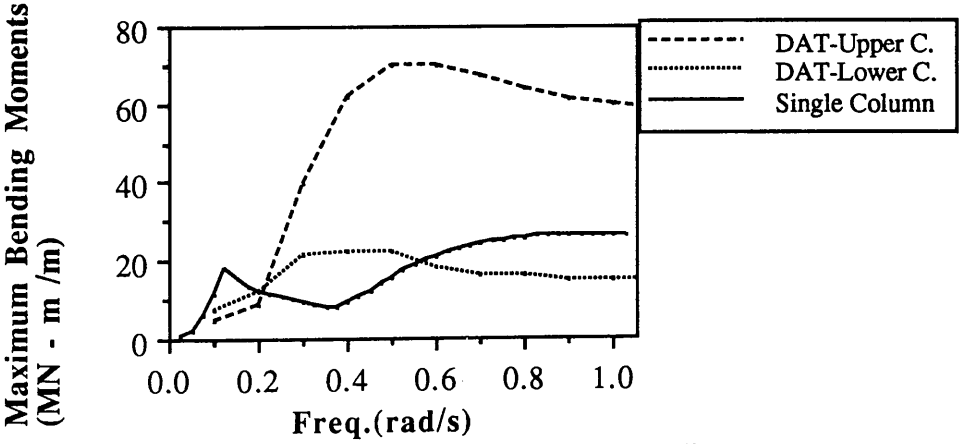

Fig.4.14 Comparison of maximum bending moment: DAT vs SAT, Cd=4.8

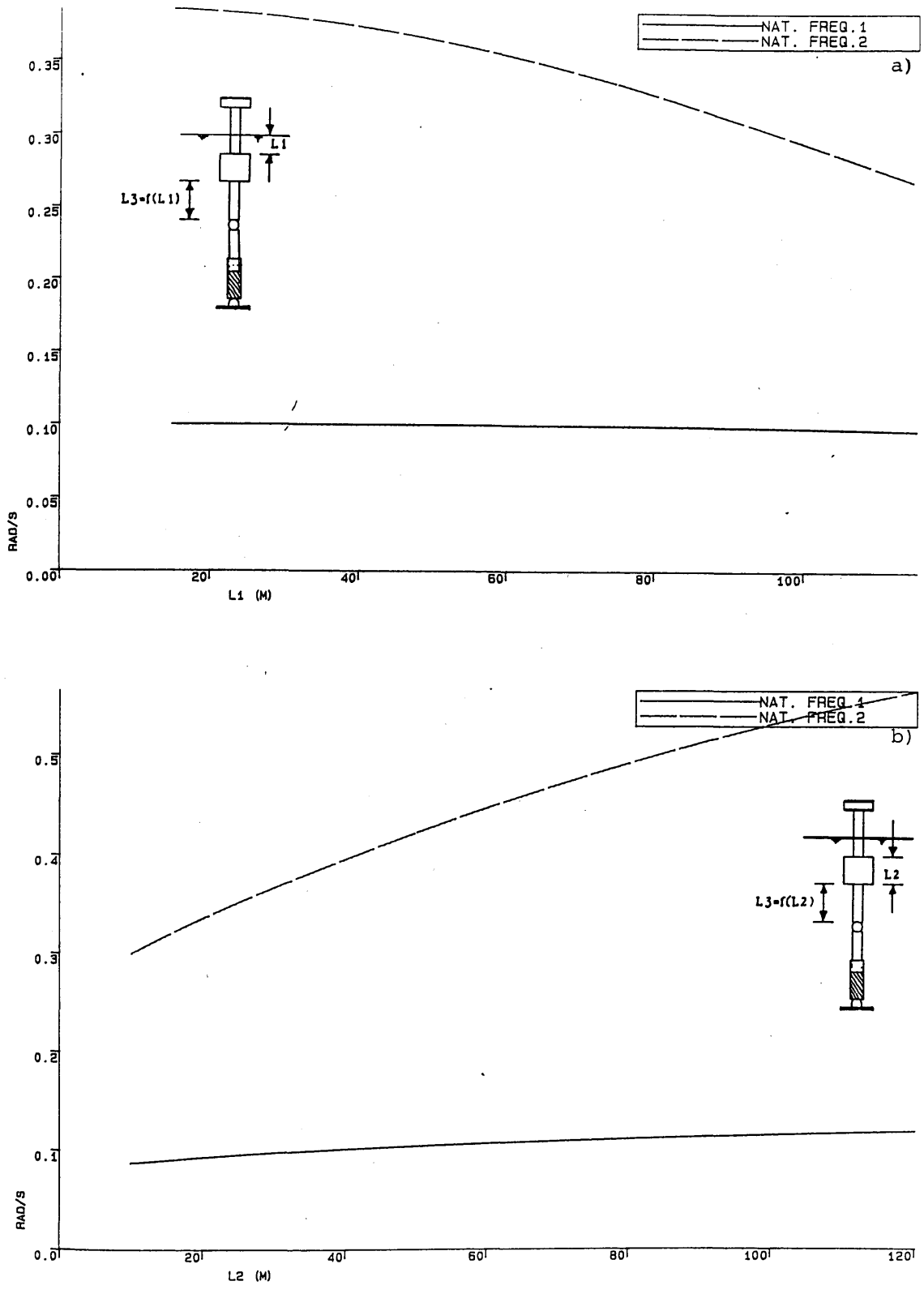

Fig.4.15 Sensitivity of natural frequencies to geometric changes

a) Place of buoyancy chamber b) Length of buoyancy chamber

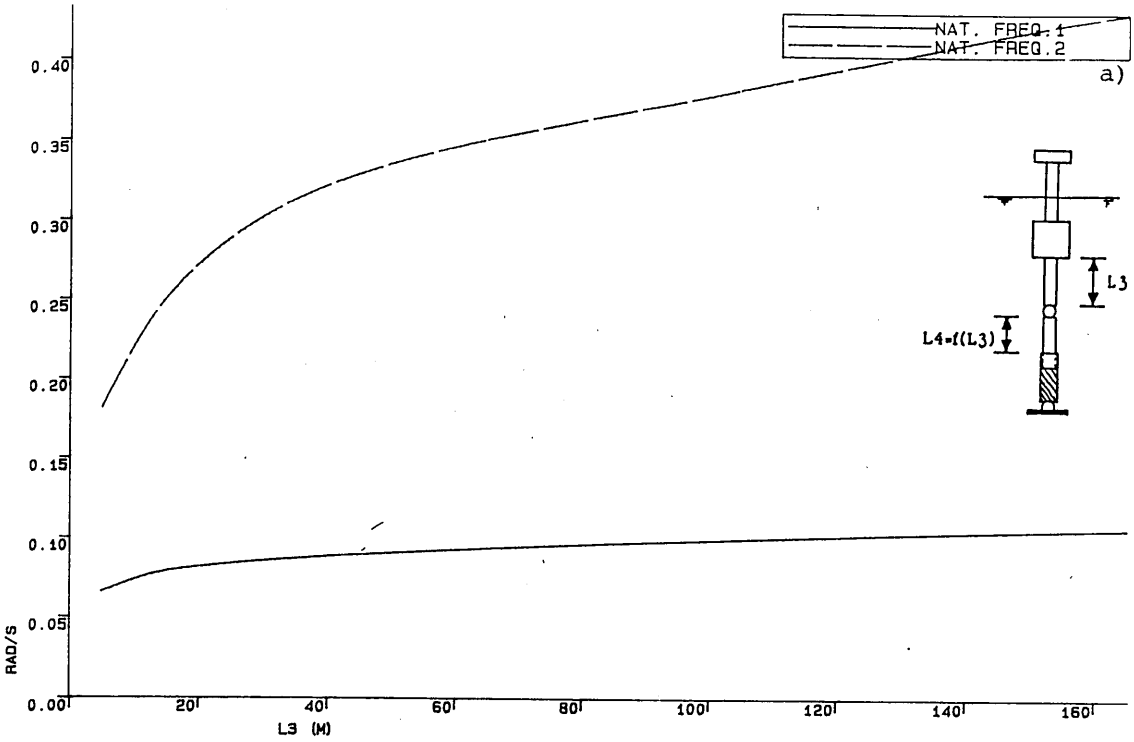

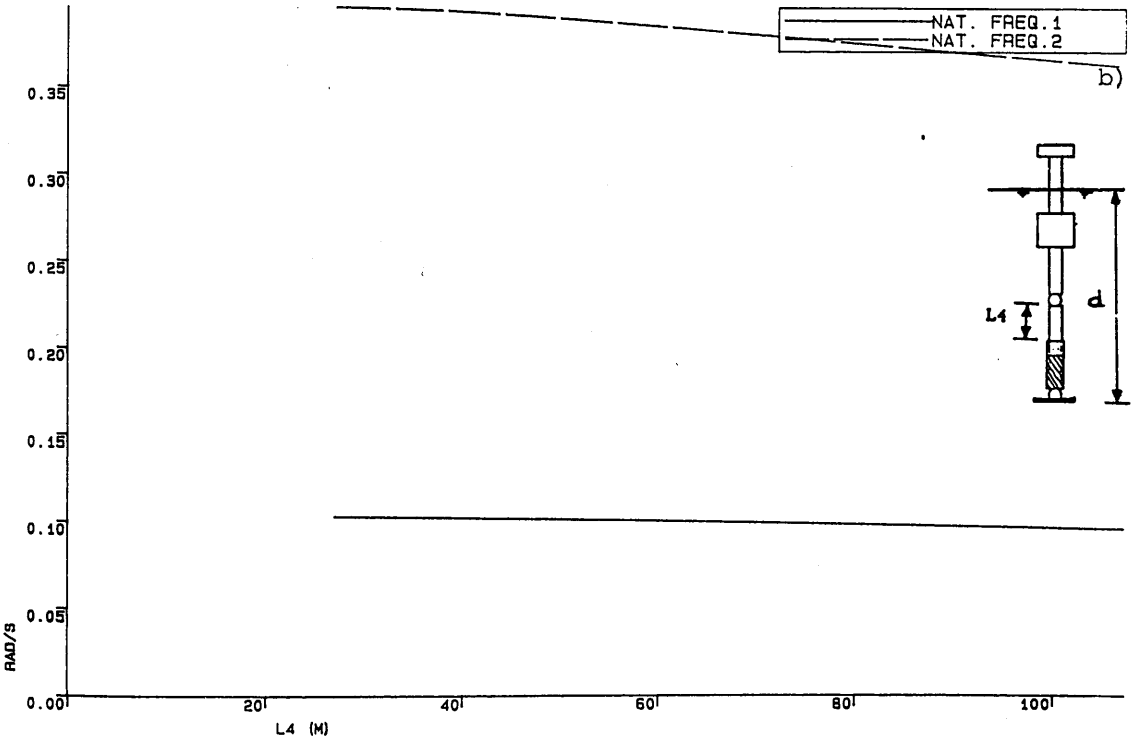

Fig.4.16 Sensitivity of natural frequencies to geometric changes

a) Place of intermediate joint b) Depth of water

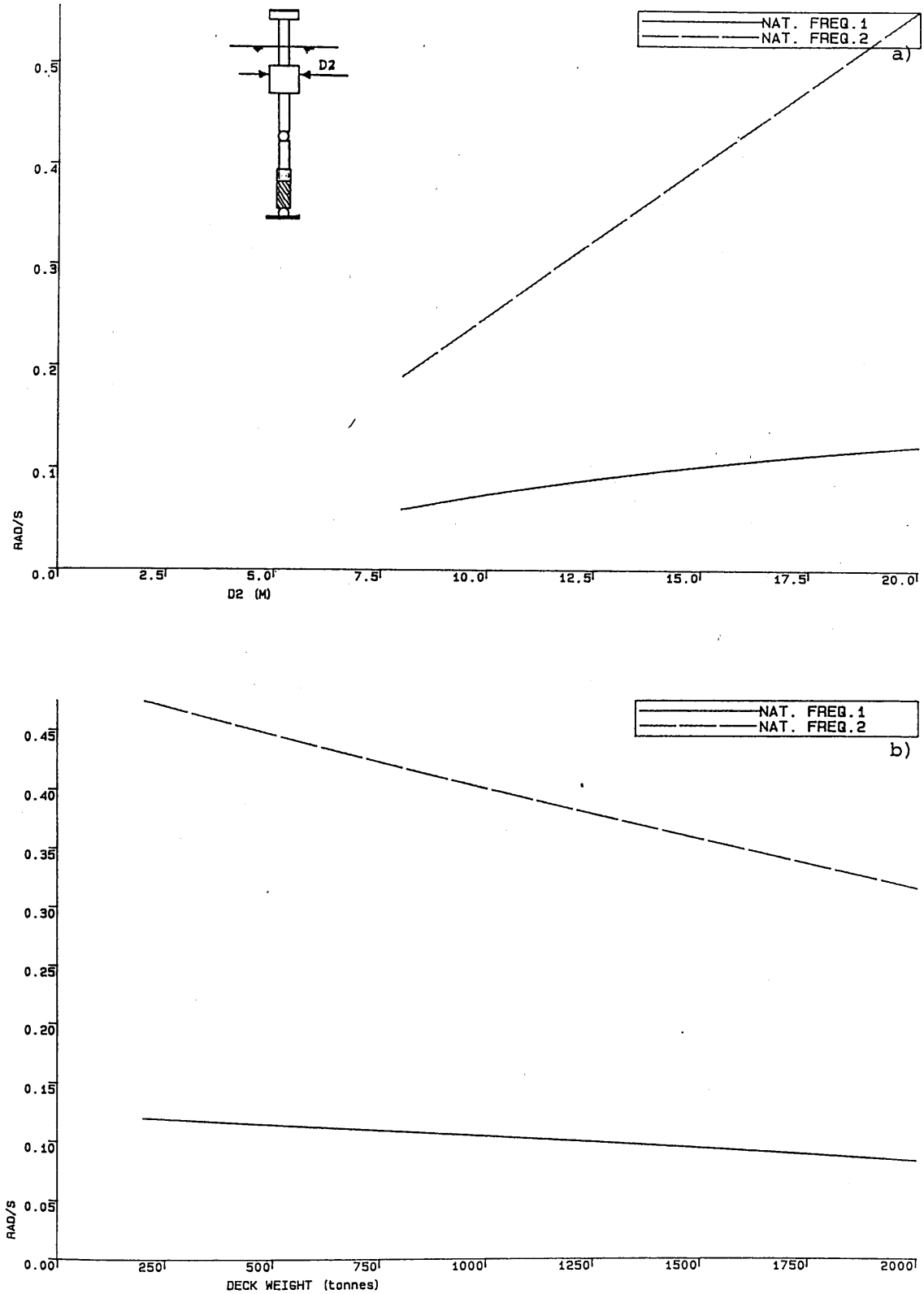

Fig.4.17 Sensitivity of natural frequencies to geometric changes.

a) Diameter of buoyancy chamber b) Deck weight

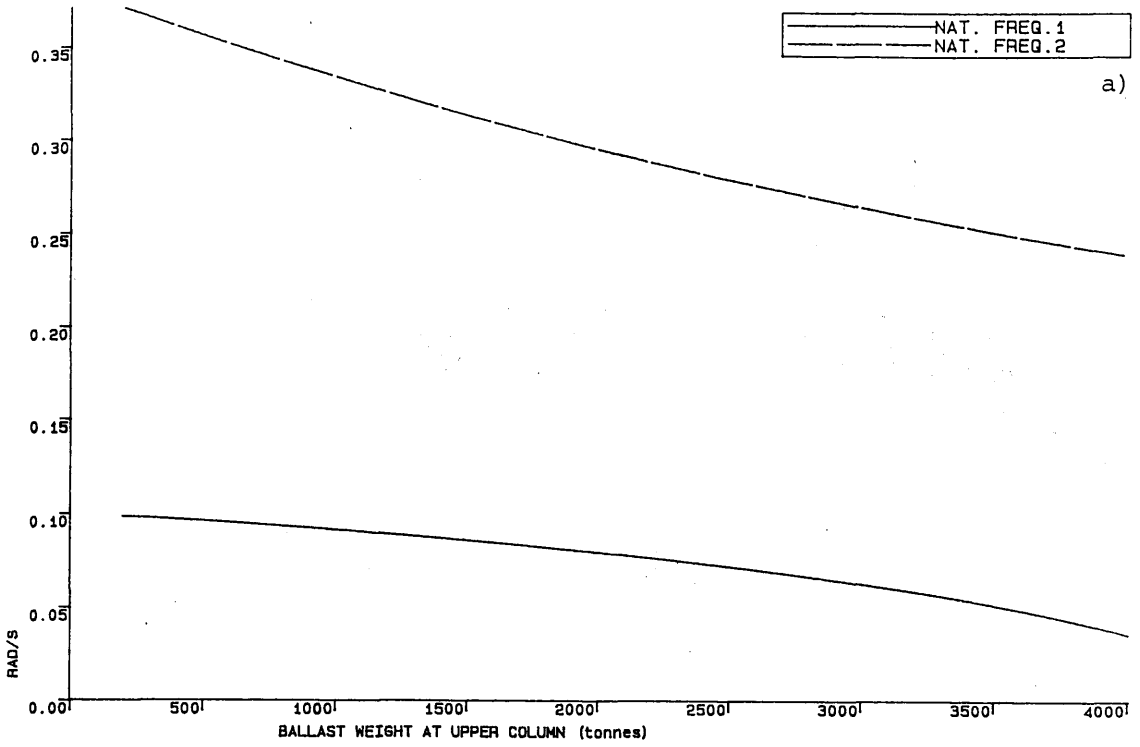

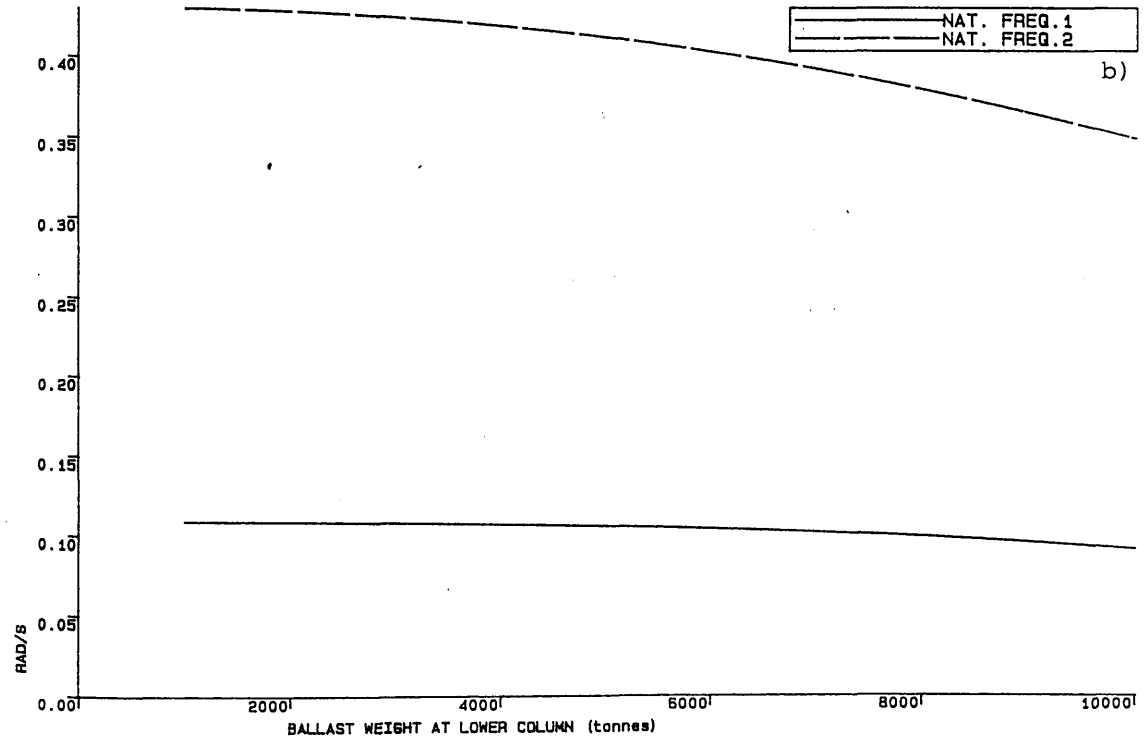

Fig.4.18 Sensitivity of the natural frequencies to the ballast weight

a) Upper column b) Lower column

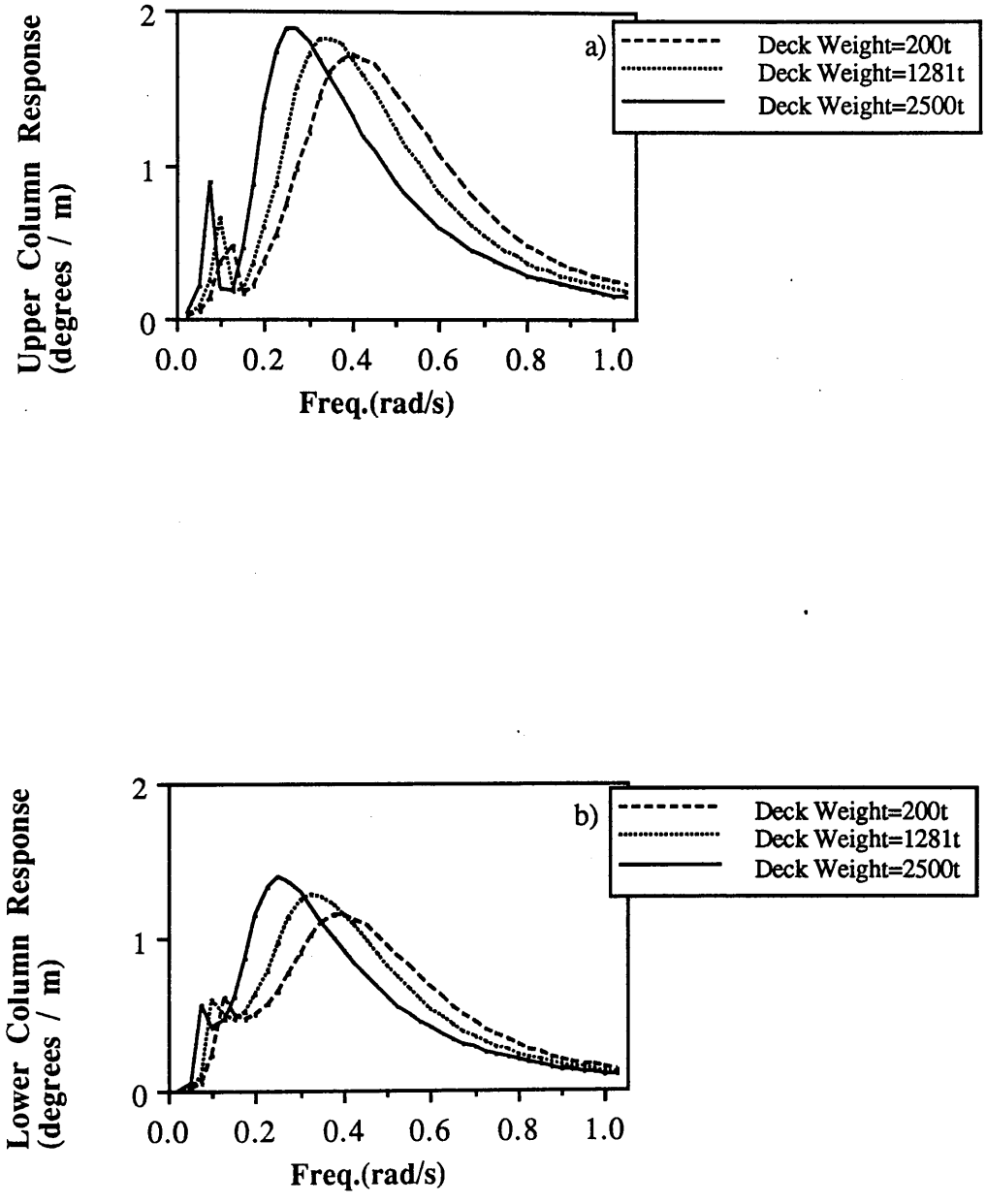

Fig.4.19 The effect of deck weight variation on the motion response

a) Upper column b) Lower column

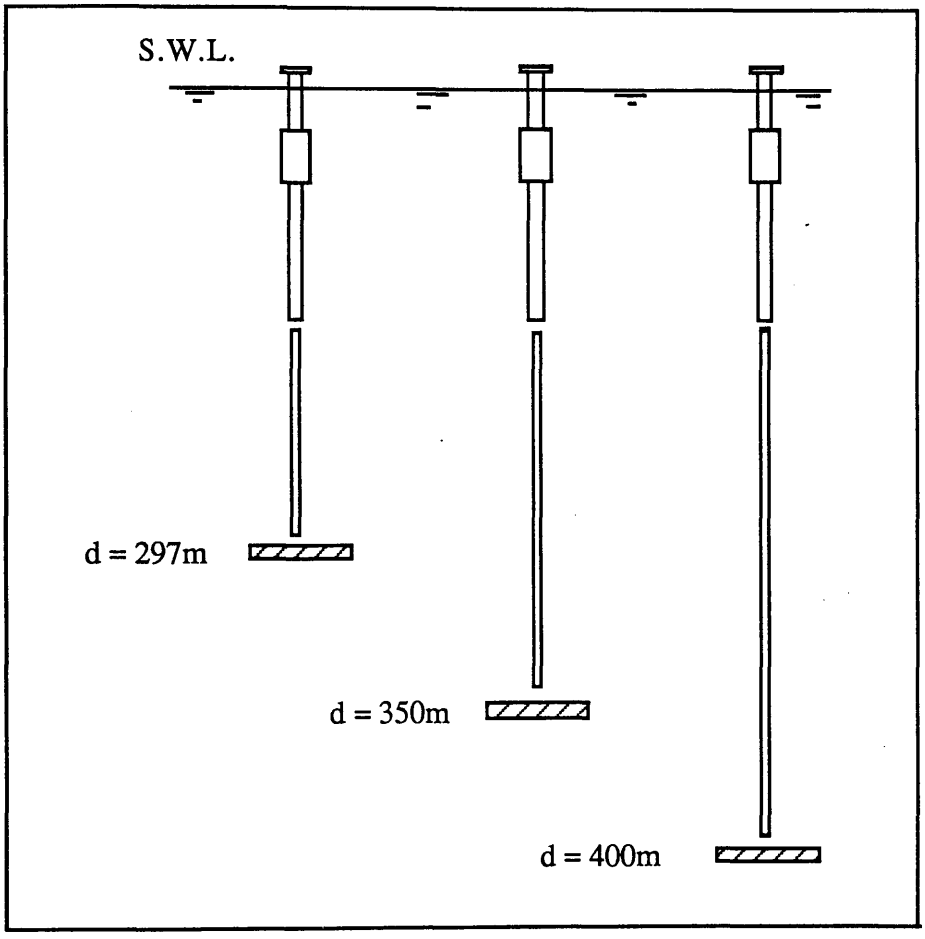

Fig.4.20 Three articulated tower configuration

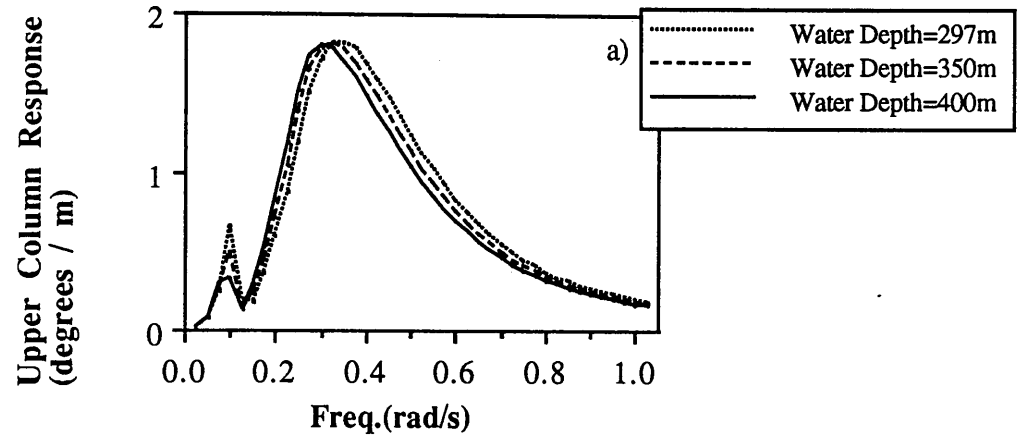

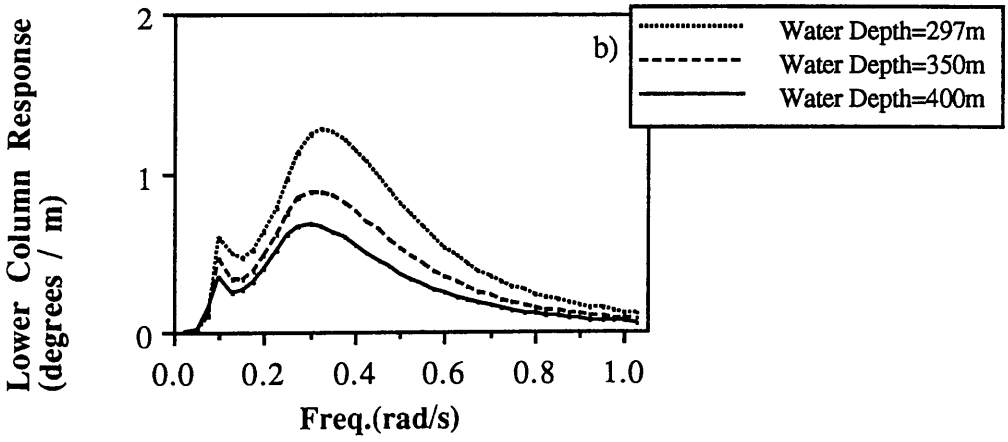

Fig.4.21 The effect of water depth variation on the motion response

a) Upper column b) Lower column

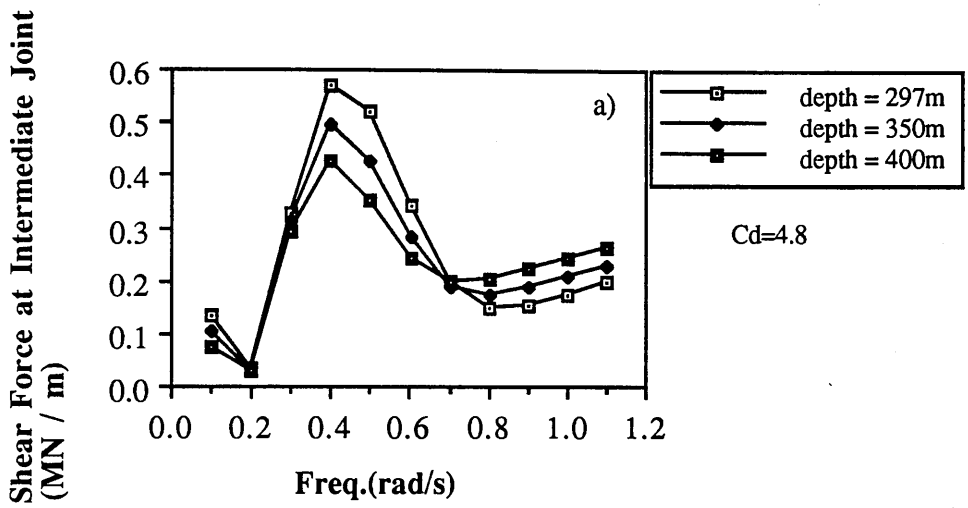

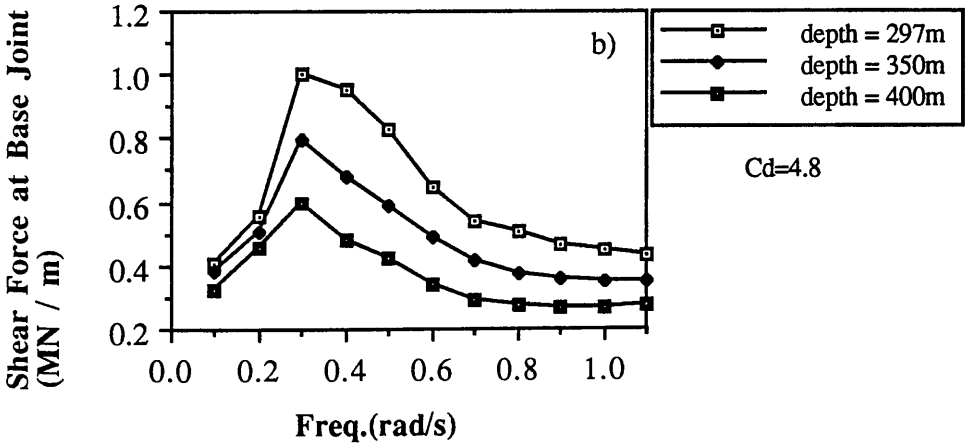

Fig.4.22 The effect of water depth variation on the joint forces

a) Intermediate joint b) Base joint

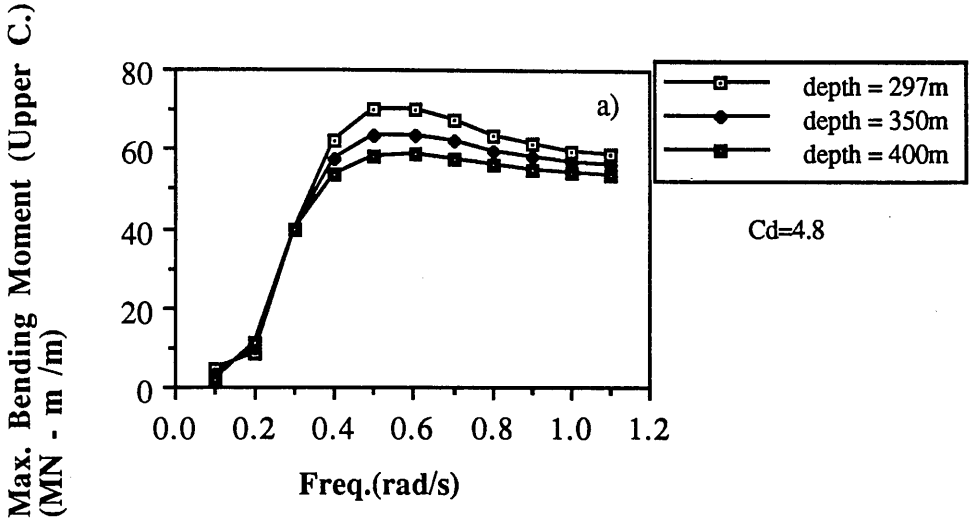

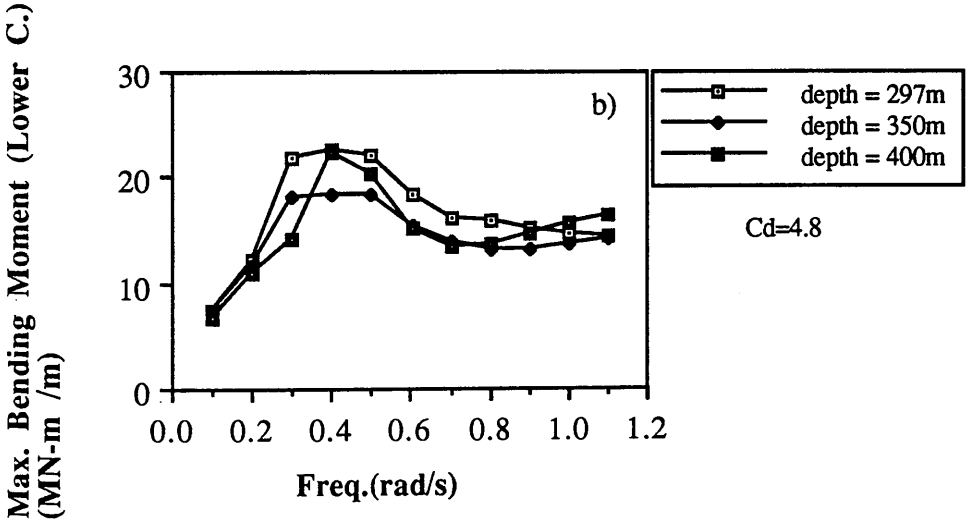

Fig.4.23 The effect of water depth variation on the max. bending moment

a) Upper column b) Lower column

CHAPTER 5

COUPLED DOUBLE ARTICULATED TOWER AND SHIP SYSTEM

5.1 GENERAL DESCRIPTION

Some of the properties of the double articulated tower (DAT) concept are discussed in Chapter 4. One of the most common usages of DAT is as a mooring base for floating production and storage vessels. The general configuration for the DAT-Ship system is shown in Fig.5.1. The articulated tower is connected to a ship by means of a rigid yoke. The rigid yoke has a universal joint on top of the DAT that allows the yoke to roll, pitch and weather vane independent of the tower. The buoyancy chamber at the upper column provides the overall restoring force for the system. The system distinguishes itself from that of single articulated based systems by the addition of a universal joint at the middle of the tower. The use of this intermediate universal joint significantly reduces the structural weight of the system as compared with the single articulated tower design. The third universal joint is placed between the lower column and the base. The base is designed to transmit the mooring loads induced by the permanently moored storage vessel from the base universal joint to the ocean floor.

The presence of the ship restricts the motions of the upper column. The modes of motion for this system are shown in Fig.5.2. The first mode is well known planery motion of the vessel against the buoyancy restoring forces due to the upper column buoyancy chamber. The second mode of motion is the so-called 'elbowing oscillations' of the tower. This motion can be excited in a high sea state (second natural period, T_n=25.5 s).

Third and higher modes are the structural periods of the lower and upper columns. Analysis of the structural periods of the system by using modal technique is beyond the scope of this study.

Several papers have discussed the behaviour of DAT based FPSs. Among them are Wolfram and Gunderson(1979), Haverty et al. (1982), Houlie et al. (1983), Natvig and Berta(1983), Dumazy and Leturq(1983), Römeling et al (1984), Chaudhuri (1986), and Brendling and Wilson(1987). The studies considered in these papers are all related to the overall behaviour of the system in irregular uni- or multi-directional seas and they reflect

mostly experimental model test and/or finite element application oriented studies. The results presented in these references consider the behaviour of a prototype configuration and do not examine the effect of geometric changes on the important parameters in the design stage.

In this study a more simplistic approach is followed in order to understand the behaviour of the system in waves and to point out some important parameters which govern the design of such systems.

Two different mathematical models are considered. The first one has 2-DOF, which assumes that the ship performs surge oscillations only, neglecting the heave and pitch oscillations. The second one considers the system as a 5-DOF system including the arbitrary yoke angle-stiffness and ship heave-pitch motions. The results of the two mathematical models are compared with each other as well as with the experimental measurements carried out at the Hydrodynamics Laboratory. The shear force and bending moment distributions along the double articulated tower with the ship connected to it are shown. Chapter 5 ends with some parametric studies which examine the effect of various geometrical changes on the system responses as well as on the yoke forces including the yoke length and the yoke orientation.

5.2 MOTION EQUATION FOR COUPLED DOUBLE ARTICULATED TOWER AND SHIP SYSTEM

5.2.1 SIMPLE MODEL FOR COUPLED DAT-SHIP SYSTEM, 2-DOF

In order to investigate the behaviour of the DAT-ship system in regular waves the ship is assumed to be a rigid extension of the upper column. This assumption is similar to the one which is described in Chapter 3, Section 3.2.1. During the oscillations of the system around the equilibrium position, the yoke remains parallel to the water surface(see Fig.5.3).

The motion equations which describe the system's behaviour under the wave excitation forces are similar to those of the double articulated tower(see Chapter 4). In order to take into account the presence of the ship, some coefficients should be modified. In addition, the moment term, M_{ES}, due to the surge forces on the ship, is added to the right hand side of the motion equation. The 2-DOF motion equation of the system is given as follows

$$\begin{bmatrix} A_{11} & A_{12} \\ A_{21} & A_{22} \end{bmatrix} \begin{Bmatrix} \ddot{\theta}_1 \\ \ddot{\theta}_2 \end{Bmatrix} + \begin{bmatrix} B_{11} & B_{12} \\ B_{21} & B_{22} \end{bmatrix} \begin{Bmatrix} \dot{\theta}_1 \\ \dot{\theta}_2 \end{Bmatrix} + \begin{bmatrix} K_{11} & 0 \\ 0 & K_{22} \end{bmatrix} \begin{Bmatrix} \theta_1 \\ \theta_2 \end{Bmatrix} = \begin{Bmatrix} M_{E1} \\ M_{E2} + M_{ES} \end{Bmatrix} \tag{5.1}$$

Eq.(5.1) has been derived from Lagrange's equation by including the coupling effects between the lower and upper columns. The terms appearing in Eq.(5.1) can be written as follows(extra terms due to the presence of the ship are typed in italic characters).

$$A_{11} = m_{11}l^2_{11} + m_{12}l^2_{12} + m_{13}l^2_{13} + m_{14}l^2_{14} + (m_{21}+m_{22}+m_{23}+m_{24}+m_{25})L^2_1 + \rho[V_{11}h^2_{11}+V_{12}h^2_{12}+(V_{21}+V_{22}+V_{23})L^2_1] + 2\,(M+M_{AD,X})L^2_1$$

$$A_{22} = m_{21}l^2_{21} + m_{22}l^2_{22} + m_{23}l^2_{23} + m_{24}l^2_{24} + m_{25}l^2_{25} + \rho(V_{21}h^2_{21}+V_{22}h^2_{22}+V_{23}h^2_{23}) + (M+M_{AD,X})(L_2+CL)^2$$

$$A_{12} = A_{21} = [m_{21}l_{21} + m_{22}l_{22} + m_{23}l_{23} + m_{24}l_{24} + m_{25}l_{25} + \rho(V_{21}h_{21}+V_{22}h_{22}+V_{23}h_{23})]L_1 + (M+M_{AD,X})(L_2+CL)L_1$$

$$B_{11} = (1 / 3\pi)\,\rho\, C_D \omega\, \theta_{1,max} \{D_5((l_5+\varepsilon_1)^4 - \varepsilon^4_1) + D_4((l_4 + l_5 +\varepsilon_1)^4 - (l_5+\varepsilon_1)^4)\} + 0.5\,\rho\, C^B_D BT\, L^3_1 \omega\theta_{1,max}$$

$$B_{12} = (4/9\pi)\,\rho\, C_D \omega\, \theta_{2,max}\, L_1 \{D_3((\varepsilon_2/2 + l_3)^3 - (\varepsilon_2/2)^3) + D_2((\varepsilon_2/2 + l_3 + l_2)^3 - (\varepsilon_2/2 + l_3)^3) + D_1((\varepsilon_2/2 + l_3 + l_2 + l_1)^3 - (\varepsilon_2/2 + l_3 + l_2)^3)\}$$
$$+0.5\,\rho\, C^B_D BT\, L_1 (L_2 + CL)^2 \omega \theta_{2,max}$$

$$B_{21} = (2/3\pi)\,\rho\, C_D \omega\, \theta_{1,max}\, L_1^2 \{D_3((\varepsilon_2/2 + l_3)^2 - (\varepsilon_2/2)^2) + D_2((\varepsilon_2/2 + l_3 + l_2)^2 - (\varepsilon_2/2 + l_3)^2) + D_1((\varepsilon_2/2 + l_3 + l_2 + l_1)^2 - (\varepsilon_2/2 + l_3 + l_2)^2)\}$$
$$+0.5\,\rho\, C^B_D BT\, L^2_1 (L_2 + CL) \omega \theta_{1,max}$$

$$B_{22} = (1/3\pi)\,\rho\, C_D\, \omega\, \theta_{2,max} \{D_3((\varepsilon_2/2 + l_3)^4 - (\varepsilon_2/2)^4) + D_2((\varepsilon_2/2 + l_3 + l_2)^4 - (\varepsilon_2/2 + l_3)^4) + D_1((\varepsilon_2/2 + l_3 + l_2 + l_1)^4 - (\varepsilon_2/2 + l_3 + l_2)^4)\} + 0.5\,\rho\, C^B_D BT (L_2 + CL)^3 \omega \theta_{2,max} \quad (5.2)$$

The wave forces on the double articulated tower can be obtained from Morison's formula. It is assumed that the fluid motion is unaffected by the presence of the ship. Wave exciting forces on the ship are presented in terms of the Froude-Krylov forces including the diffraction effects in an approximate way. The assumptions concerning fluid loading are discussed in detail in Chapter 2. The viscous damping forces due to the ship are calculated by assuming that the ship is represented by an oscillating plate which has a cross sectional area of $T_S \times B_S$.

The motion equation can be solved by introducing the solution terms as given in Eq.(4.17). The total surge motion of the ship consists of the addition of the upper and lower column responses observing the phase differences

$$x_{SHIP} = L_1 \sin\theta_1 + (L_2 + CL)\sin\theta_2 \quad (5.3)$$

The axial forces on the yoke mechanism can be calculated by replacing the yoke structure with a fictitious axial force vector and writing the equation of motion of the rest of the system.

$$F_R = F_{Px} + F_{Ax} - (M + M_{AD,x})\omega^2 x_{SHIP} \quad (5.4)$$

The application of a 2-DOF mathematical model on the coupled system is discussed in Section 5.2.3.

5.2.2 DETAILED MODEL FOR COUPLED DAT-SHIP SYSTEM, 5-DOF

The motion of the DAT-ship system in the plane of wave propagation can be defined by a five degrees of freedom (5-DOF) model. This model couples the angular motion of the double articulated tower to the surge, heave and pitch of the ship by a yoke of finite stiffness. A schematic diagram of the 5-DOF system is shown in Fig.5.4 in which the origin of the system is centered at the undisturbed equilibrium position of the ship. The motions of the system are assumed to take place about the static equilibrium position with small amplitudes. It is also assumed that the joints on the yoke are frictionless.

The equations of motion of the 5-DOF system are derived by considering the equilibrium of forces and moments on the double articulated tower and on the ship.

Heave Motion of the Ship

$$(M + M_{AD,y})\ddot{y} + B_{yy}\dot{y} + K_{yy}y = F_{Ty} - F_R \sin\alpha \tag{5.5}$$

where M is the mass of the ship; $M_{AD,y}$ the added mass of the ship in heave; B_{yy}, the damping coefficient in heave; K_{yy}, the stiffness coefficient of the ship in heave; F_{Ty}, the heave forces on the ship due to regular waves (see Eq.(2.12)); α, the yoke inclination angle and F_R, the axial yoke force.

Surge Motion of the Ship

$$(M + M_{AD,x})\ddot{x} + B_{xx}\dot{x} = F_{Tx} + F_R \cos\alpha \tag{5.6}$$

where $M_{AD,x}$ is the added mass of the ship in surge; B_{xx}, the damping coefficient in surge and F_{Tx}, the surge forces on the ship due to regular waves (see Eq.(2.9))

Pitch Motion of the Ship

$$(I_{\psi\psi} + I_{AD,\psi})\ddot{\psi} + B_{\psi\psi}\dot{\psi} + K_{\psi\psi}\psi = M_{T\psi} - F_R[H\cos\alpha + (L_S/2)\sin\alpha] \qquad (5.7)$$

where $I_{\psi\psi}$ is the mass moment of inertia of the ship in pitch; $I_{AD,\psi}$, added mass moment of inertia of ship in pitch; $B_{\psi\psi}$, damping coefficient in pitch; $K_{\psi\psi}$, stiffness coefficient of ship in pitch; $M_{T\psi}$, wave induced moments on ship in pitch(see Eq.(2.14)).

Angular Motion of the Double Articulated Tower

$$\begin{bmatrix} A_{11} & A_{12} \\ A_{21} & A_{22} \end{bmatrix}\begin{Bmatrix} \ddot{\theta}_1 \\ \ddot{\theta}_2 \end{Bmatrix} + \begin{bmatrix} B_{11} & B_{12} \\ B_{21} & B_{22} \end{bmatrix}\begin{Bmatrix} \dot{\theta}_1 \\ \dot{\theta}_2 \end{Bmatrix} + \begin{bmatrix} K_{\theta\theta,1} & 0 \\ 0 & K_{\theta\theta,2} \end{bmatrix}\begin{Bmatrix} \theta_1 \\ \theta_2 \end{Bmatrix} = \begin{Bmatrix} M_{E1} + F_R L_1 \cos\alpha \\ M_{E2} + F_R(L_2 + CL)\cos\alpha \end{Bmatrix} \qquad (5.8)$$

where A_{11},A_{12},A_{21},A_{22} are inertia terms; B_{11},B_{12},B_{21},B_{22} , damping terms; $K_{\theta\theta,1}$, $K_{\theta\theta,2}$, stiffness coefficients of lower and upper column, respectively; θ_1,θ_2, angular response of the lower and upper columns, respectively; M_{E1}, M_{E2}, wave exciting moments on the lower and upper column, respectively.

Compatibility Equation

The kinematic compatibility equation takes into account the surge, heave and pitch motions of the ship, the upper and lower column rotations, the initial yoke angle and yoke stiffness. Fig.5.4 shows a diagram of the deflected configuration of the system. It can be seen in this figure that the following geometrical relationship holds for the axial yoke force:

$$F_R = c\{y \sin \alpha - x \cos \alpha + [H \cos \alpha + (L_S / 2)\sin \alpha]\psi - (\theta_1 L_1 + \theta_2(L_2 + CL))\cos \alpha\} \quad (5.9)$$

where c is stiffness coefficient for the yoke or $c = AE/L_y$; A, cross sectional area of the yoke; E, modulus of elasticity and L_y, yoke length.

The compatibility equation couples the five motion equations describing the system's response.

Solution of Equations of Motion

Eqs.(5.5)-(5.8) can be written in matrix form as

$$[M]\{\ddot{X}\} + [B]\{\dot{X}\} + [K]\{X\} = \{F\} \quad (5.10)$$

The mass, damping and stiffness matrices and the definition of the terms are given as follows:

$$[M] = \begin{bmatrix} (M + M_{AD,y}) & 0 & 0 & 0 & 0 \\ 0 & (M + M_{AD,x}) & 0 & 0 & 0 \\ 0 & 0 & (I_{\psi\psi} + I_{AD,\psi}) & 0 & 0 \\ 0 & 0 & 0 & A_{11} & A_{12} \\ 0 & 0 & 0 & A_{21} & A_{22} \end{bmatrix}$$

$$[B] = \begin{bmatrix} B_{yy} & 0 & 0 & 0 & 0 \\ 0 & B_{xx} & 0 & 0 & 0 \\ 0 & 0 & B_{\psi\psi} & 0 & 0 \\ 0 & 0 & 0 & B_{11} & B_{12} \\ 0 & 0 & 0 & B_{21} & B_{22} \end{bmatrix}$$

$[K] = K_{ij}$ where, i = 1, 5 and j = 1, 5

$$\{X\}^T = \{y,\ x,\ \psi,\ \theta_1,\ \theta_2\}$$

$$\{F\}^T = \{F_{Ty},\ F_{Tx},\ M_{T\psi},\ M_{E1},\ M_{E2}\}$$

in which

$M = \rho L_S B_S T_S$,

$M_{AD,y} = \rho\ (\pi/2)(B_S/2)^2 C_{VH} L_S$,

$B_{yy} = 2\zeta[(M+M_{AD,y})K_{yy}]^{0.5}$,

$K_{yy} = \rho g L_S B_S$,

$M_{AD,x} = \rho\ (\pi/4) B_S^2\, C_{VS} T_S$

$B_{xx} = (1/2)\ \rho\ C_{DS}\ B_S T_S$

$I_{\psi\psi} = (M/12)(D_B^2+L_S^2)$

$I_{AD,\psi} = \rho\ (\pi/2)\ (L_S/2)^4 C_{VP} B_S$

$B_{\psi\psi} = 2\ \zeta\ [(\ I_{\psi\psi}+I_{AD,\psi})\ K_{\psi\psi}]^{0.5}$

$K_{\psi\psi} = \rho\ g\ \overline{GM}_L\ L_S\ B_S\ T_S$

ζ = damping ratio

$\overline{GM}_L$ = longitudinal metacentric height of ship

The terms, A_{11}, A_{12}, A_{21}, A_{22}, B_{11}, B_{12}, B_{21}, B_{22}, $K_{\theta\theta,1}$, $K_{\theta\theta,2}$ are related to the double articulated tower motion equations. Since these coefficients are the same as given in Eq.(4.26) they will not be repeated here.

The coefficients K_{ij} are as follows:

$K_{11} = K_{yy} + c \sin^2\alpha$

$K_{12} = - c \cos\alpha \sin\alpha$

$K_{13} = c\ [\ H \cos\alpha + (L_S/2) \sin\alpha]\ \sin\alpha$

$K_{14} = - c\ L_1 \cos\alpha \sin\alpha$

$K_{15} = - c\ (L_2+CL) \cos\alpha \sin\alpha$

$K_{21} = -c \cos\alpha \sin\alpha$

$K_{22} = c \cos^2\alpha$

$K_{23} = - c [H \cos\alpha + (L_S/2) \sin\alpha] \cos\alpha$

$K_{24} = c L_1 \cos^2\alpha$

$K_{25} = c (L_2+CL) \cos^2\alpha$

$K_{31} = c \sin\alpha [H \cos\alpha + (L_S/2) \sin\alpha]$

$K_{32} = - c \cos\alpha [H \cos\alpha + (L_S/2) \sin\alpha]$

$K_{33} = K_{\psi\psi} + c [H \cos\alpha + (L_S/2) \sin\alpha]^2$

$K_{34} = - c L_1 \cos\alpha [H \cos\alpha + (L_S/2) \sin\alpha]$

$K_{35} = -c (L_2+CL) \cos\alpha [H \cos\alpha + (L_S/2) \sin\alpha]$

$K_{41} = -c L_1 \sin\alpha \cos\alpha$

$K_{42} = c L_1 \cos^2\alpha$

$K_{43} = - c [H \cos\alpha + (L_S/2) \sin\alpha] L_1 \cos\alpha$

$K_{44} = K_{\theta\theta,1} + c L_1^2 \cos^2\alpha$

$K_{45} = c (L_2+CL) \cos^2\alpha L_1$

$K_{51} = - c (L_2+CL) \sin\alpha \cos\alpha$

$K_{52} = c (L_2+CL) \cos^2\alpha$

$K_{53} = - c [H \cos\alpha + (L_S/2) \sin\alpha] (L_2+CL) \cos\alpha$

$K_{54} = c L_1 (L_2+CL) \cos^2\alpha$

$K_{55} = K_{\theta\theta,2} + c (L_2+CL)^2 \cos^2\alpha$

Eq.(5.10) is a homogeneous, second-order, linear differential equation. Therefore, the solutions are assumed to take the following form

$$\{X\} = \begin{Bmatrix} y_1 \sin \omega t + y_2 \cos \omega t \\ x_1 \sin \omega t + x_2 \cos \omega t \\ \psi_1 \sin \omega t + \psi_2 \cos \omega t \\ \theta_{11} \sin \omega t + \theta_{12} \cos \omega t \\ \theta_{21} \sin \omega t + \theta_{22} \cos \omega t \end{Bmatrix} \tag{5.11}$$

The next step is to apply these solutions to Eq.(5.10). This yields the following matrix equation.

$$A_{ij}X_j=B_i \tag{5.12}$$

In order to solve the above equation, the computer program, a NAg subroutine, F04AEF is employed. The results are nondimentionalised with respect to the wave amplitude.

5.2.3 COMPARISON OF TWO MATHEMATICAL MODELS: 2-DOF VS 5-DOF

The results of the two mathematical models are compared in this section. A coupled double articulated tower-ship configuration, shown in Fig.5.5, is considered. The ship is modelled as a rectangular box-shaped barge. Using the 1:125 scaled model given in Fig.5.5, a set of model tests are performed in the Hydrodynamics Laboratory of the University of Glasgow. The detail of the test procedure is left to Chapter 7. The outcome of model tests is compared with theoretical predictions in Figs.5.6-5.10.

Fig.5.6 shows the surge motion values of the ship. The system has a very low natural frequency in the first mode of oscillation (natural period, T_n=442s). This is predicted correctly in the 5-DOF model. The 2-DOF model seems to agree with the experimental results more closely for one set of experimental data. On the other hand, the experimental data for the surge mode of motion is subject to some error. In order to show the bound of error the maximum and minimum values of surge data are chosen and are plotted in Fig.5.6. The scattering in surge data is partly due to the slowly varying motions superposed on the high frequency oscillations and due to the errors which occur during the measurement of wave heights. The magnitude of the overall surge behaviour is also a function of wave damping which effects the magnitudes of the surge oscillation (see Wicher and van Sluijs (1979)). The high order surge responses are read from the chart recorder and normalized with respect to wave amplitudes. Since the values are very small, any error in this process leads to large differences.

In comparing the lower column top displacement(see Fig.5.7), the trend predicted by the 5-DOF mathematical model is closer to the experimental results than that predicted by the 2-DOF model. The higher resonance values shown in Fig.5.7 indicate the peak at the second mode natural frequency. Fig.5.8 shows a comparison of the axial yoke

predictions. The yoke force calculation is a function of surge response in the 2-DOF mathematical model(see Eq.(5.4)). Therefore, higher surge values lead to higher yoke force predictions. On the other hand, the trend and magnitude of axial yoke forces calculated by the 5-DOF mathematical model are in good agreement with model test data. The wave force value which is determined by using Froude-Krylov approximation is quite conservative in the high frequency range(see Chapter 2 Section 2.2.4). This could be the reason for the over predicted axial force values. Fig.5.9 and 5.10 show a comparison between the experimental data and predictions for the heave and pitch motion responses of the ship.

Comparisons between the motion response and the test measurements (Figs.5.6-5.10) validate the 5-DOF mathematical model. Although easier to use and to run in the computer, the results obtained from the 2-DOF model are conservative. The trend of the motion and structural responses does not follow the experimental data. It is concluded that the 5-DOF model is more suitable for analyzing the behaviour of coupled DAT-ship systems.

5.3 CALCULATION OF SHEAR FORCE AND BENDING MOMENT DISTRIBUTION ALONG THE DOUBLE ARTICULATED TOWER WHEN IT IS COUPLED WITH A SHIP

The shear forces and bending moments along the columns are calculated by integrating the structural load acting on the differential circular beam elements of the upper and lower columns. The procedure is similar to one which is described in Chapter 4, Section 4.3.2. The detailed formulation of the load, shear force and bending moment calculation procedure is described in Appendix A. The only difference of procedure used for the DAT concept is the axial force component due to the presence of the ship. The inphase and outphase components of the yoke forces are added into the calculation as external forces. The shear force and bending moment distributions for a unit wave amplitude are given in Figs.5.11 and 5.12 for the wave frequencies 0.4 rad/s and 1.0 rad/s, respectively.

The structural response values of a double articulated tower-ship system are compared with those of an equivalent single articulated tower-ship system. Fig.5.13 compares the SF and BM distribution along the of the SAT- and DAT-ship systems when the wave frequency is 0.4rad/s. As shown in Fig.5.13, the second articulation reduces the bending moment values by about 50%. Fig.5.14 shows that the maximum shear forces of the double articulated tower-ship system are less than those of the single articulated ship system up to a wave frequency of about 0.7 rad/s. However a maximum shear force occurs on the double articulated tower ship system when the wave frequency is about 0.8 rad/s. Fig.5.15 compares maximum bending moment values of the single articulated tower-ship system with maximum bending moment values predicted along the upper and lower columns of the double articulated tower-ship system. As is seen from Fig.5.15, throughout the wave frequency range there is a reduction of about 50% in the bending moments in the case of the double articulated tower.

5.4 PARAMETRIC STUDIES

The parametric studies which will be presented in this section can be categorized as follows.
The variations of

- drag coefficient, C_D
- inertia coefficient, C_M
- yoke length and yoke orientation, and
- water depth.

In these parametric studies, the 5-DOF mathematical model is used. Four motion response values namely, heave, pitch, lower column surge and ship surge are obtained by using the configuration given in Fig.5.5.

It is observed that the horizontal displacement of the lower column top and axial yoke forces are more sensitive to geometrical changes than the ship surge, heave and pitch motions. In the parametric studies, only three values namely, the surge response of the

ship, the horizontal displacement of the lower column top and the axial yoke forces, are considered.

The damping forces present in the system are due largely to the viscous drag forces on the upper and lower columns. In calculating the viscous forces, there is a need to predict the relative motion of the tower first. Then the relative motion values give the necessary damping forces for the system. The iteration procedure is required until convergence is reached in the motion calculation.

In the first parametric study, the effect of C_D variation is considered. The experimental data is also included in order to compare the variation in viscous force with the prediction. Fig.5.16 shows that the horizontal displacement of the upper column top does not vary for the different C_D values, whereas the lower column top response and the axial yoke force values show a closer trend with the experiment when higher C_D values are used(see Figs.5.17 and 5.18). As with the stand-alone double articulated tower, the best agreement between the predictions and measurement is obtained when the drag coefficient for the circular column is 4.8. This C_D coefficient is a relative value which takes into account the other uncertainties present in viscous damping calculation.

In the second part of the parametric studies, the effect of variation of the column inertia coefficient C_M for the vertical cylinder on the surge responses of the coupled system and on the yoke forces is investigated. It can be seen from Fig.5.20 that when the C_M coefficient increases from 1.5 to 2.5 the maximum horizontal displacement of the lower column top increases by about 25%. On the other hand surge response of the upper column remain unchanged as the C_M values vary (see Fig.5.19). Fig.5.20 shows that an increase in C_M from 1.5 to 2.5 yields a 50% increase in the yoke forces.

The motion response and axial yoke values are calculated for different yoke inclination angles. The yoke angle is not always parallel to the sea surface(see Fig.5.5). The yoke angle varies as the ship loads or offloads the oil. In addition, the tidal effects change the S.W.L and consequently the yoke angle. Three yoke inclination angles are

considered in this study. These are -5, zero and +5 degrees. Figs 5.22 and 5.23 show that the motion response values do not vary appreciably when the yoke angle changes. Fig.5.24 shows that the inclination angle causes small changes on the axial yoke force in the frequency range between 0.2 and 0.6. Figs.5.25 and 5.27 present the experiment measurement recorded for different yoke inclination angles. Except for the ship surge response, the effect of the yoke inclination angle is very small. The error in surge motion measurement, as discussed previously, is the main reason for the scattering in surge values.

The effect of yoke length variation on the yoke force is studied by altering the yoke length between 40 and 82.5 metres. It is found that there is no significant change in the motion response and axial yoke values as the yoke size increases (see Figs.5.28-5.30).

Finally, the effect of water depth on surge responses of the system and on the axial yoke forces is investigated. Figs.5.31, 5.32 and 5.33 show that an increase of water depth from 289m to 400m (about 38% increase) yields a very small decrease in column motion response and axial yoke force values.

5.5 CONCLUSIONS

Two different mathematical models were developed to predict the motion response and yoke forces of a coupled double articulated tower and ship system. These models were implemented into the computer programs to perform the response and force predictions for the coupled system.

The results of the mathematical models were compared with each other and with the experimental measurements. It was found that generally the 5-DOF modelling gives considerably lower predictions than those given by the 2-DOF modelling. It was also observed that the 5-DOF model agrees well with the experimental measurements.

Parametric studies performed for the DAT-ship system showed that the effect of variations in yoke length and yoke angle was not significant on motion responses or on

the axial yoke force values.

The second mode of vibration is the oscillation of the intermediate universal joint. It is necessary for the coupled articulated tower and tanker systems to have a second natural period larger than the maximum expected wave period to avoid resonance. Apart from the first and second modes of vibration, the structural periods of the lower and upper columns must also be determined. Bishop and Price (1979) applied the modal analysis techniques to a single tower. The application of this method to the double articulated tower may be considered as a future study.

The best agreement between the predictions and the measurement was obtained for the double articulated tower-ship system when a drag coefficient of 4.8 was used for circular columns. Parametric studies revealed that as the wave inertia coefficient for the columns increased from 1.5 to 2.5 the surge response of the upper column remained unchanged and an increase of about 25% in surge response of the lower column was predicted. The axial yoke forces increased by about 60%. The surge response and the axial yoke force predictions were found to be insensitive to the water depth variations when the water depth increased from 289m to 400m.

The dynamic motion and structural response comparisons carried out between the single articulated tower-ship system and double articulated tower-ship system showed that the second articulation gives rise to a reduction of about 50% in maximum bending moment value.

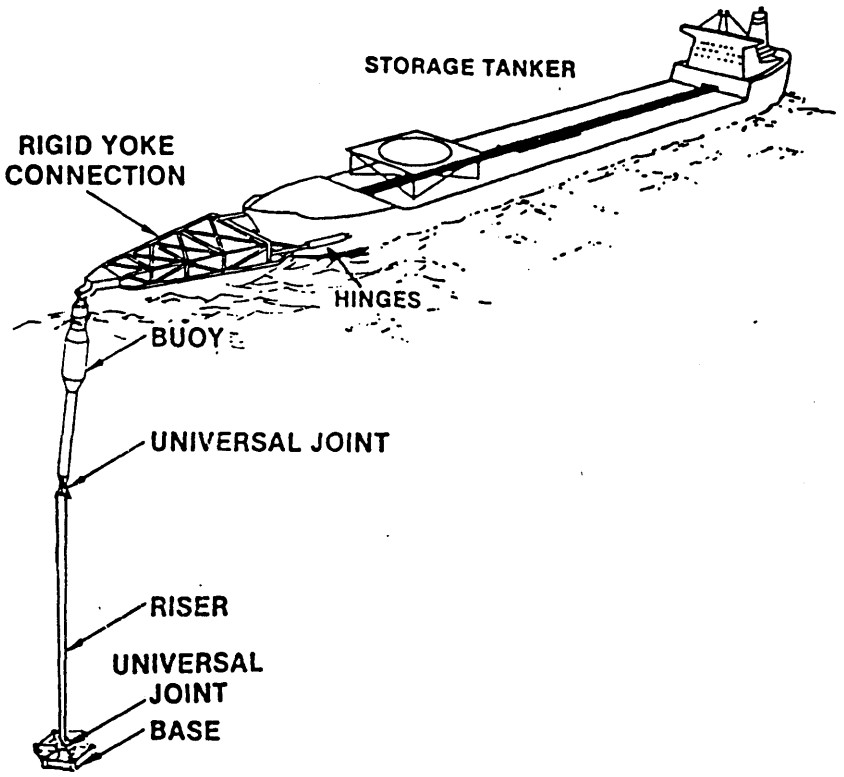

Fig.5.1 Double articulated tower and ship configuration (Houlie et al (1983))

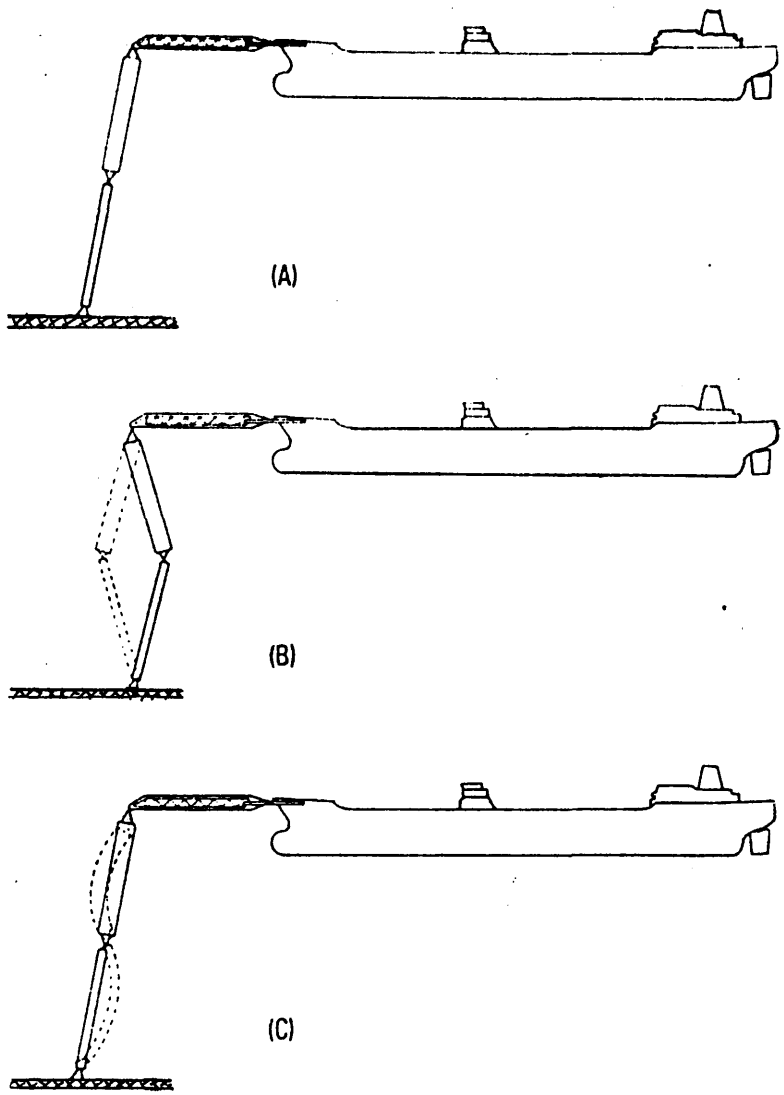

Fig.5.2 Mode of oscillations of DAT when it is coupled with a ship (Wolfram and Gunderson(1979)) a) First mode b)Second mode (elbowing motion) c) Structural bending oscillation of the DAT

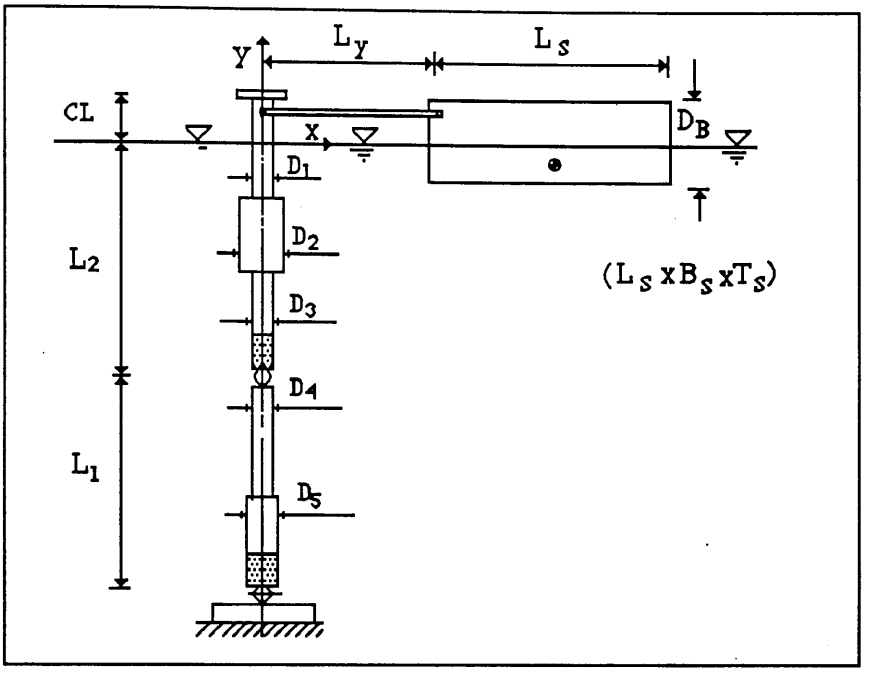

Fig.5.3 Coordinates of 2-DOF system

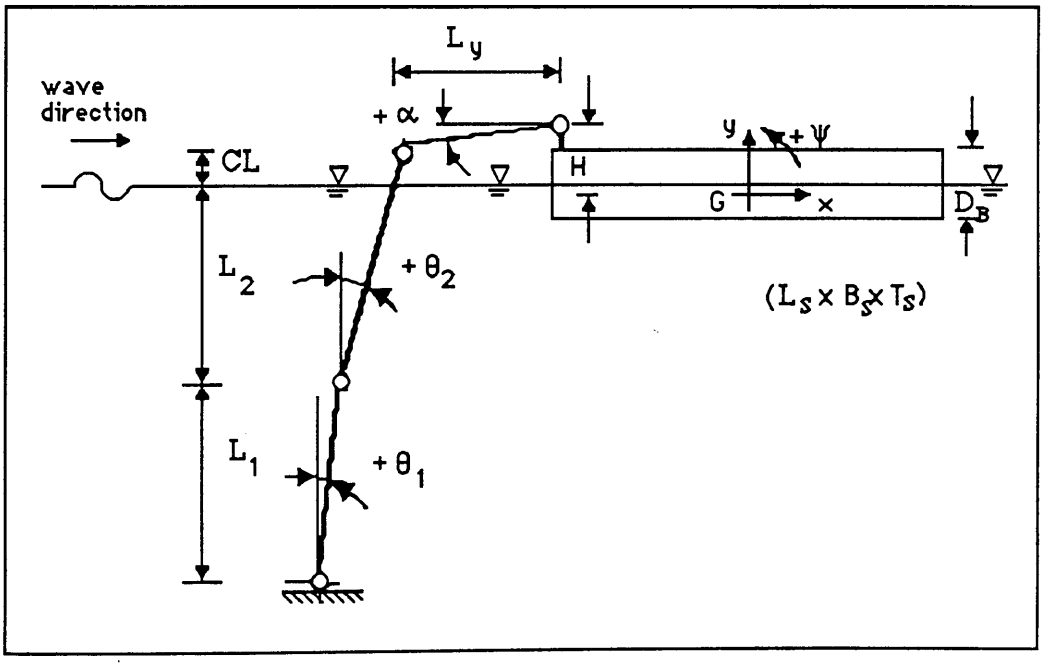

Fig.5.4 Coordinates of 5-DOF system

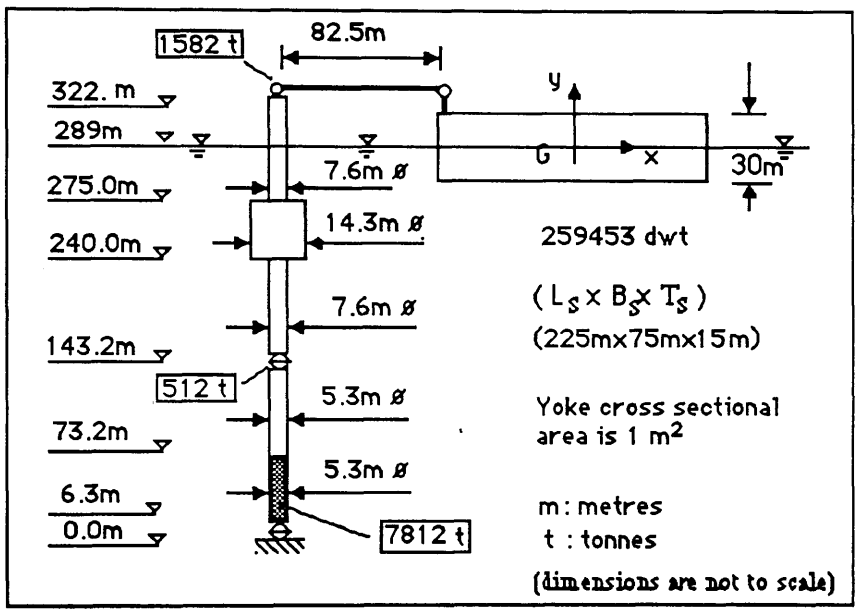

Fig.5.5 Double articulated tower-ship configuration

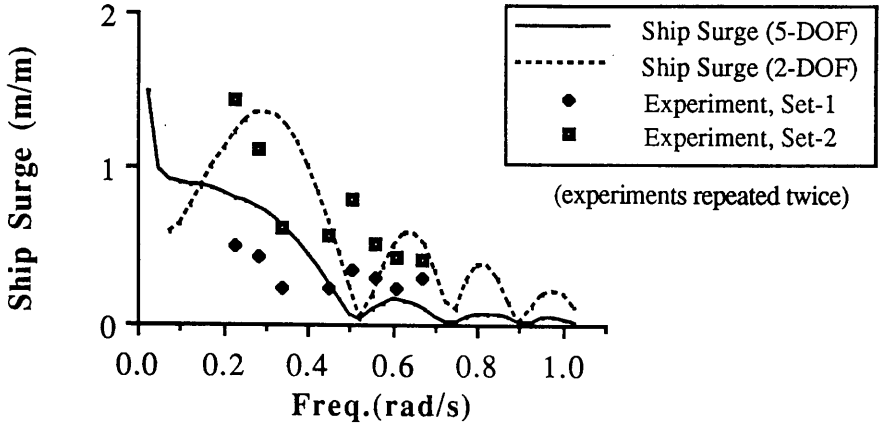

Fig.5.6 Comparison between theoretical and experimental results of surge motion of ship

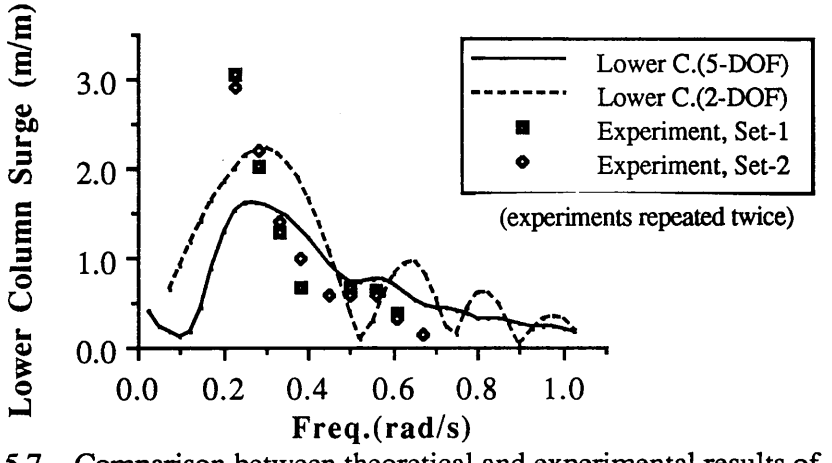

Fig.5.7 Comparison between theoretical and experimental results of horizontal displacement of lower column top(elbowing motion)

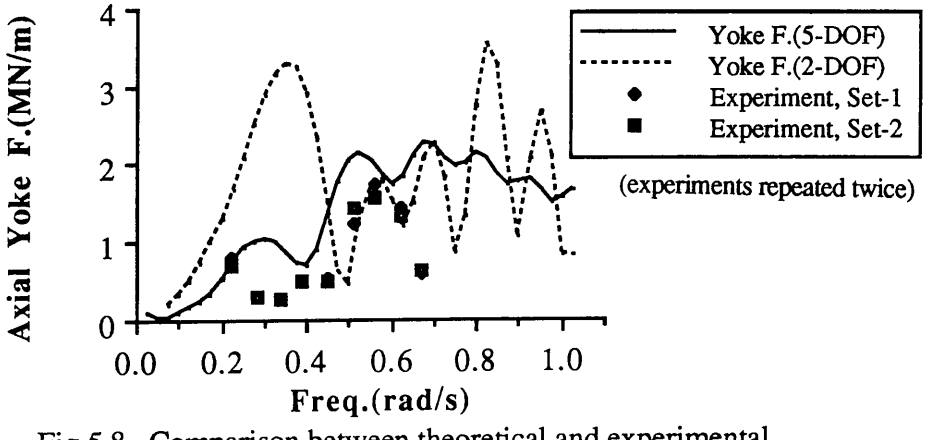

Fig.5.8 Comparison between theoretical and experimental results of axial yoke forces

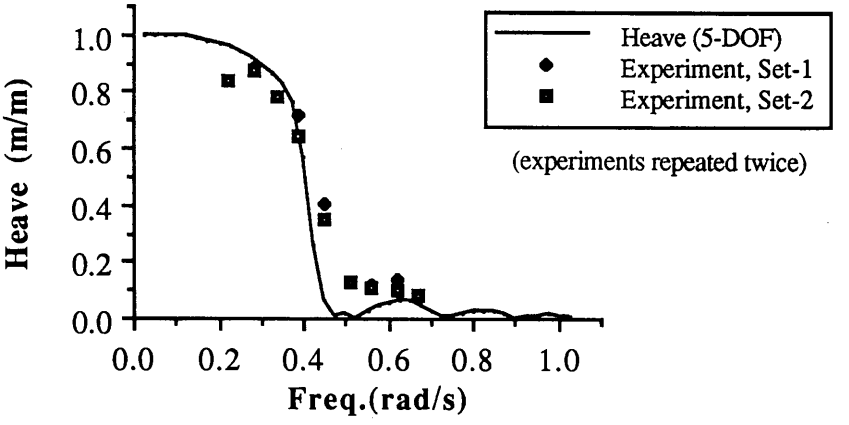

Fig.5.9 Comparison between theoretical and experimental results of heave motion of ship

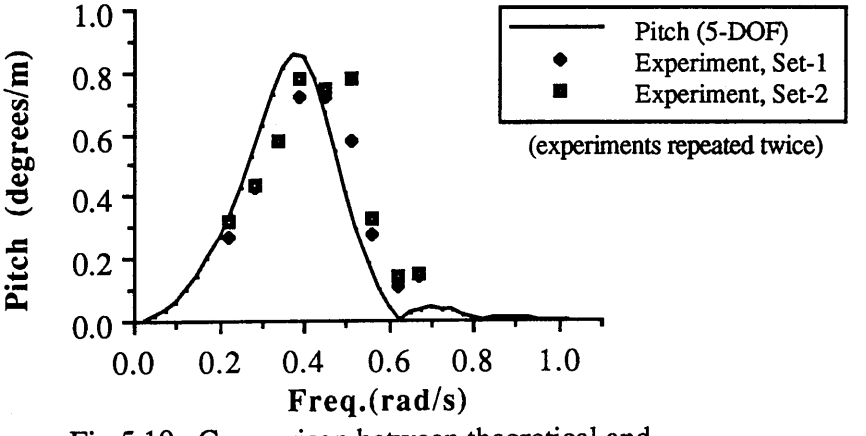

Fig.5.10 Comparison between theoretical and experimental results of pitch motion of ship

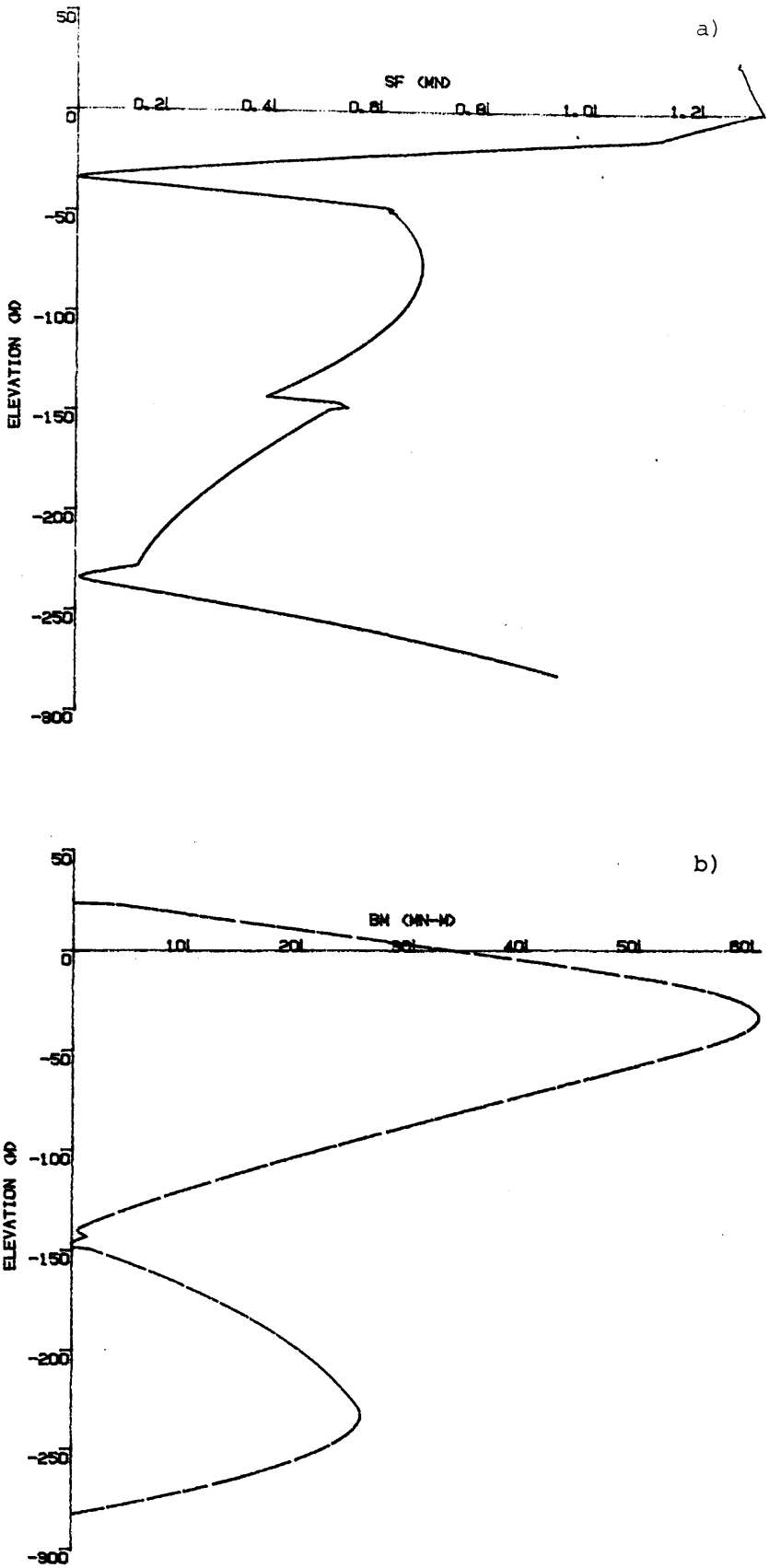

Fig.5.11 Shear force and bending moment distribution along tower when it is coupled with ship, $\omega = 0.4$rad /s $H_W = 2$m $C_D = 4.8$ a) Shear force b) Bending moment

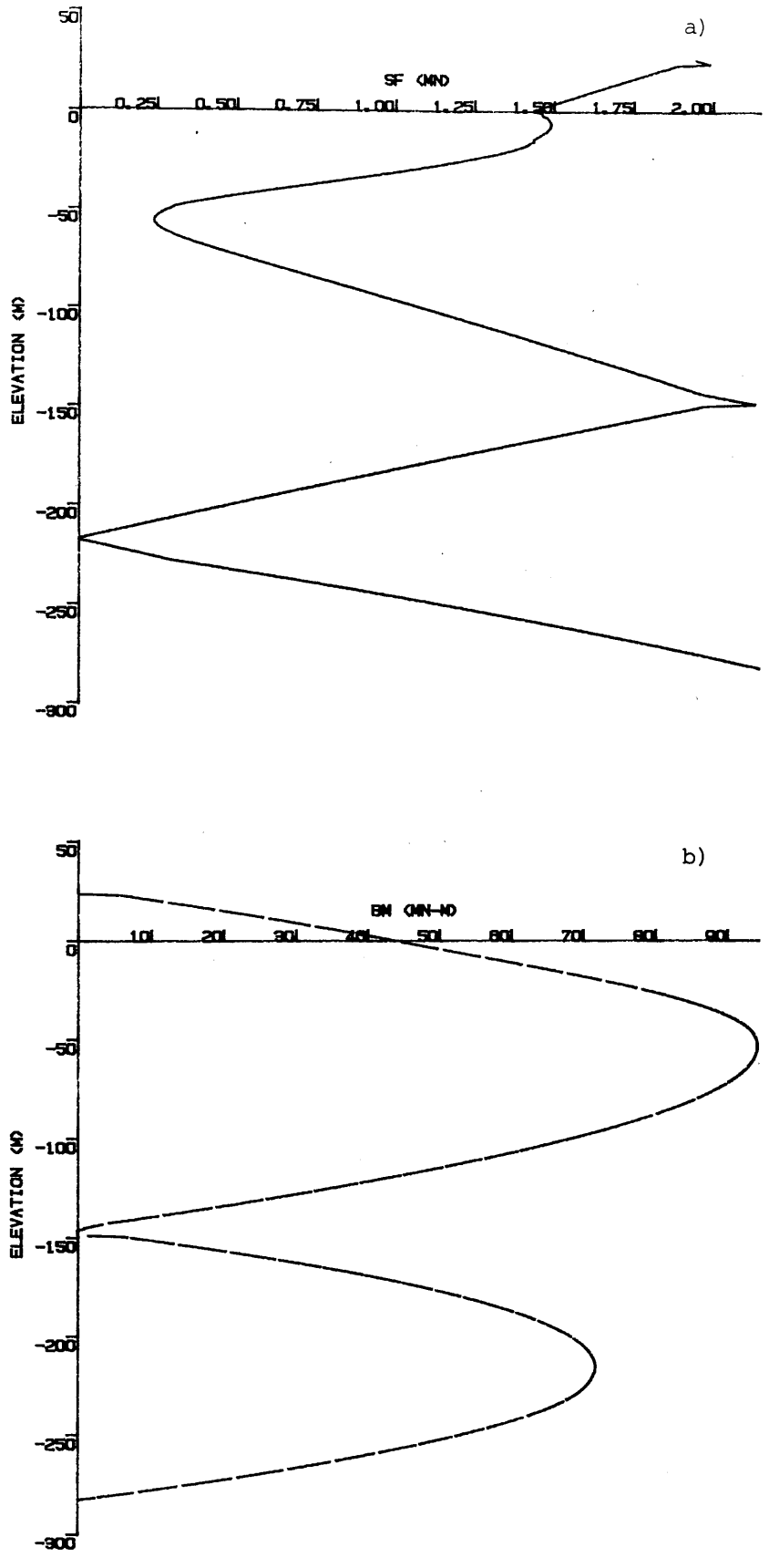

Fig.5.12 Shear force and bending moment distribution along tower when it is coupled with ship, $\omega = 1.0$ rad /s $H_W = 2$m, $C_D = 4.8$ a) Shear force b) Bending moment

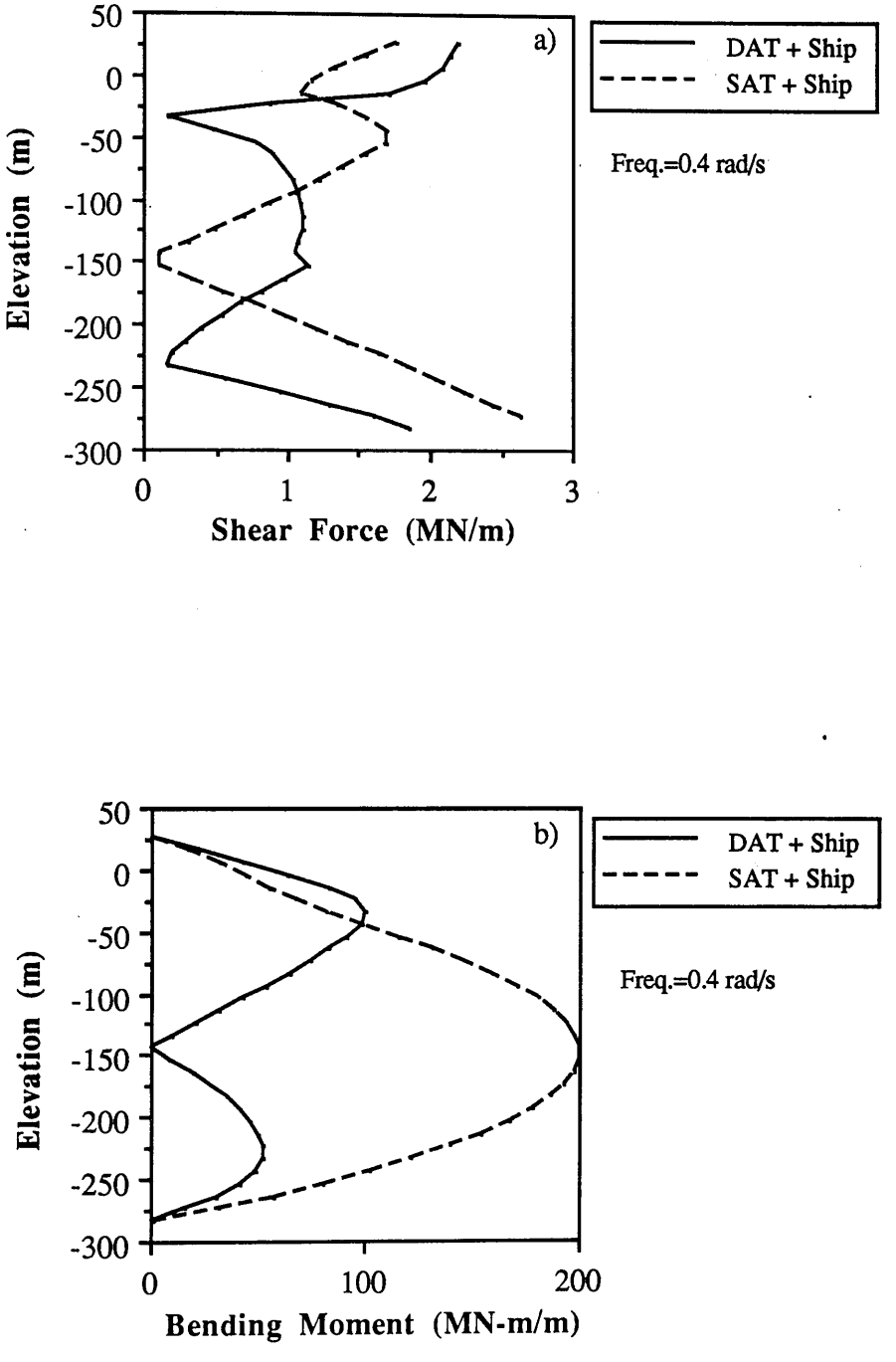

Fig.5.13 Comparison of a) Shear force, b) Bending moment distribution along tower in coupled system: double articulated tower vs single articulated tower

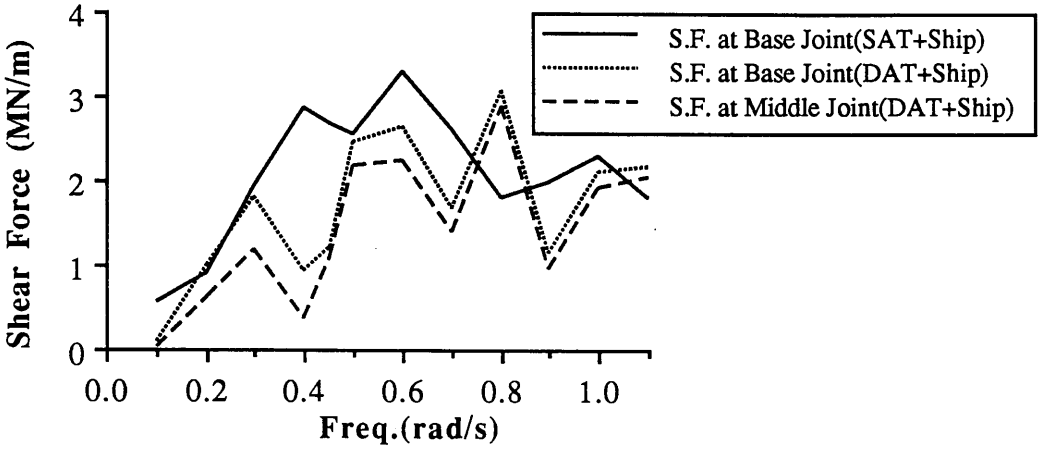

Fig.5.14 Comparison of shear forces at base joint in coupled system: double articulated tower vs single articulated tower

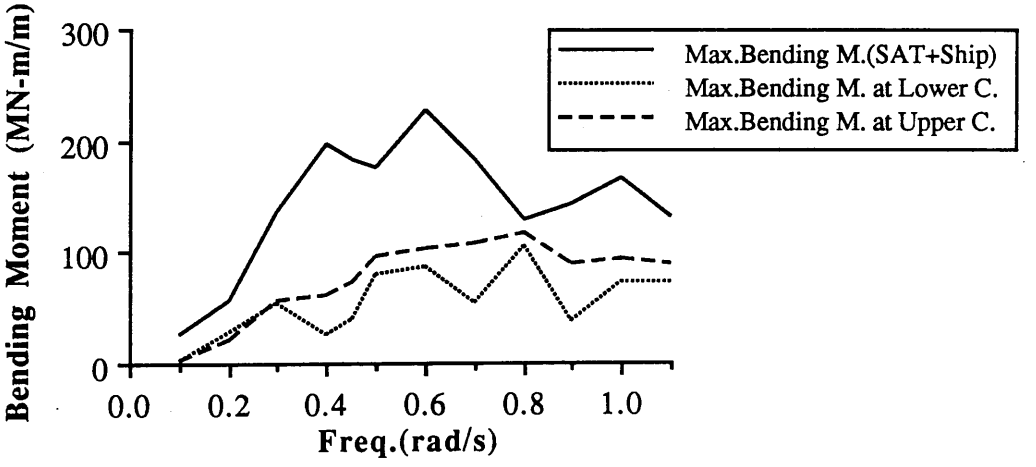

Fig.5.15 Comparison of maximum bending moments in coupled system: double articulated tower vs single articulated tower

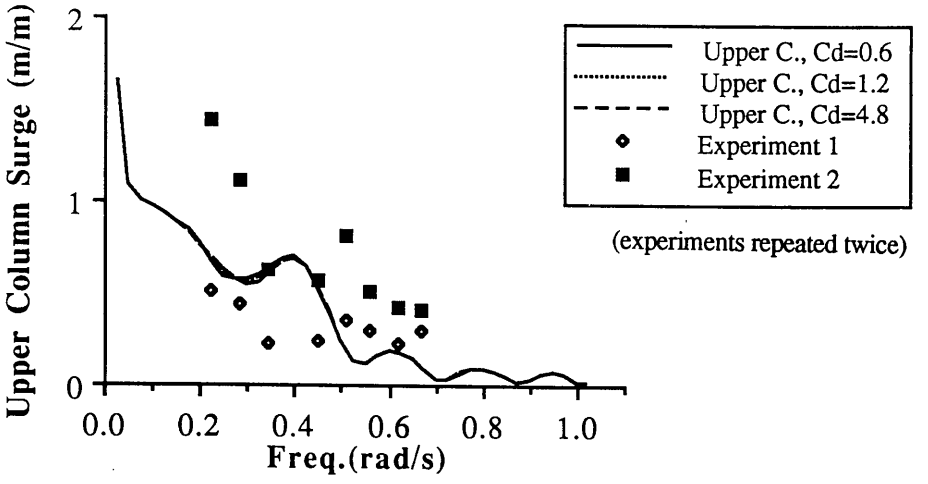

Fig.5.16 Effect of drag coefficient variation on horizontal displacement of upper column top

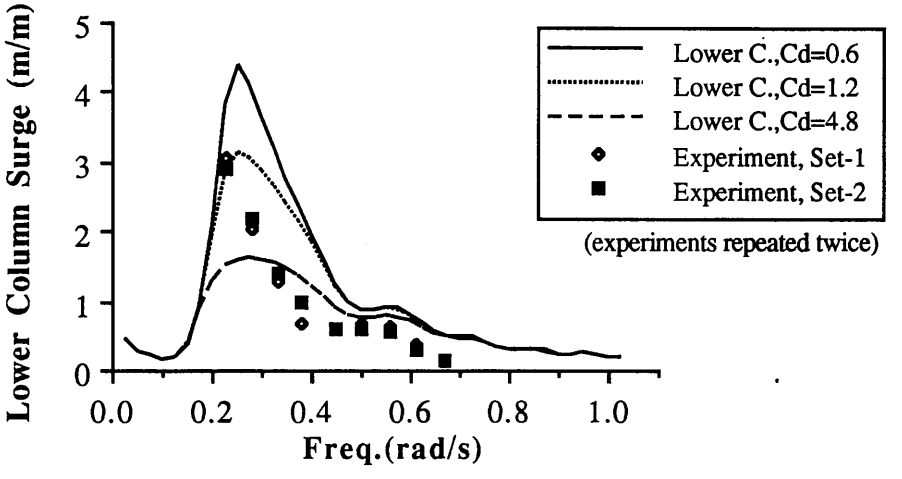

Fig.5.17 Effect of drag coefficient variation on horizontal displacement of lower column top(elbowing motion)

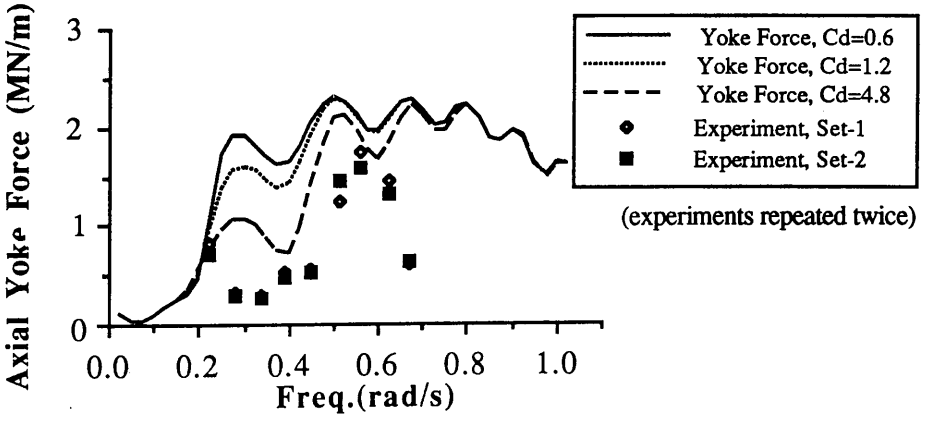

Fig.5.18 Effect of drag coefficient variation on axial yoke forces

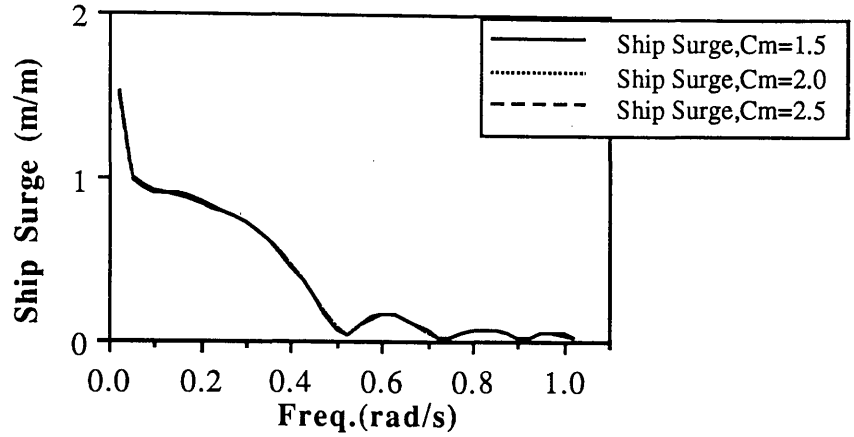

Fig.5.19 Effect of inertia coefficient variation on surge motion of ship

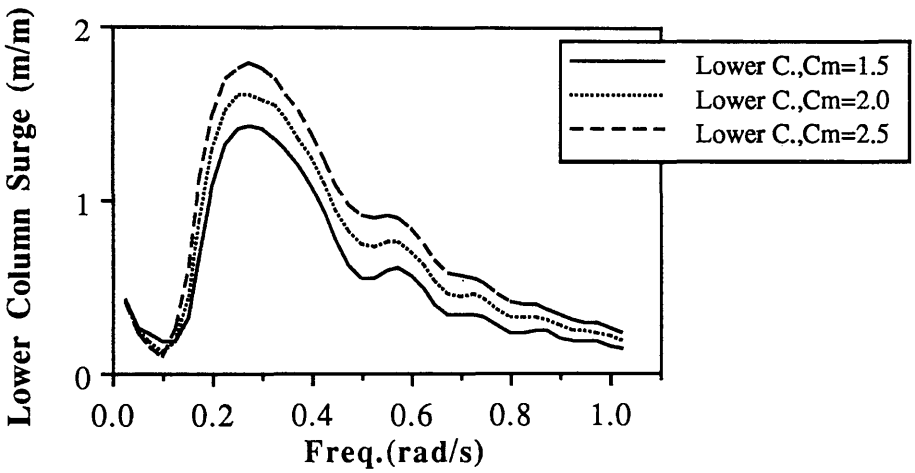

Fig.5.20 Effect of inertia coefficient variation on horizontal displacement of lower column top(elbowing motion)

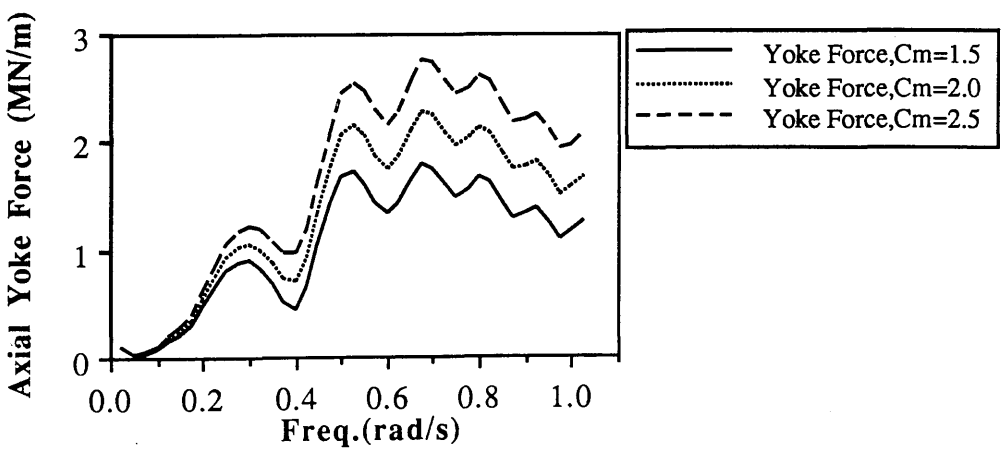

Fig.5.21 Effect of inertia coefficient variation on axial yoke forces

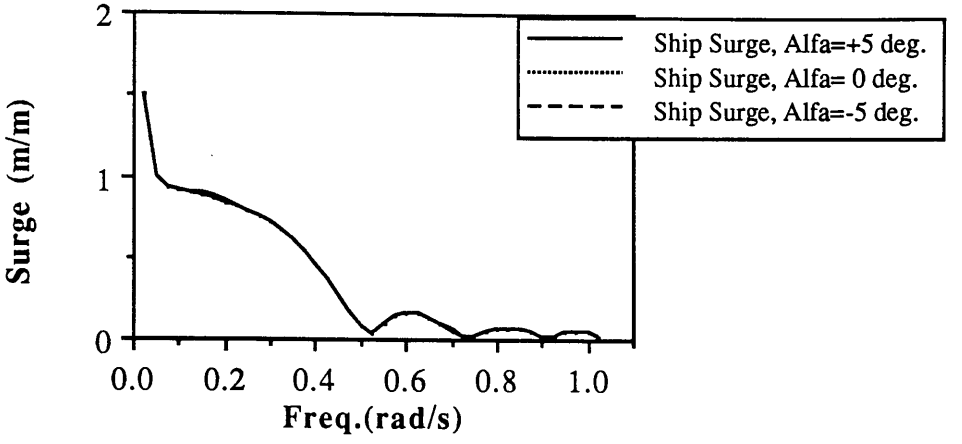

Fig.5.22 Effect of variation in yoke angle on surge motion of ship

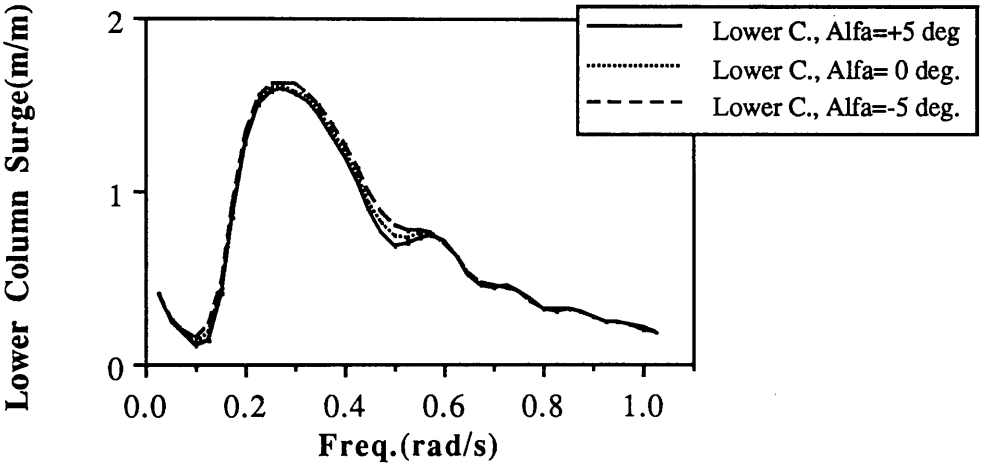

Fig.5.23 Effect of variation in yoke angle on horizontal displacement of lower column top(elbowing motion)

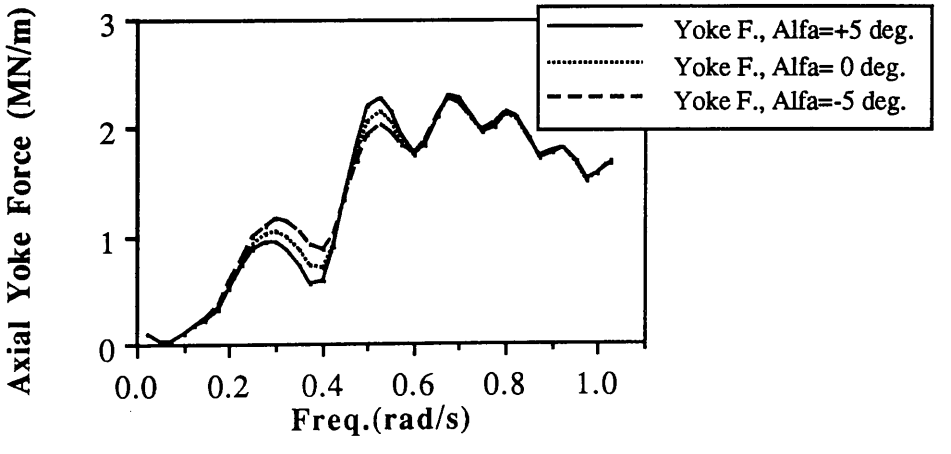

Fig.5.24 Effect of variation in yoke angle on axial yoke forces

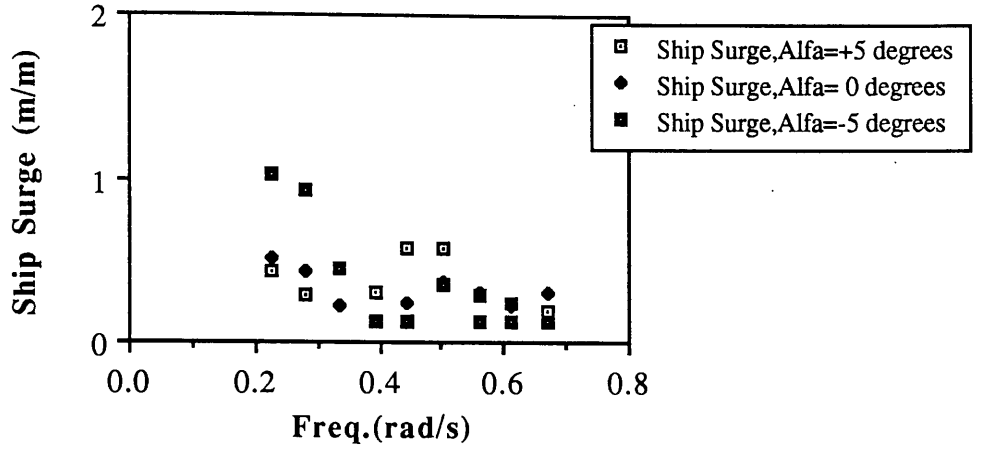

Fig.5.25 Effect of variation in yoke angle on experimental surge motion of ship

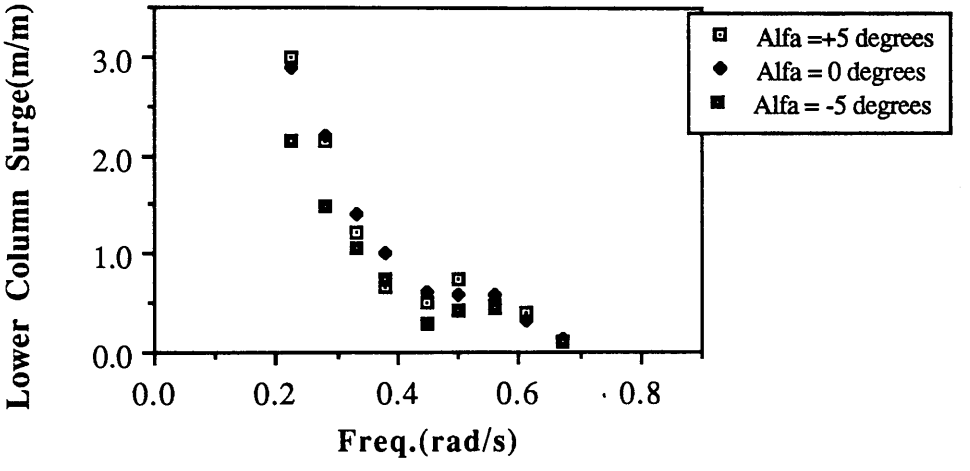

Fig.5.26 Effect of variation in yoke angle on experimental lower column top response

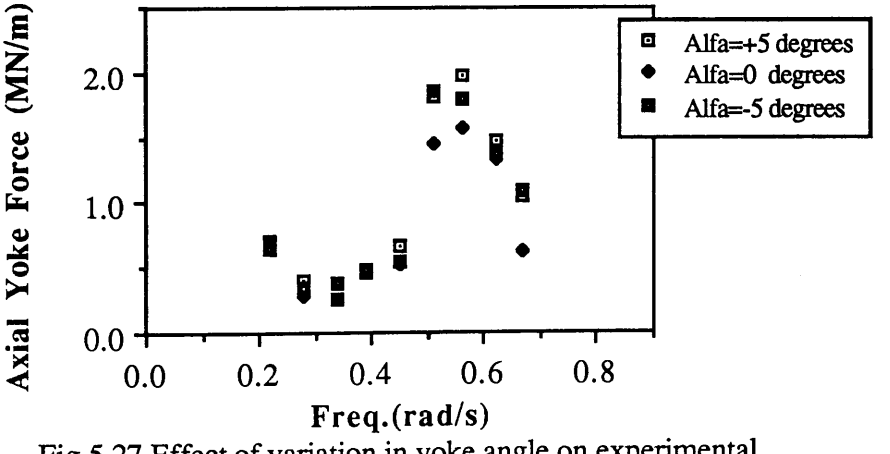

Fig.5.27 Effect of variation in yoke angle on experimental axial yoke forces

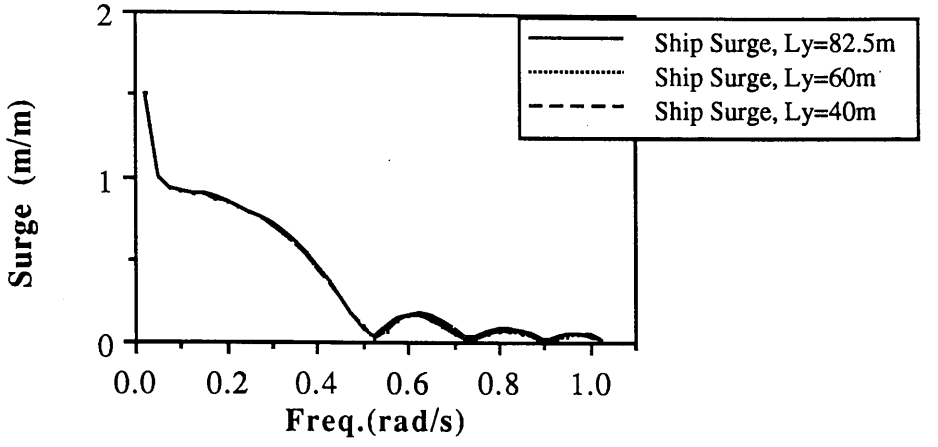

Fig.5.28 Effect of variation in yoke length on surge motion response of ship

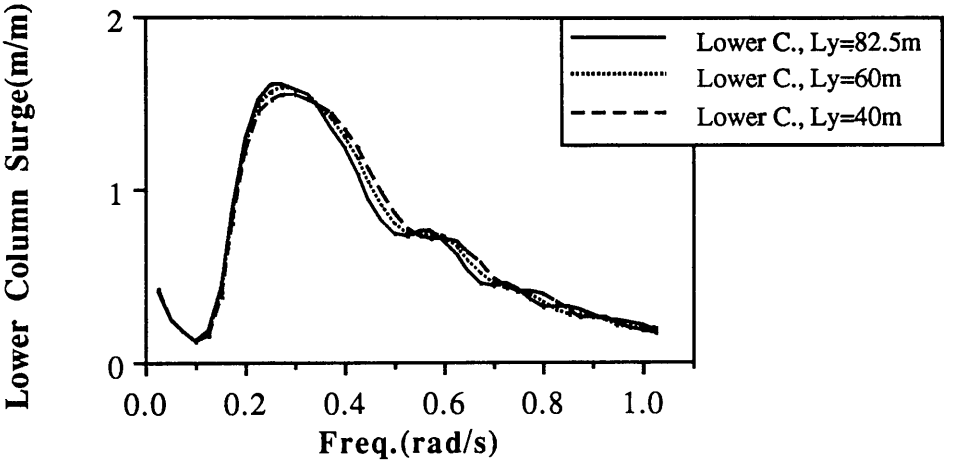

Fig.5.29 Effect of variation in yoke length on horizontal displacement of lower column top(elbowing motion)

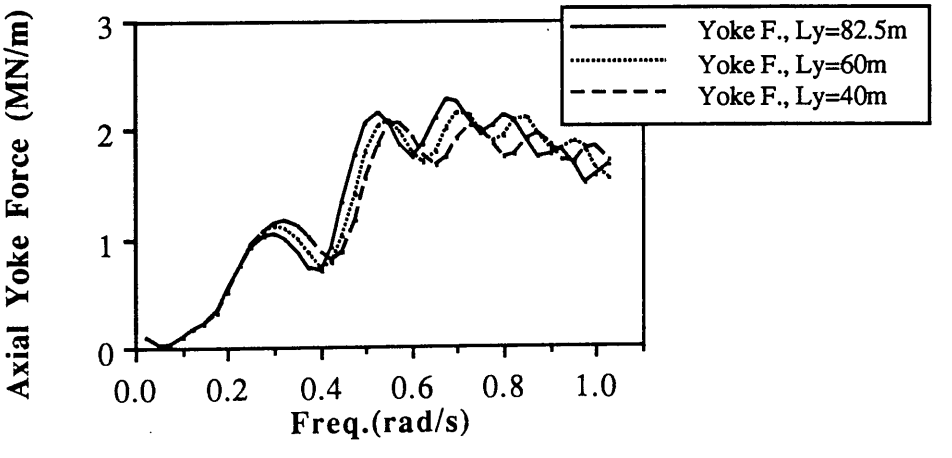

Fig.5.30 Effect of variation in yoke length on axial yoke forces

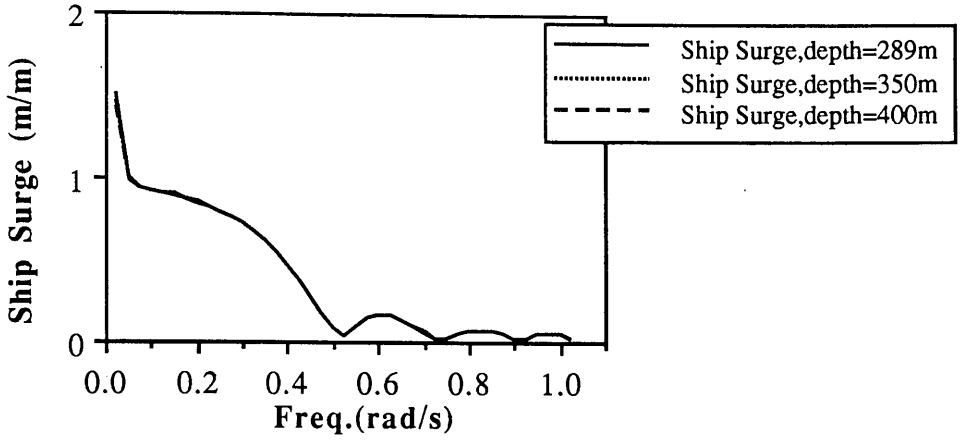

Fig.5.31 Effect of water depth variation on surge motion of ship

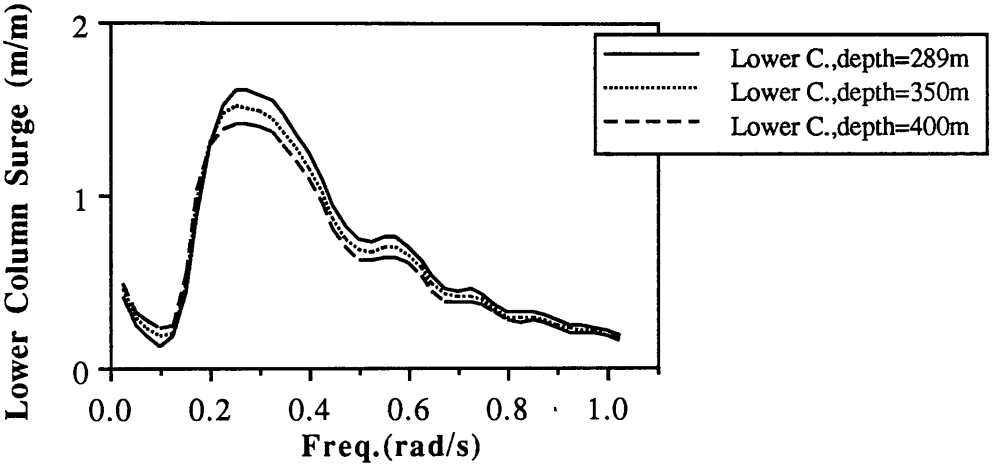

Fig.5.32 Effect of water depth variation on horizontal displacement of lower column top(elbowing motion)

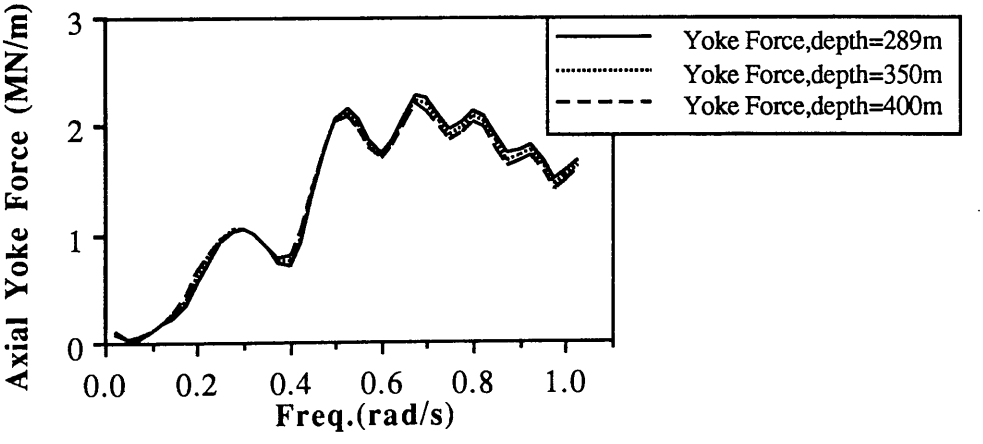

Fig.5.33 Effect of water depth variation on axial yoke forces

CHAPTER 6

TIME DOMAIN ANALYSIS

6.1 GENERAL DESCRIPTION

Up to this chapter, all analytical calculations have been performed in the frequency domain by replacing the non-linearities in the equation of motion by linear approximations. Because of the presence of nonlinear damping and drift force as well as nonlinear restoring forces, the motion equations for the coupled articulated tower and ship systems are generally nonlinear. Time domain simulation of the motion equation of an articulated tower in waves and current allows various non-linearities to be accounted for, including

- the drag component of Morison's equation with the true relative water particle velocity,
- variation in the instantaneous water surface,
- variation of the wave excitation forces and moments with displacement at the tower, and
- variation in the buoyant stiffness of the articulated tower as it rotates.

In the following section, the development of the time domain simulation is studied for single articulated tower motion prediction. The results obtained from the time domain work are compared with the frequency domain solutions. In Section 6.3 a nonlinear motion equation of the coupled articulated tower and ship system is considered. In Section 6.4 a yaw motion equation of a rigid yoke moored ship is derived and solved in the time domain.

6.2 APPLICATION TO SINGLE ARTICULATED TOWER MOTION EQUATION

The equation of motion of a single articulated tower can be written in general form, including all non-linearities, as follows

$$\left(I_{\theta\theta} + I_{AD,\theta}\right)\ddot{\theta} + B_{\theta\theta}\dot{\theta} + g(\rho\nabla\overline{KB} - W\overline{KG})\sin\theta = M_I + M_D \qquad (6.1)$$

where $I_{\theta\theta}$ is mass moment of inertia; $I_{AD,\theta}$, added mass moment of inertia; $B_{\theta\theta}$, damping coefficient; g, gravitational acceleration; ∇, total buoyancy of the tower; W, total mass of the tower; $\overline{KB}$, centre of buoyancy; $\overline{KG}$, centre of gravity and θ, pitch angle of the tower. M_I and M_D are the moments at the universal joint due to wave inertia forces and drag forces, respectively.

The moment due to wave inertia forces is given in the following expression

$$M_I = \int_{-d}^{\zeta_a \cos(kx-\omega t)} \rho C_M \frac{\pi D^2}{4} \left(\dot{U}_x \cos\theta - \dot{U}_y \sin\theta\right)(y+d)dy \qquad (6.2)$$

where ρ is the water density; C_M inertia coefficient; D diameter of the tower; ζ_a, wave amplitude and d depth to the articulated joint. $\dot{U}_x$ and $\dot{U}_y$ represent water particle accelerations in x and y directions, respectively (see Chapter 2 ,Table 2.1). The terms in Eq.(6.2) are also defined in Fig.6.1.

Upper limit of the integration indicates that the integration is performed up to the instantaneous water surface. This integration is performed numerically by introducing the summation sign in Eq.(6.2), as follows

$$M_I = C_1 \sum_{i=1}^{N} C_{Mi} D_i^2 e^{ky_i} \left[\sin(kx_i - \omega t)\cos\theta + \cos(kx_i - \omega t)\sin\theta\right](d + y_i)\Delta y \qquad (6.3)$$

where C_1 is a constant ($=\rho\frac{\pi}{4}gk\zeta_a$); N is the number of elements up to the instantaneous water surface; C_{Mi} inertia coefficient of the ith element; D_i diameter of ith element and x_i and y_i the horizontal and vertical coordinates of the centre of ith element with respect to the earth fixed coordinate system.

The instantaneous length of the tower oscillating in regular waves is given by the following equation

$$l_i = \frac{d}{\cos(\theta)} + \zeta_i \tag{6.4}$$

where ζ_i is the wave elevation at the point where the tower pierces the surface (see, Fig.(6.1)). Hence, the number of elements at each time step can be calculated as follows

$$N = \frac{l_i}{\Delta y} \tag{6.5}$$

The moment of the forces proportional to the velocity square is given by

$$M_D = \int_{-d}^{\zeta_i} 0.5\rho C_D D V_R |V_R| (y + d)\, dy \tag{6.6}$$

where V_R is relative velocity, $V_R = (V_C + U_x)\cos\theta - U_y \sin\theta - \dot{\theta}(y + d)$; V_C is the current velocity; C_D is the drag coefficient; U_x and U_y are water particle velocity in x and y directions (see, Table 2.1) and finally, the term $\dot{\theta}(y + d)$ is the angular velocity.

For numerical calculations, Eq.(6.6) can be written as a summation of N elements over the tower:

$$M_D = C_2 \sum_{i=1}^{N} C_{Di} D_i V_{Ri} |V_{Ri}| (y_i + d) \Delta y \tag{6.7}$$

where

$$V_{Ri} = (V_{Ci} + U_{xi})\cos\theta - U_{yi} \sin\theta - \dot{\theta}(y_i + d)$$

and $C_2 = 0.5\rho$.

The variables in the motion equation can be classified as follows:

Terms which are time dependent,

- $\theta, \dot{\theta}, N_r, x_i, y_i, \nabla, \overline{KB}, I_{AD,\theta}$

Terms whose magnitude varies along the tower,

- D, C_M, C_D, V_C

Constant values,

- $C_1, C_2, k, \omega, \overline{KG}, W, \Delta y$

To determine the dynamic oscillations of the tower, the equation of motion is integrated in the time domain by the forward time step routine. This requires that the displacement and velocities of the system be known at t=0 and that the forces be known as functions of the time or motion for t>0 (initial value problem). At each time step, the linear accelerations are computed from the displacements and velocities. Then the displacements and velocities at the next time step are found by an integration method for stepping the solution forward. This procedure is repeated until a required final time is reached.

The numerical integration procedure is evaluated using a NAG subroutine, D02BBF. This subroutine implements a variable step length Runge-Kutta-Merson method with an appropriate interpolation technique. The required values can be obtained at specified points during the simulation.

An articulated tower configuration was adopted from Snowden et al. (1985) as shown in Fig.6.2. Fig.6.3 shows a typical output of the time domain simulation program.

In order to avoid numerical stability problems, the external forces are increased exponentially over the initial 50 s of total 250 s simulation period. The reason for using the exponential ramp function is that the articulated tower may react unfavourably to the initial imposition of large wave induced loads.

The intermediate output is generated so that there are 20 data samples per cycle of wave frequency. The simulation time is kept constant at 250 s for high frequencies 0.4~1.0 rad/s. Thus, the number of the samples in total is variable with respect to the wave frequency. The simulation time for the lower frequencies (0.06~0.3 rad/s) is kept longer -1000 s - in order to obtain a large number of cycles.

The results obtained from time domain simulation of the motion equation are compared with the frequency domain results in Figs.6.4 and 6.5. The experimental results which are reproduced from Snowden et al (1985) are also presented in these figures. Angular response values calculated using both frequency and time domain analysis agree quite well with measurements. However, frequency domain analysis over predicts the angular response value in the region of the natural frequency.

The shear forces at the base joint are calculated for the single articulated tower using the procedure presented in Appendix A. Comparison of the shear force values in frequency and time domain solutions shows that the values are quite close to each other in the lower frequency region. In frequency regions higher than 0.6rad/s, the time domain simulation technique solution agrees better with the experimental results.

In order to investigate the effect of the instantaneous water surface variation on the motion response of the tower, the simulation is repeated for two different wave heights. The results are normalized with respect to wave amplitude. Fig.6.6 shows that the wave height increment increases the damping and that the less motion response values are obtained especially in the region of the natural frequency. Fig.6.7 shows that shear forces behave linearly with wave amplitude.

6.3 APPLICATION TO COUPLED ARTICULATED TOWER AND SHIP MOTION EQUATION

The behaviour of the articulated tower and ship system under regular wave forces was discussed in Chapter 3. In deriving the motion equations, a linearization procedure was employed. The motion equation was solved in the frequency domain. In this section, motion equations of ship surge and tower oscillation will be solved in the time domain.

A time domain simulation procedure was applied to a coupled tower ship system by Gernon and Lou (1987). They considered the hawser connection between the tower and the ship.

In this analysis, a rigid connection will be considered. The purpose of this study is to test the accuracy of the linearization procedure employed in Chapter 3.

The motion equations of the coupled system are given as follows:

Surge motion of the ship

$$(M + M_{AD,x})\ddot{x} + B_{xx}\dot{x} = F_{Tx} - F_R \tag{6.8}$$

where $M_{AD,x}$ is the added mass of the ship in surge; B_{xx}, the damping coefficient in surge and F_{Tx}, the surge forces on the ship due to regular waves

Angular motion of the tower

$$(I_{\theta\theta} + I_{AD,\theta})\ddot{\theta} + B_{\theta\theta}\dot{\theta} + g(\rho\nabla\overline{KB} - W\overline{KG})\sin\theta = M_I + M_D + F_R L_1 \tag{6.9}$$

Yoke forces can be written in terms of motion amplitudes of the ship and the tower

and stiffness of the yoke as follows

$$F_R = c\,(x - \theta L_1) \tag{6.10}$$

The system configuration given by Snowden et al (1985) is considered (see, Fig.3.1). Typical results of the time domain analysis are shown in Fig.6.8. The motion and structural response values are obtained for various frequencies at a unit wave height. The results are presented as open circles in Figs.6.9-6.11. The values from the linearized model were found to agree quite well with the results from the time domain simulation of the non-linear system.

6.4 APPLICATION TO YAW MOTION EQUATION OF A YOKE MOORED SHIP

In this section, the yaw motion equation of a rigid yoke moored ship will be examined under several environmental conditions. This nonlinear problem can only be solved by employing a time domain simulation procedure. Similar attempts have already been made to simulate the ship motions for positioning at a definite point (see, Faltinsen et al(1979), Clarke et al(1983), Nienhuis(1986) and Chakrabarti&Cotter(1988)). Three dimensional description of the problem is quite complex. Therefore, a simplified approach is followed in this section.

It is assumed that the vessel is free to weatherwane about a fixed point (e.g. a spar buoy or an articulated tower). The effect of the rolling of the vessel as well as the contribution of the roll motion to the hydrodynamic coefficients are neglected. The environmental forces consist of the steady wind and current forces, the steady component of the second order forces, and incident wave forces. The equations of motion in yaw can, therefore, be written as a second order differential equation including all environmental forces and nonlinear terms. The coordinate system is given in Fig.6.12.

The equation of motion can be written in the following form

$$I\ddot{\mu} = N_{PR} + N_{AC} + N_{DR} + N_{CU} + N_{WI} \tag{6.11}$$

where I is mass and added mass moment of inertia, or

$$I = \frac{1}{3}(m + m_{AD,\bar{z}})(X_S^3 - X_B^3)$$

$m = \rho B_S T_S$ and $m_{AD,\bar{z}} = \rho\frac{\pi}{4}T_S^2$ are the unit mass and added mass of the vessel in $\bar{z}$ direction, respectively; X_B and X_S are the bow and stern coordinate of the vessel, respectively; N_{PR} , moment due to pressure forces; N_{AC}, moment due to acceleration forces; N_{DR}, moment due to second order steady wave drift forces; N_{CU}, moment due to current forces and N_{WI}, moment due to wind forces.

The moment due to the environmental forces originating from wind,waves and current and the hydrodynamic reaction forces will be discussed in the following.

Moment due to wave pressure forces

$$N_{PR} = -\int_{X_B}^{X_S}\int_{-B_S/2}^{B_S/2}\int_{-T_S}^{0}\bar{x}\left(\frac{\partial p}{\partial \bar{z}}\right)d\bar{y}d\bar{z}d\bar{x} \tag{6.12}$$

in which $p = -\rho\frac{\partial\phi}{\partial t}$. The definition of wave potential in oblique seas is given in Appendix B.

The moment due to acceleration forces

$$N_{AC} = m_{AD,\bar{z}}\left(\int_{X_B}^{X_S}\bar{x}\dot{U}_{\bar{z}}d\bar{x}\Big|_{\substack{\bar{z}=0\\ \bar{y}=-T_S/2}}\right) \tag{6.13}$$

in which $\dot{U}_{\bar{z}} = -g\zeta_a k_2 e^{k\bar{y}}\sin(k_1\bar{x} - k_2\bar{z} - \omega t)$.

Moment due to wave drift forces

$$N_{DR} = \bar{F}_{DR,\bar{z}} l_O \tag{6.14}$$

in which l_O is the distance between the vessel centre of gravity and the fixed point and $\bar{F}_{DR,\bar{z}}$ is the steady wave drift force on the ship in $\bar{z}$ direction.

An asymptotic formula, derived by Faltinsen et al. (1979) was used in calculating the drift forces on the ship. This approximation is valid when the wave length of the incident regular sinusoidal waves is small compared to the characteristic cross-dimension of the body. Therefore, the steady wave drift forces on the ship are given as follows

$$\bar{F}_{DR,\bar{z}} = \rho g \zeta_a^2 [\frac{B_S}{3} \sin(\alpha_{WA} - \mu) \pm (\frac{L_S - B_S}{2}) \sin^2(\alpha_{WA} - \mu)]$$

where the plus-sign is valid when $0 \le \mu \le \pi$ and the minus-sign is valid when $\pi < \mu \le 2\pi$. The axial and transverse components of the drift forces are shown in Fig.6.13.

Moment due to current forces

$$N_{CU} = \frac{1}{2} \rho T_S \int_{\bar{x}_B}^{\bar{x}_S} C_{DCU} V_{RC} |V_{RC}| \bar{x} d\bar{x} \tag{6.15}$$

where $V_{RC} = V_C \sin(\alpha_{CU} - \mu) - \bar{x}\dot{\mu}$; C_{DCU}, drag coefficient in transverse direction.

This semi-empirical equation makes use of the cross flow principle given by Faltinsen et al. (1979). In this method, it was assumed that the transverse drag forces per unit length along the hull were independent of forward speed, and proportional to the square of the local angular yaw velocity. The advantage of the above equation is that it takes account of the alteration of the incident velocity due to yaw motion along the length of the ship.

Moment due to wind forces

$$N_{WI} = \frac{1}{2}\rho_a f_B L_S C_{DWI} V_{RW}^2 l_O \tag{6.16}$$

where ρ_a is air density; f_B, freeboard; C_{DWI}, drag coefficient of the above water part of the hull; V_{RW}, instantaneous wind velocity, or

$$V_{RW} = V_W \sin(\alpha_{WI} - \mu) - l_O\dot{\mu}$$

The axial and transverse yoke forces were calculated by combining the external wave, wind and current forces with motion induced inertia and hydrodynamic reaction forces in the time domain.

Axial Yoke Forces

$$F_{YOKE,\bar{x}} = \underbrace{F_{PR\bar{x}} + F_{AC\bar{x}} + F_{DR\bar{x}}}_{\text{wave forces}} + F_{CU\bar{x}} + F_{WI\bar{x}} - \underbrace{(M + M_{ADz})l_O\omega^2}_{\text{axial rotational forces}}$$

Transverse Yoke Forces

$$F_{YOKE,\bar{z}} = \underbrace{F_{PR\bar{z}} + F_{AC\bar{z}} + F_{DR\bar{z}}}_{\text{wave forces}} + F_{CU\bar{z}} + F_{WI\bar{z}} - \underbrace{(M + M_{ADz})l_O\ddot{\mu}}_{\text{transverse rotational forces}}$$

Wave forces on the ship in axial and transverse directions are given in Appendix B. The other components are defined as follows

Forces due to second order wave forces in x direction

$$F_{DR\bar{x}} = \frac{2}{3}\rho g\zeta_a^2\frac{B_S}{2}\cos(\alpha_{WA} - \mu)$$

Forces due to current in x direction

$$F_{CU\bar{x}} = [\frac{0.075}{(\log Re - 2)^2}]\frac{1}{2}\rho S V_C^2 \cos(\alpha_{CU} - \mu)\left|\cos(\alpha_{CU} - \mu)\right|$$

where, $Re = V_C \cos(\alpha_{CU} - \mu) L_S / \nu$

The current is assumed to be constant versus depth for the ship draught.

Forces due to steady wind in x direction

$$F_{WI\bar{x}} = \frac{1}{2}\rho_a C_{DWI} A_T V_W^2 \cos(\alpha_{WI} - \mu)\left|\cos(\alpha_{WI} - \mu)\right|$$

where $A_T = f_B B_S + 800\,m^2$ (for super structure).

Forces due to current in z direction

$$F_{CU\bar{z}} = \frac{1}{2}\rho T_S \int_{X_B}^{X_S} C_{DCU} V_{RC}\left|V_{RC}\right| d\bar{x}$$

where, $V_{RC} = V_C \sin(\alpha_{CU} - \mu) - \bar{x}\dot{\mu}$

Forces due to steady wind in z direction

$$F_{W\bar{z}} = \frac{1}{2}\rho_a C_{DWI} A_L V_W^2 \sin(\alpha_{WI} - \mu)\left|\sin(\alpha_{WI} - \mu)\right|$$

where $A_L = f_B L_S + 800\,m^2$ (for super structure).

The single degree of freedom motion equation of the system was solved in the time domain. The output was generated so that there were 20 data samples per cycle of the wave frequency. The simulation time was kept constant at 1000 seconds. Thus, the number of samples in total was variable with respect to the frequency.

Three groups of simulation studies were carried out. The direction and magnitude of wind and current forces were kept constant while varying the direction, magnitude and frequency of wave forces in the first group of studies. The results of these simulations are shown in Tables 6.1-6.8. In the Tables the yaw angle (in degrees) corresponds to a steady angle after the articulated tower-ship system reaches an equilibrium state under wave, wind and current forces. Similarly, oscillatory components of the axial and transverse yoke forces, as well as the steady forces at the base joint, are given in these Tables.

In some conditions the solution took longer to settle down. Therefore, the running time was kept as long as 5000 s in these frequencies. No unstable behaviour was experienced in these runs.

Fig.6.14 shows the results of time-domain simulations carried out to predict the motion and structural response of the yoke moored ship.

Tables 6.1, 6.2, 6.5 and 6.7 show that wave excitation is the dominant environmental force in the prediction of steady yaw angle. Examination of these tables also reveals that maximum axial and transverse yoke forces occur when the direction of wave approach makes a 90 degree angle with wind and current directions.

Table 6.3 shows that, while the magnitudes of axial yoke forces are linearly proportional to wave amplitudes, the magnitudes of yaw angles, transverse yoke forces and steady axial forces show non-linear trends with increasing wave amplitudes.

Table 6.4 shows the variation of motion and structural response values of the wave excitation frequency changes. Table 6.4 illustrates that axial yoke forces are the most sensitive design parameters to changes in wave frequencies.

Tables 6.5 and 6.6 show that motion and structural response values of the yoke moored ship system are not sensitive to variations in wind direction and speed under the particular conditions considered here.

Tables 6.7 and 6.8 show that the steady yaw angle values of the coupled system increase as the current direction angle and velocity increase. However, amplitudes of axial and transverse yoke forces and steady joint forces, are not sensitive to changes in current direction and speed. Since the wave encounter frequency values were calculated as a function of current velocity, Table 6.8 shows significant variations in the amplitudes of axial and transverse yoke forces.

6.5 CONCLUSIONS

Time domain simulation procedures for nonlinear motion equations were considered in this chapter. In the first two section, the nonlinearities due to the presence of an articulated tower were considered. Frequency and time domain analysis were compared for unit wave amplitude to validate the drag linearity assumption as well as the nonlinear equation and the computer simulation. As figures indicate both techniques agree quite well with each other. In the case of single articulated tower, the time domain simulation technique solution agrees better with the experimental results. It was shown that the increment in the wave height introduces extra damping in the region of the natural frequency.

In order to examine the effect of the joint occurrence of wave, wind and current forces, the motion and structural response values of a rigid yoke moored ship system were calculated in the time domain. A parametric study was carried out by changing the direction and magnitude of an environmental force while keeping the other forces the same. Maximum axial and transverse yoke forces occurred when the direction of wave made a 90 degrees angle with wind and current directions. It was also found that neither the wind and current speeds nor their directions had a significant effect on axial and transverse yoke force predictions.

Table: 6.1 Motion and Structural Response due to Co-Linear Wave, Wind and Current

Wave Freq. (rad/s)	Yawing Angle (deg.)	Axial Yoke F. (MN)	Transverse Y. F. (MN)	Steady Joint F.(Hor.) (MN)
0.80	0.00	6.6	0.0	2.6
.Constant values during the simulation : Wave height, 8m; current velocity, 1.5m/s; wind velocity, 22m/s;				

Table: 6.2 Effect of Wave Direction

Wave Direction (deg.)	Yawing Angle (deg.)	Axial Yoke F. (MN)	Transverse Y. F. (MN)	Steady Joint F.(Hor.) (MN)
0	-6.97	6.6	1.0	2.5
-30	-28.16	6.6	0.3	2.3
-45	-37.93	6.5	1.1	1.7
-60	-49.25	6.5	1.6	1.4
-90	-73.40	6.7	2.4	2.2
Constant values during the simulation : Wave height, 8m; wave frequency, 0.8 rad/s; current velocity, 1.5m/s; current direction, 0 deg.; wind velocity, 22m/s; wind direction,-90 deg.				

Table: 6.3 Effect of Wave Height

Wave Height (m)	Yawing Angle (deg.)	Axial Yoke F. (MN)	Transverse Y. F. (MN)	Steady Joint F.(Hor.) (MN)
4	-33.06	3.3	0.9	0.7
8	-37.93	6.5	1.1	1.8
12	-40.77	9.9	0.9	5.7
Constant values during the simulation : Wave direction, -45deg.; wave frequency, 0.8 rad/s; current velocity, 1.5m/s; current direction, 0 deg.; wind velocity, 22m/s; wind direction,-90 deg.				

Table: 6.4 Effect of Wave Frequency

Wave Freq. (rad/s)	Yawing Angle (deg.)	Axial Yoke F. (MN)	Transverse Y. F. (MN)	Steady Joint F.(Hor.) (MN)
0.80	-37.93	6.5	1.1	2.6
1.00	-37.93	8.1	1.0	2.6
1.20	-37.93	8.2	0.9	2.6
Constant values during the simulation : Wave direction, -45deg.; wave height, 8m; current velocity, 1.5m/s; current direction, 0 deg.; wind velocity, 22m/s; wind direction,-90 deg.				

Table: 6.5 Effect of Wind Direction

Wind Direction (deg.)	Yawing Angle (deg.)	Axial Yoke F. (MN)	Transverse Y. F. (MN)	Steady Joint F.(Hor.) (MN)
0	-17.20	6.8	2.4	2.5
-30	-18.06	6.8	2.5	2.5
-45	-18.28	6.9	2.6	2.5
-60	-18.76	6.9	2.6	2.5
-90	-19.49	7.0	2.7	2.5

Constant values during the simulation : Wave height, 8m; wave frequency, 0.8 rad/s; wave direction, 0deg.; current velocity, 1.5m/s; current direction, -90 deg.; wind velocity, 22m/s.

Table: 6.6 Effect of Wind Velocity

Wind Velocity (m/s)	Yawing Angle (deg.)	Axial Yoke F. (MN)	Transverse Y. F. (MN)	Steady Joint F.(Hor.) (MN)
10	-17.82	6.8	2.5	2.5
20	-18.15	6.9	2.5	2.5
30	-18.84	6.9	2.6	2.5

Constant values during the simulation : Wave height, 8m; wave frequency, 0.8 rad/s; wave direction, 0 deg.; current velocity, 1.5m/s; current direction, -90 deg.; wind direction, -45 deg.

Table:6.7 Effect of Current Direction

Current Direction (deg.)	Yawing Angle (deg.)	Axial Yoke F. (MN)	Transverse Y. F. (MN)	Steady Joint F.(Hor.) (MN)
0	-6.97	6.6	1.0	3.1
-30	-9.70	6.5	1.4	2.7
-45	-12.48	6.5	1.8	2.5
-60	-15.18	6.7	2.2	2.5
-90	-19.49	7.0	2.7	2.5

Constant values during the simulation : Wave height, 8m; wave frequency, 0.8 rad/s; wave direction, 0deg.; current velocity, 1.5m/s; wind direction, -90 deg.; wind velocity, 22m/s.

Table: 6.8 Effect of Current Velocity

Current Velocity (m/s)	Yawing Angle (deg.)	Axial Yoke F. (MN)	Transverse Y. F. (MN)	Steady Joint F.(Hor.) (MN)
0.5	-8.18	6.8	1.2	2.4
1	-10.14	7.5	1.4	2.5
1.5	-12.48	6.5	1.8	2.6

Constant values during the simulation : Wave height, 8m; wave frequency, 0.8 rad/s; wave direction, 0 deg.; current direction, -45 deg.; wind velocity, 22 m/s; wind direction, -90 deg.

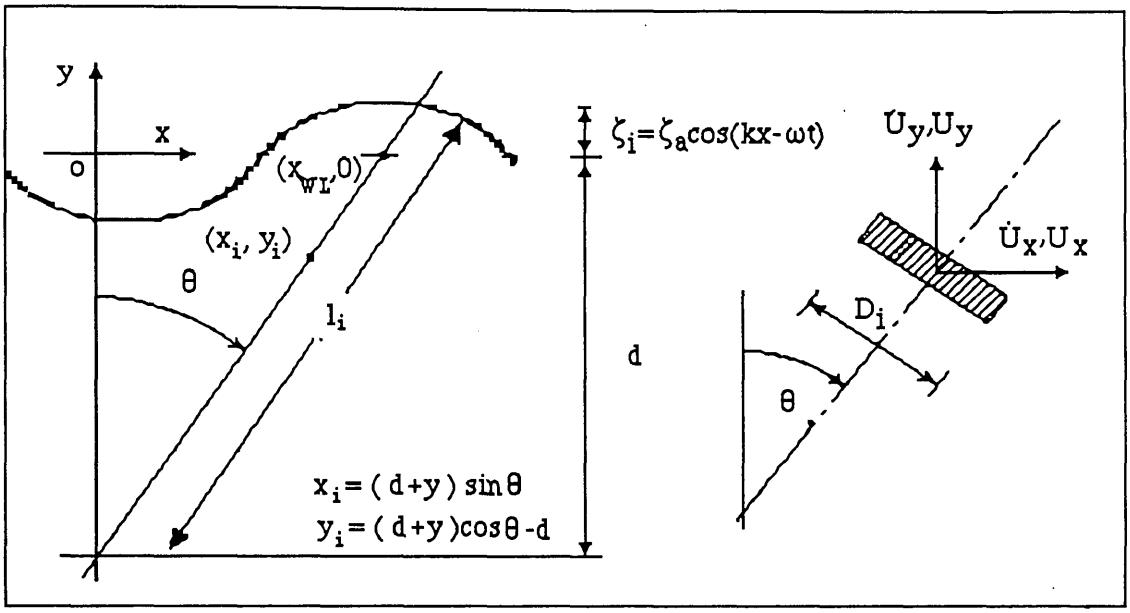

Fig.6.1 Coordinate system for large angle oscillations of articulated tower

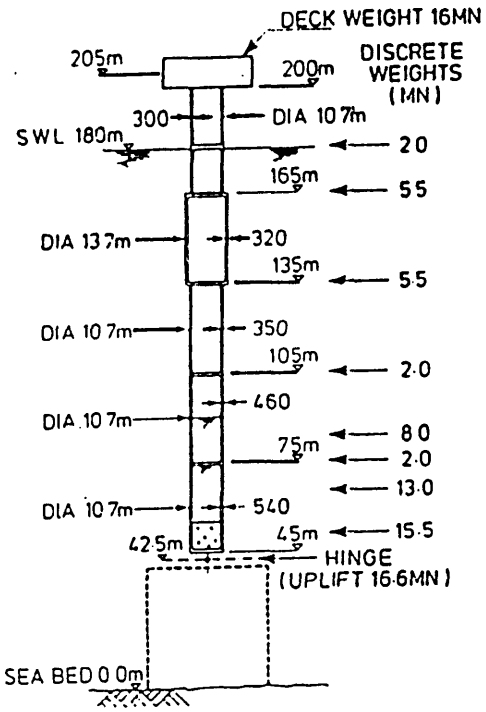

Fig.6.2 Single articulated tower configuration (Snowden et al, 1985)

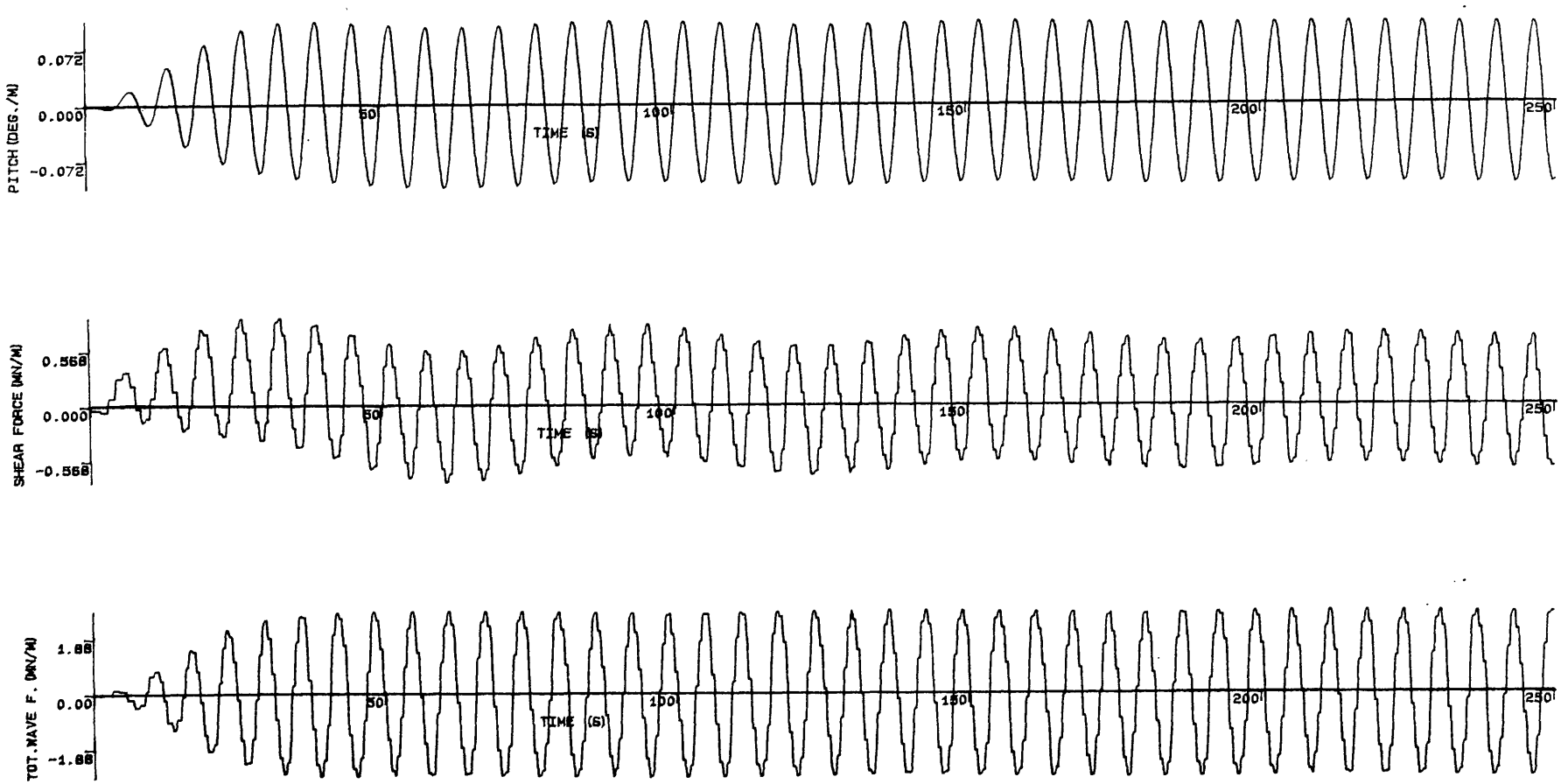

Fig.6.3 Single articulated tower motion simulation. Freq.=1.0rad/s, Hw=2m,
ramp function applied during first 50 sec

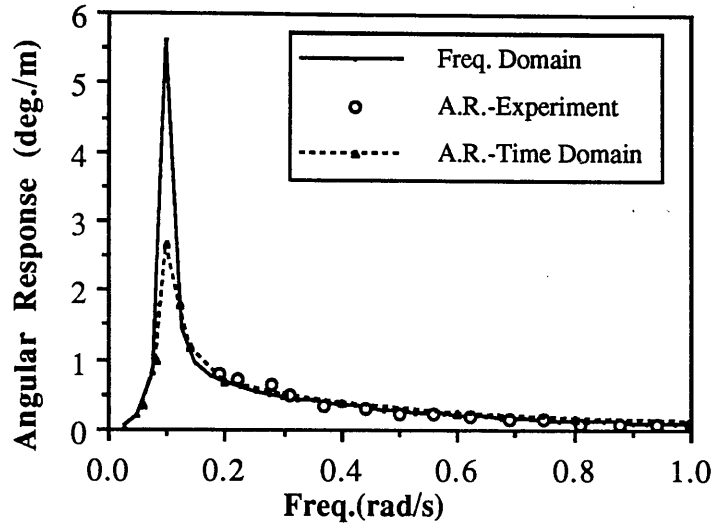

Fig.6.4 Comparison of angular response values obtained in frequency and time domain (H_W=2m)

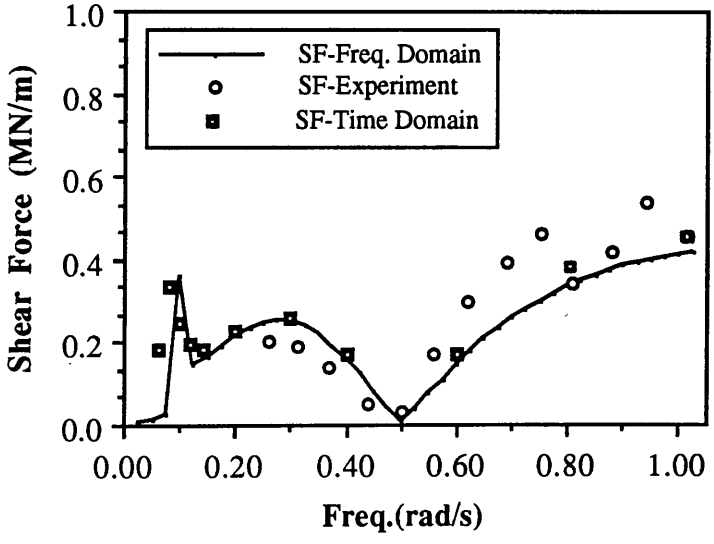

Fig.6.5 Comparison of shear force at base joint obtained in frequency and time domain (H_W=2m)

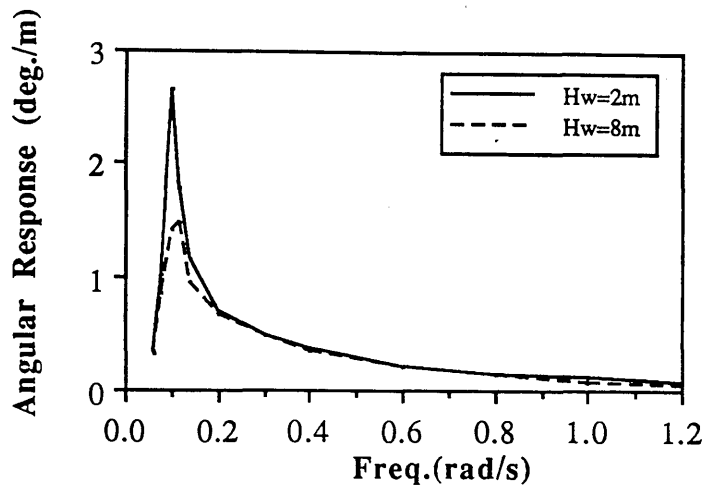

Fig.6.6 Effect of wave height variation on angular response of tower

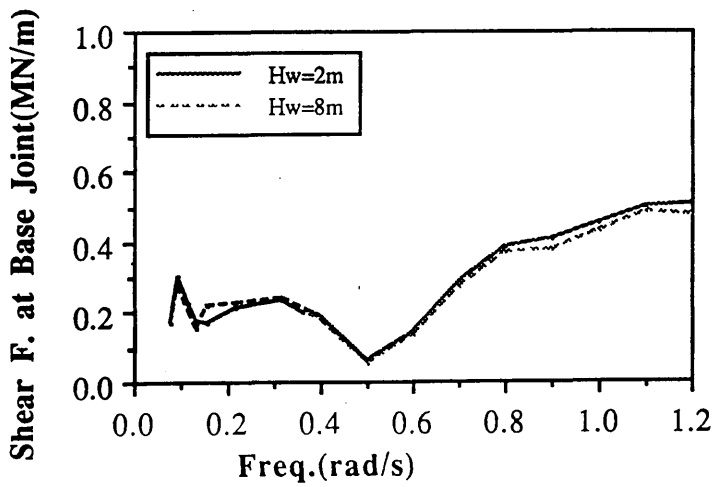

Fig.6.7 Effect of wave height variation on shear force at joint

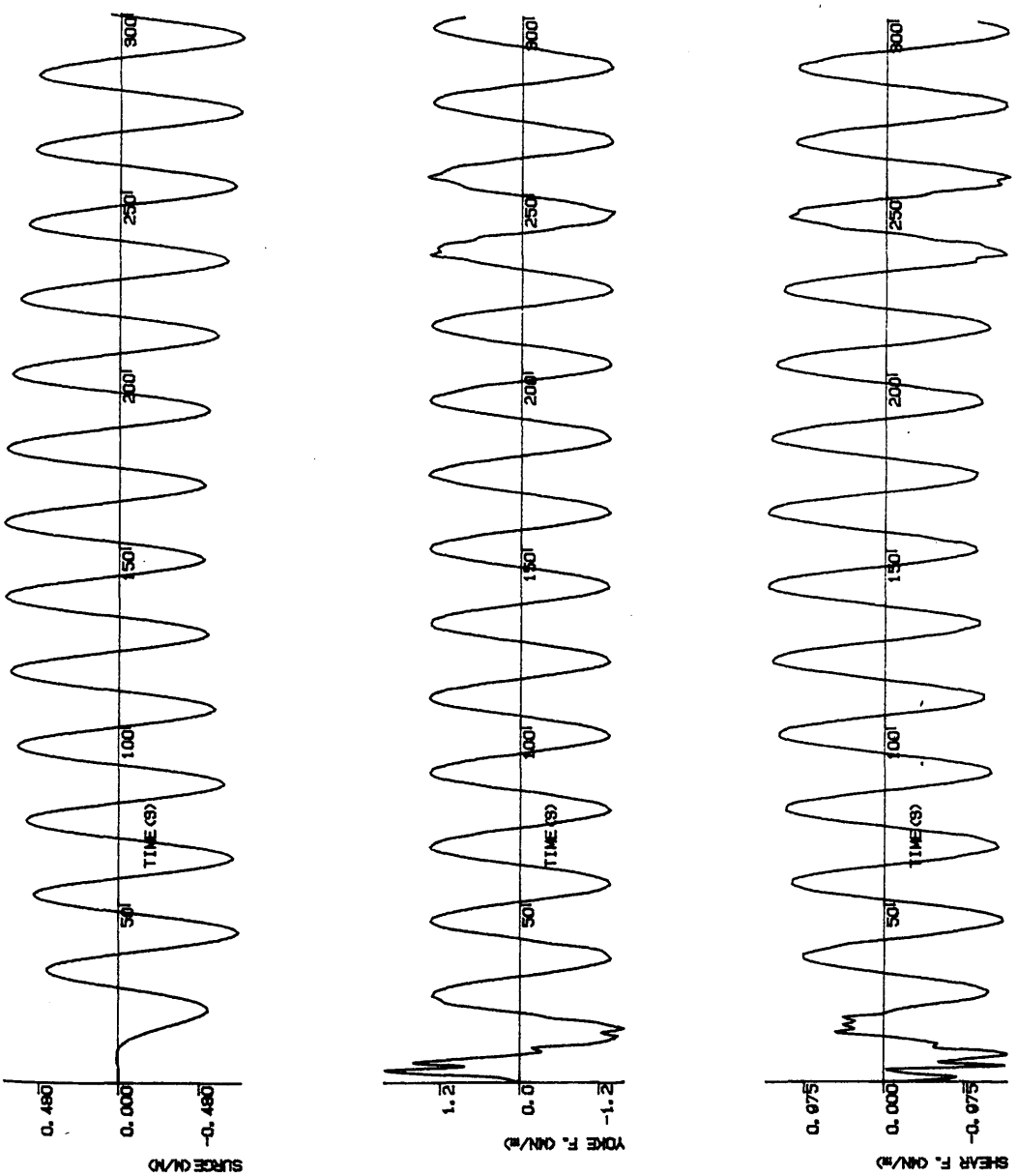

Fig.6.8 Coupled articulated tower and ship motion simulation. Freq.=0.3rad/s, Hw=2m, ramp function applied during first 60 sec

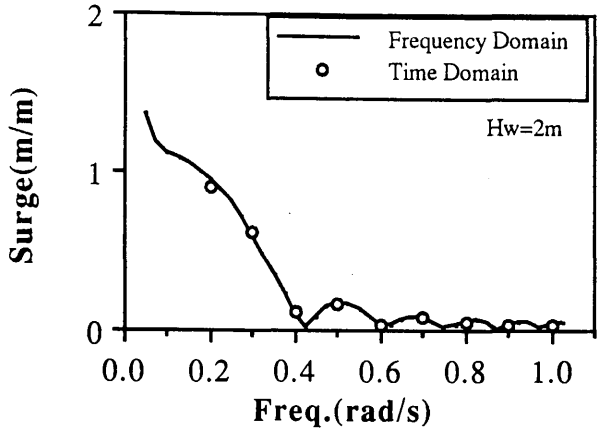

Fig.6.9 Comparison of surge response: frequency domain vs time domain

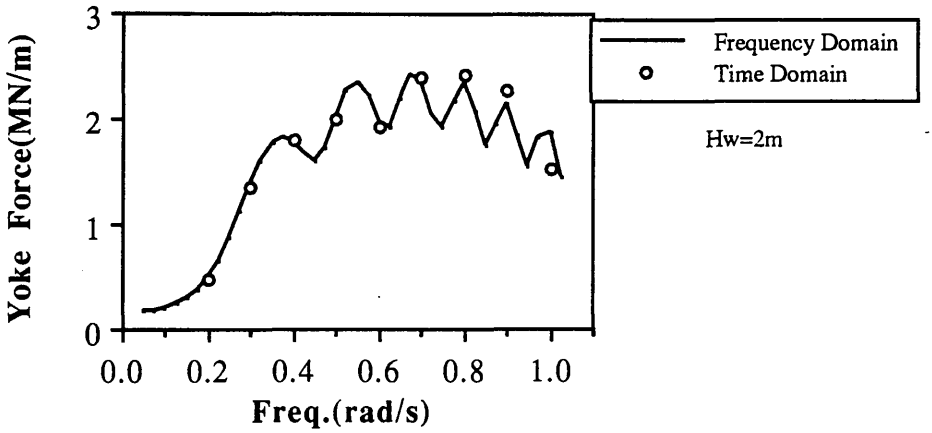

Fig.6.10 Comparison of yoke force: frequency domain vs time domain

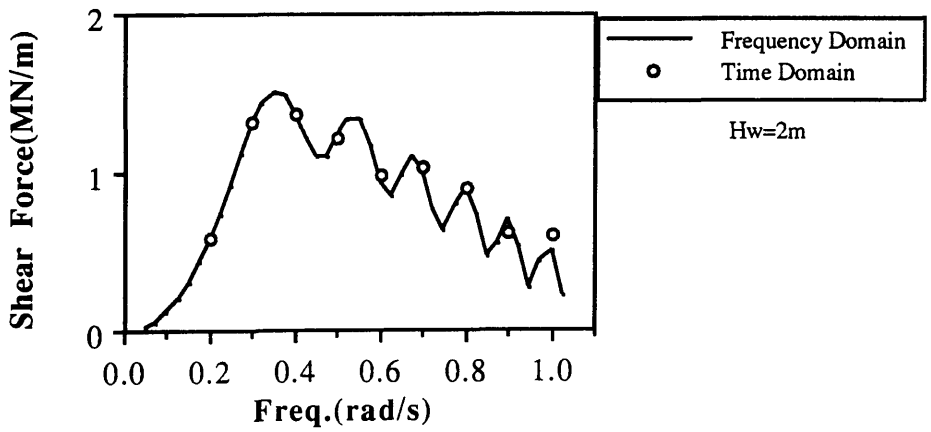

Fig.6.11 Comparison of shear force: frequency domain vs time domain

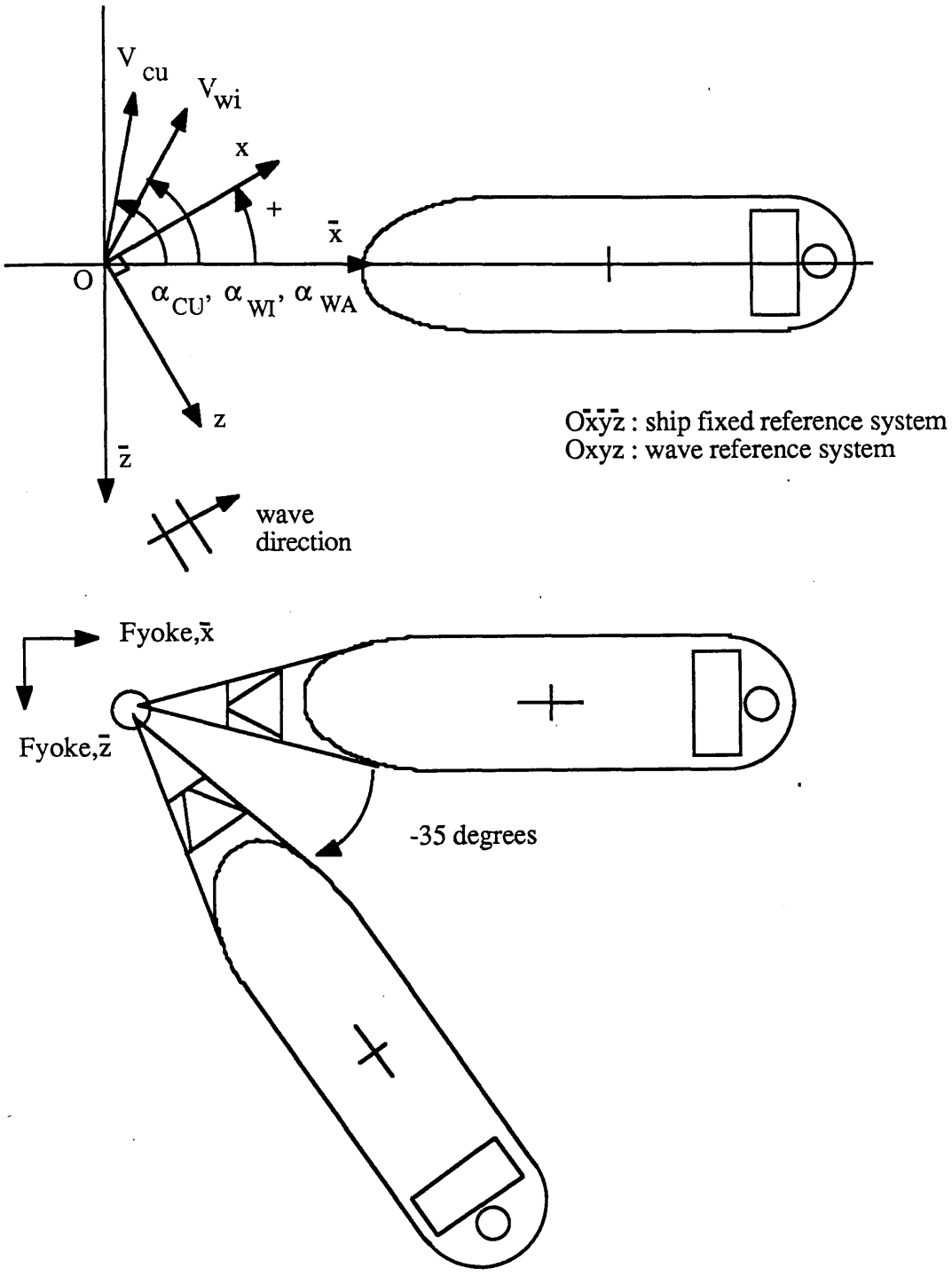

Fig.6.12 Environmental forces and their directions acting on the articulated tower-tanker system

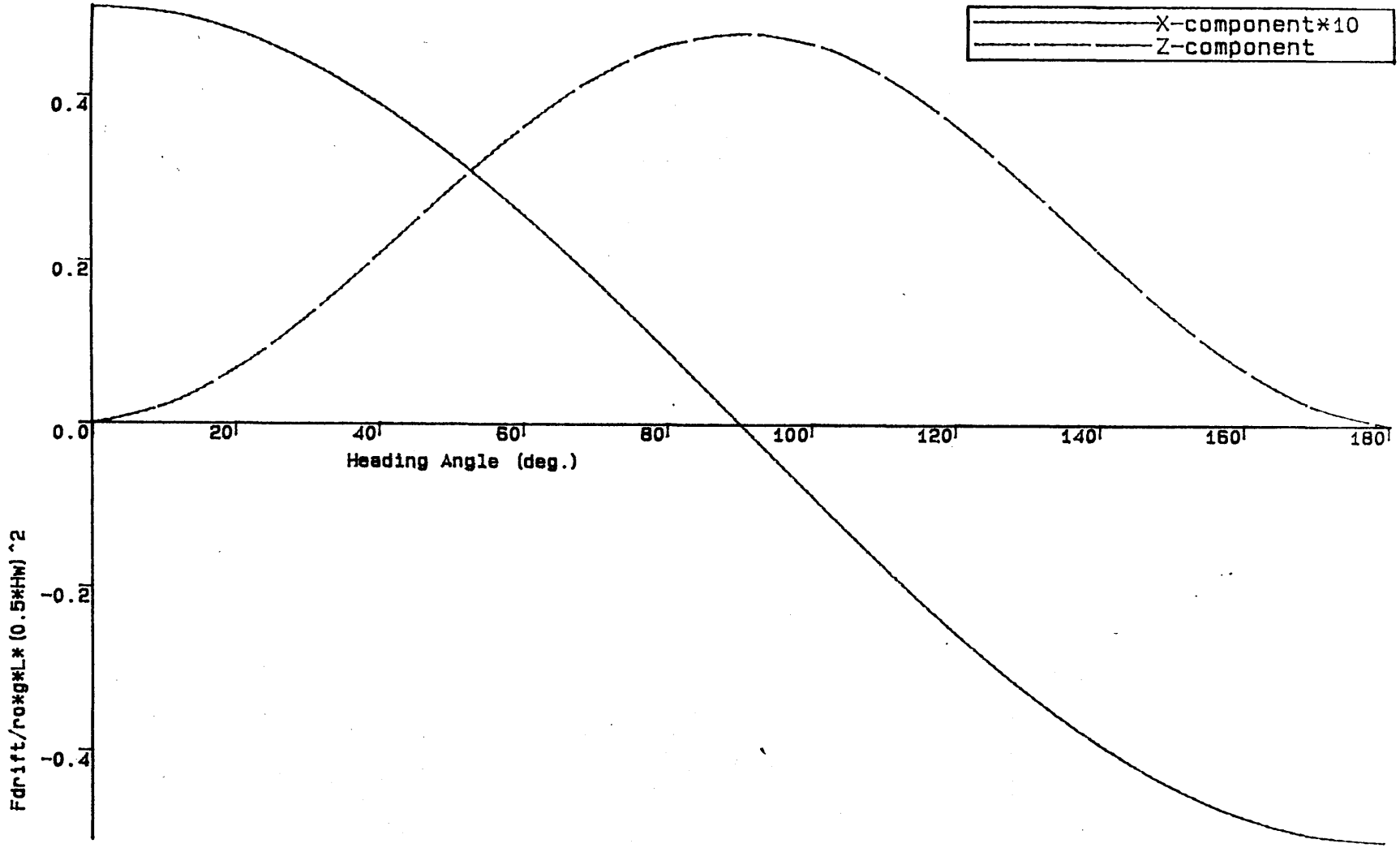

Fig.6.13 Non-dimensionalized drift forces on ship

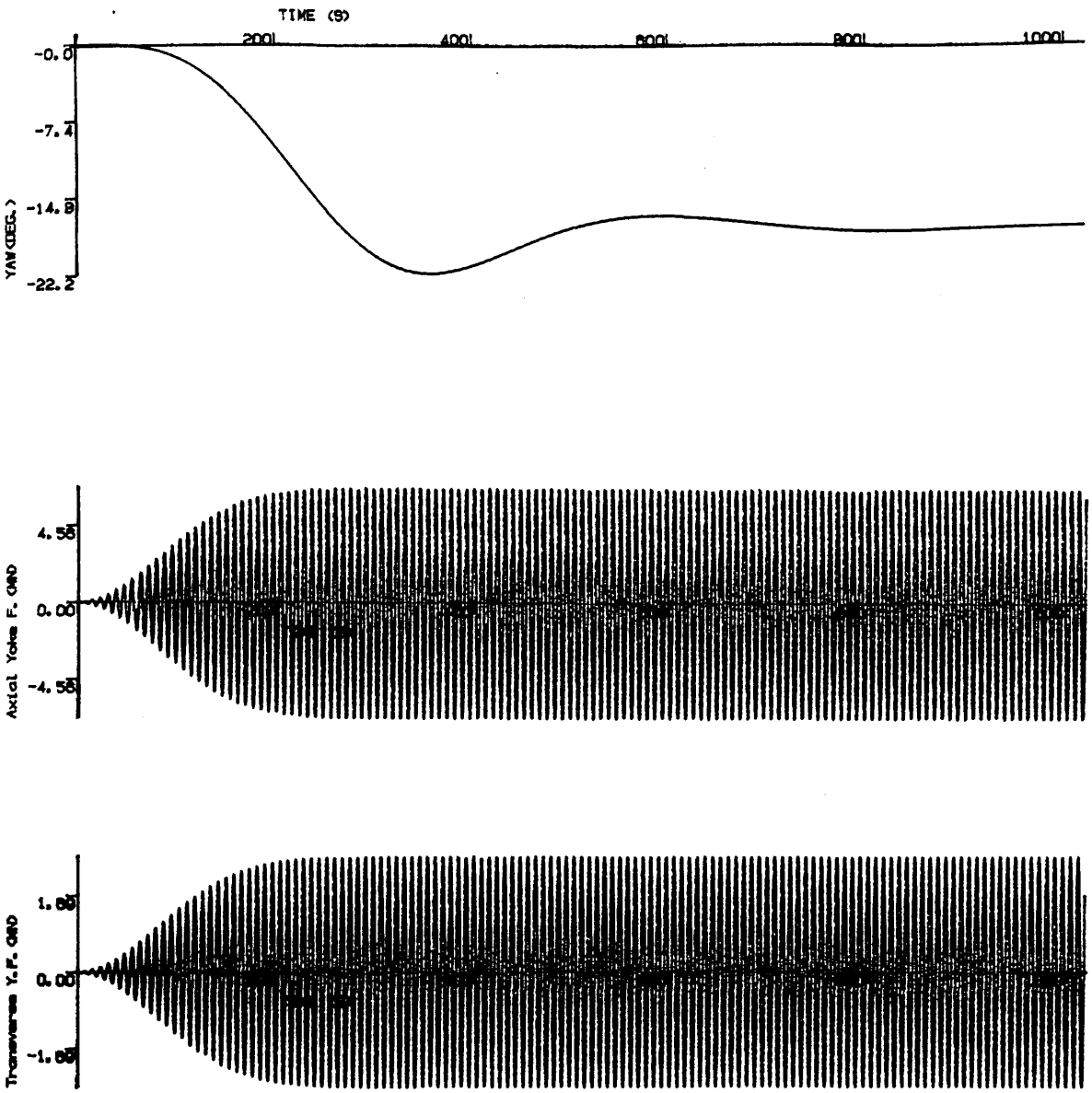

Fig.6.14 Time domain simulation curves; wave height, 8m; wave frequency, 0.8rad/s; wind velocity; 22m/s; current velocity, 1.5m/s; wave direction, 0 deg; current direction,-90 deg ; wind direction, -30 deg

CHAPTER 7

EXPERIMENTAL WORK

7.1 GENERAL DESCRIPTION

In order to validate the analytical calculations carried out for the coupled double articulated tower and ship system a series of experiments was conducted. The experimental set-up, the techniques used for the analysis of measurements and the results of measurement are described in this chapter.

The facilities at the Hydrodynamics Laboratory of the University of Glasgow were used. The wave tank used is 77m long, 4.6m wide and 2.4 deep.

Regular waves are created by an electro-hydraulic, plunger type wave maker fitted along one end of the tank. The other end of the tank is fitted with a passive wave absorber or beach.

In order to measure wave heights, resistance type wave probes were placed across the tank width ~10.5m in front of the wave maker. These probes induced electrical signals whose strength varied with the varying wave height. These electrical signals were amplified and recorded by a chart recorder for further analysis.

The calibration of wave probes was performed by lifting the wave probes 5cm and recording the deflection on the chart recorder. The range of waves which can be produced by the wave maker in the test tank is shown in Fig.7.1. The regular wave measurements were performed in the absence of any experimental model.

The scale of the models selected was 1:125 so that a 300 m water depth could be represented in the model scale.

The experimental results were scaled according to Froude's law of similarity. If the model and full scale Froude number is the same (i.e. $(F_r)_{MODEL} = (F_r)_{FULL}$ where $F_r = v / \sqrt{gL}$) the following table can be obtained for the scale used in this chapter:

TABLE 7.1

Dimension	Scale Factor	Values
Length	α	125
Volume	α^3	1953125
Velocity	$\sqrt{\alpha}$	11.18
Time	$\sqrt{\alpha}$	11.18
Forces	$\alpha^3 \times 1.025$(correction for water density)	2001953.1

In this chapter, the description of model tests in regular waves is presented. These tests are:

- motion response measurements with a double articulated tower over a range of wave frequencies and wave heights,
- motion response and the yoke force measurements with a coupled double articulated tower and a rectangular box-shaped barge
- motion response measurements for a barge model moored by means of linear springs located on the fore and aft ends of the model.

The wave frequency and wave height range considered for each set of test are given in Table 7.2.

TABLE 7.2

	Model Scale		Full Scale	
	Freq.(Hz)	Wave Height(cm)	Freq.(rad/s)	Wave Height(m)
DAT (alone)	0.4-1.2	4.0-7.0	0.2-0.7	5.0-9.0
DAT+Barge	0.4-1.2	2.5-5.0	0.2-0.7	3.0-6.3
Barge (Spring moored)	0.4-1.2	2.0-6.0	0.2-0.7	2.5-7.5

In addition to the measurements listed above, the added mass, drift force coefficients and still water and wave damping coefficients for the barge model were measured. The numerical filtering procedure developed to analyze the data obtained from the free oscillation tests in waves is described in Appendix C.

7.2 DOUBLE ARTICULATED TOWER MODEL TESTS

The double articulated tower was constructed in two parts, namely the upper and the lower column (see Fig.7.2). They were connected to each other by means of a universal joint (see Fig.7.3). The lower column was also connected to the tank bottom using another universal joint mechanism. This arrangement makes the tower free to move in all directions about the universal joint except to yaw about its own axis. The columns are constructed from PVC piping. The lower column was ballasted using leadshot. The main dimensions of the model and ballast weight distribution are shown in Fig.7.4.

The model was instrumented with a LED-selspot system to measure the displacements of upper and lower columns. The selspot system is an optoelectronic device employing cameras to perceive the location of a light source. The infrared light from a Light Emitting Diode (LED) is focused on the detector surface. The photo current occurring on the surface can be used to obtain two signals linearly related to the X and Y coordinates of the LED.

During the experiments two cameras were used to measure the upper and lower column oscillations, independently. One camera was placed on the side of the tank. The other camera was accommodated in a water tight case and placed under the water. The tank width was well within the range of the camera for detecting the signals. On the other hand, the distance between the LED and the under water camera had to be kept below 1.5m in order to get a clear focus on the signal. The effect of the presence of the under water camera case on the column oscillation was assumed to be negligible.

Calibration of LED's was performed by moving the camera 5cm towards the wave maker. Calibration checks were performed on all channels every alternate day.

Each run was initiated by taking a zero measurement in calm water. Before a test run was recorded, the wave maker was started and a period of time allowed for the waves to arrive at the model. The data was recorded into a computer with an time interval of

0.0625 s. A generous time interval was allowed for the tank to calm between test runs.

From the horizontal displacements of the top end of the upper and lower columns, the angular responses in the plane of regular waves were obtained. In order to investigate the effect of wave height the tests were repeated with different wave heights at each frequency. The average value of the displacement amplitude was computed and normalized with respect to the average incident wave amplitude. These normalized values were plotted against the wave frequency as shown in Fig.4.4. As was discussed in Chapter 4 the actual displacements were less than those obtained theoretically, particularly near the natural frequencies of the system where the displacements were large.

7.3 COUPLED DOUBLE ARTICULATED TOWER AND BARGE MODEL TESTS

The existing model for the double articulated tower was connected with a rectangular box shaped barge by means of a rigid yoke. A typical lay out of the experimental set-up is shown in Fig.7.5. The tests were carried out in order to measure the heave and pitch response of the model barge, as well as upper and lower column response of the double articulated tower model in head sea condition in regular waves. The axial yoke forces on the yoke mechanism were also measured for three different inclination angles.

The barge model consisted of 4 compartments which were constructed using PVC plates and the base for the yoke mechanism (see Fig.7.6).

The motion response of the upper and lower columns as well as the heave and pitch responses of the barge were measured using the LED-selspot system and LVDTs (Linear Variable Differential Transformers), respectively. The measurement using the LED-selspot system was described in Section 7.2.

The heave and pitch motion responses of the barge model were measured by a pair of gravity type LVDT vertical displacement transducers with a ±20cm range. As shown

in Fig.7.5, they were attached to the subcarriage and connected with piano wires to the fore and aft sides of the deck of the barge model. The wires were suspended over a pulley to measure the vertical displacement at both sides. The weights of the transducers were balanced by counter weights to avoid any inertia effects on the transducers due to motion of the model. The data gathered from the transducers were stored in files on the VAX11/730 computer. They were also recorded simultaneously on charts by the multi-channel pen recorder.

The yoke mechanism chosen was an 'A' frame construction (see Figs.7.7 and 7.8). The barge side of the yoke mechanism was designed to be adjustable to a required height so that several inclination angles could be tested. The barge-yoke hinges were fabricated so as to permit only relative pitch. The material brass was chosen for the 'A' frame because of its light weight. A load cell which measures the axial yoke force was placed between the 'A' frame yoke and the universal joint on top of the upper column. The universal joint on the top of the column was made from an aluminium universal joint which was free to oscillate in two degrees of freedom (pitch and yaw). Therefore, it was possible to measure the axial yoke forces accurately.

The experiment was carried out twice to check the repeatability of the results. The results were compared with the analytical predictions in Figs.5.6-5.10. In order to investigate the effect of yoke inclination angle, the experiments were repeated with several inclination angles. As can be seen in Fig.5.27, the yoke angle has a negligible effect on the axial yoke forces.

The natural period of the DAT-barge system was computed from the recorded data as 416s (full scale). The coupled system was simply pulled by means of a nylon string and released. The progressively decreasing oscillation of the system around the rest position was recorded. The free oscillation test was repeated several times for different initial amplitudes. Fig.7.9 shows a typical result of the free oscillation tests.

The second order forces which are proportional to the square of the wave amplitude cause the coupled system to experience a static offset in the high frequency region. Since

the load measuring device was mounted on the axial yoke mechanism, it was not possible to measure the steady drift forces acting on the system. Therefore, an attempt was made to investigate the contribution of the barge to the static offset due to second order forces. In order to carry out this investigation, the rectangular box shaped barge was tested alone in regular waves. The results from these experiments are discussed in the following section.

7.4 SPRING MOORED BARGE MODEL TESTS

7.4.1 TESTS IN CALM WATER

The barge was moored at the centre of the subcarriage with two linear springs on the fore and aft. The test set-up and model configuration for the mooring system are shown in Fig.7.10 and 7.11, respectively. The springs were pretensioned so that they were prevented from becoming slack during the test. Two sets of springs having different stiffness values were used. Fig.7.12 shows the linearity of the springs. The spring coefficients were 12.9 kg/m for Spring No.1 and 6.4 kg/m for Spring No.2.

Free oscillation of the barge was obtained by pulling on one of the mooring lines until the lines were stretched and then releasing it. The surge displacement of the barge was measured by a selspot measuring system. The natural period of the system was calculated as the average of the peak-to-peak values of the positive (or negative) peaks.

The added-mass and damping coefficients for the barge model at different natural periods (i.e. different stiffness coefficients) were computed from the free oscillation tests in still water as follows.

In still water, the extinction test produces a low-frequency decaying oscillation in surge motion or in the mooring line load which may be given by the following differential equation:

$$M_{Tx}\ddot{x} + b_x\dot{x} + k_x x = 0 \tag{7.1}$$

where, x is surge displacement; M_{Tx}, total mass (=M+$M_{AD,x}$); $M_{AD,x}$, added virtual mass in surge mode of motion; b_x, damping coefficient; k_x, stiffness coefficient and the dots represent the derivatives with respect to time.

The general solution of this equation can be written as follows (see Thomson (1981)).

$$x = x_a e^{-\zeta\omega_n t}\sin\left(\sqrt{1-\zeta^2}\,\omega_n t + \phi\right) \tag{7.2}$$

in which, t is time; x_a, maximum amplitude of the oscillation; ϕ, phase angle; ω_n, natural frequency and ζ, damping factor.

The damping factor is defined as the ratio of damping

$$\zeta = \frac{b_x}{b_c},\ b_c = 2M_{Tx}\omega_n \tag{7.3}$$

The logarithmic decrement can be defined as the natural logarithm of the ratio of any two successive amplitude. The expression then becomes

$$\delta = \ln\frac{x_n}{x_{n+1}} \tag{7.4}$$

Therefore, the damping coefficient of the barge in still water is given as

$$b_x = \frac{\delta}{\pi}M_{Tx}\omega_n \tag{7.5}$$

Knowing the natural frequency and the spring constant of the system the total mass, M_{Tx} is then computed

$$M_{Tx} = \frac{k_x}{\omega_n^2} \tag{7.6}$$

and the added virtual mass, $M_{AD,x}$ can be calculated as the difference between the total mass M_{Tx} and the displaced mass, M

$$M_{AD,x} = M_{Tx} - M \tag{7.7}$$

Figs.7.13 and 7.14 shows the added mass and logarithmic decrement values, respectively.

7.4.2 TESTS IN REGULAR WAVES

Wave Damping Measurement

In this part of the experimental work, the free oscillation tests were repeated in regular waves. As with the tests in still water, the barge was pulled by means of a nylon string and was set a transient low-frequency oscillation which decayed at a rate dependent on the damping in the system. Thus, the natural period of the system and its damping factor at different wave exciting frequencies were determined from these runs.

The data for surge motion in regular waves include the decaying long period oscillation and the high frequency oscillation. In order to obtain the low frequency oscillations it was necessary to preprocess the experimental data to remove the wave frequency motions. If the high frequency is filtered out from the recorded data, then the filtered data should satisfy Eq.(7.1).

The experimental data was low pass filtered using a digital filter with a cut-off frequency of 0.37 Hz and a span rate of N=71. The filtering process and the design procedure for the digital filter were explained in Appendix C.

Fig.7.15 shows an example of filtered data. Assuming Eq.(7.1) to be a linear differential equation with constant coefficients, the steady state solutions of the low-frequency surge motions take a form similar to that of the free oscillation. The added mass and damping coefficients are computed from filtered decaying oscillation in the same manner.

It was noted that for the same spring constant the natural frequencies of the moored barge in still water were the same as those in regular waves. This means that the added mass coefficient in the low-frequency surge motion in combination with high-frequency head waves corresponds to the added mass coefficient in still water conditions. However, a large difference was recognized in the damping. The reason for this is that the regular waves contribute an additional damping superimposed on the still water low-frequency damping(see Wichers and van Sluijs (1979)). This contribution is dependent on the wave height and the wave frequency and independent of the spring constant of the system. Fig.7.16 shows that there is no clear trend for damping increment in waves. However, the magnitude of the wave damping is of the same order as the viscous still water damping coefficient.

Drift Force Coefficient Measurement

In addition to the surge motion measurement of the barge, the load on the mooring line was measured by means of a load cell placed at the fixed-end of the bow spring.

The experimental data were recorded on the computer for further analysis. They were also simultaneously recorded on the pen recorder charts. Test results were analyzed by using the existing computer programs in the VAX11/730 system. Program DATAAVE was used to find the average value of the load cell signal. This value was multiplied with an appropriate calibration factor to obtain the steady forces on the axial direction of the motion. Another data analysis program, called DATARMS, was used to calculate the r.m.s. values of wave heights. Assuming that the wave trains are sinusoidal the wave amplitude can be calculated by

Amp. = $\sqrt{2}$ (r.m.s. value). (7.8)

Making the mean drift forces nondimensional the drifting coefficients of the barge can be calculated as a function of wave frequency. The steady drift force due to regular waves is made nondimensional as follows:

$$R^2(\omega) = \frac{\bar{F}_D(\omega)}{\frac{1}{2}\rho g B \zeta_a^2} \tag{7.9}$$

where, g is gravitational acceleration (m/s^2); B, barge breadth (m); ζ_a, wave amplitude (m) and ω, wave angular frequency (rad/s).

The regular wave measurements were taken in the absence of the model in order to obtain the undisturbed incident wave height.

The value of the steady drift force coefficient generally increases with the increase in the frequency of the regular waves. The difference in the steady loads due to different spring constants is shown in Fig.7.17.

The drift coefficients were obtained from experimental measurements and compared with the analytical predictions in Fig.7.18 (see also Chapter 2 Section 2.3.3). It can be seen from this figure that Kwon's formula gives a better correlation with model test results for the rectangular barge model.

Having determined the wave drift coefficient, the surge of a moored structure due to wave groups and due to irregular waves may be predicted. The latter case has been discussed in Section 2.3.4 and in Section 3.6.

7.5 CONCLUSIONS

The experiments described in this chapter are aimed at measuring the motion response of the coupled system and the axial forces acting on the yoke mechanism. This work verifies the analytical method described earlier and establishes some limitations of the calculation procedure.

The variation of damping coefficients of the barge not only with different spring coefficients but also with the wave height and frequency are studied. It has been found that damping coefficient in waves is dependent on the wave height and the wave frequency and independent of the spring constant of the system.

Comparisons between the predictions and the measurements indicate that the semi-empirical formula given by Kwon agrees better with the measurements than Fujii's formula.

It should be noted that the motions and forces in wave groups and in irregular waves were not measured in this experimental work. Since there is a low frequency component present in wave groups and in irregular waves the natural frequency of the system will be excited. The system, therefore, performs large oscillations and consequently large mooring loads occur. The analytical treatment of this problem has been made for one degree-of-freedom systems in irregular seas in Section 3.6. The application of irregular wave analysis for a multi-degrees of freedom system is suggested as a logic for the future work.

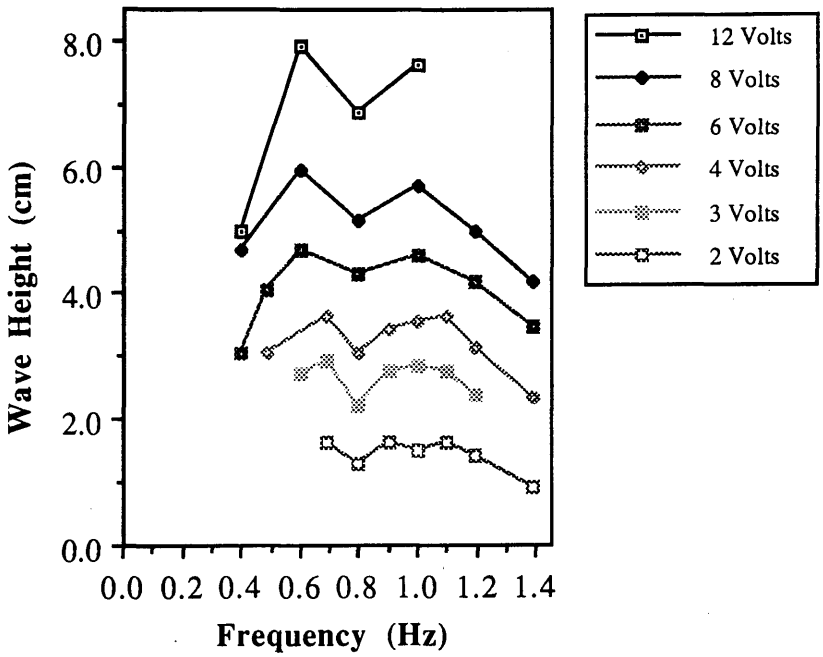

Fig.7.1 Wave height vs frequency for constant drive voltage
(Tests were carried out on February 26, 1988)

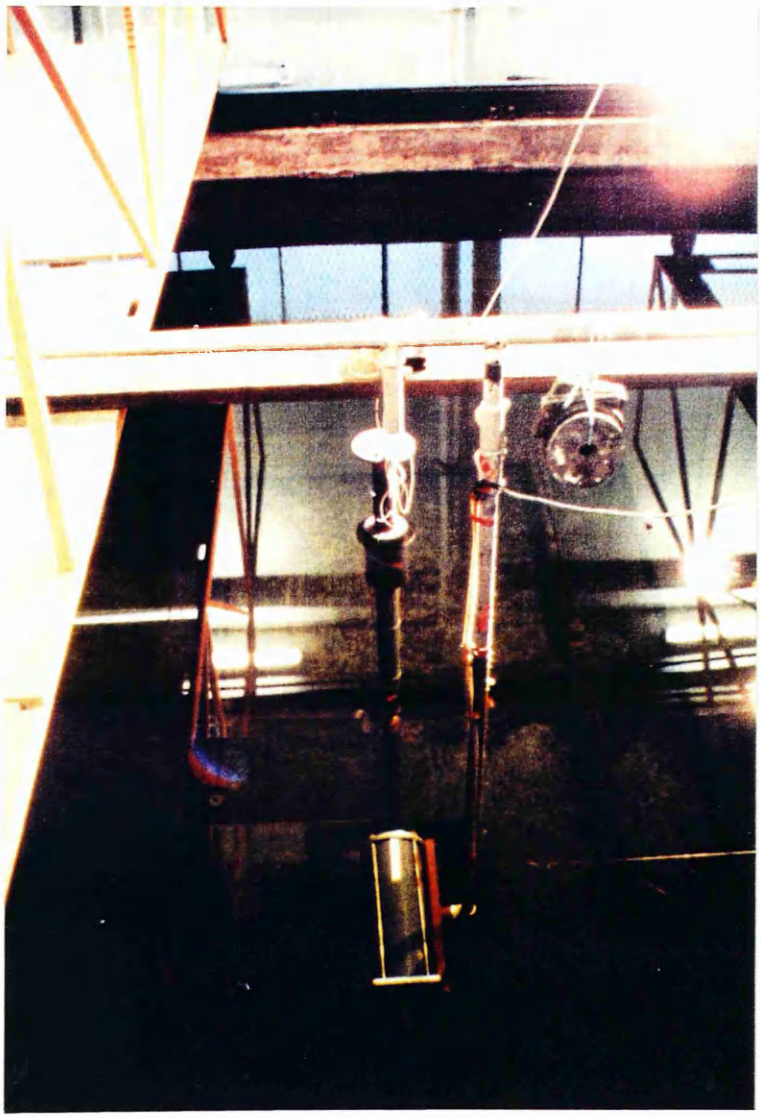

Fig.7.2 Double articulated tower model test set-up

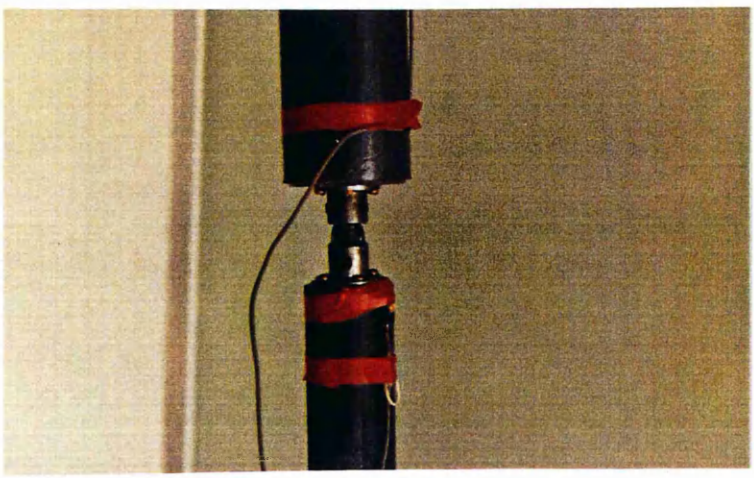

Fig.7.3 Universal joint mechanism connecting upper and lower columns

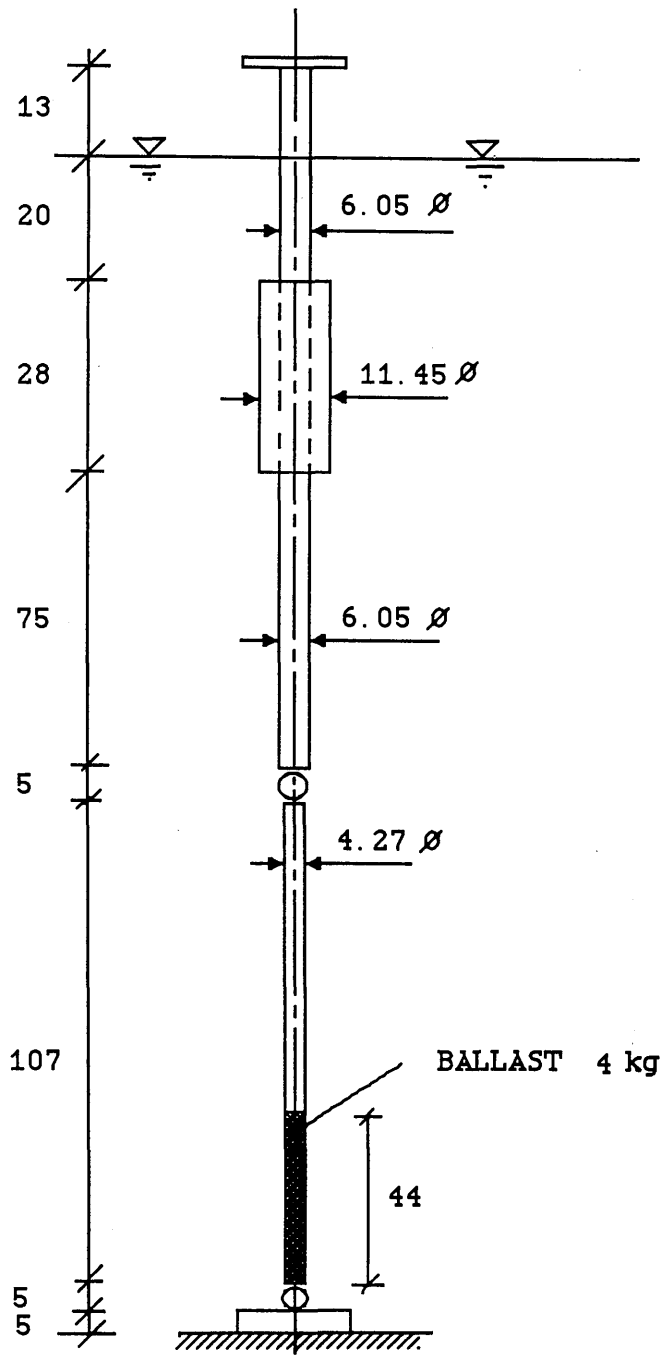

Fig.7.4 Double articulated tower model test configuration

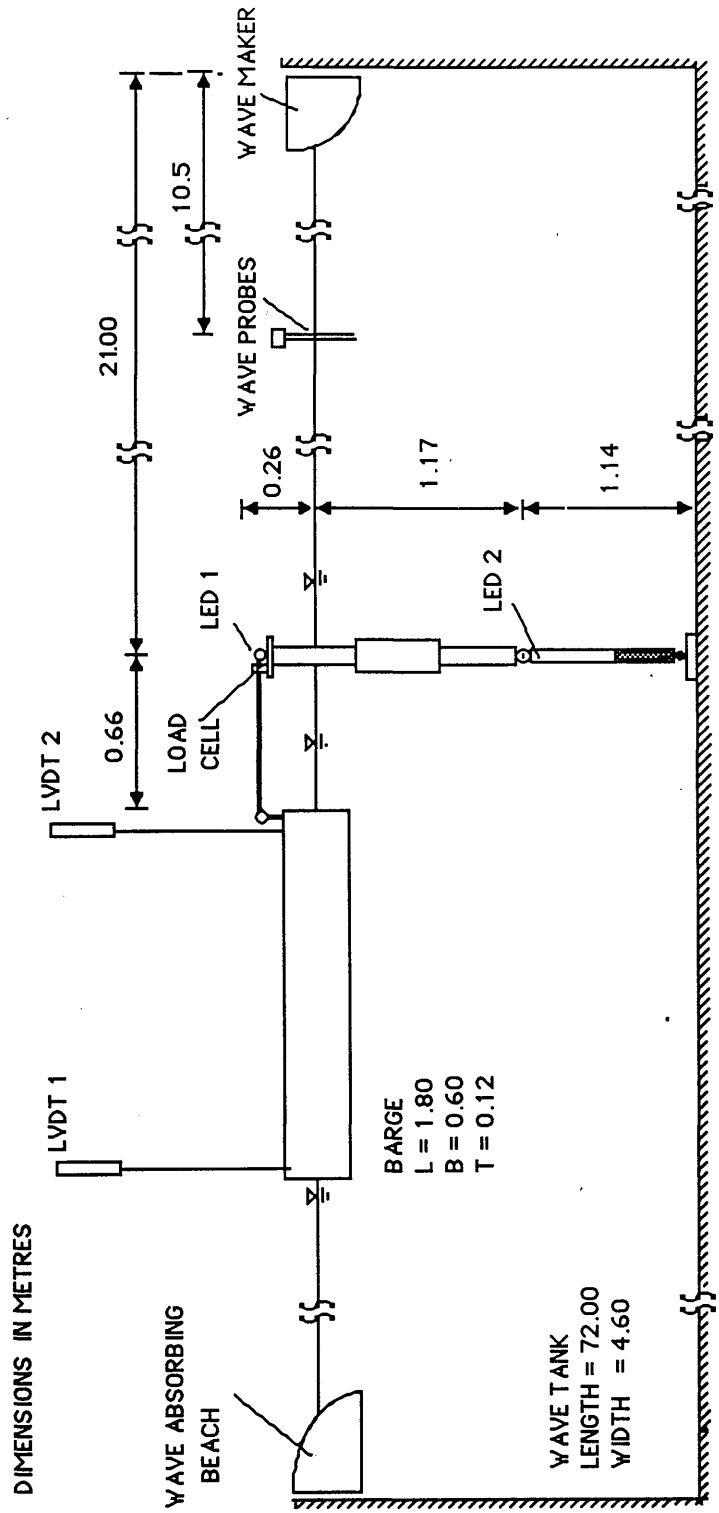

Fig.7.5 Wave tank set-up of coupled model

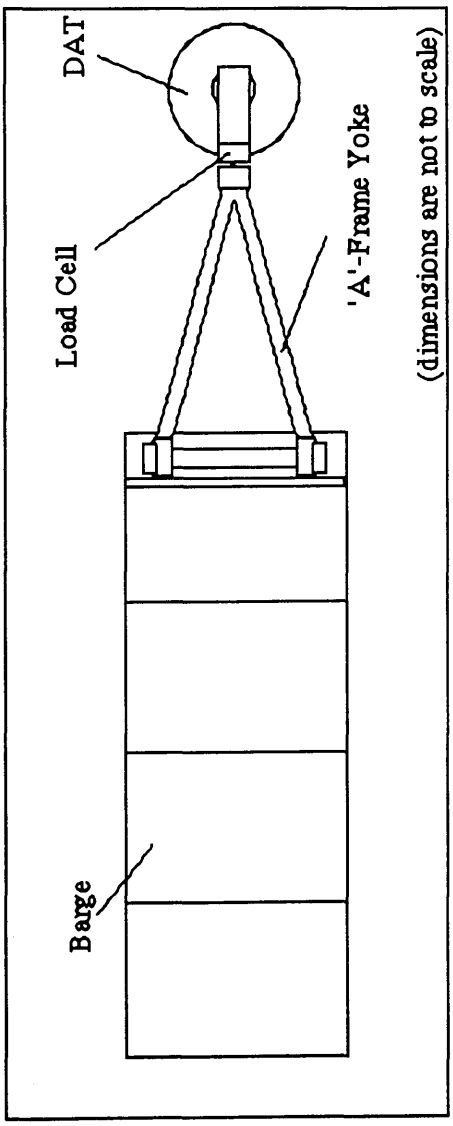

Fig.7.6 Top view of coupled DAT and barge system

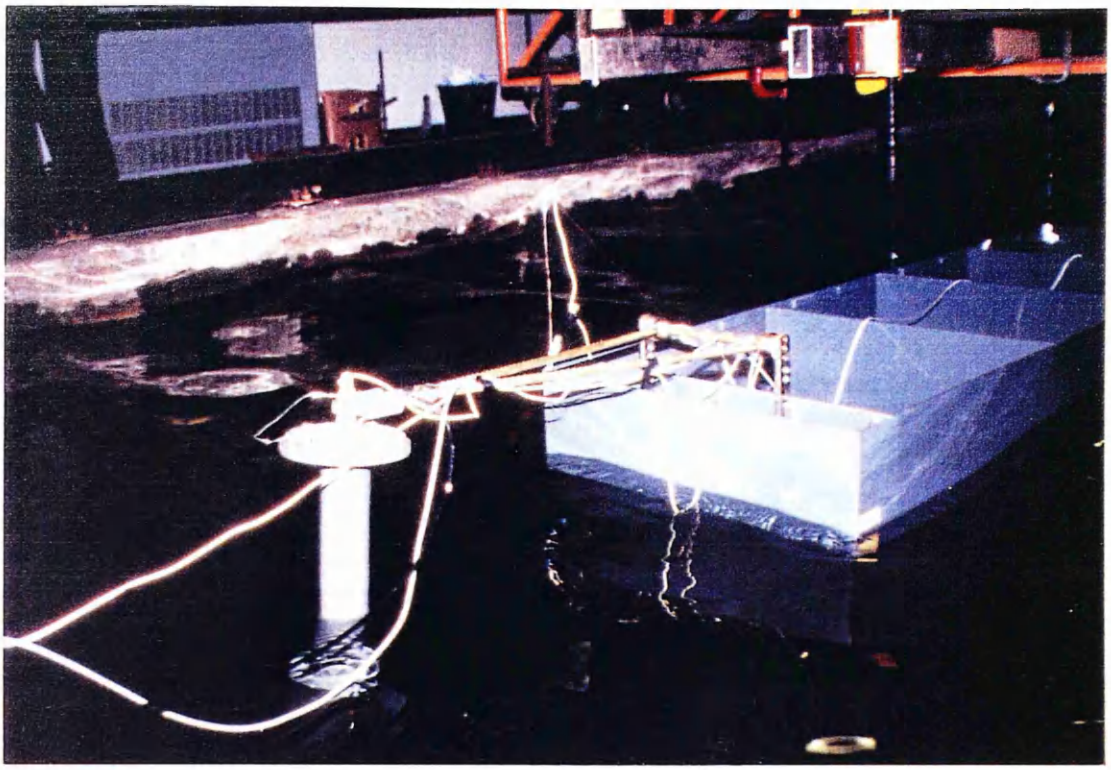

Fig.7.7 Details of rigid yoke connection between DAT and barge

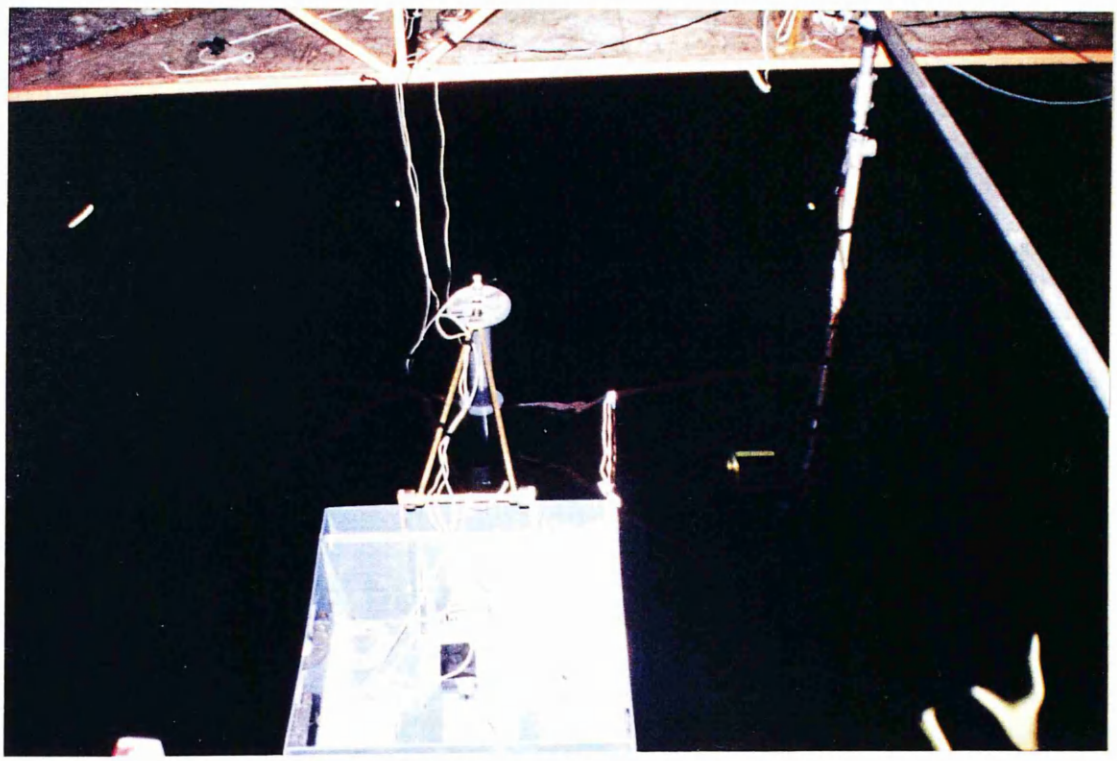

Fig.7.8 Top view of rigid yoke connection between DAT and barge

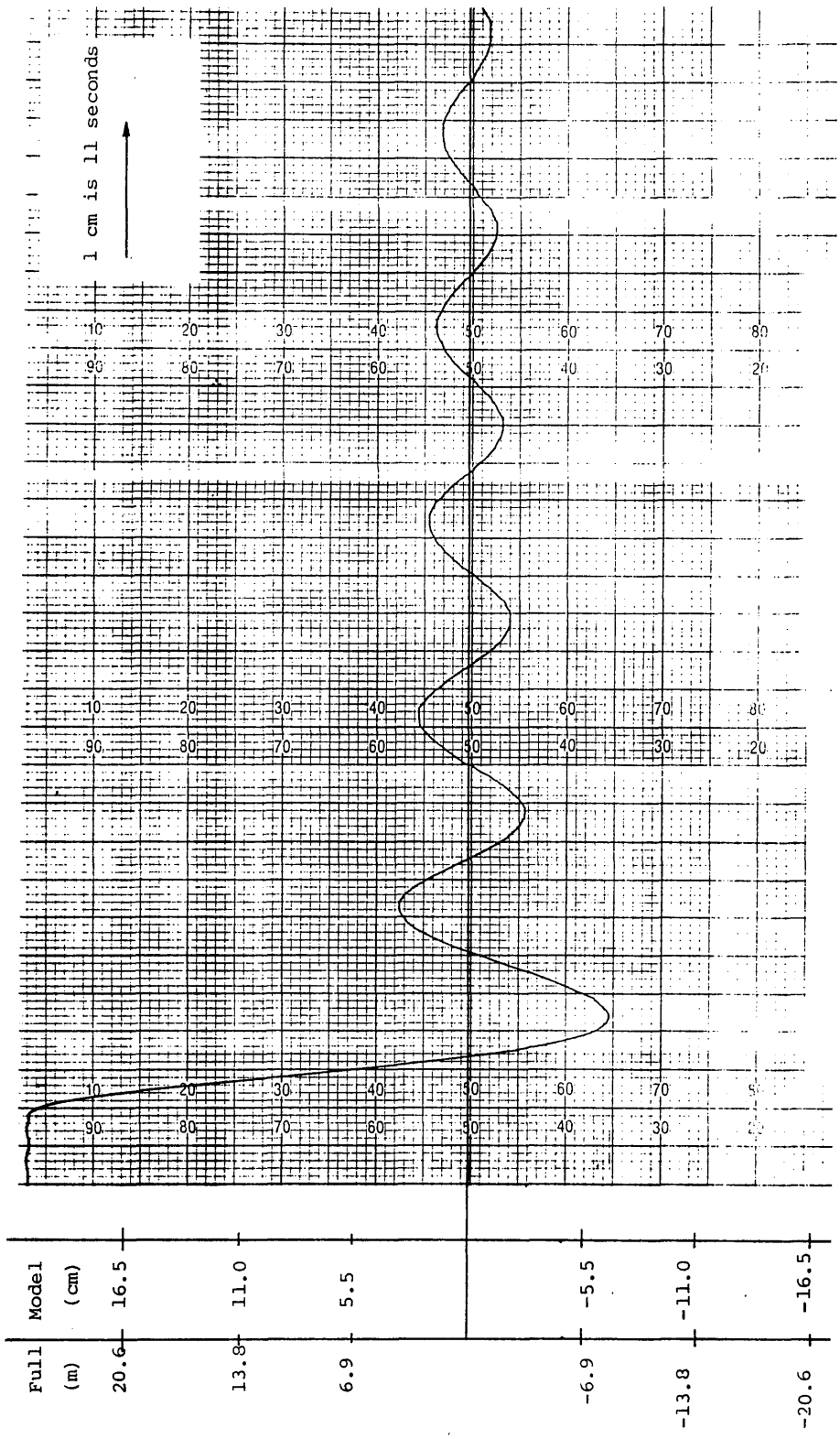

Fig.7.9 Free oscillation test in calm water

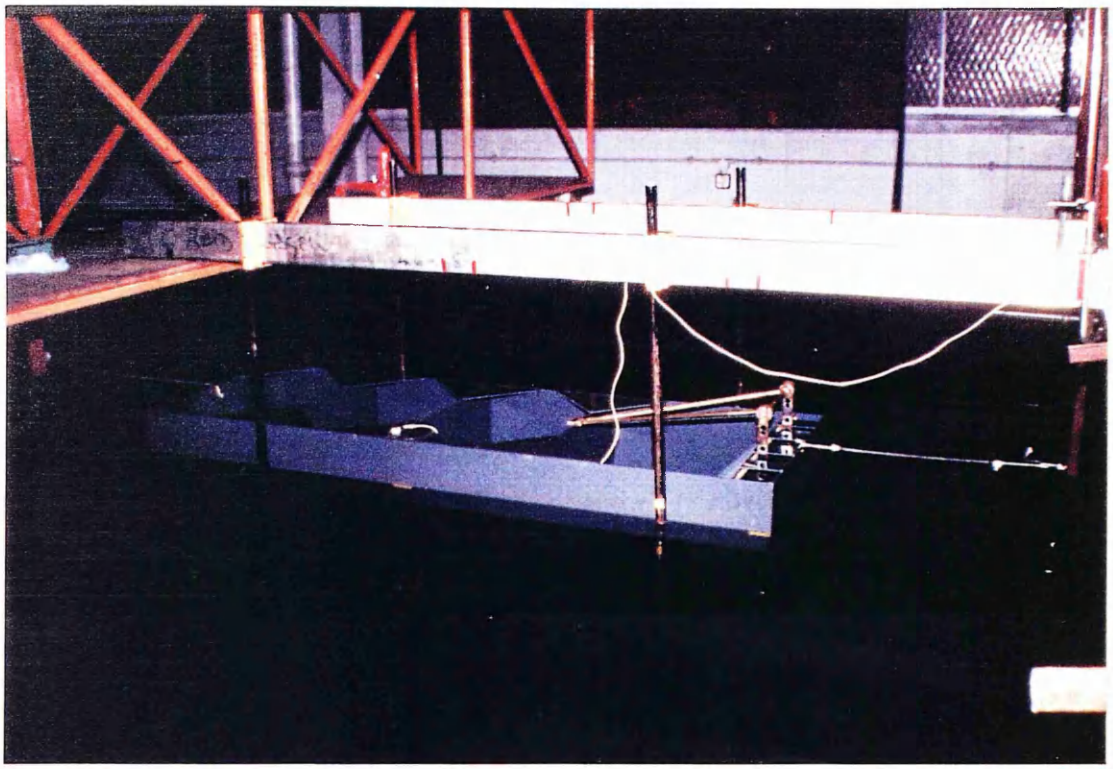

Fig.7.10 Wave tank set-up of spring moored barge model

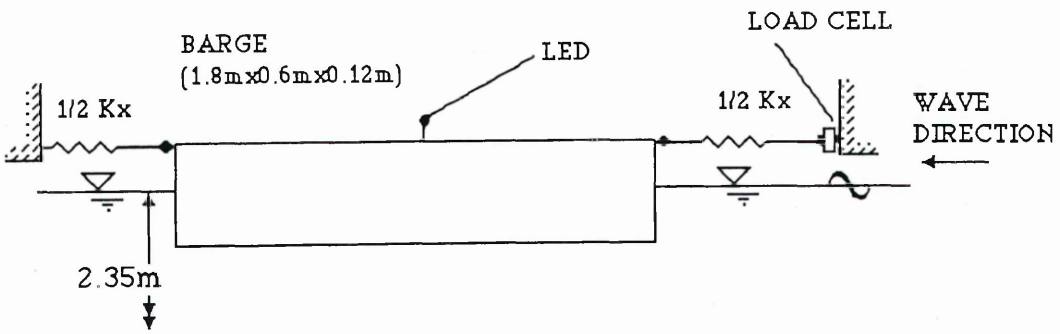

Fig.7.11 Spring moored barge model configuration

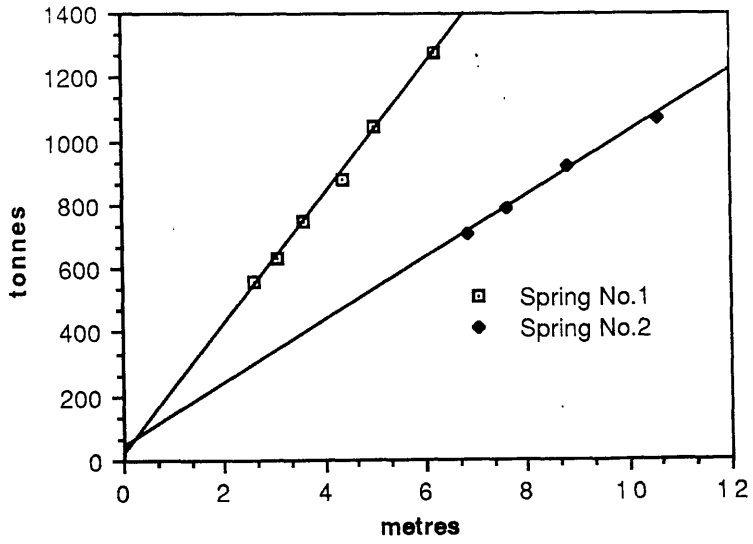

Fig.7.12 Total restoring force vs. static displacement

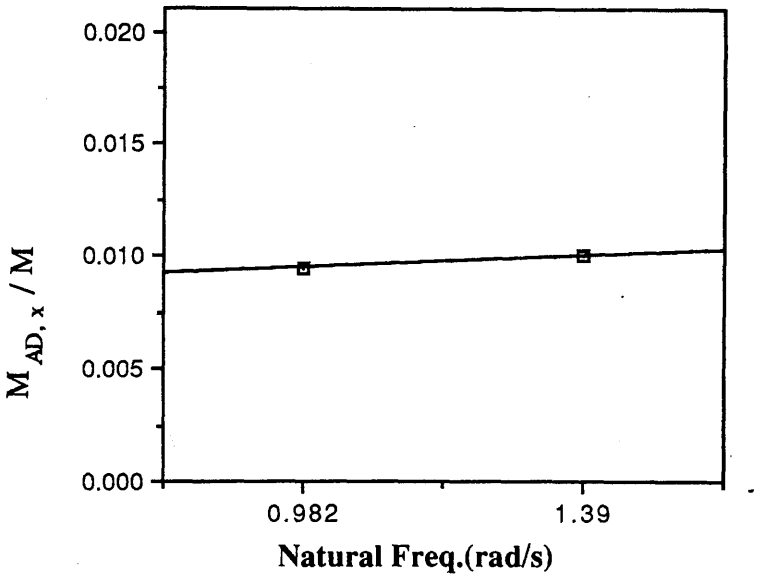

Fig.7.13 Surge added mass over mass ratio

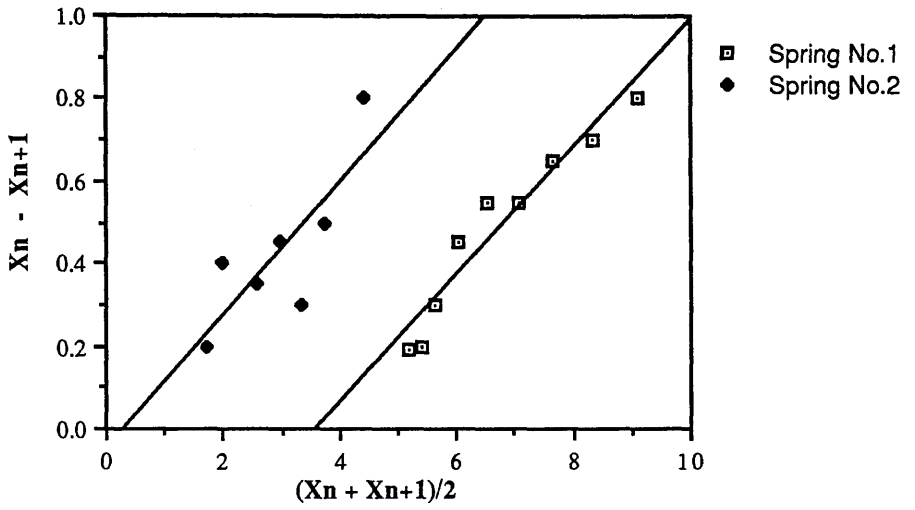

Fig.7.14 Logarithmic decrement values for two different spring moorings

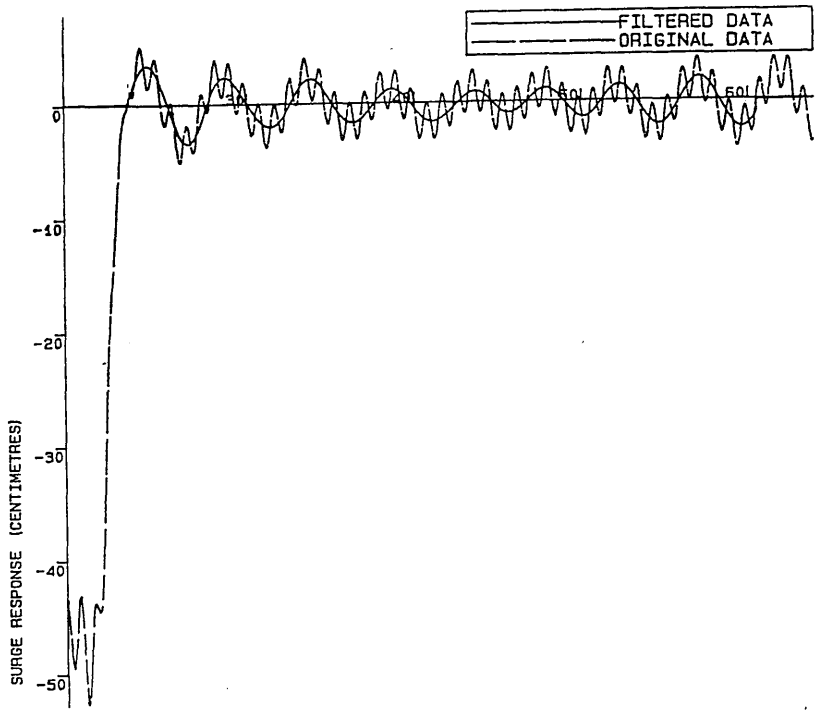

Fig.7.15 Filtered data of surge motion test in regular waves (Spring No.2)

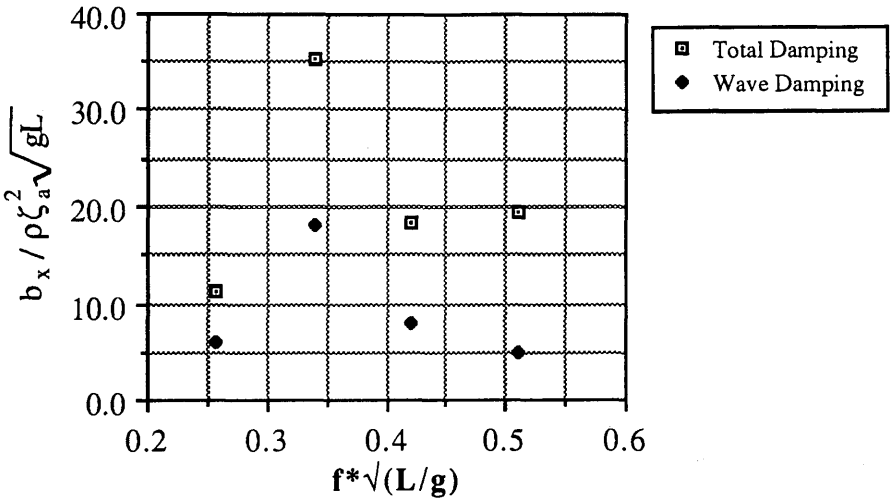

Fig.7.16 Nondimensional total and wave damping coefficients in regular waves

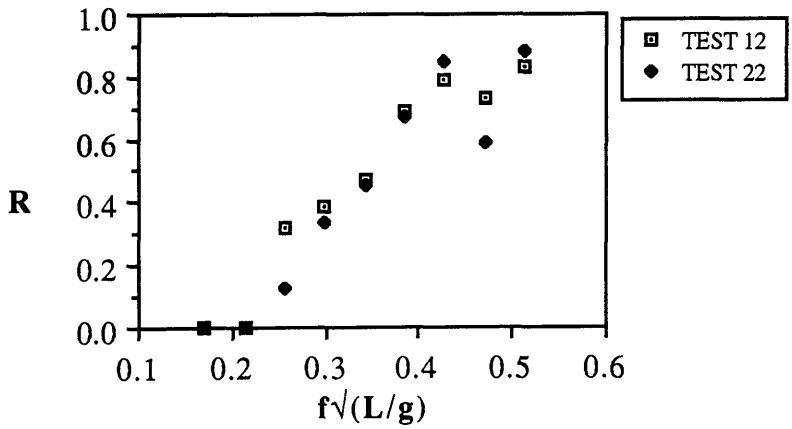

Fig.7.17 Effect of different spring coefficients on drift coefficient

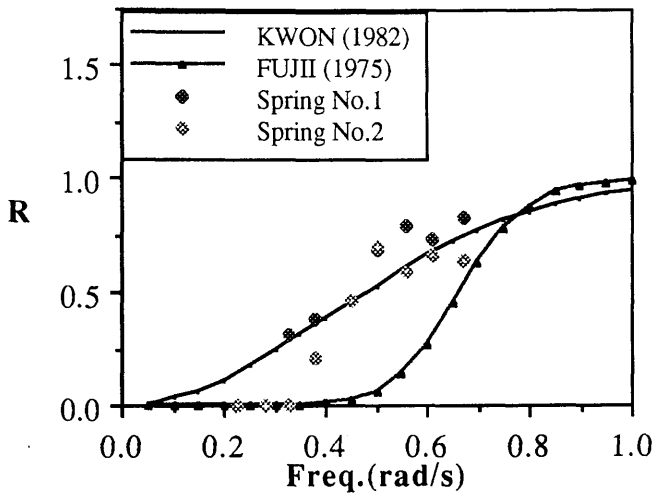

Fig.7.18 Drift force coefficient for rectangular box shaped barge

CHAPTER 8

CONCLUSIONS

8.1 GENERAL CONCLUSIONS OF THESIS

Compliant systems need more attention than fixed offshore structures in terms of dynamic analysis and in terms of different environmental loading conditions. It is necessary, therefore, to know the motion and structural response characteristics of the system in the initial design stage.

In this thesis it was shown that simplified motion equations for the coupled systems give quite good approximations. Mathematical models were verified with experimental measurements conducted at the Hydrodynamics Laboratory of Glasgow University and with previous investigations published in the literature. It is believed that these mathematical models are useful tools in the initial design stage.

The environmental forces can be calculated by using some approximate and/or empirical formula taking into account the physical properties of the system. Among the steady forces acting on the coupled tower-ship system, the current forces are found to be quite significant. On the other hand, the second order slowly varying wave forces cause the largest motion and structural response values on the coupled systems. The method given by Pinkster results in the predictions of slowly varying wave forces on the system which correlate quite well with experimental test measurements provided that the appropriate drift coefficients are used in the calculations.

Parametric studies show that the surge oscillations of the coupled articulated tower and ship system due to dynamic wind force are quite sensitive to the magnitude of the damping ratio.

The directional wave analysis reveals that more realistic strength calculations to determine the maximum stress level and fatigue life of the structure as well as motion response calculations to determine accurate down-time etc. will result when the effect of short-crested waves is taken into account.

The double articulated tower concept was introduced at greater depths as a measure of reducing bending moment values. In this study, it was found that introducing a second articulation worsens the motion characteristics. The high angular oscillations of the tower lead to higher shear force and bending moment values.

When the double articulated tower is connected to a ship with a rigid yoke mechanism, the shear force and bending moment values along the tower are considerably reduced due to the presence of the second articulation. This is due to the inertia provided by the ship reducing the motions.

The elbowing oscillation of the double articulated tower was observed experimentally and analytically. The peak frequency of this response amplitude operator is very close to the peak of the dominant sea spectrum for this particular configuration. Therefore, during the design stage, one should ensure that the peak frequency of the wave spectrum does not coincide with the second natural frequency of the double articulated tower.

The parametric studies reveal that coupled articulated tower and ship system motion characteristics are insensitive to water depth and yoke length variations. For the double articulated tower configuration it is possible to achieve required natural frequencies by changing the geometry of the buoyancy chamber.

The studies using the time domain simulation techniques show that the nonlinearities due to the presence of the tower are insignificant. It is concluded that the linearization procedure adopted in the frequency domain is acceptable. On the other hand, the other nonlinearities e.g. nonlinear wave damping, time depended added mass etc. are still subject to discussion.

The results of parametric studies on the joint occurrence of various environmental forces indicate that in defining the design wave, wind and current conditions, a prediction method based on the time-domain simulation provides an excellent tool.

8.2 RECOMMENDED FUTURE WORK

Given fast running computer programs, three dimensional source distribution techniques could be adapted in calculating accurately the wave forces and hydrodynamic coefficients on the ship. These forces could then be used in the motion equations given in this thesis.

In designing the coupled articulated tower and ship systems for deep waters, flexural modes of the tower should be taken into account. The effect of wave slamming and asymmetric loading on the tanker hinges should also be considered.

Measuring drift forces acting on the ship in short crested waves is subject to recent investigation (Pinkster (1988) and Nwogu and Isaacson (1989)). The effect of these second order forces on yoke mechanism and the universal joints of the tower would be a continuation of the present research.

The reason behind the large damping values on the double articulated tower motion when it is oscillating in waves still requires a further investigation.

APPENDIX A

SHEAR FORCE AND BENDING MOMENT CALCULATIONS

This Appendix describes a calculation procedure to predict the shear force and bending moment distributions along a single and a double articulated column. In the first section of the Appendix, a single articulated tower configuration is considered. The mooring forces due to a ship is also taken into account in the calculations. In the second section, a double articulated tower is considered as a stand alone structure and as a structure coupled with a ship.

The previous reported studies on the calculation of the shear force (SF) and bending moment (BM) distributions on articulated towers can be summarized as follows:

A vertical flexible column in regular waves was examined by Bishop and Price (1979). They adopted the Timoshenko beam theory to determine the principal modes and natural frequencies. The shear force and bending moment distributions for each mode were given separately.

Kirk and Bose (1982) considered three deep water articulated towers subject to random wave excitation. They compared r.m.s. values of SF and BM distributions on the three different tower configurations.

Eatock Taylor and Drake (1984) calculated the SF and BM distributions on a large diameter articulated tower subject to excitation due to regular waves. They also examined the effect of increasing water depth on the SF and BM distributions.

McNamara and Lane (1984) modelled the double articulated tower using discrete point masses (finite elements) with rigid links connected by torsional springs. The SF and BM distributions were given for the double articulated tower configuration designed for Thistle Field, North Sea.

In this study the articulated tower is assumed to be rigid so that the other flexural modes of vibration can be eliminated. The tower is divided into small strips. The forces on each strip are assumed to arise from the fluid inertia and drag forces, structural inertia, gravity and buoyancy forces.

i) Calculation of SF and BM Distributions for Single Articulated Tower

Assuming that the column is inclined at an angle of θ from the vertical axis (see Fig.A-1), the force acting on a strip of the column can be written as follows

$$dP = dF_I + dF_D - [(y+d)dB + (y+d)dW]\ddot{\theta} - (y+d)\dot{\theta}dC - g(dB - dW)\theta \tag{A-1}$$

where, dP is the total force per unit length; dF_I, inertia force; dF_D, drag force; dB, buoyancy; dW, weight; dC, damping coefficient; g, gravitational acceleration; d, water depth; θ, $\dot{\theta}$, $\ddot{\theta}$ angular motion,velocity and acceleration, respectively.

If we introduce the solution of $\theta = X_1 \sin \omega t + X_2 \cos \omega t$ and its first and second derivatives to Eq.(A-1), the following expression can be obtained

$$\begin{aligned} dP = dF_I + dF_D &- \{\omega^2[(y+d)dB + (y+d)dW] - g(dB - dW)\} \\ &\times (X_1 \sin \omega t + X_2 \cos \omega t) - (y+d)(\omega)(X_1 \cos \omega t - X_2 \sin \omega t)dC \end{aligned} \tag{A-2}$$

It is assumed that the influence of the drag force and damping on wave frequency motions is negligible in comparison with the inertia forces. Therefore, Eq.(A-2) is reduces to the following form

$$\begin{aligned} dP = dF_I &+ \{\omega^2[(y+d)dB + (y+d)dW] - g(dB - dW)\} \\ &\times (X_1 \sin \omega t + X_2 \cos \omega t) \end{aligned} \tag{A-3}$$

The shear forces at the universal joint can be calculated by summing the forces along the column as follows

$$F_{JX} = \int_{-d}^{CL} dP \tag{A-4}$$

where, CL denotes the distance between the SWL and the deck. Eq.(A-4) can be written in terms of in-phase and out-phase components as follows

$$F_{JX1} = F_I + [\omega^2(B\overline{KB} + W\overline{KG}) - g(B - W)]X_1 \tag{A-5}$$

$$F_{JX2} = [\omega^2(B\overline{KB} + W\overline{KG}) - g(B - W)]X_2 \tag{A-6}$$

where,

$$B\overline{KB} = \int_{-d}^{0} (y + d)dB \qquad B = \int_{-d}^{0} dB$$

$$W\overline{KG} = \int_{-d}^{CL} (y + d)dW \qquad W = \int_{-d}^{CL} dW$$

$$F_I = -\frac{\pi}{8} C_M \rho g H_W D^2 (1 - e^{-kd})$$

The maximum shear forces at the universal joint :

$$(F_{JX})_{MAX.} = \sqrt{F_{JX1}^2 + F_{JX2}^2} \tag{A-7}$$

The shear force and bending moment values at a given elevation, y is calculated as follows

$$SF(y) = F_{JX} - \int_{-d}^{y} P dy \tag{A-8}$$

$$BM(y) = \int_{-d}^{y} SF(y)dy \tag{A-9}$$

The integral expressions given above are obtained by carrying out simple cumulative additions starting from the universal joint. The bending moment at the top of the tower should be zero. However, in practice it will probably have a small value. This can be eliminated by applying a correction force at each strip. The magnitude of correction force is proportional to the distance between the universal joint and the strip.

In addition to the external forces acting on the column, a mooring force at the top of the column should be included in the force calculations. This force resultant arises due to the wave and motion induced forces on the floating structure which is connected to the column by means of a permanent mooring. In order to include the mooring forces into the SF and BM calculations, it is necessary to modify Eq.(A-4) as follows

$$F_{JX} = F_E + \int_{-d}^{CL} dP \tag{A-10}$$

where F_E is the mooring force acting at the top of the tower (see Fig.A-1).

ii) Calculation of SF and BM Distributions for Double Articulated Tower

The approach used in calculating the SF and BM distributions along the double articulated tower is similar to the approach used in the single articulated tower case. A particular attention should be paid to the calculation of the shear forces at the intermediate joint. The same notation as in the preceeding section is used. First number of the subscripts denotes the column number while the second number denotes the in-phase and out-phase components (see Fig.A-2)

$$F_{JX1} = F_{JX2} + \int_{-d}^{-L_2} dP_{X1} \tag{A-11}$$

$$F_{JX2} = \int_{-L_2}^{CL} dP_{X2} \tag{A-12}$$

where,

$$dP_{X1} = dF_{I11} + \{\omega^2[(y+d)dB_1 + (y+d)dW_1] - g(dB_1 - dW_1)\} \times (\theta_{11}\sin\ \omega t + \theta_{12}\cos\ \omega t)$$

$$dP_{X2} = dF_{I21} + \{\omega^2[(y+L_2)dB_2 + (y+L_2)dW_2] - g(dB_2 - dW_2)\} \times (\theta_{21}\sin\ \omega t + \theta_{22}\cos\ \omega t)$$

Eqs. (A-11) and (A-12) can be written in the form of in-phase and out-phase components as follows

$$\left.\begin{aligned} F_{JX11} &= F_{JX21} + F_{I11} + A_1\theta_{11} \\ F_{JX12} &= F_{JX22} + A_1\theta_{12} \end{aligned}\right\} \tag{A-13}$$

$$\left.\begin{aligned} F_{JX21} &= F_{I21} + A_2\theta_{21} \\ F_{JX22} &= A_2\theta_{22} \end{aligned}\right\} \tag{A-14}$$

where,

wave forces,

$$F_{I21}\sin\ \omega t = \int_{-L_2}^{0} dF_{I21} \qquad F_{I11}\sin\ \omega t = \int_{-d}^{-L_2} dF_{I11}$$

buoyancy moment,

$$B_2\overline{KB}_2 = \int_{-L_2}^{0} (y+L_2)dB_2 \qquad B_1\overline{KB}_1 = \int_{-d}^{-L_2} (y+d)dB_1$$

mass moment,

$$W_2\overline{KG}_2 = \int_{-L_2}^{CL}(y + L_2)dW_2 \qquad W_1\overline{KG}_1 = \int_{-d}^{-L_2}(y + d)dW_1$$

buoyancy,

$$B_2 = \int_{-L_2}^{0} dB_2 \qquad B_1 = \int_{-d}^{-L_2} dB_1$$

mass,

$$W_2 = \int_{-L_2}^{CL} dW_2 \qquad W_1 = \int_{-d}^{-L_2} dW_1$$

and,

$$A_1 = \omega^2(B_1\overline{KB}_1 + W_1\overline{KG}_1) - g(B_1 - W_1)$$

$$A_2 = \omega^2(B_2\overline{KB}_2 + W_2\overline{KG}_2) - g(B_2 - W_2)$$

$$F_{I11} = -\frac{\pi}{8}C_M\rho g H_W D_1^2(e^{-kL_2} - e^{-kd})$$

$$F_{I21} = -\frac{\pi}{8}C_M\rho g H_W D_2^2(1 - e^{-kL_2})$$

The maximum shear forces at the base and intermediate joints are given, respectively, as follows

$$(F_{JX1})_{MAX.} = \sqrt{F_{JX11}^2 + F_{JX12}^2} \qquad \text{(A-15)}$$

$$(F_{JX2})_{MAX.} = \sqrt{F_{JX21}^2 + F_{JX22}^2} \qquad \text{(A-16)}$$

SF and BM distributions on the lower and upper columns can be calculated as follows

$$SF_1(y) = F_{JX1} - \int_{-d}^{y} P_{X1} dy \tag{A-17}$$

$$SF_2(y) = F_{JX2} - \int_{-L_2}^{y} P_{X2} dy \tag{A-18}$$

$$BM_1(y) = \int_{-d}^{y} SF_1(y)\, dy \tag{A-19}$$

$$BM_2(y) = \int_{-L_2}^{y} SF_2(y)\, dy \tag{A-20}$$

When a ship is coupled to the double articulated tower the mooring forces F_E must be included in the total external forces(see Eq.(A-12)):

$$F_{JX2} = F_E + \int_{-L_2}^{CL} dP_{X2} \tag{A-21}$$

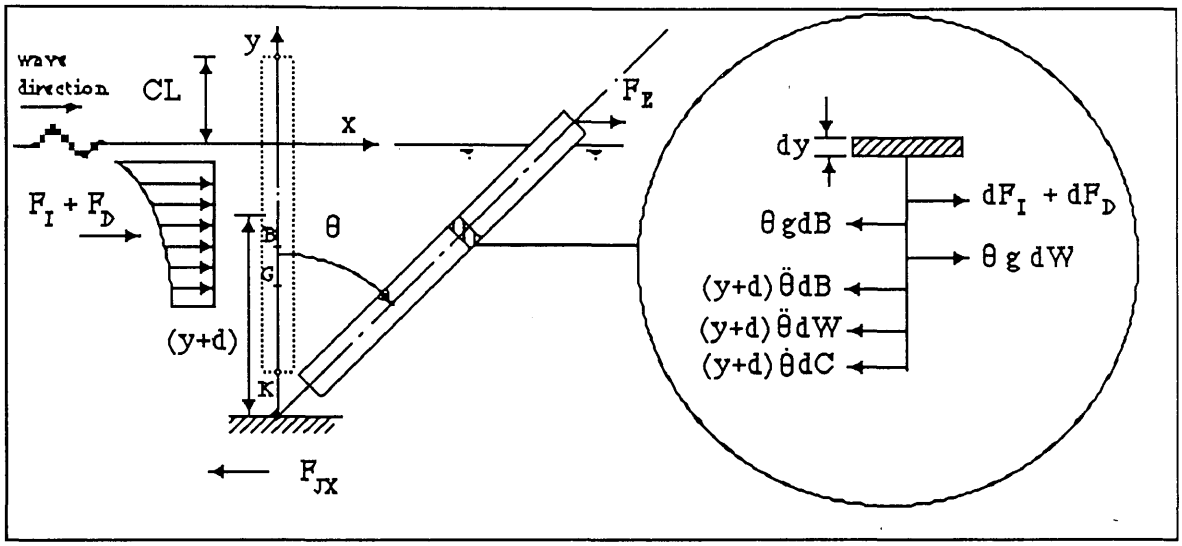
wave
direction
CL
y
x
F_E
$F_I + F_D$
B
G
K
θ
(y+d)
F_{JX}
dy
$dF_I + dF_D$
θ gdB
θ g dW
(y+d) θ̈dB
(y+d) θ̈dW
(y+d) θ̇dC

Fig.A-1

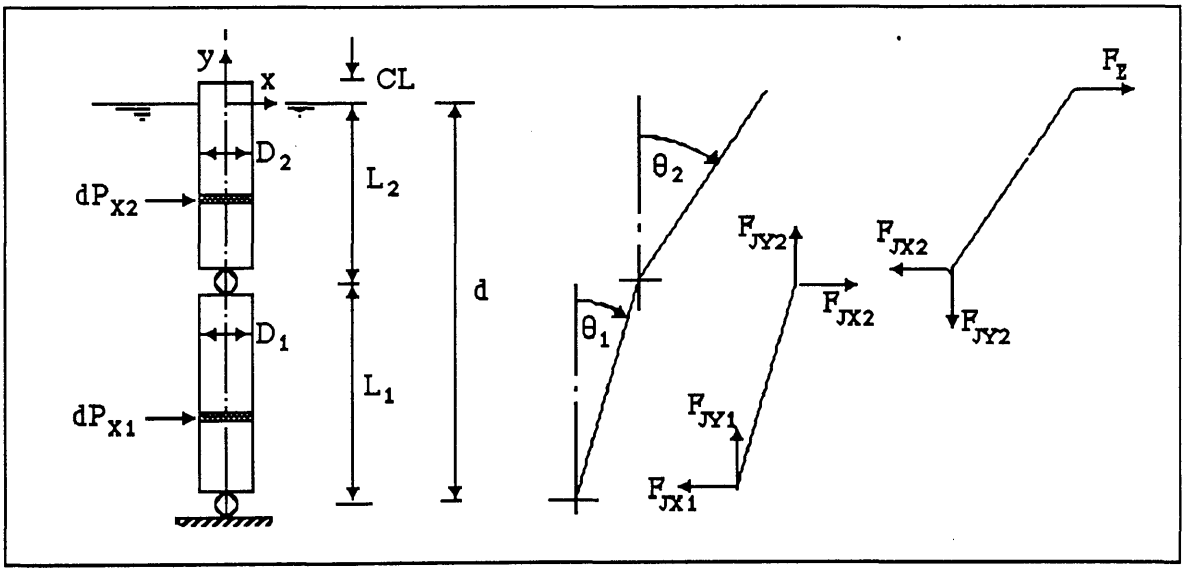
y
x
CL
D_2
D_1
dP_{X2}
dP_{X1}
L_2
L_1
d
θ_2
θ_1
F_{JY2}
F_{JX2}
F_{JY1}
F_{JX1}
F_E

Fig.A-2

APPENDIX B

CALCULATION OF WAVE INDUCED FORCES AND MOMENTS IN OBLIQUE SEAS

The oncoming wave potential defined in the wave reference system Oxyz can be written as

$$\phi = \frac{g\zeta_a}{\omega} e^{ky} \sin(kx - \omega t) \tag{B-1}$$

The coordinate axes, x is positive in the wave propagation direction, y is positive in upward direction and z is perpendicular to the x-y plane. It was assumed that the structure reference system, $\bar{O}\bar{x}\bar{y}\bar{z}$ has a rotating angle around the y axes (see Fig.B-1). Therefore, the velocity potential with respect to a rotated axes can be written as

$$\phi = \frac{g\zeta_a}{\omega} e^{k\bar{y}} \sin(k_1\bar{x} - k_2\bar{z} - \omega t) \tag{B-2}$$

in which, $k_1 = k \cos \alpha$, $k_2 = k \sin \alpha$ and α is the wave propagation direction.

The pressure forces on the vessel in $\bar{x}$ direction can be given as follows

$$F_{P\bar{x}} = - \int_{X_B}^{X_S} d\bar{x} \int_{-B_S/2}^{B_S/2} d\bar{z} \int_{-T_S}^{0} \left(\frac{\partial p}{\partial \bar{x}}\right) d\bar{y} \tag{B-3}$$

where, X_B and X_S are the bow and stern coordinate of the vessel, respectively, p is the linear hydrodynamic pressure, and

$$p = - \rho \frac{\partial \phi}{\partial t} \tag{B-4}$$

Carrying out the above integral for a rectangular box shaped barge gives the following expression

$$F_{P\bar{x}} = -\rho g \zeta_a \frac{2}{k_2 k} \sin\left(\frac{B_S}{2} k_2\right)(1 - e^{-kT_S})(a_1 \cos \omega t + b_1 \sin \omega t) \qquad \text{(B-5)}$$

where, $a_1 = \cos(k_1 X_S) - \cos(k_1 X_B)$ and $b_1 = \sin(k_1 X_S) - \sin(k_1 X_B)$.

The pressure forces on the barge in $\bar{z}$ direction is given as

$$F_{P\bar{z}} = -\int_{X_B}^{X_S} d\bar{x} \int_{-B_S/2}^{B_S/2} d\bar{z} \int_{-T_S}^{0} \left(\frac{\partial p}{\partial \bar{z}}\right) d\bar{y} \qquad \text{(B-6)}$$

Following the similar procedure the pressure forces in $\bar{z}$ direction can be obtained as

$$F_{P\bar{z}} = \rho g \zeta_a \frac{2}{k_1 k} \sin\left(\frac{B_S}{2} k_2\right)(1 - e^{-kT_S})(a_1 \cos \omega t + b_1 \sin \omega t) \qquad \text{(B-7)}$$

If the vessel is long enough, the small body theory may be used for determining the excitation forces due to a non-uniform acceleration of the fluid (see Hooft, 1982). Following this theory, the wave acceleration forces in surge direction can be determined as a function of wave particle acceleration at ends on the vessel and associated added-mass coefficients. In the case of a rectangular box shaped barge, the acceleration forces in $\bar{x}$ direction can be written as follows:

$$F_{A\bar{x}} = m_{AD,\bar{x}} \left(\int_{-B_S/2}^{B_S/2} \dot{U}_{\bar{x}}\Big|_{\substack{\bar{x}=X_B \\ \bar{y}=-T_S/2}} d\bar{z} + \int_{-B_S/2}^{B_S/2} \dot{U}_{\bar{x}}\Big|_{\substack{\bar{x}=X_S \\ \bar{y}=-T_S/2}} d\bar{z} \right) \qquad \text{(B-8)}$$

where, $m_{AD,\bar{x}} = \rho\frac{\pi}{4}T_S^2$ and $\dot{U}_{\bar{x}}$ is the water particle acceleration in $\bar{x}$ direction.

The wave acceleration forces on the barge in $\bar{z}$ direction can be approximated as follows

$$F_{A\bar{z}} = m_{AD,\bar{z}}\left(\int_{X_B}^{X_S} \dot{U}_{\bar{z}}\Big|_{\substack{\bar{z}=0 \\ \bar{y}=-T_S/2}} d\bar{x}\right) \tag{B-9}$$

in which $m_{AD,\bar{z}} = \rho\frac{\pi}{4}T_S^2$ and $\dot{U}_{\bar{z}}$ is the water particle acceleration in $\bar{z}$ direction. In the above formula, it was assumed that the acceleration forces are acting at the centre of the barge. The expressions given below are used in (B-8) and (B-9) for the water particle acceleration in $\bar{x}$ and $\bar{z}$ direction, respectively

$$\dot{U}_{\bar{x}} = g\zeta_a k_1 e^{k\bar{y}} \sin(k_1\bar{x} - k_2\bar{z} - \omega t)$$

$$\dot{U}_{\bar{z}} = -g\zeta_a k_2 e^{k\bar{y}} \sin(k_1\bar{x} - k_2\bar{z} - \omega t)$$

The moment due to the pressure due to the wave pressure forces around the point O (see Fig.B-1) can be written as

$$N_{PR} = -\int_{X_B}^{X_S}\int_{-B_S/2}^{B_S/2}\int_{-T_S}^{0} \bar{x}\left(\frac{\partial p}{\partial \bar{z}}\right)d\bar{y}d\bar{z}d\bar{x} \tag{B-10}$$

After the integrations

$$N_{PR} = 2\rho g\zeta_a(1 - e^{-kT_S})\left(\frac{1}{k}\right)\sin\left(k_2\frac{B}{2}\right)[\beta_1 \sin(\omega t) - \alpha_1 \cos(\omega t)] \tag{B-11}$$

where,

$$\alpha_1 = (\frac{1}{k_1^2})[\sin(k_1 X_S) - \sin(k_1 X_B)] + (\frac{1}{k_1})[X_B \cos(k_1 X_B) - X_S \cos(k_1 X_S)]$$

$$\beta_1 = (\frac{1}{k_1^2})[\cos(k_1 X_S) - \cos(k_1 X_B)] + (\frac{1}{k_1})[X_S \sin(k_1 X_S) - X_B \sin(k_1 X_B)]$$

In similar way the moment due to acceleration forces are given by

$$N_{AC} = m_{AD,\bar{z}} \left(\int_{X_B}^{X_S} \bar{x}\dot{U}_{\bar{z}}\Big|_{\substack{\bar{z}=0 \\ \bar{y}=-T_S/2}} d\bar{x} \right)$$

or

$$N_{AC} = -m_{AD,\bar{z}} g\zeta_a k_2 e^{-kT_S/2}[-\beta_1 \sin(\omega t) + \alpha_1 \cos(\omega t)] \qquad \text{(B-12)}$$

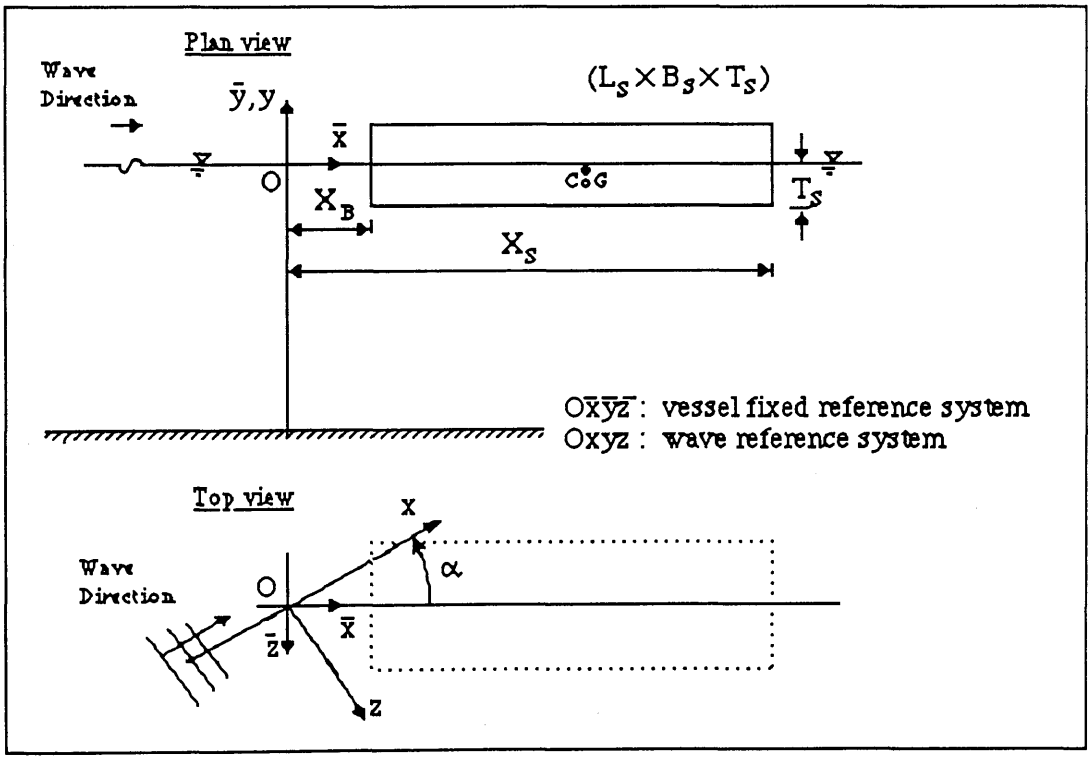

Fig.B-1 Coordinate system

APPENDIX C

DIGITAL FILTERING

The time history of the motion recorded from SELSPOT is a combination of the low frequency natural decay and the wave frequency harmonics about the local mean. In order to find the motion decay in regular waves the wave frequency harmonics should be removed.

The output signal is a sum of linearly weighted present and a number of previous samples of the input signal. In recursive filter structures the output depends both on the input and on the previous outputs. The non-recursive filter has, however, a finite memory with linear phase characteristics and requires a large number of input terms (~700 terms in order to obtain relatively sharp cut-off frequency response).

A non-recursive digital filter with a Hamming window is selected to cut-off the higher frequencies from the time series data (see Bozic 1979). The mathematical form of the filter can be written as follows

$$y_m = \frac{T\omega_c}{\pi} \sum_{n=-N}^{N} W_n \frac{\sin nT\omega_c}{nT\omega_c} x_{m-n}$$

where, x_m is the input signal at the mth time step; y_m, the output filtered signal at the mth time step; T, the sampling interval; ω_C the cut-off frequency; W_n, the Hamming window; N, the half span of the filter.

The frequency response of a filtered time series can be improved by using a window function. With a help of a window function we can choose the appropriate windowing coefficient and the span rate of N. The Hamming window is given by

$$W_n = 0.54 + 0.46 \cos \frac{n\pi}{N}$$

The Hamming window function is applied to the input signal to create the sharp cut-off as an ideal filter has. The span number of N is dependent upon the required accuracy of the output signal. It is noted that a part of the signal data will be lost at the beginning and at the end of the output signal depending on the span rate N.

Fig.C-1 shows the effect of several span rates on the shape of Hamming window for different sampling intervals. A small sampling intervals requires a higher span rate in order to achieve the expected gain. In Fig.C-1, the cut-off frequency selected is 0.4 Hz.

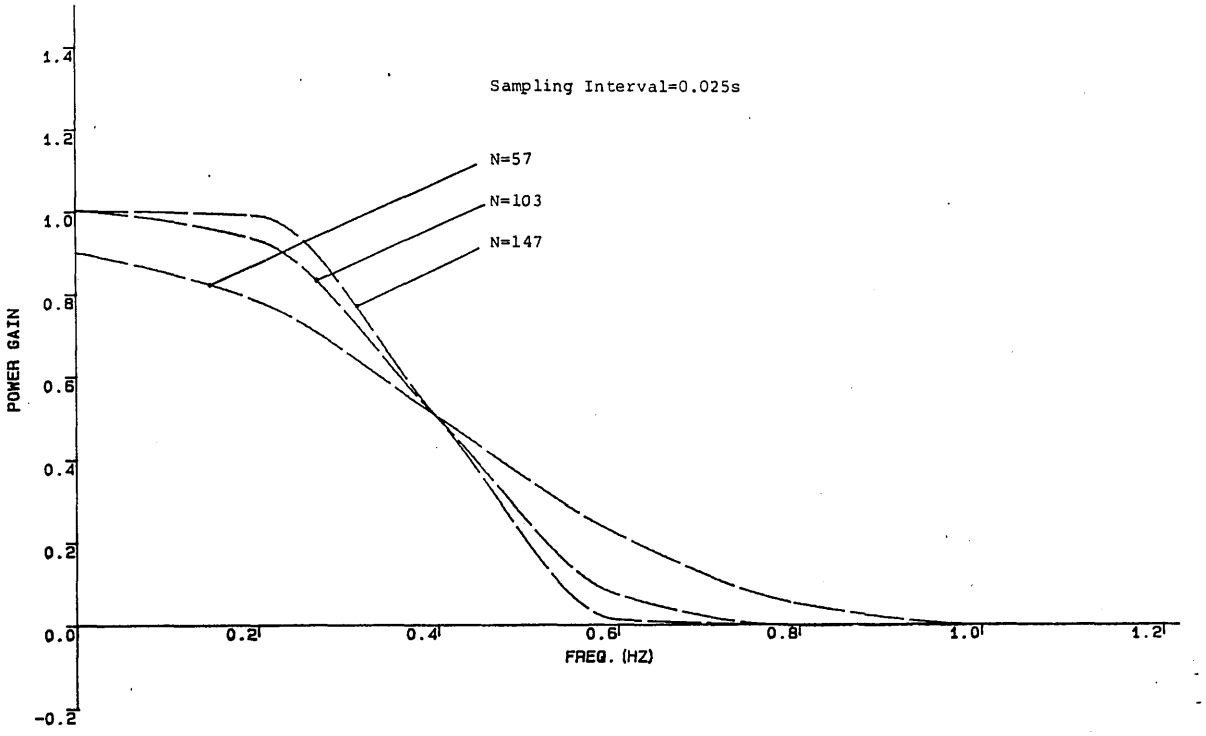

HAMMING WINDOW

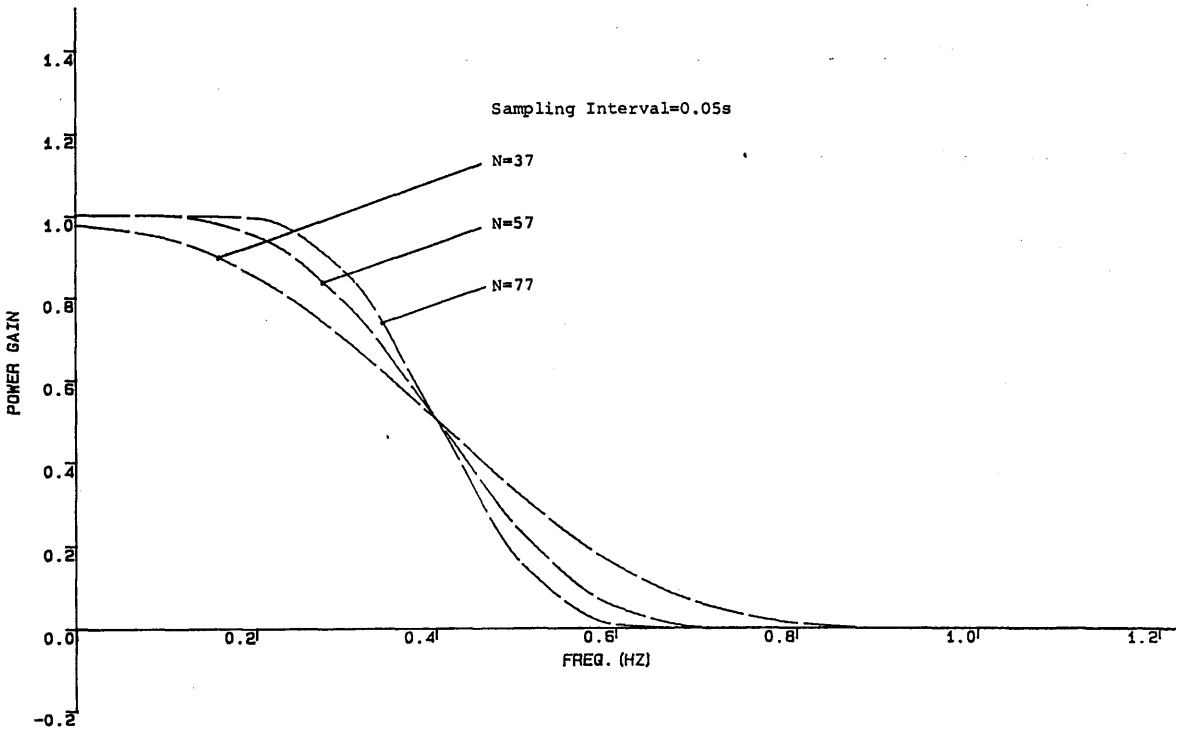

HAMMING WINDOW

Fig.C-1 Effect of span rates on shape of Hamming window

REFERENCES

Andersson, L. and Matsson, B. 1983. A Program for Dynamic and Structural Analysis of Offshore Structures, *Proc. of the 2nd Inter. Symp. on Practical Design of Ships and Mobile Units*, pp.51-61.

Arai, S., Nekado, Y. and Takagi, M. 1977. Study on the Motion of a Moored Vessel among the Irregular Waves, *Naval Arch. and Ocean Engng.*, SNAJ, Vol.15, pp.68-81.

Arthur, R. S. 1949. Variability in Direction of Wave Travel in Ocean Surface Waves, *Ann. Newyork Acad. Sci.*, Vol.51, No.3, pp.511-522.

Bishop, R. E. D. and Price, W. G. 1979. *Hydroelasticity of Ships*, Cambridge University Press, Chapter 12, pp.388-407.

Bowers, E.C. 1976. Long Period Oscillations of Moored Ships Subject to Short Wave Seas, *RINA Transactions*, Paper No. W4, pp.181-191.

Bozic, S. M. 1979. *Digital and Kalman Filtering*, Edward Arnold Pub. Ltd.

Brebbia, C. A. and Walker, S. 1979. *Dynamic Analysis of Offshore Structures*, Newnes-Butterworths, London.

Brendling, W. and Wilson, D. 1987. Theoretical and Experimental Investigation of the Low Frequency Motions of a SALM and Tanker, *Proc. of a Workshop on Floating Structures and Offshore Operations*, Wageningen, the Netherlands.

Butt, H.G., Kokkinowrachos, K. and Troeder, C. 1984. Articulated Production Tower for Deep Water, *Proc. of the 16th Annual Offshore Tech. Conf.*, Paper No. OTC 4821, Houston, pp.367-377.

Butt, H.G., Salewski, J., Wagner, P., Grallert, M., and Kokkinowrachos, K. 1980. Test-Conat a Large Scale Test in the Vicinity of the Research Platform 'NORDSEE'. *Proc. of the European Offshore Technology Conference*, EUR 267, London, pp.559-567.

Caldwell, J. B. and Gammage, W. E. 1977. A Method for Analysis of a Prototype Articulated Multiline Marine Production Riser System, *Jou. of Pressure Vessel Technology*, ASME, pp.170-175.

Chakrabarti, S. K. 1970. Dynamics of Single Point Mooring in Deep Water (Discussion on Proc. Paper 7700, Nov. 1970),*Journal of Waterway, Port, Coastal and Ocean Division*, ASCE, Vol.97, No.WW3, pp. 588-590.

Chakrabarti, S. K. 1980. Steady and Oscillating Drift Forces on Floating Objects, *Journal of Waterway, Port, Coastal and Ocean Division*, ASCE, WW2, pp. 205-228.

Chakrabarti, S. K. 1984a. Steady Drift Force on Vertical Cylinder-Viscous vs. Potential, *Applied Ocean Research,* Vol.6, No.2, pp.73-82.

Chakrabarti, S. K. 1984b. Technical Note: On the Formulation of JONSWAP Spectrum, *Applied Ocean Research*, Vol.6, No.3, pp.175-176.

Chakrabarti, S. K. and Cotter, D. C. 1978. Analysis of a Tower-Tanker System, *Proc. of the 10th Annual Offshore Tech. Conf.*, Paper No. OTC 3202, Houston, pp.1301-1310.

Chakrabarti, S. K. and Cotter, D. C. 1979. Motion Analysis of Articulated Tower, *Journal of Waterway, Port, Coastal and Ocean Division,* ASCE, Vol.105, No.WW3, pp.281-292.

Chakrabarti, S. K. and Cotter, D. C. 1984. Hydrodynamic Coefficients of a Mooring Tower, *Journal of Energy Resources Technology*, ASME, Vol.106, pp.183-190.

Chakrabarti, S. K. and Cotter, D. C. 1988. Motions of Articulated Towers and Floating Structures, *Proc. of the 7th Inter. Conf. on Offshore Mech. and Artic Engng.*, ASME, Houston.

Chaudhuri, J. 1986. Conceptual Designs for Deepwater SALM-Tanker Systems, *Intr. Conf. on Developments in Deeper Waters*, RINA, Paper No.3, London.

Clarke, D., Gedling, P. and Hine, G. 1983. The Application of Maneouvring Criteria in Hull Design Using Linear Theory, *Trans. RINA*, Vol.124.

Clauss, G. , Sükan, M. and Schellin, T. E. 1982. Drift Forces on Compact Offshore Structures in Regular and Irregular Waves. *Applied Ocean Research*, Vol.4, No.4., pp.208-218.

Clough, R. W. and Penzien, J. 1974. *Dynamics of Structures*, McGraw-Hill, New York.

Davenport, A. G. 1967. Gust Loading Factors, *Jou. of the Structural Division*, ASCE, Vol.93, No.ST3, pp.11-34.

Dean, R. G. 1977. Hybrid Method of Computing Wave Loading, *Proc. of the 9th Offshore Tech. Conf.*, Houston, Paper No. 0TC 3029 .

DnV (1974) Rules for Construction and Certification of Fixed Offshore Structures, Oslo.

Drake, K. R. 1984. Dynamics of Large Diameter Articulated Columns in Waves, Ph.D. Thesis, University College of London.

Drake, K. R., Eatock-Taylor, R. and Matsui, T. 1984. Drift of an Articulated Cylinder in Regular Waves. *Proc. Royal Soc. London*, A 394, pp.363-385.

Drawe III, W.J., Raj, A. and Rawston, P.J. 1986. Technical and Economic Considerations in Developing Offshore Oil and Gas Prospects Using Floating Production Systems, *Marine Technology*, SNAME, Vol. 23, No.3, pp. 253-270.

Dumazy, C. and Leturq, M. 1983. Behaviour of a Floating Vessel/Articulated Column System, *Proc. of the 15th Annual Offshore Tech. Conf.*, Paper No. OTC 4547, Houston.

Eatock Taylor, R. and Drake, K. R. 1984. Design Considerations for Articulated Columns, *Developments in Floating Production Systems*, RINA, London.

Faltinsen, O. M., Kjaerland, O., Liapis, N. and Walderhaug, H. 1979. Hydrodynamic Analysis of Tankers at Single Point Mooring Systems, *Inter. Conf. on Behaviour of Off-Shore Structures.*, BOSS'79, Imperial College, London, England, pp.177-206.

Fujii, H. and Takahashi, T. 1975. Experimental Study on the Resistance Increase of a Ship in Regular Oblique Waves, *Proceedings of the 14th ITTC*, Ottowa.

Gernon, B. J. and Lou, J. Y. K. 1987. Dynamic Response of a Tanker Moored to an Articulated Loading Platform, *Ocean Engng*, Vol.14, No.6, pp.489-512.

Goda, Y. 1985. *Random Seas and Design of Maritime Structures*, University of Tokyo Press.

Goodfellow Associates Limited. 1986. *Offshore Engineering : Developments of Small Oilfields*, Graham&Trotman Ltd.

Harris, R. I. 1970. The Nature of the Wind, *Proc. of the Seminar on the Modern Design of Wind-sensitive Structures*, The Inst. of Civil Engineers, London.

Havelock, T.H. 1940. The Pressure of Water Waves upon a Fixed Obstacle, *Proceedings of Royal Society of London*, Series A, No. 963, Vol. 175, pp.409-421.

Haverty, K. F., McNamara, J. F. and Moran, B. 1982. Finite Dynamic Motions of Articulated Offshore Loading Towers, INTERMARITEC'82, Paper No. IMT 82-110/01, Hamburg, pp.145-157.

Hogben, N. 1976. Wave Loads on Structures, *Proc. of the First Inter.Conf. on the Behaviour of Offshore Structures*, BOSS'76, Vol.1, pp.187-219.

Hooft, J.P. 1982. *Advanced Dynamics of Marine Structures*, John Wiley and Sons, New York.

Horner,S. F. 1965. *Fluid Dynamic Drag*, Ed. by the author, New Jersey.

Houlie, M. Stansberg, C. T. and Wereskiold, P. 1983. Model Tests with a SPM System in Short Crested Waves, *Proc. of the 15th Annual Offshore Tech. Conf.*, Paper No. OTC 4644, Houston.

Jain, R. K. and Kirk, C. L. 1977. The Dynamic Response of a Double Articulated Offshore Loading Structure to Non-Colinear Waves and Current, *Conf. on the Applied Mechanical Engineering*, Yale University.

Kaimal, J. C. et al. 1972. Spectral Characteristics of Surface-Layer Turbulance, *Jou. Royal Meteorological Soc.*, Vol.98, pp.563-589.

Kareem, A. and Dalton, C. 1982. Dynamic Effects of Wind on Tension Leg Platforms, *Proc. of the 14th Annual Offshore Tech. Conf.*, Paper No. OTC 4229, Houston.

Kim, C. H. and Luh, P. A. 1982. Prediction of Pitching Motions and Loads of an Articulated Loading Platform in Waves,*Proc. of the 14th Annual Offshore Tech. Conf.*, Paper No. OTC 4247, Houston.

Kinsman, B. 1965. *Wind Waves* , Prentice-Hall, Inc.

Kirk, C. L. , Shanks, J. M. and Langley, R. S. 1985. Dynamic Analysis and Design of Articulated Spar Buoys, SERC Cohesive Program on Compliant Structures, Project 4.1, No.16.

Kirk, C. L. and Bose, P. 1982. Dynamic Response of Articulated Platforms in Random Seas. *Inter. Conf. on Flow Induced Vibrations in Fluid Engineering*, BHSA Fluid Engineering, Cranfield, England, pp.77-103.

Kirk, C. L. and Jain, R. K. 1977. Response of Articulated Towers to Waves and Current, *Proc. of the 9th Annual Offshore Tech. Conf.*, Paper No. OTC 2798, Houston.

Kokkinowrachos, K. and Mitzlaf, A. 1981. Dynamic Analysis of One- and Multi-Column Articulated Structures, *Inter. Symp. on Hydrodynamics in Ocean Engng.*,the Norwegian Inst. of Tech., Norway, pp.837-862.

Kokkinowrachos, K., Hoefeld, J. and Mitzlaff, A. 1985 . Evaluation of Experiences from Three Large-size Tests in the North Sea within the Design Procedure of Offshore Structures, *Inter. Conf. on Behaviour of Off-Shore Structures*, BOSS'85, Amsterdam, pp.135-151.

Korbijn, F. 1979. Computer Simulation of Slow and High Frequency Motion and Loads of the STATFJORD"A" Articulated Loading Platform in Irregular Sea, DnV Tech. Report, No.791049-I and -II.

Kwon, Y.J. 1982. The Effect of Weather Particularly Short Sea Waves on the Ship Speed Performance. Ph.D. Thesis, Faculty of Engineering, University of Newcastle-upon-Tyne.

Langley, R. S. and Kirk, C. L. 1982. Random Dynamic Analysis of an Offshore Single Anchor Leg Storage System, *Applied Ocean Research,* Vol.4, No.4, pp.232-246.

MacCamy, R.C. and Fuchs, R.A. 1954. Wave Forces on Piles: A Diffraction Theory, U.S. Army Corps of Engineers, Beach Erosion Board, Technical Memorandum No. 69.

Mack, R. C. et al. 1981. Fulmar, the First North Sea SALM/VLCC Storage System, *Proc. of the 13th Annual Offshore Tech. Conf.*, Paper No. OTC 4041, Houston.

Maruo, H. 1960. The Drift of a Body Floating on Waves, *Jou. of Ship Research*, Vol.4, No.3, pp.1-10.

McNamara, J. F. and Lane, M. 1984. Practical Modeling for Articulated Risers and Loading Columns, *Jou. of Energy Resources Technology*, Vol.106, December, pp.444-450.

Millar, J. L., Hughes, H. and Dyer, R. C. 1979. First Year's Operation Experience of the Deepest SPM in the World, *Proc. of the 11th Annual Offshore Tech. Conf.*, Paper No. OTC 3561, Houston.

Mitsuyasu et al. 1975. Observation of the Directional Spectrum of Ocean Waves Using a Coverleaf Buoy, *Jou. Physical Oceanogr.*, Vol.5, No.4, pp.750-760.

Molin, B. 1979. Second-Order Diffraction Loads upon Three-Dimensional Bodies, *Appl. Ocean Research*, Vol.1, No.4, pp.197-202.

Morison, J. R., O'Brien, M. P., Johnson, J. W. and Schaaf, S. A. 1950. The Force Exerted by Surface Waves on Piles, *Petroleum Transactions*, AIME, Vol.189, pp.149-154.

Muga, B. J. and Fong, H. 1976. Wave Forces Induced on VLCCs, *Proc. of the 8th Annual Offshore Tech. Conf.*, Paper No. OTC 2535, Houston.

Naess, A. 1980. Loads and Motions of an Articulated Loading Platform with Moored Tanker, *Proc. of the 12th Annual Offshore Tech. Conf.*, Paper No. OTC 3841, Houston.

Naftzger, R. A. and Chakrabarti, S. K. 1980. Dynamic Behavior of Floating Storage Vessel, *Jou. of the Waterway, Port, Coastal and Ocean Div.*, ASCE, Vol.106, No.WW2, pp.157-167.

Natvig, B. J. and Berta, M. 1983. Comprehensive Dynamic Analysis of Offshore Loading Concepts, *Proc. of the 15th Annual Offshore Tech. Conf.*, Paper No. OTC 4499, Houston.

Newman, J. N. 1967. The Drift Force and Moment on Ships in Waves, *Jou. of Ship Research*, Vol.11, pp.51-60.

Newman, J. N. 1974. Second Order, Slowly Varying Forces on Vessels in Irregular Waves, *Proc. of Inter. Symp. on Dynamics of Marine Vehicles in Waves*, London, pp.182-186.

Nienhuis, U. 1986. Simulations of Low Frequency Motions of Dynamically Positioned Offshore Structures, *Trans. RINA*.

Nwogu, O. and Isaacson, M. 1989. Drift Motions of a Floating Barge in Regular and Random Multi-Directional Waves, *Proc. of the 8th Inter. Conf. on Offshore Mech. and Artic Engng.*, Vol.II, ASME, the Hague.

OCIMF(Oil Companies International Marine Forum). 1977. Prediction of Wind and Current Loads on VLCCs, London.

Olsen, O. A., Braathen, A., Loken, A. E., Nyhus, K. A., and Torset, O. P. 1978. Slow and High Frequency motions and Loads of Articulated Single Point Mooring Systems for Large Tankers, *Norwegian Maritime Research*, No.2, pp.14-28.

Olson, R. E., Olsen, D. R., Rullman, J. D. and Vasser, F. G. 1983. Hondo Field Development and Operations, *Proc. of the 15th Annual Offshore Tech. Conf.*, Paper No. OTC 4542, Houston.

Östergaard, C. and Schellin, T. E. 1987. Comparison of Experimental and Theoretical Wave Actions on Floating and Compliant Offshore Structures, *Applied Ocean Research*, Vol.9, No.4, pp.192-213.

Pinkster, J. A. 1974. Low Frequency Phenomena Associated with Vessels Moored at Sea, *Society of Petroleum Engineers Journal*, No. 4837.

Pinkster, J. A. 1979. Mean and Low Frequency Wave Drifting Forces on Floating Structures, *Ocean Engng.*, Vol.6, pp.593-615.

Pinkster, J. A. 1988. The Influence of Directional Spreading of Waves on Mooring Forces, *Proc. of the 20th Offshore Tech. Conf.*, Paper No. OTC 5629, Houston.

Pinkster, J. A. and van Oortmerssen, G. 1977. Computation of the First and Second Order Wave Forces on Oscillating Bodies in Regular Waves, *Proc. of the 2nd Intr. Conf. on Numerical Ship Hydr.*, University of Calif., Berkeley, pp.136-156.

Ractliffe, A. T. and Clarke, D. 1980. Development of Comprehensive Simulation Model of a Single Point Mooring System, *Trans. RINA*

Remery, G. F. M. and Hermans, A. J. 1971. The Slow Drift Oscillations of a Moored Object in Random Seas, *Proc. of the 3rd Annual Offshore Tech. Conf.*, Paper No. OTC 1500, Houston.

Remery, G. F. M. and van Oortmerssen, G. 1973. The Mean Wave, Wind and Current Forces on Offshore Structures and Their Role in the Design of Mooring Systems, *Proc. of the 5th Annual Offshore Tech. Conf.*, Paper No. OTC 1741, Houston.

Romeling, J. U., Marol, P. and Sand, S. E. 1984. Bi-Articulated Tower Tested in Directional Waves, *Sym. on Description and Modelling of Directional Seas*, Tech. Uni. of Denmark.

Sarpkaya, T. and Isaacson, M. 1981. *Mechanics of Wave Forces on Offshore Structures*, Van Nostran Reinhold Company, New York.

Schellin, T. E. and Koch, T. 1985. Calculated Dynamic Response of an Articulated Tower in Waves, *Proc. of the 4th Inter. Conf. on Offshore Mech. and Artic. Engng.*, ASME, Dallas.

Smulders, L. H. and Remery, G. F. 1979. The Mooring of a Tanker to a Single Point Mooring by a Rigid Yoke, *Proc. of the 11th Annual Offshore Tech. Conf.*, Paper No. OTC 3567, Houston.

Snowden, D. P. , Warren, J. G. and Bury, M. R. C. 1985 . The Development of Hyrodynamic Analysis for Articulated Column-Based Floating Production Systems, *Inter. Conf. on Behaviour of Off-Shore Structures*, BOSS'85, Amsterdam, pp.545-556.

Sorheim, H. R. 1980. Analysis of Motion in Single Point Mooring Systems, *Modelling, Identification and Control,* Vol.1, No.3, pp.165-186.

Standing, R. G. , Rowe, S. J. and Brendling, W. J. 1986. Jacket Transportation Analysis in Multidirectional Waves, *Proc. of the 18th Annul Offshore Tech. Conf.,* Paper No. OTC 5283, Houston.

Standing, R. G., Dacunha, N.M.C. and Matten, R.B. 1981. Mean Wave Drift Forces: Theory and Experiment, NMI Report No. R124.

Teigen, P. S. 1983. The Response of a TLP in Short-Crested Waves, *Proc. of the 15th Offshore Tech. Conf.*, Paper No. OTC 4642, Houston.

Thomson, W. T. 1981. *Theory of Vibration with Applications*, Prentice-Hall, New Jersey.

van Oortmerssen, G. 1976. The Motions of a Moored Ship in Waves, Doctoral Thesis, MARIN Publ. No. 510, Wageningen, The Netherlands.

Wagenaar, M. G. and Davison, C. 1983. Self Installable: Floating Production Facility Requires Only Light Support Craft, *Proc. of the 15th Annual Offshore Tech. Conf.*, Paper No. OTC 4544, Houston.

Wichers, J. E. W. and van Sluijs, M. F. 1979. The Influence of Waves on the Low-Frequency Hydrodynamic Coefficients of Moored Vessels, *Proc. of the 11th Annual Offshore Tech. Conf.*, Paper No. OTC 3625, Houston.

Wolfram Jr., W. R. and Gunderson, R. H. 1979. Structural Design of Production Risers and Offshore Production Terminals, *Proc. of the 11th Annual Offshore Tech. Conf.*, Paper No. OTC 3535, Houston.

Wu, S. 1987. Hydro-Structural Design Aspects of Articulated Towers, Ph.D. Thesis, University of Glasgow.

Wu, S. C. and Tung, C. C. 1975. Random Response of Structures to Waves and Current Forces, Sea Grand Pub., Report No. UNC-SG-75-22.

Yilmaz, O. 1990. Calculation of Wave Forces on a Tanker, Departmental Report, Glasgow Uni., NAOE-90-22.